

**CONTENTS**

**BIOSCIENCES**

**Altered energy transfer in Phycobilisomes of the Cyanobacterium, *Spirulina Platensis* under the influence of Chromium (III)** 1 - 3  
Ayya Raju, M. and Murthy, S. D. S.

**Biotransformation of 11 $\beta$ , 17 $\alpha$ -dihydroxy-4-pregnene-3, 20-dione-21-o-succinate to a 17-ketosteroid by *Pseudomonas Putida* MTCC 1259 in absence of 9 $\alpha$ -hydroxylase inhibitors** 4 - 7  
Rahul Patel and Kirti Pawar

**Influence of nicking in combination with various plant growth substances on seed germination and seedling growth of Noni (*Morinda Citrifolia* L.)** 8 - 10  
Karnam Jaya Chandra and Dasari Daniel Gnana Sagar

**Quantitative analysis of aquatic Macrophytes in certain wetlands of Kachchh District, Gujarat** 11 - 13  
J.P. Shah, Y.B. Dabgar and B.K. Jain

**Screening of crude root extracts of some Indian plants for their antibacterial activity** 14 - 18  
Purvesh B. Bharvad, Ashish R. Nayak, Naynika K. Patel and J. S. S. Mohan

Short Communication

**Heterosis for biometric characters and seed yield in parents and hybrids of rice (*Oryza Sativa* L.)** 19 - 20  
M. Prakash and B. Sunil Kumar

**CHEMISTRY**

**Adsorption behavior and thermodynamics investigation of Aniline-n-(p-Methoxybenzylidene) as corrosion inhibitor for Al-Mg alloy in hydrochloric acid** 21 - 24  
V.A. Panchal, A.S. Patel and N.K. Shah

**Grafting of Butyl Acrylate onto Sodium Salt of partially Carboxymethylated Guar Gum using Ceric Ions** 25 - 31  
J.H. Trivedi, T.A. Bhatt and H.C. Trivedi

**Simultaneous equation and absorbance ratio methods for estimation of Fluoxetine Hydrochloride and Olanzapine in tablet dosage form** 32 - 36  
Vijaykumar K. Parmar, Uday H. Thorat, Girish K. Jani and Laxman M. Prajapati

**COMPUTER SCIENCE**

**Bootstrapping of phone models for a large vocabulary continuous speech recognition for Gujarati** 37 - 40  
Himanshu N. Patel and Paresh V. Virparia

**Natural Language Interface for Student Information System (NLSIS)** 41 - 44  
Amisha Shingala, Rinku Chavda and Paresh Virparia

**PRAJÑĀ**  
Volume 19, 2011

**Journal of Pure and Applied Sciences**



**SARDAR PATEL UNIVERSITY**  
VALLABH VIDYANAGAR  
Gujarat - 388 120, INDIA  
www.spuvvn.edu

# **PRAJÑĀ - Journal of Pure and Applied Sciences**

(Abbreviation: *PRAJÑĀ - J. Pure & Appl. Sci.*)

## **Patron**

**Prof. Harish Padh**  
Vice-Chancellor

## **Managing Editor**

**Prof. T. V. Ramana Rao**  
B. R. D. School of Biosciences  
Sardar Patel University  
Vallabh Vidyanagar, Gujarat - 388 120  
spu.prajna@gmail.com

## **Editorial Board**

**Prof. S. J. Bhatt**  
Dept. of Mathematics  
subhashbhaib@yahoo.co.in

**Prof. Rema Subhash**  
Dept. of Home Science  
remasubhash@yahoo.com

**Prof. D. K. Raval**  
Department of Chemistry  
aanal.virat@gmail.com

**Prof. K. N. Joshipura**  
Dept. of Physics  
knjoshipura@yahoo.com

**Prof. Satish Manocha**  
Dept. of Materials Science  
sm\_manocha@rediffmail.com

**Prof. D. Lakshminarayana**  
Department of Electronics  
dlnvvn@yahoo.com

**Prof. K. S. Rao**  
Dept. of Biosciences  
kayesrao@yahoo.com

**Prof. Darshan Choksi**  
Dept. of Computer Science  
dbchoksi@yahoo.com

**Prof. Ashok Shanubhogue**  
Department of Statistics  
a\_shanubhogue@yahoo.com

Since 1991 Sardar Patel University has been regularly publishing the *PRAJÑĀ - Journal of Pure and Applied Sciences* with an aim of providing a platform to Academicians, Researchers and Scientists for the rapid dissemination of original scientific work carried out in the University Departments, Affiliated Colleges and Research Laboratories located in Gujarat. All articles published in *PRAJÑĀ* are deemed to reflect the individual views of the authors and not the official points of view of the Sardar Patel University.

**A Peer Reviewed Journal**

**Indexed in Indian Science Abstracts**

**Published by the Registrar, Sardar Patel University, Vallabh Vidyanagar, Gujarat - 388 120**

**Printed at Sardar Patel University Press, Vallabh Vidyanagar, Gujarat-388 120**

## **MATHEMATICS**

**A Mathematical model for a growth curve of rice crop** 45 - 46  
R. Lakshmi and V. Ravichandran

**On a new sequence of functions defined by a generalized Rodrigues formula** 47 - 49  
J.C. Prajapati, N.K. Ajudia and A.K. Shukla

Corrected Version of Vol. 18: 115-116(2010)  
**Mean labeling for some new families of graphs** 50 - 51  
S.K. Vaidya and Lekha Bijukumar

## **PHYSICS**

**Correlations among atomic properties and estimates on exotic atoms** 52 - 55  
Pooja Bhowmik, Ramji H. Patel and K.N. Joshipura

**Crystal quartz windows for far-infrared interferometer of SST-1** 56 - 59  
Asha Adhiya and Rajwinder Kaur

**Decay widths of  $B_c \rightarrow J/\Psi \pi^+$  in CPPv model** 60 - 62  
Arpit Parmar, Kaushal Thakkar, Bhavin Patel and P.C. Vinodkumar

**DFT studies on electronic structure and elastic properties of CoN: Zinblende and Rocksalt Structures** 63 - 67  
Jameson Maibam, B. Indrajit Sharma, Ramendu Bhattacharjee, R.K. Thapa and R.K. Brojen Singh

**Electrical transport properties of Tungsten Ditelluride (WTe<sub>2</sub>) Crystals** 68 - 70  
Priyanka Desai, D.D. Patel, D.N. Bhavsar and A.R. Jani

**Electron impact total cross sections for Ethylene Oxide** 71 - 74  
Avani Y. Barot, Minaxi Vinodkumar and Bobby Antony

**Infrared spectra of charge transfer complexes of Proteoglycan** 75 - 78  
Pravinsinh I. Rathod, Vishal Patel and A. T. Oza

**Optical Properties of Tin Monosulphide And Tin Monoselenide Single Crystals** 79 - 81  
B.B. Nariya, A.K. Dasadia and A.R. Jani

**Structural Characterization and Transport Properties of CVT Grown ZrSe<sub>3</sub> and ZrS<sub>3</sub> Crystals** 82 - 84  
A.K. Dasadia, B.B. Nariya and A.R. Jani

**Theoretical calculation of electron impact total cross sections for HCl molecule over a wide range of impact energies (0.1 eV – 2000 eV)** 85 - 89  
Mayuri Y. Barot, Harshad Bhutadia, Minaxi Vinodkumar

## **STATISTICS**

**A case study of hybrid microcircuit assembly process using Taguchi design method and response surface method** 90 - 92  
D.P. Raykundaliya and A. Shanubhogue

**Acceptance decision rule for Type-I generalized half logistic distribution** 93 - 96  
K. Rosaiah, R.R.L. Kantam and V. Rama Krishna

**On variance estimation for the Greg estimator** 97 - 99  
P.A. Patel and R.D. Chaudhari

**Guidelines for Contributors** 100 - 101

***PRAJÑĀ - Journal of Pure and Applied Sciences***

Volume 19, December 2011



An Official Publication of  
**Sardar Patel University**  
Vallabh Vidyanagar, Gujarat - 388 120, India

[www.spuvvn.edu](http://www.spuvvn.edu)

E-mail: [spu.prajna@gmail.com](mailto:spu.prajna@gmail.com)



**Sardar Patel University**

is grateful to

**Prof. Vithalbhai A. Patel**

**Humboldt State University, Arcata, California, USA,  
whose generous donation to organize academic activities  
in the name of Shri Ishwarbhai Ambalal Patel (Shertha) helped  
to meet a part of tge publication cost of PRAJNA Journal.**

\* \* \* \* \*

**The Editorial Board of PRAJNA is grateful to all those experts who  
rendered their valuable services as referees for reviewing  
the papers received for this volume of the Journal.**

\* \* \* \* \*

**The computational assistance received from Miss. Jigisha Vaghela and Mr. Sahaj Gandhi,  
Doctoral Research Students of of Biosciences and Physics Departments  
respectively for making of this volume of  
PRAJNA Journal is also gratefully acknowledged.**



## ALTERED ENERGY TRANSFER IN PHYCOBILISOMES OF THE CYANOBACTERIUM, *SPIRULINA PLATENSIS* UNDER THE INFLUENCE OF CHROMIUM (III)

Ayya Raju, M. and Murthy, S.D.S.\*

Department of Biochemistry, S.V. University, Tirupati-517 502, A.P., India

### ABSTRACT

Phycobilisomes act as major light harvesting complex in photosystem II of cyanobacteria. In this investigation an attempt has been made to study the effect of chromium (Cr) in the energy transfer of phycobilisomes. Our results indicate that chromium (III) (50 and 100  $\mu$ M) is able to cause alterations in absorption and energy transfer with intact cells at 100  $\mu$ M concentration during short term incubation. The phycobilisomes isolated from chromium (50 $\mu$ M) treated cells also exhibited changes in absorption as well as fluorescence emission properties in the red shift in the peak position. Thus chromium acts as an energy transfer inhibitor both under *in vitro* and *in vivo* conditions.

**Key words :** Absorption, Allophycocyanin, Cyanobacteria, Fluorescence, Phycocyanin.

### INTRODUCTION

Phycobiliproteins (PBPs) are unique light harvesting pigment proteins present in cyanobacteria, red algae and cryptomonads, but not in higher plants. Unlike plant light harvesting chlorophyll (Chl) proteins, these PBPs are arrayed in subcellular structures which are known as phycobilisomes (PBSs). These structures allow the pigments to get arrayed geometrically in a manner which help to optimize the capture light and transfer of energy [1-4]. The major components of PBSs are the bilin containing proteins: Phycoerythrin (PE), Phycocyanin (PC) and Allophycocyanin (APC). The last two pigment proteins PC and APC are present in cells of cyanobacteria and red algae [5 - 6], while PE is available component and its presence is resulted by the available quality of light [7-9].

The energy transfer in the PBSs (PE  $\rightarrow$  Chl *a*) can be influenced by several environmental factors such as Hg [10], Cu [11]. Studies related to the effect of Cr (III) on energy transfer studies are scanty. Hence in this investigation an attempt has been made to study the effect of Cr both short term (10 min) and long term (12 h) using intact cells of *Spirulina platensis* as well as isolated PBSs.

### MATERIALS AND METHODS:

*Spirulina platensis* trichomes were grown in Zarrouk's medium [12] at  $25 \pm 2^\circ$  C under continuous illumination ( $15 \text{ Wm}^{-2}$ ). *In vivo* experiments were conducted by incubating the cells with Cr (100  $\mu$ M) for 10 min under continuous stirring. For *in vitro* studies the cells were treated with Cr ions (50  $\mu$ M) for 12 h and the PBSs have been isolated. The PBSs isolated were according to the method of Gantt *et al* [13] with slight modifications. The PBSs were recovered from the 1.0 M region as an intense blue band. Sucrose was removed from the isolated PBSs by using dialysis, with against 0.75 K.  $\text{PO}_4$  (pH 7.0) buffer. PBSs and intact cells both were used for spectral measurements. The absorption spectra of intact cell suspension and PBSs were taken by using a Hitachi - 557 double beam, spectrophotometer as described by Murthy *et al* [14]. The emission spectral of cell samples and PBSs were measured by using Perkin-Elmer spectrofluorometer [14]. Cells equivalent to 15  $\mu$ g of Chl were used for spectral measurements, where as PBSs equivalent to 30  $\mu$ g of protein was used for both absorption as well as fluorescence emission measurements.

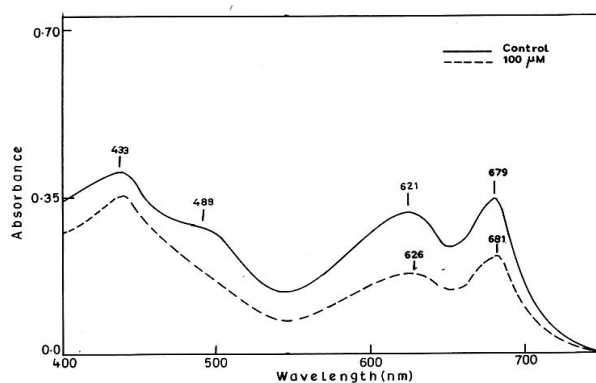


Fig. 1 Effect of 'Cr' ions on the absorption spectra of intact cells of *Spirulina platensis*.

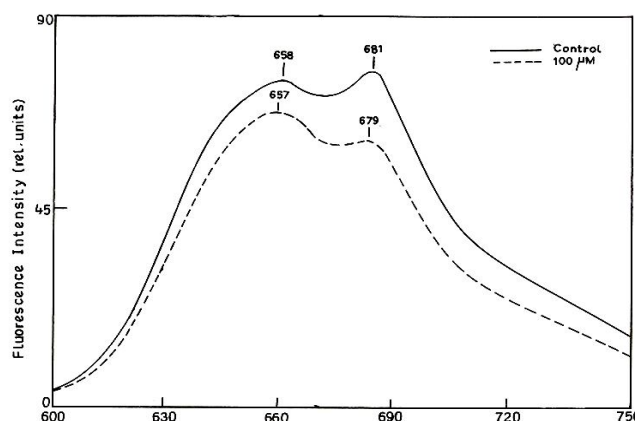


Fig. 2 Effect of 'Cr' on phycocyanin fluorescence emission spectra of the intact cells.

### RESULTS AND DISCUSSION:

Initially after giving the Cr ions (100  $\mu$ M) treatment for 10 min, the absorption characteristics of different pigment proteins present in the control cells of *Spirulina platensis* was measured. The peak at 433 nm is due to the solet band of Chl *a*; at 488nm the peak is due to carotenoids, at 621 nm is due to the absorption of PC and peak at 679 nm is due to the absorption of Chl *a* [15]. The

\*Corresponding author: sdsurthy@rediffmail.com

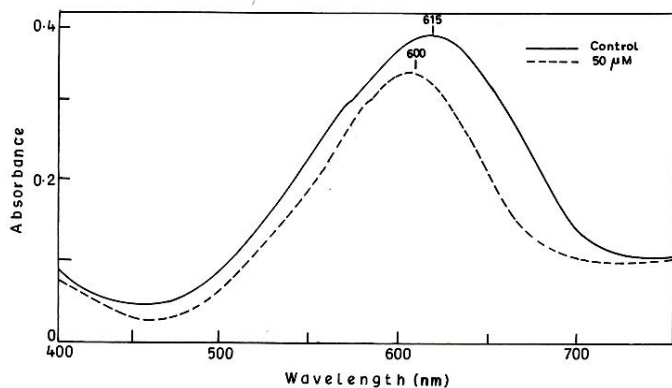


Fig. 3 Absorption spectra of isolated PBSs from control and 'Cr' treated cells.

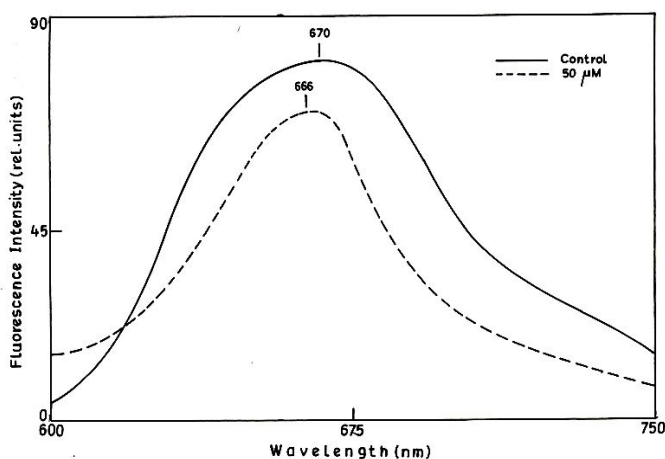


Fig. 4 Fluorescence emission spectra of isolated PBSs from control and 'Cr' treated cells.

treatment of intact cells of *Spirulina* with different concentrations chromium (100  $\mu\text{M}$ ) caused drastic decrease in phycocyanin absorption by marginally affecting the Chl *a* and carotenoid absorption. In addition there is a 5 nm red shift of PC indicating the structural alterations in PBSs regarding the chromophore attachment with apoprotein (Fig. 1). Similar observations were made by Murthy *et al* [14] in *Spirulina* under mercury stress. Since chromium affected the phycocyanin absorption quite extensively further studies were made by measuring room temperature phycocyanin fluorescence. The control cells excited with 545 nm light beam exhibited an emission peak at 658 nm which indicates that the energy is transferred from PC to Chl *a* [14; 16]. Figure 2 shows the phycocyanin fluorescence emission spectra of chromium treated *Spirulina* intact cells. With the treatment of Cr ions drastic decrease was noticed in the fluorescence emission intensities and with 100  $\mu\text{M}$  of chromium ions almost 50 % of loss in the fluorescence intensity of phycocyanin was observed. It clearly demonstrates that selected heavy metal (Cr) induced alterations in the energy transfer from PC to Chl *a* by inducing the structural changes in the phycobiliproteins.

To correlate the results of *in vivo* experiments with *in vitro* experiments, phycobilisomes have been isolated from control as well as Cr (50  $\mu\text{M}$ ) treated cells (12 h) by using sucrose density gradient. After removal sucrose the spectral properties have been measured (Fig 3 and 4). The absorption spectra of PBSs exhibit a main peak at 615 nm. The PBSs isolated from 50  $\mu\text{M}$  of Cr treated cells, caused a decrease in the absorption of PC by 40% and shifted the peak position from 615 nm to 600 nm. Since the absorption properties are related to the fluorescence emission of PC, PBSs samples which were isolated from chromium exposed

(50  $\mu\text{M}$ ) *Spirulina* cells were used for the measurement of phycocyanin fluorescence emission. Chromium is able to cause 42% decrease in the fluorescence intensity and blue shift in the emission peak from 670 nm to 666 nm. The decrease in the fluorescence intensity indicates the change in the energy transfer and blue shift gives information about structural changes in the PBSs (Fig 4).

Similar reports were made by Murthy *et al* [14] during the toxic effect of mercuric chloride ( $\text{HgCl}_2$ ) on the spectral properties of phycobiliproteins in the same organism. Thus chromium is able to cause alterations in the energy transfer from PC to Chl *a* in the *Spirulina* both under *in vivo* as well as *in vitro* conditions by inducing changes in PBSs.

#### ACKNOWLEDGEMENT

Prof. S. D. S. Murthy is thankful to University Grants Commission for providing Major Research Project (2011-2014).

#### REFERENCES

- [1] Gantt, E. (1981) Phycobilisomes. *Ann. Rev. Plant Physiol.* **32**: 327-347.
- [2] Glazer, A. (1984) Phycobilisome: A macromolecular complex specialized for light energy transfer. *Biochim. Biophys. Acta* **768**, 29.
- [3] Grossman, A. R., Schaefer, M.R., Chiang, G. G. and Collier, J. L. (1993a) The phycobilisomes: A light harvesting complex responsive to environmental conditions. *Microbiol. Rev.* **57**: 725-749.
- [4] Zhao, F. and Qin, S. (2006) Evolutionary analysis of phycobiliproteins: Implications for their structural and functional relationships. *J. Mol. Evol.* **63**: 330-340.
- [5] Bryant, D. A., Grglielmi, G., Tandeau de Marsac, N., Castets, A.M. and Cohen-Bazire, G. (1979) The structure of cyanobacterial phycobilisomes: A Model. *Arch. Microbiol.* **123**: 113-127.
- [6] Gantt, E., Lipschutz, C.A Grabowski, J. and Zimmerman, B.K. (1979) Phycobilisomes from blue-green and red algae. Isolation criteria and dissociation characteristics. *Plant Physiol.* **63**: 615-620.
- [7] Bogorad, L. (1975) Phycobiliproteins and complementary chromatic adaptation. *Ann. Rev. Plant Physiol.* **26**: 369-401.
- [8] Tandeau, N. de Marsac and Cohen-Bazire, G. (1977) Molecular composition of cyanobacterial phycobilisomes. *Proc. Natl. Acad. Sci. U. S. A.* **74**: 1635-1639.
- [9] Bryant, D. A. (1982) Phycoerythrocyanin and Phycoerythrin: properties and occurrence in cyanobacteria. *J. Gen. Microbiol.* **128**: 835-844.
- [10] Murthy, S.D.S. (1991) Studies on bioenergetic processes of cyanobacteria: Analysis of the selected heavy metal ions on energy linked process. Ph. D thesis, Jawaharlal Nehru University, New Delhi.
- [11] Ranjani, R. (2002) Characterization of heavy metal ions induced damage in photochemical functions of the cyanobacteria. Ph. D thesis, Sri Venkateswara University, Tirupati.
- [12] Zarrouk, C. (1966) Contribution a l'etude d'une cyanophyce influence de diverse facteurs physiques et chimiques sur la croissance et la photosynthese de *Spirulina maxima*, (Setch et Gardner) Geitler, Ph.D. Thesis, University of Paris, Paris.

- [13] Gantt, E., Lipschutz, C. A., Grabowski, J. and Zimmerman, B.K. (1979) Phycobilisomes from blue-green and red algae. Isolation criteria and dissociation characteristics. *Plant Physiol.* **63**: 615-620.
- [14] Murthy, S.D.S., Sabat, S.C. and Mohanty, P. (1989) Mercury induced inhibition of photosystem II activity and changes in the emission of fluorescence from phycobilisome in intact cells of the cyanobacterium *Spirulina platensis*. *Plant Cell Physiol.* **30**: 1153-1157.
- [15] Fork, D.C. and Mohanty, P. (1986) Fluorescence and other characteristics of blue-green algae (Cyanobacteria), red algae and cryptomonads. In: *Light Emission by Plants and Bacteria* (Govindjee, Amsez, I. and Fork, D.C., eds.) pp. 451-496, Academic Press, New York.
- [16] Singhal, G. S. Mohanty, P. and Govindjee, (1981) Effect of preheating intact cells on pigments revealed by absorption and fluorescence spectra. *Z. Pflanzen-physiol.* **103**: 217-228.



## BIOTRANSFORMATION OF 11 $\beta$ , 17 $\alpha$ -DIHYDROXY-4-PREGNENE-3, 20-DIONE-21-O-SUCCINATE TO A 17-KETOSTEROID BY *PSEUDOMONAS PUTIDA* MTCC 1259 IN ABSENCE OF 9 $\alpha$ -HYDROXYLASE INHIBITORS

Rahul Patel\* and Kirti Pawar

Ashok and Rita Patel Institute of Integrated Study and Research in Biotechnology and Allied Sciences,  
New Vallbh Vidyanagar, Anand 388 121, Gujarat, India

### ABSTRACT

Growing cells of *Pseudomonas putida* MTCC 1259 were used for biotransformation of a steroid with cortical side chain, 11 $\beta$ ,17 $\alpha$ -dihydroxy-4-pregnene-3,20-dione-21-O-succinate. Separation of the steroidal components of fermentation extracts was done by TLC with an optimized solvent system. The precursor and different product steroids were found to separate satisfactorily in a 2:4 mixture of benzene:ethyl-acetate. A 17-ketosteroid was found to accumulate in the fermentation medium after 120 h incubation at 37 °C under aerobic incubation without addition of any ring cleavage inhibitors which suggested a desirably low 9 $\alpha$ -hydroxylase activity in the strain. The biotransformation product was characterized to be Adrost-4-ene-3,17-dione on the basis of FTIR spectroscopic analysis. The pathway of corticosteroid side chain cleavage by the organism was worked out. The absence of C-1(2)-dehydrogenated product in the fermentation broth indicated a low activity of C-1(2)-dehydrogenase enzyme in the strain. The strain is found suitable for production of 17-ketosteroids from precursors having cortical side chains.

**Key words :** steroid bioconversion; 17-ketosteroid production; 9 $\alpha$ -hydroxylase inhibitors; chromatographic separation of steroids

### INTRODUCTION:

Steroid modification or synthesis is one biotechnological process having potential applications in pharmaceutical industries due to the complex structure of steroid molecule and requirement of complicated, multi-step schemes for the chemical synthesis of steroid compounds. The basic ring structure of some steroid derivatives is sensitive to cleavage by a wide variety of chemicals. Chemical synthesis also requires the use of reagents such as pyridine, sulfur trioxide or selenium dioxide which are hazardous to the health of production staff and constitute a serious environmental disposal problem. There are plenty of steroid drugs available in market, and much research is on going to modify steroid drugs to more potent derivatives with longer half-lives in the blood stream, having simpler delivery methods, more specific and one having no or less side-effects. This can be achieved by microbial bioconversion [1].

Microbial cleavage of steroid side-chains has been an extensively researched subject because of the potential utility of this reaction for the production of high value therapeutic pharmaceuticals. Side-chain degradation has been studied by first blocking ring-degradation. It has been found in several studies using *Mycobacteria* that hydroxylation of the terminal carbons is the first step [2]. Wide varieties of fungi are capable of side-chain cleavage of progesterone [3]. During side-chain cleavage of progesterone, usually 17-acetate is formed by introduction of oxygen between C-17 and C-20 then an esterase cleaves the acetate leaving the 17-hydroxy steroid, testosterone. Then the 17-hydroxyl group is oxidized to 17-ketone, some of the organisms may form the 1-dehydrogenated derivatives. Adrost-4-ene-3,17-dione [AD], and Androsta-1,4-diene-3,17-dione [ADD] are among several important compounds obtained by degradation of steroid side-chain which may be useful for the production of androgens, estrogens and other compounds by further chemical modification. 1-dehydrotestolactone may also be produced which is approved for the treatment of mammary cancer. Androst-4-ene-3,17-dione can be chemically converted to spironolactone which is an important drug in the treatment of hypertension. Androst-4-ene-3,17-dione may also be chemically reduced to give testosterone and some derivatives that have important medicinal uses [3].

Pseudomonads are able to grow in different environments and have broad metabolic versatility and genetic plasticity. Also some important reactions for steroid bioconversion are reported with these groups of organisms. Screening of microorganisms able to grow on bile acids and in the presence of organic solvents

led to the isolation of *Pseudomonas putida* ST491 [1]. When grown in 5 g l<sup>-1</sup> lithocholic acid in the presence of diphenyl ether, 60% of the substrate was cleaved to AD (75% yield), with ADD (17% yield) and pregna-1,4-dien-3-on-20-al (8% yield) as secondary products. If the organic solvent was replaced by Triton X-100 in the aqueous conversion medium, 40% of the substrate was converted to ADD alone [1]. *Pseudomonas* mutant had converted compound-S directly to prednisolone, showing that organism is capable of 1-dehydrogenation along with 11 $\beta$ -hydroxylation [4]. According to one report, [5] 19-hydroxyandrostenedione was converted to estrone by a *Pseudomonas*. They proposed that the organism 1-dehydrogenated the steroid and then the hydroxymethyl group was removed by aldol cleavage.

The study was initiated with an aim to cleave side chain of a corticosteroid using *Pseudomonas putida* MTCC 1259 which was known to successfully degrade side chain of cholesterol [6]. Emphasis was to accumulate 17-ketosteroids without addition of inhibitors for enzymes responsible for cleavage of steroid ring system.

### MATERIALS AND METHODS:

**Materials:** The general chemicals and media components required for the study were purchased from Hi Media, Glaxo, Qualigens, Merck and S D fine Chemicals.

**Microorganisms:** The strain *Pseudomonas putida* MTCC 1259 was purchased from Microbial Type Culture Collection, Institute of Microbial Technology, Chandigarh, India. The strain was maintained on nutrient agar slants supplemented with appropriate inducer steroid (1 mg l<sup>-1</sup>) and stored in a refrigerator at 4 °C. The organisms were sub-cultured every month.

**Bioconversion of 11 $\beta$ ,17 $\alpha$ -dihydroxy-4-pregnene-3,20-dione-21-O-succinate by growing cells:** Medium containing g l<sup>-1</sup>, Beef Extract (1.5), Peptone (5), NaCl (5), Yeast Extract (1.5), Inducer steroid (1 mg l<sup>-1</sup>) was prepared and pH adjusted to 7. Medium (20 ml) was dispensed in series of 100 ml conical flasks and sterilized at 121 °C for 15 mins and allowed to cool to room temperature. Three flasks were inoculated with actively growing culture of *Pseudomonas putida* MTCC 1259 in the same medium. After overnight growth at 37 °C on a 110 rpm shaking platform, steroid substrate (4 mg) dissolved in 0.5 ml ethyl acetate (or as specified) was added in each flask. Sample (2 ml) was withdrawn every 24 hours and extracted twice with equal volume of ethyl acetate. The organic layers were decanted, pooled, dried over sodium sulphate and solvent evaporated by

\*Corresponding author : r.jpatel@rediffmail.com

keeping the tubes in boiling water bath and residual steroid re-dissolved in 0.1 ml ethyl acetate. Aliquots were taken for qualitative analysis by thin layer chromatography.

**Thin Layer Chromatography of steroids:** Method described by [7] was used for qualitative analysis of the bioconversion products. Slurry of silica gel (5%) was prepared in distilled water and allowed to swell for 5 min, layered on a clean glass plate and allowed to air dry. The plates were activated in a hot air oven at 110 °C for 30 mins and allowed to cool to room temperature. Extracted steroid samples were spotted along with the authentic precursor with the help of capillary tube. The plates were developed in a mobile phase having mixture of benzene: ethyl acetate optimized for better separation of steroid samples. The solvent was allowed to evaporate at 50 °C for 15 mins and plates were sprayed with 60% sulphuric acid for preparing steroid chromogens. The plates were heated in a hot air oven for 110 °C for 30 mins for visualization of chromogens.

**Identification of Steroids:** Identification of the steroids was done by comparing the color and Rf of the spots with the authentic samples. Confirmation of identification was done by FTIR spectroscopy. For isolation of steroids for IR spectroscopy, preparative TLC as described by [8] using the solvent system optimized for separation of the desired steroids. The separated steroids were visualized in a chamber of iodine vapors, positions of steroids marked; silica gel was scrapped from the marked area and extracted thrice with ethyl acetate. Ethyl acetate was recovered, steroid sample concentrated in a powder form, recrystallized from either methanol or acetone and submitted for FTIR analysis using **FTIR spectrometer, Perkin Elmer make, model Spectrum GX, wave number range:** 30-15600 cm<sup>-1</sup> suitable for liquid, solid and gas samples, operating mode NIR and MIR with NIR source optical system 15,200 – 1,200 cm<sup>-1</sup>, beam splitter KBr: 7,800 - 370 cm<sup>-1</sup> with optimum range: 7,800 - 1,200 cm<sup>-1</sup> and detector MIRTGS: 10,000 - 220 cm<sup>-1</sup>.

## RESULTS AND DISCUSSION:

Bioconversion products of 11 $\beta$ ,17 $\alpha$ -dihydroxy-4-pregnene-3,20-dione-21-O-succinate by *P. putida* MTCC 1259 have been shown in table 1. A prominent bluish green spot appeared on the TLC plate along with the precursor that showed

reddish brown spot. Product forming bluish green spot was supposed to be accumulating as intensity of the spot increased with increasing time of incubation.

Although it was possible to identify the product steroids from the precursor steroids using 5 : 1 benzene : ethyl acetate as a mobile phase, to obtain the individual compounds with highest purity using preparative TLC, it was necessary to attain maximum possible separation of product steroids. Hence, it was decided to optimize the mobile phase composition for 11 $\beta$ ,17 $\alpha$ -dihydroxy-4-pregnene-3,20-dione-21-O-succinate and its bioconversion products. During chromatographic separation of steroids choice of proper mobile phase and optimization of mobile phase are important as the product steroids are closely related compounds which makes their separation difficult. In first step 1 : 1 mixture of acetone : ethyl acetate and 5 : 1 mixture of benzene : ethyl acetate as a mobile phase solvent system was screened for separation of precursor steroid and its bioconversion product.

Although visualization of the product was possible, separation of the product from precursor was very low. So it was decided to optimize the composition of mobile phase for which, the ability of different composition of mobile phase (5 : 1, 4 : 2, 3 : 3, 2 : 4, 1 : 5 benzene : ethyl acetate) to separate precursor from product was checked by spotting steroids extracted from 2 ml bioconversion medium of *P. putida* MTCC 1259 along with authentic precursor.

**Table-1:** Bioconversion products of hydrocortisone succinate by *P. putida* MTCC 1259 as seen on TLC analysis

Time	192 hrs	240 hrs		336 hrs
Spot	Green	Green	Golden	Green
Rf	0.0967	0.0793	0.174	0.079
Spot intensity	+	+++	++	++++

+ Score of spot intensity

**Table 2:** Effect of mobile phase composition on Rf of bioconversion products of *P. putida* MTCC 1259 on TLC plate

Ratio of Benzene: Ethylacetate	Precursor (Spot 1)	Rf of Golden spot (Spot 2)	Rf of Green Spot (Spot 3)
5 : 1	At origin	0.1	0.079
4 : 2	At origin	0.36	0.45
3 : 3	At origin	0.36	0.72
2 : 4	At origin	0.45	0.87
1 : 5	At origin	0.63	0.90

It is clear from Table 2 that 2 : 4 mixture of benzene : ethyl acetate shows maximum separation of bioconversion products. It was also obvious that two major products were formed golden (spot-2) and Green (spot-3). Authentic precursor did not move past the origin in all the tested combinations of benzene and ethyl acetate. It was also observed that authentic hydrocortisone succinate was poorly soluble in ethyl acetate. Also, products solubility in ethyl acetate was higher than in benzene. Hence it was decided to use 2 : 4 benzene : ethyl acetate mixture as the developing solvent for TLC during future experiments.

Although product steroids can be identified by the color and Rf of the spot, FTIR spectra provides an important tool for further confirmation of this analysis. Figure 3 represents FTIR spectrum of authentic precursor used for bioconversion. Figure 4 and 5 depict the FTIR spectra of spot-2 (golden) and

spot-3 (green) respectively. Upon inspection of FTIR spectrum of spot-2, prominent peaks were observed at 1647 and 1711 cm<sup>-1</sup> indicating the presence of 3-keto group. Absence of peak at 1730-1750 cm<sup>-1</sup> suggests absence of 17-keto group. Broad absorptions in the range of 2800-3400 cm<sup>-1</sup> indicate presence of aliphatic stretch, indicating that the succinate side chain of the precursor has not been cleaved. Absorbance at 2850 and 2981 cm<sup>-1</sup> indicated the presence of methyl or methylene groups. The comparison of IR spectra of hydrocortisone succinate and spot-2 indicates only minor changes in the steroid ring (additional peak at 1711.23 cm<sup>-1</sup> in spot-2). Similar spectral analysis have been suggested while explaining 1,2-dehydrogenation of 17,21-dihydroxypregn-4-ene-3,20-dione. Their product showed had I.R. spectrum bands (KBr) at: 3400 cm<sup>-1</sup> (OH); 2958 cm<sup>-1</sup> (CH); 1718 cm<sup>-1</sup> (CO); 1666 cm<sup>-1</sup>, 1620 cm<sup>-1</sup>, 1607 cm<sup>-1</sup> ( $\Delta$ 1,4-3-one) indicating 1,2-dehydrogenation of hydrocortisone to prednisolone. As observed from the suggestions in the IR spectra

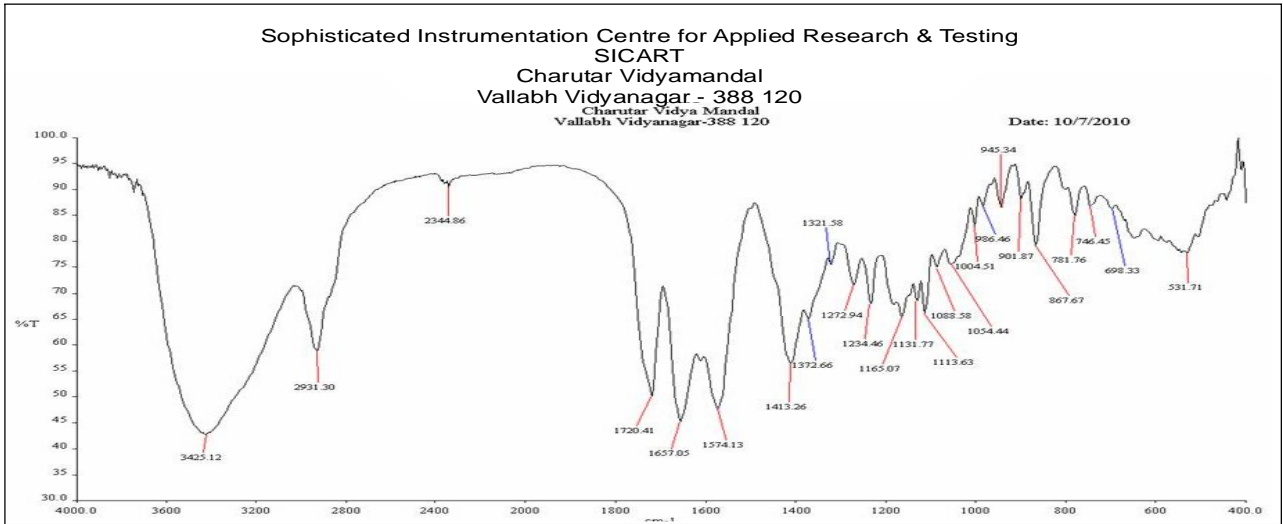


Figure-3 : FTIR spectra of Hydrocortisone succinate – sodium salt, copied from [11] with permission

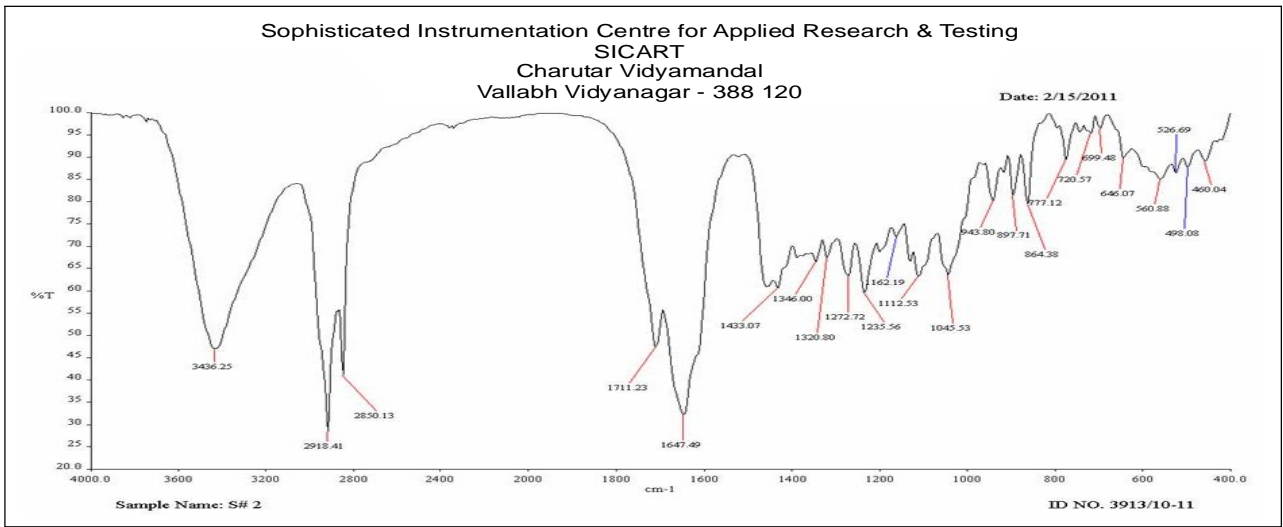


Figure-4: FTIR spectrum of bioconversion product of hydrocortisone succinate by *P. putida* MTCC 1259 (Golden spot or Spot-2)

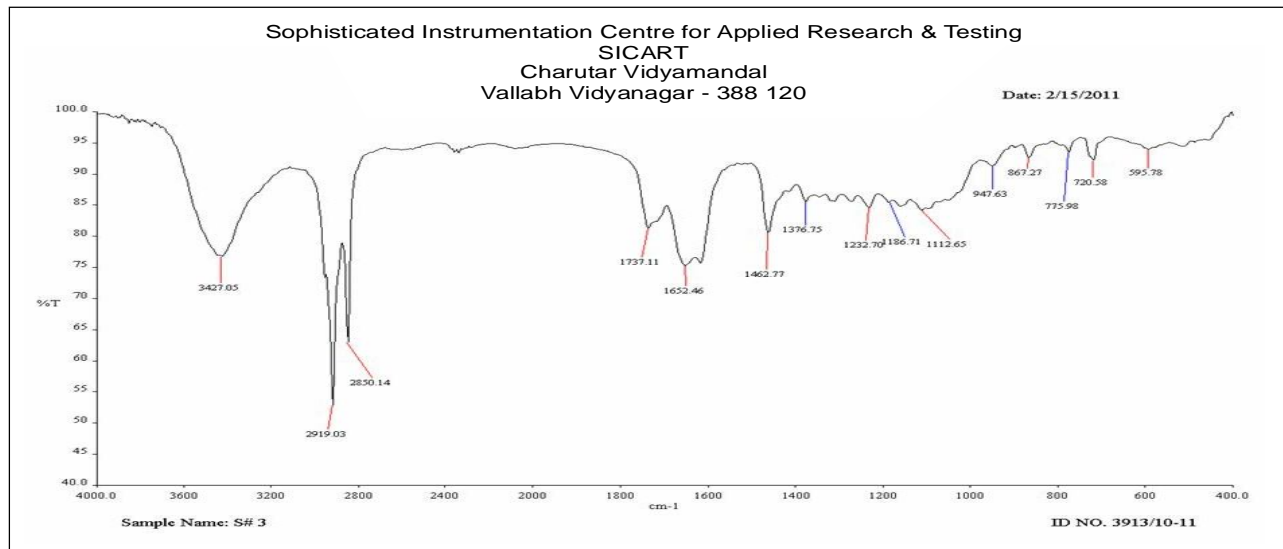
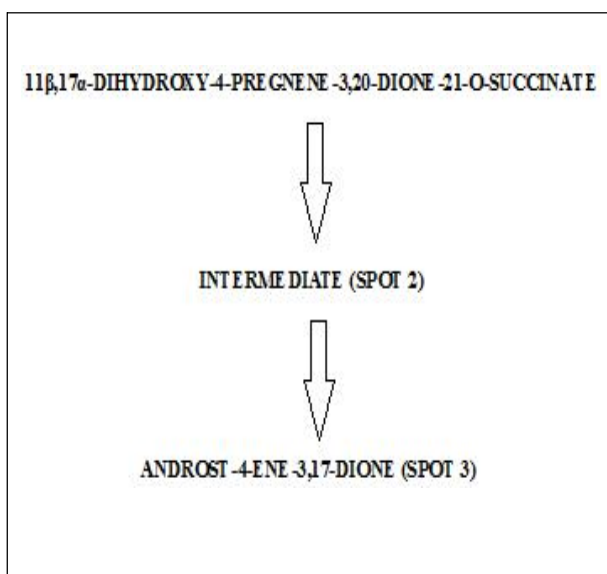


Figure-5: FTIR spectrum of bioconversion product of hydrocortisone succinate by *P. putida* MTCC 1259 (Greenspot or spot-3)

analysis by [9] where the C-H stretch of an aliphatic compound (or fragment) have been analysed. He observed the asymmetric C-H stretch of the methyl and methylene groups ( $2960$  and  $2930$   $\text{cm}^{-1}$ , respectively) occurring at slightly higher frequency than symmetric vibrations ( $2875$  and  $2855$   $\text{cm}^{-1}$ , respectively for methyl and methylene). He further suggested that most part, this simple rule holds true for most common sets of vibrations. Naturally there are always exceptions, and a breakdown of the rationale may occur when other effects come into play, such as induced electronic, spatial or entropy-related effects. The identification peaks suggested for prednisolone by [10] during bioconversion of hydrocortisone are IR  $\nu_{\text{max}}$  (KBr,  $\text{cm}^{-1}$ )  $3050$ ,  $2980$ ,  $1658$ ,  $1624$ ,  $1600$  supporting the inferences of the present investigation.

Whereas, observing the FTIR spectra of spot-3 a prominent peak at  $1737$   $\text{cm}^{-1}$  indicated the presence of 17- keto group, hence, side -chain of this product steroid had been cleaved. Absorbance at  $1652$   $\text{cm}^{-1}$  indicate the presence of 4-ene,3-one. Absence of prominent peaks in  $1600$   $\text{cm}^{-1}$  suggests absence of C1-2 double bond. Hence the compound may be Androst-4-ene-3,17-one. Presently it can be concluded that the side-chain of hydrocortisone succinate was successfully cleaved. The pathway for side chain cleavage of can be stated as:



#### ACKNOWLEDGEMENTS:

The authors thank Charutar Vidyamandal, Vallabh Vidya Nagar, Anand, Gujarat, India for extending all the facilities for successful completion of this work. The authors like to acknowledge Microbial Type Culture Collection, Institute of

Microbial Technolgy, Chandigarh, India for providing the strains used for the study and Sophisticated Instrumentation Centre for Applied Research and Training (SICART), Vallabh Vidya Nagar, Anand, Gujarat, India for the IR Spectral analysis of steroid samples.

#### REFERENCES:

- [1] Fernandes, P., Cruz, A., Angelova, B., Pinheiro, H. M. and Cabral J. M. S. (2003) Microbial conversion of steroid compounds: recent developments. *Enzyme and Microbial Technology*, **32**: 688–705.
- [2] Zaretskaya, I. I., Kogan, L. M., Tikhomirova, O. B., Sis, J. D., Wulfson, N. S., Zaretskii, V. I., Zaikin, V.G., Skryabin, G. K. and Torgov, I. V. (1968) Microbial hydroxylation of the cholesterol side chain. *Tetrahedron*, **24**: Issue 4: 1595-1600.
- [3] Miller, T. L. (1972) Steroid Fermentations. In *Comprehensive Biotechnology* (Murrey, M. and Young, E.), Pergamon Press, USA, Vol 4. pp. 297-316.
- [4] Takeda, R., I., Nakanishi, J. Terumichi, M. Uchida, M. Katsumata, M. Chibayahsi, and H. Nawa. (1959) Transformation of Reichstein's Substance S to prednisolone by *Pseudomonas*. *Tetrahedron Letters* No. 18:17-19.
- [5] Dodson, R. M., and R. D. Muir. 1961. Microbiological transformations. VI. The microbiological aromatization of steroids. *J. Amer. Chem. Soc.* **83**:4627-4631.
- [6] Pawar, K. and Bhatt, M. (2011) Accumulation of a Pharmacologically important 17-ketosteroid during Side Chain Cleavage of Cholesterol by *Pseudomonas putida* MTCC 1259. *World Journal of Science and Technology*, **1**: No 5: 62-65.
- [7] Shinde K (2000): Biotransformation of some steroid drug precursors to 17-ketosteroids by mixed bacterial culture. Ph. D Thesis, Devi Ahilya Vishwavidyalaya, Indore (MP) India.
- [8] Coates, J. (2000) Interpretation of Infrared Spectra: A practical approach. In *Encyclopedia of analytical chemistry* (Meyers, R. A., Meyers) John Wiley & Sons Ltd Press, USA, pp. 10815-10837.
- [9] Ghasemi, Y., Sara, R. A., Mohammad, H. M., Mohammad, J. R., Mohammad, B. G., Fatemeh, N., Narges, N., Rezvan, P., Seyed, B., Mosavi, A. and Shadman, S. (2008) Dehydrogenation, C-20 Ketone Reduction and Side-chain Cleavage of Hydrocortisone in *Chlamydomonas reinhardtii* Cultures. *Molecules*, **13**: 2416-2425.
- [10] Lad N. (2010) *Optimization of parameters for hydrocortisone succinate bioconversion*. M. Sc. Microbiology Dissertation thesis, Sardar Patel University, Vallabh Vidya Nagar, Anand, Gujarat, India.



## INFLUENCE OF NICKING IN COMBINATION WITH VARIOUS PLANT GROWTH SUBSTANCES ON SEED GERMINATION AND SEEDLING GROWTH OF NONI (*Morinda citrifolia* L.)

Karnam Jaya Chandra and Dasari Daniel Gnana Sagar<sup>1\*</sup>

Department of Biotechnology, Acharya Nagarjuna University, Nagarjunanagar -522510, A.P., India

<sup>1</sup> Department of Botany & Microbiology, Andhra Christian College, Guntur -522001, A. P., India

### ABSTRACT

A study was carried out to investigate the effect of various concentrations of plant growth substances in combination with nicking on the germination of Noni (*Morinda citrifolia* L.). Freshly extracted Noni seeds were nicked first and then treated with various concentrations (100-1000ppm) of Gibberellic acid, Indole-3-Butyric acid, Naphthalene-1-acetic acid, 6-Benzyl-amino-purine, Potassium nitrate, Kinetin and nicking along with control (seeds soaked in water) for a period of 24 hours. The highest germination percent, shoot length, root length, fresh and dry weights were recorded in seeds treated with Gibberellic acid at 800 ppm concentration (96.33%, 7.92 and 3.34cm, 1.408 and 0.076g); followed by Indole-3- Butyric acid (89.26%, 6.53 and 2.97cm, 1.312 and 0.068g); Naphthalene-1-acetic acid (73.61%, 5.36 and 2.84cm, 1.293 and 0.066g); 6-Benzyl-amino-purine (65.33%, 5.28 and 2.62cm, 1.255 and 0.061g); Potassium nitrate (55.86%, 3.92 and 2.14cm, 1.201 and 0.041g) and Kinetin (54.16%, 4.11 and 2.38cm, 1.221 and 0.043g) at 1000ppm concentration; followed by nicking alone (39.42%, 1.98 and 1.14cm, 1.050 and 0.015g). Whereas poor response was observed in control with low germination percent (34.28%), shoot length (1.72cm), root length (1.11cm), fresh weight (1.020g) and dry weight (0.011g).

**Key words:** plant growth substances, germination, *Morinda citrifolia* L.

### INTRODUCTION

*Morinda citrifolia* L. commonly known as Indian Noni, is one of the most significant sources of traditional medicine [1, 2]. *Morinda citrifolia* L. belongs to the family Rubiaceae [3]. Noni is also known as Indian mulberry. Various parts of the plant, including its leaves, fruit, bark and roots, have been used for over 2000 years to treat several diseases such as high blood pressure and diabetes, and to cure eye problems, skin wounds, throat problems, respiratory ailments, constipation, and stomach pains [4]. About 160 valuable phytochemicals have been identified in this plant, and the major compounds are polyphenols, organic acids and alkaloids [5].

Dormancy is a condition in which seeds do not germinate even when the environmental conditions (water, temperature and aeration) are permissive for germination [6, 7]. The Noni seeds have a problem of seed dormancy thus limiting its commercial cultivation. Noni seeds are buoyant and hydrophobic due to air chamber and durable, water repellent, fibrous seed coat. Noni is easy to propagate from seeds and the primary disadvantage of seed propagation is that without seed treatment and applied heat, uniformity of seed germination may be unreliable and seedling production may take 6-12 months for germination and 9-12 more months before they are ready to transplant.

Hence, untreated seeds need several months to a year for germination but their germination period can be reduced to a month using techniques such as trimming, heating or chemical scarification etc. Pre sowing chemical treatments have generally been used to enhance seed germination and seedling vigor. Various methods have been used by seed scientists and technologists to break seed dormancy. Stratification plays an important role as a stimulator that helps to break dormancy [7]. In order to accelerate this method, it can be combined with some treatments such as chemical applications or mechanical seed coat removal [8]. Many investigators have studied the effects of exogenous growth regulators on seed germination. Gibberellins are believed to be important in controlling the germination of seeds in nature [9].

Scarifying the hard seed coat by nicking or puncturing significantly reduces the germination time, improves germination percentage and promotes uniform sprouting. Scarifying can be done by blending machine, nail cutter etc. [10]. Hence, present research was carried to study the effect of various plant growth substances along with nicking to improve the germination percent in Noni seeds.

### MATERIALS & METHODS

The present investigation was conducted at Department of Biotechnology, Acharya Nagarjuna University, Guntur, Andhra Pradesh, India. Noni seeds were brought from Tirumala hills, lie between 79° 19' to 79° 23' East and 13° 37' to 13° to 43' both latitude in the Chittoor District of Andhra Pradesh, India. Fully ripened, soft and white colored Noni fruits were collected. The pulp of the Noni fruit was washed thoroughly with water to obtain Noni seeds. Noni seeds were dried under shade for 2 to 3 days. Seeds were stored in the airtight container at room temperature.

The shade dried Noni seeds were nicked using an ordinary fingernail clipper to create an opening in the tough seed coat, so that water and air may enter and contact the embryo. This clipping can increase the germination percent and also reduce the time required for germination from several months to only 4 weeks or more. The nicked seeds were treated with different concentrations (100-1000ppm) of Gibberellic acid (GA), Indole-3-Butyric acid (IBA), Naphthalene-1-Acetic acid (NAA), 6-Benzyl-amino-purine (BAP), Potassium nitrate (KNO<sub>3</sub>), Kinetin (KN) and nicking alone along with control (seeds soaked in water) for a period of 24 hours. Ten imbibed seeds were placed in petri dishes lined with two layers of Whatmann No.1 filter papers, moistened with sterile distilled water to provide humidity. Petri dishes were placed in an incubator at 25°C with 70-80% humidity. The number of seeds germinating everyday in each treatment was counted for calculating the final germination percent in each treatment and same temperature and humidity are maintained throughout the growth of the seedlings for a period of six weeks.

The fresh weight was calculated, root and the shoot length of the seedlings were measured using a transparent plastic ruler. The seedlings were placed in an oven at 80°C for 24 hours and dry weights were recorded.

\*Corresponding author: drddaniel@rediffmail.com

The experiment was conducted with eight treatments like Gibberellic acid (GA), Indole-3-Butyric acid (IBA), Naphthalene-1-Acetic acid (NAA), 6-Benzyl-amino-purine (BAP), Potassium nitrate (KNO<sub>3</sub>), Kinetin (KN) with various concentrations (100-1000ppm) and nicking alone along with control (seeds soaked in water) for a period of 24 hours in three replications in a completely randomized design (CRD). Data on germination percent (%); shoot length (cm); root length (cm); fresh weight (g) and dry weight (g) was collected and ANOVA was carried out using IRRISTAT software package.

## RESULTS AND DISCUSSION

### Seed germination (%)

The treatments differed significantly for the character studied. The data on the effect of various concentrations of growth substances on the nicked Noni seed germination are presented in Table - 1. At 800 ppm, Gibberellic acid was found to be significantly superior over other treatments and control for seed germination percent (96.33), followed by Indole-3-Butyric acid (89.26) and Naphthalene-1-Acetic acid (73.61) at 1000ppm concentration, whereas other growth hormones like 6-Benzyl-amino-purine (65.33), Potassium nitrate (55.86) and Kinetin (54.16) were significantly superior at 1000ppm concentration over nicking alone (39.42) and control treatment (34.28%).

### Shoot length and root length (cm)

The data on the effect of various concentrations of growth substances on the length of the shoot and root are presented in Table - 2. The hormone Gibberellic acid recorded maximum shoot length (7.92) and root length (3.34) at 800ppm concentration whereas Indole - 3- Butyric acid (6.53 and 2.97) and Naphthalene-1-Acetic acid (5.36 and 2.84), 6-Benzyl-amino-purine (5.28 and 2.62), Potassium nitrate (3.92 and 2.14) and Kinetin (4.11 and 2.38) were found to be significantly superior for root length and shoot length at 1000ppm concentration over nicking alone (1.98 and 1.14) and control (1.11 and 1.72). In general, it was observed that shoot length was more when compared to root length for all the treatments tested, might be due to application of hormones which had a physiological effect on plant growth.

### Fresh weight and dry weight (g)

The data on the effect of various concentrations of growth substances on the fresh and dry weights of nicked Noni seed are presented in Table - 3. Fresh weight and dry weight were found to be superior at 800ppm concentration when tested with Gibberellic acid (1.408 and 0.076) which was significantly superior over other treatments like Indole- 3-Butyric acid (1.312 and 0.068), Naphthalene-1-Acetic acid (1.293 and 0.066), 6-Benzyl-amino-purine (1.255 and 0.061), Potassium nitrate (1.201 and 0.041) and Kinetin (1.221 and 0.043) at 1000ppm concentration than

nicking alone (1.050 and 0.015). Control treatment recorded the least fresh weight and dry weights (1.02 and 0.011).

Seed dormancy and germination are complex traits of higher plants that are influenced by a large number of genetic and environmental factors. Present study on Noni seeds indicated that application of Gibberellic acid (GA) induced higher germination percent, shoot length and root length, fresh and dry weight when compared with soaking of seeds for 24 hours in Indole - 3- Butyric acid, Naphthalene-1-acetic acid, 6-Benzyl-amino-purine, Kinetin, Potassium nitrate, nicking alone and control treatments. From the above investigations it was observed that *Morinda citrifolia*. L. seed germination and other parameters studied were highest in 800 ppm concentration of Gibberellic acid (GA) along with nicking followed by Indole-3- Butyric acid (IBA), Naphthalene-1-acetic acid (NAA), 6-Benzyl-amino-purine(BAP), Kinetin and Potassium nitrate; this is due to the effect of Gibberellic acid on seed germination along with scarification or nicking. Kockemann [11] reported that growth substances serve to regulate the germination of seeds. These growth regulators when applied exogenously or naturally occurring exert either stimulatory or inhibitory effects under different conditions and concentrations either as germination stimulators or germination inhibitors. Davies [12] mentioned that Gibberellins (GA) is an essential phytohormone induces many aspects of plant development including seed germination. Pandey and Sinha [13] reported that GA induced the synthesis of  $\alpha$ -amylase and other hydrolytic enzymes during the early stages of seed germination. Similarly, Raliton [14] also found the accelerating effect of Gibberellic acid in seed germination of *Morus indica*.

**Table - 1** Effect of Gibberellic acid, Indole- 3- Butyric acid, Naphthalene-1- acetic acid, 6-Benzyl-amino-purine, Potassium nitrate, Kinetin and nicking on germination of Noni seeds.

Concentration (ppm)	Germination (%)					
	GA <sub>3</sub>	IBA	NAA	BAP	KNO <sub>3</sub>	KN
Control	34.28	34.28	34.28	34.28	34.28	34.28
Nicking alone	39.42	39.42	39.42	39.42	39.42	39.42
100	46.6	42.53	42	40.66	40.66	41.96
200	50.16	47.06	43.2	41.91	44.41	42.93
300	51.9	51.41	48.78	46	46.9	44.86
400	58.3	53	52.26	50.58	47.55	46.5
500	62.21	62.61	60.66	55.45	52.83	47.83
600	75.36	72.16	62.91	60.73	52.16	51.61
700	83	78.13	65.62	63.5	55.1	52.26
800	96.33	84.43	69.25	63.76	55.66	52.66
900	95.83	85.4	73.5	65.16	54.63	53.66
1000	94.5	89.26	73.61	65.33	55.86	54.16
Mean	68.05	63.67	56.92	53.40	49.10	47.52
CD (5%)	2.36	2.53	2.45	2.74	2.50	3.05
CV (%)	2.0	2.3	2.5	3.0	3.0	3.8

**Table - 2** Effect of Gibberellic acid, Indole - 3- Butyric acid, Naphthalene-1- acetic acid, 6-Benzyl-amino-purine, Potassium nitrate, Kinetin and nicking on shoot and root length of Noni seedlings.

Concentration (ppm)	GA <sub>3</sub>		IBA		NAA		BAP		KNO <sub>3</sub>		KN	
	SL(cm)	RL (cm)	SL (cm)	RL (cm)	SL (cm)	RL (cm)						
Control	1.72	1.11	1.72	1.11	1.72	1.11	1.72	1.11	1.72	1.11	1.72	1.11
Nicking alone	1.98	1.14	1.98	1.14	1.98	1.14	1.98	1.14	1.98	1.14	1.98	1.14
100	4.11	1.72	3.41	1.45	2.13	1.47	2.25	1.35	1.88	1.15	1.96	1.14
200	4.20	1.73	3.92	1.52	2.52	1.51	2.52	1.61	1.92	1.33	2.07	1.22
300	4.42	1.83	4.06	1.75	2.81	1.84	2.91	1.85	2.12	1.46	2.14	1.35
400	4.86	2.04	4.31	2.11	3.42	1.91	3.32	2.02	2.53	1.65	2.41	1.57
500	5.15	2.14	5.02	2.33	3.86	2.01	3.42	2.07	2.61	1.61	2.64	1.71
600	5.23	2.21	5.21	2.42	4.15	2.21	4.11	2.15	2.82	1.71	2.80	1.85
700	5.58	2.37	5.36	2.51	4.33	2.36	4.33	2.21	3.06	1.75	3.06	1.92
800	7.92	3.24	5.71	2.56	4.36	2.42	4.48	2.45	3.54	1.86	3.53	2.03
900	7.42	3.31	5.82	2.61	4.61	2.51	4.71	2.58	3.63	1.91	3.60	2.04
1000	7.32	3.34	6.53	2.97	5.36	2.84	5.28	2.62	3.92	2.14	4.11	2.38
Mean	5.27	2.28	4.64	2.12	3.57	2.02	3.55	2.00	2.71	1.61	2.73	1.67
CD (5%)	0.02	0.02	0.02	0.02	0.02	0.02	0.02	0.02	0.02	0.02	0.01	0.02
CV (%)	0.2	0.5	0.3	0.6	0.3	0.5	0.3	0.7	0.5	0.7	0.3	0.7

**Table - 3** Effect of Gibberellic acid, Indole-3-Butyric acid, Naphthalene-1-acetic acid, 6-Benzyl-amino-purine, Potassium nitrate, Kinetin and nicking on fresh and dry weight of Noni seeds.

Concentration (ppm)	GA <sub>3</sub>		IBA		NAA		BAP		KNO <sub>3</sub>		KN	
	FW (g)	DW (g)	FW (g)	DW (g)	FW (g)	DW (g)	FW (g)	DW (g)	FW (g)	DW (g)	FW (g)	DW (g)
Control	1.020	0.011	1.020	0.011	1.020	0.011	1.020	0.011	1.020	0.011	1.020	0.011
Nicking alone	1.050	0.015	1.050	0.015	1.050	0.015	1.050	0.015	1.050	0.015	1.050	0.015
100	1.239	0.036	1.146	0.024	1.099	0.035	1.121	0.031	1.051	0.011	1.107	0.011
200	1.244	0.039	1.151	0.025	1.149	0.040	1.131	0.033	1.099	0.014	1.116	0.015
300	1.289	0.045	1.159	0.028	1.201	0.042	1.141	0.035	1.107	0.015	1.151	0.015
400	1.319	0.049	1.171	0.031	1.210	0.045	1.181	0.036	1.131	0.018	1.181	0.019
500	1.322	0.058	1.181	0.035	1.234	0.050	1.189	0.041	1.139	0.020	1.189	0.020
600	1.325	0.064	1.188	0.038	1.238	0.051	1.196	0.043	1.156	0.023	1.196	0.024
700	1.351	0.066	1.201	0.041	1.259	0.055	1.201	0.049	1.160	0.025	1.199	0.034
800	1.406	0.074	1.241	0.045	1.262	0.058	1.206	0.053	1.181	0.028	1.206	0.038
900	1.407	0.075	1.291	0.047	1.271	0.059	1.221	0.056	1.191	0.038	1.211	0.040
1000	1.408	0.076	1.312	0.068	1.293	0.066	1.255	0.061	1.201	0.041	1.221	0.043
Mean	1.303	0.034	1.187	0.036	1.203	0.047	1.169	0.041	1.131	0.022	1.163	0.025
CD (5%)	0.014	0.002	0.013	0.02	0.014	0.002	0.014	0.02	0.014	0.002	0.013	0.002
CV (%)	0.6	1.9	0.7	2.7	0.7	2.0	0.7	2.5	0.7	4.6	0.7	4.0

Nelson [10] reported that nicking helps the seed to imbibe, causing seed coat to rupture hence, increases the seed germination rate uniformly and similarly Gibberellic acid (GA) enhances the shoot and root length simultaneously which was found comparable with the other treatments. These results were similar to the results of Singh *et al.* [15] which revealed that Noni seeds treated with GA significantly increased the height of seedling and number of leaves per seedling. Similar studies by Ponnaiyan and Vezhavendan [16] reported that hulling of seed coat or scarification of tough seed coat of Noni seeds reduce the time required for germination. The germination percent shoot length, root length, fresh and dry weight of the seeds treated with Indole-3-Butyric acid (IBA) and other plant growth substances like NAA, BAP, KN and KNO<sub>3</sub> were low when compared to Gibberellic acid treatment. This might be due to the seeds not withstanding more concentrations. Potassium nitrate is most widely used chemical for promoting seed germination. It acts synergistically with Gibberellic acid in inducing germination in tobacco seeds. However, the actual role of potassium nitrate in inducing the germination rate is not clearly known [7], potassium nitrate was found to be effective in breaking seed dormancy of many species [17]. Studies have revealed that seed dormancy and germination are under hormonal control [18, 19].

As a conclusion, the methods used in this study are practical and easily applicable for experimental studies and in the field conditions for rapid germination of Noni seeds and are useful in commercial rapid seedling production in large scale which would be essential for anti-desertification.

## REFERENCES

- [1] McClatchey, W. (2002) From Polynesian Healers to Health Food Stores: Changing Perspectives of *Morinda citrifolia* (Rubiaceae). *Integrative Cancer Therapies*, **1(2)**: 110-120.
- [2] Nelson, S. C. (2001) Noni cultivation in Hawaii. Univ. of Hawaii CTAHR- Cooperative Extension Service PD-19.
- [3] Mortan, J. F. (1992) The Ocean-Going Noni, or Indian Mulberry (*Morinda citrifolia*, Rubiaceae) and some of its "colorful" Relatives. *Economic Botany*, New York; **46(3)**: 241-256.
- [4] Wang, M. Y. and West, B. J. (2002) *Morinda citrifolia* (Noni): A literature review and recent advances in Noni Research. *Acta Pharmacologica Sineca*. **23(12)**:1127-114.
- [5] Wang, M.Y. and Su, C. (2001) Cancer preventative effect of *Morinda citrifolia* (Noni). *Annals of the New York Academy of Science*. **952**: 161-168.
- [6] Bewley, J. D. and Black, M. (1994) *Seeds. Physiology of development and germination*. Second Edition New York, Plenum Press.
- [7] Hartmann, H. T., Kester, D. E., Davies, F. jr. and Geneve, R. L. (1997) *Plant propagation principles and practices*. Sixth Edition. New Jersey, Prentice Hall.
- [8] Martinez- Gomez P. and Dicenta, F. (2001) Mechanisms of dormancy in seeds of peach (*Prunus persica* L. Batsch) cv. GF 305. *Scientia Horticulturae*, **91**: 51-58.
- [9] Lawrence. O. Copeland and Miller. B. Mc Donald (2004) *Principles of seed science and technology*. Second Edition. Kluwer Academic Publishers. pp: 107-108.
- [10] Nelson, S. C. 92006) *Morinda citrifolia* (noni), ver. 4. In: Elevitch, C. R. (ed.). Species Profiles for Pacific Island Agroforestry. Permanent Agriculture Resources (PAR), Hōlualoa, Hawai'i. <http://www.traditionaltree.org>.
- [11] Kockemann, A. (1934) Über eine keimungshemmenede substanz in frleischigen fruchten. Ber dtsn. Botany Ges., **52**: 523-526
- [12] Davies, P. J. (1995) *Plant Hormones: Physiology, Biochemistry and Molecular Biology*. (Dordrecht, The Netherlands: Kluwer Academic publishers).
- [13] Pandey, S. N. and Sinha, B. K. (2001) *Plant Physiology*, Third Edition, Vikas Publishing House Pvt. Ltd, New Delhi. 582.
- [14] Raliton, I. D. (1982) Gibberellin metabolism in plants, *Cell Biology, International Reports* **6**: 319-337.
- [15] Singh, D. R and Rai, R. B. (2005) Influence of Gibberellic acid on seed germination in Noni (*Morinda citrifolia* Linn.) of Andaman's *International. J Noni Res.*, **1**: pp. 31-35.
- [16] Ponnaiyan and Vezhavendan (2005) The effect of growth regulators and its combination with nicking on the germination of Indian mulberry (*Morinda citrifolia*. L.) *Intl. J. Noni Res* **1**: pp.23-26.
- [17] Agrawal P. K., Dadlani M., (1995) *Techniques in seed science and technology*. Second Edition. South Asian Publishers. New Delhi.
- [18] Frankland, B., (1961) Effect of gibberellic acid, kinetin and other substances on seed dormancy. *Nature*, **192**: 678-679.
- [19] Paleg, L. G., B. G. Coombe and M. S. Buttrrose (1962) Physiological effects of gibberellic acid. V. Endosperm responses of barley, wheat and oats. *Plant physiol.*, **37**: 798-803.



## QUANTITATIVE ANALYSIS OF AQUATIC MACROPHYTES IN CERTAIN WETLANDS OF KACHCHH DISTRICT, GUJARAT

J.P. Shah\*, Y.B. Dabgar<sup>1</sup> and B.K. Jain<sup>2</sup>

Gujarat Institute of Desert Ecology (GUIDE), PO Box 83, Opp. Changleshwar Temple, Mundra Road, Bhuj, Kachchh- 370001, Gujarat, India

<sup>1</sup>R.R. Mehta College of Science and C. L. Parikh College of Commerce, Palanpur, Banaskantha-385001, Gujarat, India

<sup>2</sup>Botany Department, M. G. Science Institute, Ahmedabad-380009, Gujarat, India

### ABSTRACT

A study was conducted for the aquatic macrophytes and its ecological attributes of the Kachchh district of Gujarat. In Kachchh many natural and manmade seasonal wetlands are present which serve as important gateways for the migratory waterfowl. In the present study six wetlands viz. Godhatad dam, Luna dhandh, Chhari dhandh, Pragsar lake, Changadasar talav and Jakhau intertidal were studied for western Kachchh district during 2007- 2009. The number of quadrates sampled varied according to the extent of area under vegetation cover and the size of wetlands. A number of sample plots were collected then analyzed in a nested sampling quadrat. Fifty seven different species of Aquatic macrophytes were recorded from the studied wetlands, which have included one free floating, one rooted floating, six submerge and 47 emergent species. Significantly 11 aquatic macrophyte species have been found to occur throughout the year, while other species recorded in a gap of 5 to 6 months. *Cynodon dactylon*, *Cyperus sp.* and *Creesa cretica* showed wider distribution in Kachchh wetlands. Some ecological parameters such as Species richness, Dominance, Diversity and Evenness status have been discussed in this paper.

**Key words :** wetlands, Kachchh, aquatic macrophytes

### INTRODUCTION

Wetland is the area covered by shallow water. These shallow areas are transitional zones between land and water. Vegetation studies - specific to wetlands of Gujarat are limited. The importance of aquatic macrophytes to the functioning of fresh water ecosystems has been under scored during the last few decades [1, 2, 3] because they harbor high biodiversity and influence biomass production, nutrient cycling and community dynamics [4]. Aquatic plants are key components for the well functioning of wetland ecosystem for biological productivity and support diverse organisms and there by provide lots of goods and services for the dependent people.

The western most part of the Gujarat state is recognized as the gateway of migratory waterfowl that come into the sub-continent. In spite of being arid, Kachchh district covers maximum area under wetlands.

Based on the distribution, the wetlands of Kachchh can be divided into three major types; the central inland wetlands (man-made), coastal wetlands in the southern and western region and saline wetlands (Ranns and Banni) in the northern limit. These are highly dependent on the village tanks and storage reservoirs. Kachchh being an arid area, the vegetation there is already faced with extremes of climatic and edaphic condition and it is more important to know the existing aquatic plants. In the absence of information on wetland vegetation for Kachchh region, an attempt was made to understand the baseline status of vegetation in and around the six selected wetlands. All these selected wetlands cover major types of wetland distribution in Kachchh. Information on aquatic macrophytes in any waterbody is of immense importance to understand the wetland ecosystem.

\*Corresponding author: Jhshpd@gmail.com

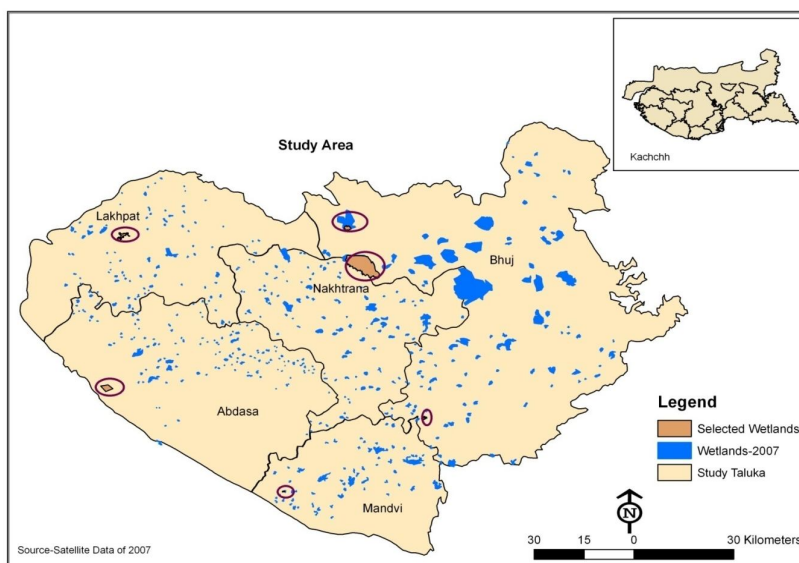


Fig. 1 Different wetlands of western Kachchh.

### Study area

Kachchh is the second largest district in the country, covering a total area of 45,652 km<sup>2</sup> and located in the north-western region of Gujarat state. Due to its unique ecological settings and geographical situation, Kachchh is classified under biotic province "3 A" (Kachchh desert) of bio-geographic zone of Indian Desert of the country [5] experiencing tropical arid climate. Most of the wetlands in arid and semi arid regions are man-made, and other natural wetlands are highly seasonal; however, they play vital role in the arid ecosystem. In some wetlands herbaceous vegetation and in certain cases, trees constitute essential grazing resources for stock farming. Since arid and semi-arid regions receive very low and erratic rainfall and experience frequent drought, livestock farming is the

predominant source of their economy. During drought period, most of the wetlands act as the natural fodder bank. This situation is true in Kachchh and especially in Banni.

Present intensive study of six wetlands Viz. Chhari Dhandh (CD), Luna Dhandh (LD), Changadasar Talav (CT), Godhatad Dam (GD), Pragsar Lake (PL) and Jakhau Intertidal (JI) (Fig. 1) was carried out in the western part of Kachchh district.

**MATERIALS AND METHODS**

Seasonal survey was done by quadrat method [6, 7] for collecting aquatic macrophytes from January 2007 to January 2009.

Plants were collected from the study area, during different seasons of the year i.e., in winter, summer and monsoon. Plant species were identified from the flora of Gujarat state [8]. The quadrat sampling method is the most popular method for ecological research and wetland delineation purposes.

The number of quadrates sampled varied according to the extent of area under vegetation cover and the size of wetlands. GPS readings were taken in each

quadrat. The number of quadrat studied were 15-20 in larger wetland, 12-15 in medium and 8-10 in small wetlands. In addition, number of sample plots also varied depending on the topography, terrain and accessibility conditions.

Status of vegetation was assessed using analysis. Species richness was obtained by enumerating the total number of species and diversity status of the aquatic macrophytes was studied using Shannon-Weiner Diversity Index and Evenness analysis was studied through statistical analysis [9, 10, 11] and "Past" software package [12].

**Shannon-Weiner Diversity Index** is calculated by using following formula.

$$\sum p_i (\log p_i) = H'$$

where  $p_i = \frac{\text{Total number of individuals of the species}}{\text{Total number of individuals of all the species}}$

**Species evenness** is calculated by using following formula.

$$J' = \frac{H'}{H'_{\max}}$$

Where  $H'$  is the number derived from the **Shannon diversity index** and  $H'_{\max}$  is the maximum value of  $H'$ , equal to:

$$H_{\max} = - \sum_{i=1}^S \frac{1}{S} \ln \frac{1}{S} = \ln S.$$

**Simpson's dominance index** is calculated by using following formula.

$$c = \sum_{i=1}^S \left( \frac{n_i}{N} \right)^2$$

Where  $n_i$  = number of individuals in the species  
 N = total number of individuals  
 S = total number of species

**Table - 1** Detail of sample plots in and around wetlands.

Name of Wetlands	Area in Ha	Total no. of Plots/ Points
Chhari Dhandh (CD)	3670.53	70
Luna Dhandh (LD)	184.87	50
Changadasar Talav (CT)	14.07	48
Godhatad Dam (GD)	217.51	65
Pragsar Lake (PL)	79.68	55
Jakhau intertidal (JI)	Open Coast	60
<b>Total</b>		<b>348</b>

**Table - 2** Wetland wise statistical analysis of the aquatic macrophytes.

Name of Wetland	Macrophytes species richness reported in wetlands	Dominance_D	Shannon_H	Evenness_e^H/S
Chhari Dhandh (CD)	8	0.20	1.69	0.67
Luna Dhandh (LD)	23	0.13	2.39	0.47
Changadasar Talav (CT)	21	0.09	2.55	0.61
Godhatad Dam (GD)	21	0.14	2.21	0.43
Pragsar Lake (PL)	26	0.16	2.30	0.38
Jakhau Intertidal (JI)	10	0.53	1.01	0.27

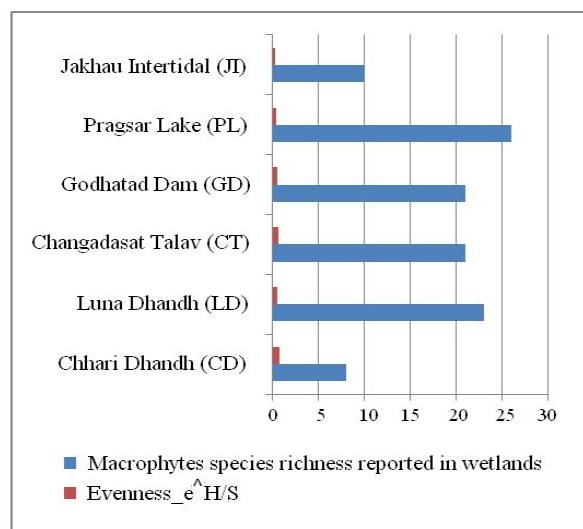


**Fig. 2** Wetland wise bar chart for evenness.

**RESULTS AND DISCUSSION**

Totally 348 quadrates were laid in and around the wetlands to record the macrophyte species. Out of 348 transect sampled, highest 70 transects were laid in Chhari Dhandh (CD) followed by 65 in Godhatad Dam (GD) and 48 in Changadasar Talav (CT) (Table - 1).

During the present study, overall 57 macrophyte species were recorded from various wetlands. Out of which 7 submerged species belonged to 7 genera and 6 families, 47 emergent species belonged to 39 genera and 22 families and one species from each rooted floating and floating pteridophytes. All the 57 Aquatic macrophyte species composition and seasonal distribution were prepared based on survey data. Out of that, only 11 species were found throughout the year.

Being mostly seasonal and dynamic, the wetland system of the Kachchh supports three major/dominant types of aquatic vegetation communities, namely 1) Submerged macrophytes such as *Hydrilla verticillata*, *Vallisneria spiralis* and *Eleocharis dulcis*, 2) Floating vegetation such as *Nymphaea sp.* observed only in two wetlands and 3) Emergent vegetation such as *Cyperus sp.* and *Cynodon dactylon*.

Aquatic macrophytes species richness was 26 in Pragsar Lake which is followed by 23 in Luna Dhandh. Changadasar Talav and Godhatad Dam showed species richness 21. The lowest species richness i.e. 8 was recorded in Chhari Dhandh. Changadasar Talav revealed highest value of Shannon-Weinner diversity index (Table - 2) which is followed by Luna Dhandh and Pragsar Lake where the diversity values were 2.39 and 2.30 respectively.

Godhatad Dam and Chhari Dhandh showed diversity index value was 2.21 and 1.69 respectively. Low diversity was recorded in Jakhau intertidal area, because of it's a coastal wetland and in fringes of coast lesser plantation. Higher species dominance was reported from Jakhau intertidal area (0.53) and lower from Changadasar Talav (0.09). Highest Evenness (0.67) was reported in Chhari Dhandh and lowest (0.27) in Jakhau Intertidal area (Table - 2).

In the present paper dominance is used to compare the same species in different wetland habitats.

Species diversity varies greatly through space and time in a given habitat and ecosystem [13]. In the present study diversity among the six wetlands the Changadasar Talav had 21 species with high diversity value of H<sup>2</sup>.55 and low dominance value 0.09 which indicates the many (6) species present with less than 20 individuals.

Due to the presence of high number of *Avicennia marina* dominance index was very high (0.53) with less evenness (0.20) in Jakhau intertidal wetland. Chhari Dhandh supported only 8 species where the diversity index was 1.69 but it has high evenness, *Cressa cretica* L. and *Cyperus exaltatus* Retz. var. *exaltatus* are the dominant species (Fig.2). Species evenness index from Luna Dhandh, Godhatad Dam and Pragsar Lake are almost similar, however, there were species representing and distributing with equal numbers.

## SUMMARY AND CONCLUSION

Out of 57 aquatic macrophytes observed in selected wetlands, 10 species were most common in study area occurred in 1 to 348 plots. *Ammannia baccifera*, *Cynodon dactylon*, *Cyperus rotundus*, *Phyla nodiflora* and *Vallisneria spiralis* were commonly observed as aquatic macrophytes in Kachchh wetlands. The outcome of the present study notes the association of rooted submerged species such as *Najas* sp. with water depth and its certain qualities. *Najas* sp. is found in association with deeper and clearer water. Emergent species grow as the periphery of the wetland gets dry. The *Typha* sp. was occurring at moderate or intermediate water depth. Submerged species like *Potamogeton* sp. were also commonly present where water depth is lower or shallow.

In the context of coastal wetlands, salt works, ports and jetty construction pose major threat to mangroves. Emergent vegetation can be useful for livestock, fishes, birds, reptiles, wild life and local people, shoreline vegetation is also important for smaller size class Crocodiles cover and food. For the inland water bodies, controlling and removing *Prosopis* would be an important task for wetland management.

This result shows that smallest wetlands in this study were habitat for infrequent species. Conserving only larger wetlands will not be sufficient to protect plant species richness.

## ACKNOWLEDGEMENT

Dr. Jagruti Shah is thankful to Dr. V. Vijaykumar, Deputy Director, GUIDE, Bhuj for providing necessary facility. The author wish to acknowledge the constant encouragement and useful suggestions is provided by senior scientist Dr. S.F. Wesley Sunderraj of Gujarat Institute of Desert Ecology, Bhuj.

## REFERENCES

- [1] Cyr, H. and Downing, J. A. (1988) Empirical relationships of photo faunal abundance to plant biomass and macrophyte bed characteristics. *Can. J. of Fish. And Aq.Sci.* **45**: 976-984.
- [2] Denny, P. (1985) The Ecology and Management of African wetland vegetation. (ed. W.Junk Publishers) 1The Hague.
- [3] Randall, R.G., Minns C. K., Cairns V. W. and Moore J. E. (1996) The relationship between an index of fish production and submerged macrophytes and other habitat features at three littoral areas in the Great Lakes. *Can. J. of Fish. and Aq. Sci.* **53**: 35-44.
- [4] Kateyo, E.M. (2007) Biodiversity of an interface zone of a nutrient-deficient lake (Nabugabo) in Uganda: macrophytes, *Afri. J. of Ecol.* **45**(2): 130-134.
- [5] Rodgers, W. A. and Panwar H. S. (1988) Planning Wildlife protected area network in India. Wildlife Institute of India, Dehra Dun. pp. 44.
- [6] Mueller-Dombois, D. and Ellensberg, H. (1967) Aims and Methods of Vegetation Ecology. (ed. Wiley), New York.
- [7] Kershaw, A. S. and Wright, C. E. (1980) Sampling test of Comparison and application of quadrat measures In: *Quantitative and Dynamic Plant Ecology*. Second edition. William Clowes and Sons Limited, London. pp: 21-39.
- [8] Hammer, Ø.; Harper, D.A.T. and Ryan, P.D. (2001) PAST: Paleontological Statistics Software Package for Education and Data Analysis. *Palaeontologia Electronica* **4**(1): 9pp. [http://palaeo-electronica.org/2001\\_1/past/issue1\\_01.htm](http://palaeo-electronica.org/2001_1/past/issue1_01.htm)
- [9] Hosmani, S. P. (2006) Trophic State Index (TSI) in conservation of Lake Ecosystems from [http://wgbis.ces.iisc.ernet.in/energy/lake2006/programme/programme/proceedings/Presentations/Lake\\_2006\\_-\\_Presentations/29\\_Dec\\_2006/Session\\_VI/Hosmani/TSI\\_IISc](http://wgbis.ces.iisc.ernet.in/energy/lake2006/programme/programme/proceedings/Presentations/Lake_2006_-_Presentations/29_Dec_2006/Session_VI/Hosmani/TSI_IISc).
- [10] Robin, L. M. and David J. C. (2001) The diversity – disturbance relationship is it generally storing and peacked? *Ecology* pp. 3479-3492.



## SCREENING OF CRUDE ROOT EXTRACTS OF SOME INDIAN PLANTS FOR THEIR ANTIBACTERIAL ACTIVITY

Purvesh B. Bharvad, Ashish R. Nayak, Naynika K. Patel and J.S.S. Mohan\*

Department of Biosciences, Sardar Patel University, Vallabh Vidyanagar - 388120, Gujarat, India

### ABSTRACT

The hexane, ethyl acetate, methanol and distilled water root extracts of twenty one plants were screened for their potential antibacterial activity against six gram positive and six gram negative bacterial strains using agar well diffusion method. The minimum inhibitory concentration (MIC) values were evaluated by serial broth dilution method for the plant extracts showing more than 7 mm zone of inhibition. Root extracts were prepared by infusion extraction method using solvents. The hexane and methanolic root extracts inhibited by 33.33% and 38.09% against *Staphylococcus epidermidis* respectively, where as methanolic root extract inhibited by 57.14% against *Micrococcus luteus*. Least to no activity was found in distilled water extracts of all plants. The MIC values were observed in the range of >8 mg/ml to 0.25 mg/ml for the tested plant extracts. This study revealed that plant extracts have greater potential as antimicrobial compound/s against microorganisms and may be used in the treatment of diseases.

**Key words :** Indian medicinal plants, antimicrobial activity, crude root extracts, MIC value

### INTRODUCTION

Medicinal plants are a source of great economic value in the Indian subcontinent. Nature has bestowed on us a very rich botanical wealth and a large number of diverse types of plant grow in different parts of the country. In India, thousands of species are known to have medicinal value to cure specific ailments since ancient times. Many works aimed to know the efficacy of different antimicrobial and phytochemical constituents of medicinal plants as possible alternatives to chemical synthetic drugs to which many infectious microorganisms have become resistant. In recent years, antimicrobial properties of Indian medicinal plants have been reported [1]. Incidents of epidemic due to drug resistant microorganisms are now a common global problem posing enormous public health concerns [2]. There has been an increasing incidence of multiple resistances in human pathogenic microorganisms in recent years, largely due to indiscriminate use of commercial antimicrobial drugs commonly employed in the treatment of infectious diseases.

Plants have been known to synthesize a variety of chemical substances, such as phenolic compounds, terpenes, steroids, alkaloids, glycosides, fats and others. However these have been found to have profound effects on chemical systems with therapeutic properties. Over 50% of all modern clinical drugs are of natural products origin and play an important role in drug development in the pharmaceutical industry. Indian medicinal plants are regularly used in various system of medicine because of minimal side effect and cost effectiveness [3].

However, a majority of traditionally used medicinal plants have not yet been systematically screened against various microbial pathogens [4]. In the last few years, a number of studies have been conducted by researchers to prove efficacy of 23 medicinal plant species against four bacteria [5], *Ceiba pentandra* and *Loranthus bengwensis* [6], *Prosopis africana* [7], *Callistemon citrinus*, *Cymbopogon citratus* and *Albizia lebbek* [8]. At present, a majority of botanical drugs under development are derived from ethanobotanical sources and traditional medicinal uses to combat the treatment paused by the microorganisms, which became resistance to antimicrobial agents. In this context, the present investigation is aimed to screen crude root extracts of 21 medicinal plants belonging to 16 different families against six gram positive and six gram negative bacteria for antibacterial activity.

\*Corresponding author: jssmohan@hotmail.com

### MATERIALS AND METHODS

#### Plant materials

Roots of twenty-one plant species belonging to 16 families were collected from different areas of Anand and Vallabh Vidyanagar (Table - 1). All the specimens were identified by referring "Flora of Gujarat state" [9] and with the help of Dr. A. S. Reddy, Plant Taxonomist, Department of Biosciences, Sardar Patel University, Vallabh Vidyanagar, Anand, Gujarat.

#### Preparation of extract

Collected roots were washed thoroughly with running tap water and dried at room temperature and powdered with grinder mixer. Extracts were prepared by sequential extraction method described by Houghton and Raman [10]. In this method, 100 gm of dry powdered material of each sample was soaked in 500 ml hexane for 24 hours at room temperature and shaken occasionally. Extracts were filtered by Whatman filter paper no.1 and filtrates were centrifuged at 3000 rpm for 10 minutes to remove any solid debris. The supernatant was collected and concentrated by solvent recovering assembly and dried completely at room temperature. The residue was dried and resuspended in to each of 500 ml ethyl acetate, methanol and distilled water sequentially for 24 hours at room temperature. The extract was filtered and filtrate was centrifuged at 3000 rpm for 10 minutes and the supernatants were collected and dried. All the fractions were stored in a refrigerator until further use.

#### Selected microorganisms

In this study, the six Gram-positive bacteria i.e. *Bacillus cereus* (ATCC 11778), *Bacillus subtilis* (ATCC 6051), *Staphylococcus aureus* (isolated), *Staphylococcus epidermidis* (ATCC 155), *Micrococcus luteus* (ATCC 4698), *Enterococcus faecalis* (isolated) and six Gram-negative bacteria i.e. *Escherichia coli* (ATCC 25922), *Salmonella typhi* (NTCC8394), *Salmonella paratyphi* (MTCC 735), *Pseudomonas aeruginosa* (ATCC 25668), *Klebsiella pneumoniae* (ATCC 15380), *Serratia marcescens* (isolated) were selected.

**Table - 1** Antibacterial activity of different (hexane, ethyl acetate, methanol and distilled water) crude root extracts of selected plant species.

Plant name (Family)	Zone of Inhibition (mm)												
	Extracts	Gram Positive						Gram Negative					
		BC	BS	SA	SE	ML	EN	EC	ST	SP	PS	SM	KP
<i>Ailanthus excelsa</i> Roxb. (Simaroubaceae)	H	0	5	1	0	4	0	0	0	0	0	2	0
	E	0	6	2	2	4	1	0	0	0	0	3	1
	M	3	4	0	0	5	2	0	2	0	4	6	0
	W	3	0	2	2	1	0	0	0	0	0	1	0
<i>Artocarpus integrifolia</i> auct.non L. f. (Moraceae)	H	7	6	0	0	7	2	3	0	0	0	6	2
	E	0	2	0	4	3	0	0	0	0	0	0	0
	M	2	4	0	8	0	0	0	0	0	0	6	0
	W	0	0	3	0	2	0	0	1	0	2	1	0
<i>Averrhoa carambola</i> L. (Averrhoaceae)	H	2	4	0	7	0	0	0	0	0	0	0	3
	E	0	2	3	0	1	0	0	0	0	0	0	0
	M	0	0	0	0	0	0	0	0	0	0	0	0
	W	0	0	0	1	0	2	0	1	3	0	0	1
<i>Bauhinia variegata</i> L. (Fabaceae)	H	5	0	0	0	3	0	0	0	0	0	4	0
	E	0	5	0	4	5	0	0	0	0	0	0	0
	M	0	0	0	4	0	0	0	0	0	0	0	0
	W	0	0	2	0	1	0	0	0	0	0	1	0
<i>Cordia dichotoma</i> Forst. (Boraginaceae)	H	7	4	0	0	0	7	0	0	0	0	0	3
	E	0	3	0	13	0	0	0	0	0	0	0	4
	M	0	5	3	6	2	4	0	7	3	8	4	4
	W	4	0	0	0	2	0	0	0	2	0	0	1
<i>Delonix regia</i> (Boj.) Raf. (Fabaceae)	H	0	0	0	6	2	0	0	0	0	0	0	0
	E	0	6	0	0	0	0	0	0	0	0	4	0
	M	3	7	2	7	0	0	2	0	3	6	0	0
	W	2	0	3	7	0	0	1	0	0	1	0	1
<i>Ficus racemosa</i> L. (Moraceae)	H	7	4	0	5	7	6	0	0	0	0	5	4
	E	0	2	1	3	0	0	0	0	0	0	2	0
	M	0	0	0	4	0	0	0	0	4	0	0	0
	W	0	0	0	2	1	0	1	0	0	0	3	0
<i>Gmelina arborea</i> L. (Verbenaceae)	H	0	6	0	0	4	0	0	0	0	0	0	0
	E	0	4	4	0	3	0	0	0	0	0	0	0
	M	0	6	4	3	6	0	0	5	4	0	0	4
	W	0	1	0	0	5	0	0	1	0	0	2	0
<i>Madhuca indica</i> J.F.Gmel (Sapotaceae)	H	6	11	0	5	3	4	0	0	0	0	3	0
	E	0	4	7	4	4	0	0	0	0	0	0	3
	M	0	7	5	6	7	9	0	9	7	8	4	6
	W	0	0	3	1	1	0	0	0	2	0	0	1
<i>Mangifera indica</i> L. (Anacardiaceae)	H	0	1	0	5	4	3	3	0	0	0	0	4
	E	0	2	0	0	0	5	0	0	0	4	1	0
	M	8	0	0	4	10	0	0	0	5	0	9	0
	W	2	0	0	2	2	0	0	1	0	1	0	0
<i>Manilkara hexandra</i> (Roxb.) Dub. (Sapotaceae)	H	4	3	2	0	3	0	0	0	0	0	2	0
	E	3	4	0	4	5	0	5	2	0	4	0	2
	M	10	10	12	7	11	10	0	10	12	10	12	12
	W	1	3	0	4	2	3	2	0	0	0	0	1
<i>Mitragyna parviflora</i> (Roxb.) Korth. (Rubiaceae)	H	11	16	0	12	11	3	4	7	0	3	10	13
	E	0	1	5	4	0	4	0	0	7	6	10	0
	M	4	0	0	3	9	0	0	0	6	0	7	0
	W	2	2	1	4	5	0	2	3	0	1	5	0
<i>Murraya paniculata</i> (L.) Jack. (Rutaceae)	H	0	0	0	10	3	0	0	0	0	0	4	0
	E	0	0	3	4	0	0	0	0	0	0	1	0
	M	0	6	3	2	0	10	3	0	3	4	3	0
	W	2	0	3	0	5	0	0	0	0	0	1	0
<i>Pithecellobium dulce</i> (Roxb.) Bth. (Fabaceae)	H	6	1	0	2	5	5	4	0	0	0	0	5
	E	0	2	5	0	5	3	0	0	0	6	0	0
	M	5	0	0	0	7	0	0	0	4	0	7	0
	W	1	0	2	0	2	0	0	4	0	6	0	0
<i>Psidium guajava</i> L. (Myrtaceae)	H	6	2	1	4	6	0	3	0	0	0	5	2
	E	0	4	0	0	2	0	0	0	0	0	7	4
	M	9	0	8	10	10	0	9	0	10	17	10	0
	W	3	0	5	0	7	0	0	0	1	0	1	1

<i>Salvadora persica</i> L. (Salvadoraceae)	H	1	5	0	1	0	1	1	0	0	0	0	3
	E	2	1	4	0	0	5	0	0	0	3	4	0
	M	7	0	0	0	6	0	0	0	0	0	7	0
	W	2	1	3	5	3	0	2	1	0	0	3	0
<i>Saraca indica</i> auct. non. L. (Fabaceae)	H	2	3	1	0	4	0	5	0	0	0	0	0
	E	2	2	0	0	3	0	0	0	0	1	1	0
	M	6	0	0	3	7	0	0	0	0	0	8	0
	W	1	0	0	0	0	0	2	0	0	1	3	1
<i>Sterculia urens</i> Roxb. (Sterculiaceae)	H	0	6	0	4	5	0	0	0	0	0	0	0
	E	0	0	2	4	0	3	0	0	0	0	4	0
	M	8	6	7	9	9	7	10	0	11	8	12	0
	W	3	0	3	0	7	4	0	1	0	0	0	0
<i>Tabebuia argentea</i> Brill. (Bignoniaceae)	H	2	4	1	3	0	0	0	0	0	0	0	0
	E	1	2	0	0	4	2	0	0	0	0	0	0
	M	3	0	13	6	0	3	0	0	0	0	0	0
	W	3	0	0	0	0	3	0	0	0	1	0	0
<i>Terminalia bellirica</i> (Gaertn.) Roxb. (Combretaceae)	H	4	3	0	0	3	4	5	0	0	0	0	0
	E	6	2	0	0	5	0	2	0	0	0	6	0
	M	0	0	0	0	5	0	0	0	0	0	0	0
	W	0	0	0	2	0	0	1	0	0	0	0	0
<i>Thespesia populnea</i> (L.) Sol. Ex Corr. (Malvaceae)	H	3	1	2	2	0	0	4	0	0	0	0	0
	E	1	2	0	0	3	0	0	0	0	0	0	0
	M	4	0	0	0	4	0	0	0	0	0	5	0
	W	1	0	0	2	2	0	0	0	0	0	3	0
Ciprofloxacin (20µg/ml)		12	11	11	9	11	11	12	19	10	7	8	16

**Table - 2** Minimum inhibitory concentration of effective plant extracts.

Plant name	Extracts	MIC (mg/ml)											
		BC	BS	SA	SE	ML	EN	EC	ST	SP	PS	SM	KP
<i>Artocarpus integrifolia</i>	M	-	-	-	0.25	-	-	-	-	-	-	-	-
<i>Cordia dichotoma</i>	M	-	-	-	-	-	-	-	-	-	>8	-	-
<i>Madhuca indica</i>	H	-	0.5	-	-	-	-	-	-	-	-	-	-
	M	-	-	-	-	-	8	-	0.5	-	>8	-	-
<i>Mangifera indica</i>	M	4	-	-	-	2	-	-	-	-	-	>8	-
<i>Manilkara hexandra</i>	M	4	0.5	0.5	-	>8	4	-	0.5	>8	>8	>8	4
<i>Mitragyna parvifolia</i>	H	4	2	-	>8	8	-	-	-	-	-	>8	>8
	M	-	-	-	-	0.25	-	-	-	-	-	-	-
<i>Murraya paniculata</i>	H	-	-	-	2	-	-	-	-	-	-	-	-
	M	-	-	-	-	-	0.25	-	-	-	-	-	-
<i>Psidium guajava</i>	M	8	-	0.5	0.25	4	-	2	-	-	>8	>8	-
<i>Saraca indica</i>	M	>8	-	-	-	-	-	-	-	-	-	-	-
<i>Sterculia urens</i>	M	8	-	0.25	-	-	1	8	-	-	>8	>8	-
<i>Tabebuia argentea</i>	M	-	-	-	-	4	-	-	-	-	-	-	-

**ABBREVIATIONS**

**BC**-*Bacillus cereus*  
**BS**-*Bacillus subtilis*  
**EC**-*Escherichia coli*  
**EN**-*Enterococcus faecalis*  
**KP**-*Klebsiella pneumoniae*  
**ML**-*Micrococcus luteus*  
**PS**-*Pseudomonas aeruginosa*  
**SE**-*Staphylococcus epidermidis*

**SA**-*Staphylococcus aureus*  
**ST**-*Salmonella typhi*  
**SM**-*Serratia marcescens*  
**SP**-*Salmonella paratyphi*  
**H**- Hexane  
**E**- Ethyl acetate  
**M**- Methanol  
**W**- Distilled water

Microbial pure cultures were obtained from MTCC (Institute of Microbial Technology, Chandigarh, India), ATCC (American type culture collection, Manassas, Virginia, USA) and NTCC (Health Protection Agency Culture Collection, UK). The bacterial cultures were grown on nutrient agar medium (Hi-Media, pH 7.4) at 37°C and all the cultures were maintained at 4°C.

**Antimicrobial screening of plant extracts**

In the present study, the antimicrobial activities of root crude extracts prepared in different solvents were screened by agar well diffusion method [11]. An inoculum size of  $1 \times 10^8$  CFU/ml of bacteria which compared with 0.5 McFarland turbidity standards was used [12]. Each plant extract of 100 µl (stock solution 100 mg/ml) was added in a previously marked sterile nutrient agar petriplates and the wells were punched with sterile cork borer and filled with each plant extract. Plates were placed in a refrigerator for 30 minutes for pre-diffusion of plant extract and then incubated at 37°C for 24 hours. After incubation all the plates were examined and zone of inhibition (excluding well diameter in mm) was measured as a property of antimicrobial activity. Antibiotic such as ciprofloxacin (20µg/ml) as a positive control and 100% DMSO and solvents i.e. hexane, ethyl acetate and methanol as a negative controls

were used. Minimum inhibitory concentration was evaluated in the range of 4.0 to 0.25 mg/ml by two fold serial broth dilution method [13] for the plant extracts showing more than 7mm inhibition zone. Bioassay was carried out in duplicate and experiments were repeated twice.

## RESULTS AND DISCUSSION

The antibacterial activity of crude root extracts extracted in hexane, ethyl acetate, methanol and distilled water of selected plant species against twelve bacterial strains and their potency were comparatively assessed by the presence or absence of zone inhibition (in mm). Successful prediction of botanical compounds from plant material is largely dependent on the type of solvent used in the extraction procedure. This study focused on plant extracts prepared in organic solvents (hexane, ethyl acetate and methanol) to obtain antimicrobial activity compared to aqueous extracts.

Crude root extracts of *Ailanthus excelsa*, *Artocarpus integrifolia*, *Averrhoa carambola*, *Bauhinia variegata*, *Cordia dichotoma*, *Delonix regia*, *Ficus racemosa*, *Gmelina arborea*, *Pithecellobium dulce*, *Salvadora persica*, *Tabebuia argentea*, *Terminalia bellarica*, *Thespesia populnea* prepared in hexane, ethyl acetate, methanol and distilled water exhibited only moderate to least activity as well as no activity against tested gram-positive and gram-negative bacteria. *Madhuca indica* methanolic root extract exhibited moderate activity against most of the tested organisms. Only hexane root extract showed good antibacterial activity against BS (Table - 1). Other extracts of *Mangifera indica* displayed moderate to least activity against most of the selected bacteria (Table - 1). Broad spectrum antibacterial activity was reported with methanol bark extract of *Mangifera indica* [14]. Methanolic root extracts of *Manilkara hexandra* exhibited good activity against SA, ML, SP, SM, KP, moderate activity against BC, BS, SE, EN, ST, PS and no activity was seen against EC (Table - 1). These results are mostly comparable with positive control ciprofloxacin (20µg/ml). However, least to no activity was observed in hexane, ethyl acetate and distilled water extracts of *M. hexandra* against most of the tested bacteria (Table - 1). Methanolic extracts of *Allium vineale*, *Chaerophyllum macropodium* and *Prangos ferulacea* showed higher antibacterial activity compare to ethanol and hexane extracts against gram-positive bacteria (BC, BS, ML, SA) [15].

The hexane root extracts of *Mitragyna parvifolia* displayed good activity against BC, BS, SE, ML, KP as well as ethyl acetate extract exhibited moderate activity against SP, PS and SM, least to no activity seen against other tested organisms (Table - 1). This plant extract appear to be more effective against gram-positive bacteria than gram-negative bacteria except *Klebsiella pneumoniae* and *Pseudomonas aeruginosa*. The results of hexane extracts of *Mitragyna parvifolia* are comparable with positive control. Similar results in Hexane and ethyl acetate root extracts of *Piqueria trinervia*- a Mexican plant were observed against eleven strains of bacteria [16]. In this study, broad spectrum antibacterial activity was seen in hexane and ethyl acetate root extracts of *Mitragyna parvifolia*. Methanolic root extracts of *Psidium guajava* demonstrated good activity against PS, moderate activity against BC, SA, SE, ML, EC, SP and SM (Table - 1). *Sterculia urens* methanolic root extract exhibited good activity against SP and SM, moderate activity against BC, BS, SA, SE, ML, EN, EC and PS and no activity was seen against other bacteria (Table - 1). *Senna siamiae* ethanolic leaf extracts showed antibacterial activity against *Salmonella typhi* [17]. In this study, methanolic root extract of *Sterculia urens* showed good antibacterial activity against *Salmonella paratyphi*.

This study demonstrated that methanolic root extracts of most of the selected plants showed more antibacterial activity than other solvent extracts. Similar observations have been

reported by Parekh and Chanda [18] in methanolic extracts of twelve medicinal plants belonging to different families provide more consistent antimicrobial activity compared to those extracted in water against *Bacillus cereus*, *Staphylococcus epidermidis*, *Enterococcus aerogenes*, *Pseudomonas vulgaris* and *Salmonella typhimurium*. Methanolic leaf extract of *Kirganelia reticulata* showed better activity compared to its chloroform and hexane extracts against *Escherichia coli*, *Pseudomonas aeruginosa*, *Salmonella typhi* and *Staphylococcus aureus* [19]. Crude methanolic extracts of leaves and roots of *Clerodendrum inerme* also showed more pronounced antimicrobial activity than benzene and aqueous extracts [20]. Acetone and ethanol extracts of *Madhuca longifolia*, *Parkia biglandulosa*, *Pterospermum acerifolium* displayed more significant antibacterial activity as compared to water extracts [21]. However, in this study a large number of extracts were active against tested bacterial strains and no activity was observed in all negative controls.

Out of 12 selected bacteria, gram-positive organisms i.e. *Micrococcus luteus* and *Staphylococcus epidermidis* were found to be the most susceptible and gram-negative bacteria i.e. *Escherichia coli*, *Salmonella paratyphi* and *Pseudomonas aeruginosa* appeared to be the most resistant organisms against all extracts of the selected plants. In this study, the hexane, ethyl acetate and methanol extracts of all plants showed more antibacterial activity as compared to water extracts. Hexane root extracts inhibited *Staphylococcus epidermidis* by 33.33%, *Micrococcus luteus* was found to be most susceptible organism and inhibited by 19.04% ethyl acetate root extracts and methanolic root extracts by 57.14% of the selected plants. Most of the plant extracts exhibited inhibitory activity against one or more tested bacteria but plant extracts displaying more than 5 mm inhibition zone were taken in to consideration for the preparation of sensitivity sequence of organisms. Sensitivity of test strains was in decreasing order: in hexane extract - SE > BC = BS > ML > SM > EN = EC = KP > ST > SA = SP = PS; in ethyl acetate extract: ML > BS = SA = SM > EC > PS = EN > BC = SE = SP > ST = KP; in methanol extract: ML > SM > SE > BC = BS > PS > SP > ST = EN > EC = KP > SA.

The observed minimum inhibitory concentration (MIC) of effective plant extracts varied in the range of 0.25 - 8 mg/ml for most of the tested bacterial strains (Table - 2). The methanolic root extracts of *Artocarpus integrifolia*, *Cordia dichotoma*, *Madhuca indica*, *Mangifera indica*, *Manilkara hexandra*, *Psidium guajava* and *Tabebuia argentea*, while hexane and methanolic root extracts of *Madhuca indica* and *Mitragyna parvifolia* demonstrated minimum inhibitory concentration in the range of 0.25 to >8 mg/ml against tested microorganisms (Table - 2). *Psidium guajava* methanolic root extract MIC values were observed at 0.25 mg/ml against SE, 0.5 mg/ml against SA, 2 mg/ml against EC, 4 mg/ml against ML, and 8 mg/ml against BC and >8 mg/ml against PS and SM (Table - 2). The MIC values of *Psidium guajava* bark extract against *Staphylococcus aureus* coincides with the MIC value (0.5mg/ml) obtained for methanol root extract in this study [14]. The MIC value for *Madhuca indica* methanolic root extracts showed 0.5 mg/ml against ST, 8 mg/ml against EN and <8 mg/ml against PS (Table - 2). The MIC values of *Sterculia urens* were found as >8 mg/ml against PS and SM, 8 mg/ml against BC and EC, 1 mg/ml against EN and 0.25 mg/ml against SA (Table - 2).

The present investigation concludes that among different plant extracts *Mitragyna parvifolia* (hexane extract), *Sterculia urens* and *Manilkara hexandra* (methanol extract) show promising antibacterial properties and could be used externally against bacterial infections. Alternatively, the active principles of these plant extracts may be characterized and tested for their safety and efficacy to uncover their therapeutic potential in modern and traditional medicine against infectious diseases.

## ACKNOWLEDGEMENT

Mr. Purvesh Bharvad thanks University Grant Commission, New Delhi for awarding "UGC research fellowship for meritorious students scheme".

## REFERENCES

- [1] Ahmed, I. and Beg, A. Z. (2001) Antimicrobial and phytochemical studies on 45 medicinal plants against multi-drug resistant human pathogens. *Journal of Ethnopharmacology*, **74**: 113–123.
- [2] Iwu, M. W., Duncan, A. R. and Okunji, C. O. (1999) New antimicrobials of plant origin. In *Perspectives on new crops and new uses*. (Ed. Janick, J.) pp. 457–462.
- [3] Jagtap, N. S., Khadabadi, S. S., Ghorpade, D. S., Banarase, N. B. and Naphade, S. S. (2009) Antimicrobial and antifungal activity of *Centella asiatica* (L.) Urban, Umbelliferae. *Research Journal of Pharmacy and Technology*, **2**: 328–330.
- [4] Aqil, F. and Ahmed, I. (2003) Broad-spectrum antibacterial and antifungal properties of certain traditionally used Indian medicinal plants. *World Journal of Microbiology and Biotechnology*, **19**: 653–657.
- [5] Mahida, Y. and Mohan, J. S. S. (2007) Screening of plants for their potential antibacterial activity against *Staphylococcus* and *Salmonella* spp. *Natural Product Radiance*, **6**(4): 301–305.
- [6] Nwachukwu, I. N., Allison, L. N.-O., Chinakwe, E. C. and Nwadiaro, P. (2008) Studies on the effects *Cymbopogon citratus*, *Ceiba pentandra* and *Loranthus bengwelensis* extracts on species of dermatophytes. *The Journal of American Science*, **4**(4): 52–63.
- [7] Kolapo, A. L., Okunade, M. B., Adejumo, J. A. and Ogundiya, M. O. (2009) Phytochemical composition and antimicrobial activity of *Prosopis africana* against some selected oral pathogens. *World Journal of Agricultural Sciences*, **5**(1): 90–93.
- [8] Seyyidnejad, S. M., Niknejad, M., Darabpoor, I. and Motamedi, H. (2010) Antibacterial activity of hydroalcoholic extracts of *Callistemon citrinus* and *Albizia lebbek*. *American Journal of Applied Sciences*, **7**(1): 13–16.
- [9] Shah, G. L. (1978) *Flora of Gujarat State*, Vol I-IV, Sardar Patel University Press, Vallabh Vidyanagar, Gujarat, India.
- [10] Houghton, P. J. and Raman A. (1998) Laboratory handbook for the fractionation of natural extracts. Chapman and Hall. London, pp. 1–28.
- [11] Perez, C., Pauli, M. and Bazaerque, P. (1990) An antibiotic assay by the agar well method. *Acta Biologica et Medica Experimentalis*, **15**: 113–115.
- [12] Perilla, M. J. (2003) *Manual for the laboratory identification of antimicrobial susceptibility testing of bacterial pathogens of public health importance in the developing world*. WHO (World Health Organization), pp: 209–214.
- [13] Chattopadhyay D., Mukherjee T., Pal P., Shah B. and Bhadra R. (1998) Altered membrane permeability as the basis of bactericidal action of methdilazine. *The Journal of Antimicrobial Chemotherapy*, **42**: 49–55.
- [14] Akinpelu, D. A. and Onakoya, T. M. (2006) Antimicrobial activities of medicinal plants used in folklore remedies in south-western Nigeria. *African Journal of Biotechnology*, **5**(11): 1078–1081.
- [15] Durmaz, H., Sagun E., Tarakci Z. and Ozgokce, F. (2006) Antibacterial activities of *Allium vineale*, *Chaerophyllum macropodium* and *Prangos ferulacea*. *African Journal of Biotechnology*, **5**(19): 1795–1798.
- [16] Esparza, R. R. D., Bye, R., Meckes, M., Lopez, J. T. and Estrada, M. J. (2007) Antibacterial activity of *Piqueria trinervia*, a Mexican medicinal plant used to treat diarrhea. *Pharmaceutical Biology*, **45**(6): 446–452.
- [17] Doughari, J. H. and Okafor, N. B. (2008) Antibacterial activity of *Senna siamae* leaf extracts on *Salmonella typhi*. *African Journal of Microbiology Research*, **2**: 42–46.
- [18] Parekh, J. and Chanda, S. (2007) Antibacterial and phytochemical studies on twelve species of Indian medicinal plants. *African Journal of Biomedical Research*, **10**: 175–181.
- [19] Shruthi, S. D., Ramachandra, Y. L. Rai, P. S. and Shetty, V. A. (2010). Antibacterial potential of leaf extracts from *Kirganelia reticulata* Baill. *International Journal of Pharmaceutical Researches and Developments-Online (IJPRD)*, **2**(6): 1–7.
- [20] Chahal, J. K., Sarin, R. and Malwal, M. (2010). Efficacy of *Clerodendrum inerme* L. (Garden quinine) against some human pathogenic strains. *International Journal of Pharma and Biosciences*, **1**(4): 219–223.
- [21] Khond, M., Bhosale, J. D., Arif, T., Mandal, T. K., Padhi, M. M. and Dabur, R. (2009) Screening of some selected medicinal plants extracts for *in vitro* antimicrobial activity. *Middle-East Journal of Scientific Research*, **4**(4): 271–278.



**SHORT COMMUNICATION**

**HETEROSIS FOR BIOMETRIC CHARACTERS AND SEED YIELD IN PARENTS AND HYBRIDS OF RICE (*ORYZA SATIVA* L.)**

**M. Prakash\* and B. Sunil Kumar**

*Department of Genetics and Plant Breeding,  
Faculty of Agriculture, Annamalai University,  
Annamalai Nagar – 608 002, India*

A study was conducted to derive the heterotic vigour of rice hybrids viz., ADTRH 1, CORH 2 and their parents IR 58025 A, IR 58025 B, IR 66R, C 20R for six yield and yield attributing characters. On the basis of per se performance, the parent C 20 R was found to be the best for the traits number of tillers per plant, number of productive tillers per plant, 1000 grain weight and grain yield per plant. The hybrid CORH 2 was found to excel the performance of ADTRH 1 both in per se performance and in magnitude and direction of heterosis.

**Key words:** Biometric traits, heterosis, hybrids, rice

Rice (*Oryza sativa* L.) is the staple food crop in India and in developing countries of the world. As the population of India has crossed one billion, there is an imperative need to increase the production of food grains by employing improved new rice varieties [2]. Hybrid rice technology is the proven technology in China and a more practical one to raise production ultimately. It was obvious that the growing demand for food grains can be met only through hybrids. Hence, the present study was carried out in rice hybrids. As the increase of yield in rice hybrids can be achieved by hybrid vigour (i. e) heterosis, more emphasis is laid on this. Exploitation of heterosis is considered to be one of the outstanding achievements of plant breeding. To know the potentiality of hybrids, study on magnitude and direction of heterosis is very important. Heterosis, a valuable expression that often result from genetic combination, has been frequently utilized for development and identification of promising hybrids for further exploitation in conventional as well as heterosis breeding programme. Hence, in the present study relative heterosis, heterobeltiosis and standard heterosis of the biometrical traits and seed yield were analysed.

For the present study, two F<sub>1</sub> hybrids and their parents were collected and the study was carried out at Plant Breeding Farm, Department of Genetics and Plant Breeding, Annamalai University, Annamalai Nagar. Nursery was prepared with raised beds of 90 cm width. Two centimeter deep furrow lines were formed and seeds of each genotype were sown. The seedlings raised in the nursery were transplanted to the main field with a spacing of 15 cm within rows and 30 cm between rows. The adopted design was RBD (Randomized Block Design) with three replications and the season was Navarai (January – May). Observations were recorded from the randomly selected ten plants in each replication for the yield and yield attributing components like plant height, number of tillers per plant, number of productive tillers per plant, number of grains per panicle, 1000 grain weight and grain yield per plant. The heterosis was calculated as the difference of F<sub>1</sub> from mid parent heterosis (MPH), standard heterosis (STH), and better parents heterosis (BPH). Heterosis was expressed as a percentage increase or decrease over MP (Mid Parent), SH (Standard Heterosis) and BP (Better Parent). The level of heterosis was tested using Student's "T" test. Heterosis measurement was simple and generally expressed as percentage increase or decrease in the performance of a hybrid in comparison with the reference variety or a parent [6].

The mean performance of the parents and hybrids are presented in Table - 1. On the basis of mean performance, the genotype CO 20 R was found to be the best parent for the traits number of tillers per plant (15.47), number of productive tillers per plant (13.90), 1000 grain weight (20.18g) and grain yield per plant (40.74g). The parent IR 66R was found to be the best for the trait, number of grains per panicle (149.58). Regarding the hybrids, CORH 2 was taller (89.00 cm) than ADTRH 1 (76.77 cm). The other yield attributing traits like number of tillers per plant (16.36), number of productive tillers per plant (14.69), number of grains per panicle (164.02), 1000 grain weight (22.57g) and grain yield per plant (54.62 g) were found to excel the performance of ADTRH 1.

In CORH 2, the relative heterosis, heterobeltiosis and standard heterosis were maximum for the character grain yield per plant (76.02, 34.07 and 54.47). The hybrid CORH 2 recorded positive and significant relative heterosis (11.77) and heterobeltiosis (4.45) for plant height. Negative significant standard heterosis (-3.72) was also obtained for this character. While the hybrid ADTRH 1 recorded the heterotic vigour in negative direction for the character plant height, similar findings were reported by [4]. Better segregants for dwarf plant types to

**Table- 1** Mean performance of parents and hybrids for yield and yield attributing characters in rice.

Sr. No	Characters	Parents				Hybrids	
		IR 58025A	IR 58025B	IR 66R	CO 20R	ADTRH 1	CORH 2
1.	Plant height (cm)	85.17	85.21	73.81	74.05	76.77	89.00
2.	Number of tillers per plant	10.22	10.31	15.38	15.47	13.17	16.36
3.	Number of productive tillers per plant	8.05	8.11	11.95	13.90	12.18	14.69
4.	Number of grains per panicle	82.20	138.05	149.58	144.94	155.95	164.02
5.	1000 grain weight (g)	19.00	19.04	20.15	20.18	20.10	22.57
6.	Grain yield per plant (g)	14.25	21.32	36.03	40.74	38.19	54.62

**Table- 2** Relative heterosis (di), heterobeltiosis (dii) and standard heterosis (diii) for yield and yield attributing characters in rice.

S.No	Characters	ADTRH 1			CORH 2		
		Relative heterosis	Heterobeltiosis	Standard heterosis	Relative heterosis	Heterobeltiosis	Standard heterosis
1.	Plant height (cm)	-4.13**	-10.48**	-17.60**	11.77**	4.45	-3.72**
2.	Number of tillers per plant	2.37**	-14.37	-6.79	26.92**	5.57**	15.78**
3.	Number of productive tillers per plant	20.59**	1.92	-7.59**	33.48**	5.68**	11.46**
4.	Number of grains per panicle	8.07**	4.26**	16.94**	15.92**	13.16**	22.99**
5.	1000 grain weight (g)	2.66**	-0.25**	-0.10**	15.09**	11.84**	12.18**
6.	Grain yield per plant (g)	33.62**	26.00	38.00**	76.02**	34.07**	54.47**

\*\* 1% level of significance

\*Corresponding author: geeth\_prakash@yahoo.co.in

prevent plant lodging can be obtained from this cross in subsequent generations. The hybrid CORH 2 recorded positive significant relative heterosis, heterobeltiosis and standard heterosis for all the biometric characters like number of tillers per plant, number of productive tillers per plant, number of grains per panicle, 1000 grain weight and grain yield per plant. Such positive heterosis might be attributed due to both epistasis and dominance. Similar findings were concluded by [3] for total number of tillers, [1] for number of productive tillers and [5] for 1000 grain weight. The hybrid ADTRH 1 showed low heterosis in negative direction for most of the characters like number of tillers per plant and 1000 grain weight. This expression of negative heterosis may be attributed to non-allelic interaction which can either increase or decrease the expression of heterosis.

In the hybrid CORH 2 for most of the cases, significant positive heterosis for grain yield was associated with heterosis for number of tillers per plant, number of productive tillers per plant, number of grains per panicle and 1000 grain weight. This indicated that heterosis for grain yield was through heterosis from individual yield component.

In general the hybrid CORH 2 recorded significantly positive heterotic vigour for all the biometrical traits when compared to the hybrid ADTRH 1 suggesting that exploitation of such hybrid could be more rewarding for breeding programmes in rice improvement.

#### REFERENCES

- [1] Ali, S. S. and Khan, M. G. (1995) Studies for heterosis and combining ability in rice. *Pakistan J. Sci. Indust. Res.*, **38** (5-6): 200-204.
- [2] Ismail, S. (2000) Food security-Daunting research tasks. *The Hindu Survey of Indian Agriculture*. pp. 31-34.
- [3] Mamta Singh, D., Maurya, M. and Singh, M. (1999) Heterosis and inbreeding depression in rice for yield and yield components using CMS system. *Oryza*, **36**(1): 24-27.
- [4] Reddy, C. D. R. and Nerkar, Y. S. (1991) Heterosis in  $F_1$  breeding depression and heritability estimates in  $F_2$  of rice crosses. *Crop Res.*, **42**(2): 288-292.



## ADSORPTION BEHAVIOR AND THERMODYNAMICS INVESTIGATION OF ANILINE-N-(p-METHOXYBENZYLIDENE) AS CORROSION INHIBITOR FOR Al-Mg ALLOY IN HYDROCHLORIC ACID.

V.A. Panchal, A.S. Patel and N.K. Shah\*

Chemistry Department, School of Sciences, Gujarat University, Ahmedabad, Gujarat - 380009

### ABSTRACT

The interfacial behavior of Aniline-N-(p-methoxybenzylidene) (ANPMB) between Al-Mg alloy and hydrochloric acid has been investigated by using weight loss method at a temperature range from 35°-65° C. The results showed that ANPMB is an excellent corrosion inhibitor for Al-Mg alloy in acidic medium. Inhibition efficiency increased with increase in the concentration of ANPMB but decreased with rise in temperature. The activation ( $E_a$ ) of corrosion and other thermodynamic parameters (such as heat of adsorption ( $Q_a$ ), entropy of adsorption ( $\Delta S^\circ_a$ ) and free energy of adsorption ( $\Delta G^\circ_a$ )) were calculated to elaborate the mechanism of corrosion inhibition. From the thermodynamic parameters, the  $\Delta G^\circ_a$  values are negative that suggest that the adsorption is of chemisorption type between the metal and inhibitor molecules. A plot of  $\log \theta/1-\theta$  vs  $\log C_{inh}$  gives a straight line indicating that the inhibitor function through adsorption following Langmuir isotherm. At 0.8% concentration of ANPMB, > 99% inhibition was observed.

**Key words:** Al-Mg alloy, Hydrochloric acid, Inhibitor, Corrosion.

### INTRODUCTION

Corrosion of aluminium and its alloys have been a subject of numerous studies due to their high technological values and wide range of industrial applications especially in aerospace and house hold industries. Aluminium and its alloys, however, are reactive materials and are prone to corrode [1].

Thermodynamically aluminium is a highly reactive metal ( $E^\circ_{Al^{+3}/Al} = -1.676$  V) [2] and because of its high affinity for oxygen ( $\Delta G^\circ_{Al_2O_3} = -1582$  kJmol<sup>-1</sup>) [3], aluminium surfaces are usually covered with thin but tightly adherent and protective film of aluminium oxide. The film is stable in solutions of pH 4.5 to 8.5, but because of its amphoteric nature, it fails to protect aluminium in strongly acid and strongly alkaline media [4]. Addition of magnesium to aluminium gives strain-hardenable alloys with increase in mechanical properties and improvement in resistance to corrosion [5, 6]. Al-Mg alloys are important materials for use in many applications such as for automobiles, containers, electric devices, etc., and are widely used in marine-atmosphere.

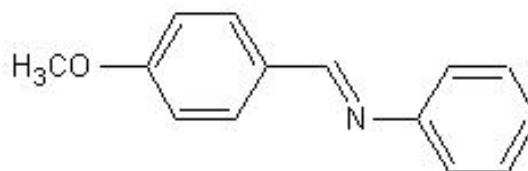
Acids have long been used in removing the scale from metal surfaces and also in pickling. Hence to avoid attack on the base metal during scale-removal and cleaning metal surfaces with acidic solutions, the use of inhibitors become necessary. The applicability of organic compounds as corrosion inhibitors for metals in acidic media has been recognized for a long time.

Aldehydes and amines are fairly good inhibitors for metals and alloys in acids and other corrosive media [7, 8]. The inhibition efficiency of Schiff bases is much greater than corresponding aldehydes and amines. This is due to the presence of a > C = N - group in azomethine [9]. From this point of view, the inhibitor (Schiff base) has been synthesized and the performance of this inhibitor in retarding the corrosion of Al-Mg alloy in hydrochloric acid has been studied.

#### Synthesis of Schiff base

The Schiff base was synthesized by condensation of aniline with p-methoxybenzaldehyde to the procedure described

by Jaeger [10]. ANPMB (m.p., 63°C, registry number, 836-41-9) is light yellow crystalline substance, insoluble in water but soluble in ethanol.



Aniline-N-(p-methoxybenzylidene) (ANPMB)

### RESULTS and DISCUSSION

Adsorption behavior, thermodynamic parameters and activation energy in the presence of inhibitor have been evaluated.

#### Adsorption behavior

Adsorption is primary and important step in inhibition by organic based film forming corrosion inhibitors. Adsorption results from the polar or charged nature of the organic molecule / ionic species first establishing a physisorption surface film which may further stabilize through chemisorption to form a donor type bond [11]. If it is assumed that the inhibition of corrosion is due to the surface coverage ( $\theta$ ) by the inhibitor molecules then value of  $\frac{w_e - w_i}{w_e}$  is a measure of the surface coverage  $\theta$  [12]. The relationship between the coverage of an interface with an adsorbed species and the concentration of the species in solution is given by Langmuir adsorption isotherm [13].

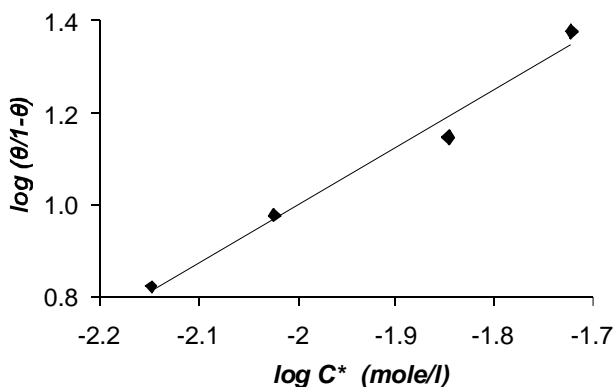
$$\theta = \frac{KC_{inh}}{1 + KC_{inh}}$$

where, K is the Langmuir adsorption constant or adsorption coefficient.

\*Corresponding author: nishchem2004@yahoo.co.in

**Table-1 :** Adsorption behavior

C (%)	C* (mole/litre x 10 <sup>-2</sup> )	log C* (mole/l)	Weight loss (mg)	θ	θ/1-θ	log (θ/1-θ)
0.15	0.7109	-2.1481	55	0.8693	6.6511	0.8228
0.20	0.9478	-2.0232	40	0.9049	9.5152	0.9784
0.30	1.4218	-1.8471	28	0.9334	14.0150	1.1465
0.40	1.8957	-1.7222	17	0.9596	23.7524	1.3757

**Fig.1 :** Langmuir plots for ANPMB in 2.0 M hydrochloric acid at 35°C.

A plot of  $\log \theta/1-\theta$  vs  $\log C_{in}$  (inhibitor concentration) (Fig-1) was drawn (from data given in Table-1) straight line was observed indicating that the inhibitor was adsorbed onto the metal surface following Langmuir isotherm.

#### Thermodynamic Parameters

If it is assumed that the inhibitor is adsorbed on the metal surface in the form of a monolayer film, covering at any instant a fraction,  $\theta$ , of the metal surface in a uniform random manner, then the heat of adsorption,  $Q_A$ , can be calculated as per Hoar and Holiday [14]. The values of the free energy of adsorption,  $\Delta G_A^\circ$ , were calculated following Abdel and Saiyed equation [15]. From the values of heats of adsorption and free energy of adsorption, values of the entropy of adsorption  $\Delta S_A^\circ$  were calculated. The values of  $Q_A$ ,  $\Delta G_A^\circ$ , and  $\Delta S_A^\circ$  for the temperature range 35°-65°C are given in Table-2. From the results, it is evident that for ANPMB, the heats of adsorption and free energy of adsorption are negative, further, the  $Q_A$  value is less negative while the free energy of adsorption is more negative in the case of a good inhibitor like ANPMB, which suggests that there is a strong interaction of the inhibitor molecules with the metal surface resulting in the spontaneous adsorption. It is observed that at higher concentration of inhibitor,  $\Delta G_A^\circ$  values are more negative, which suggest that the chemisorption of the inhibitor on the metal is a spontaneous process. The metal-inhibitor bonds are strong enough to provide excellent inhibition even at higher temperature.

The adsorption is a spontaneous process which is further supported by positive values of the entropies of adsorption,  $\Delta S_A^\circ$ . It may be generalized from the present studies, that an efficient inhibitor is characterized by a relatively greater decrease in free energy of adsorption (become more negative), positive values of entropy of adsorption and less negative value of heat of adsorption as compared to free energy of adsorption.

#### Activation energy ( $E_a$ )

$E_a$  is the apparent activation energy. It is the difference between the average energy of active molecules and the average energy of all the molecules.

A low activation energy means a fast reaction and a high activation energy means a slow reaction [16]. A high activation energy corresponds to a reaction rate that is very sensitive to temperature. Conversely, a small activation energy indicates a reaction rate that varies only slightly with temperature [17]. If a reaction has zero activation energy, its rate is independent of temperature. In some case  $E_a$  is found to be negative which indicates that the rate decreases as the temperature is raised; such behavior is a signal that the reaction has a complex mechanism.

In the present work the  $E_a$  values have been calculated from the plot of  $\log \rho$  (corrosion rate) vs  $1/T$  (Table-3 and Fig-2). In the uninhibited acid, the  $E_a$  value was 14.3 kcal/mol. The value of  $E_a$  at 0.8% of ANPMB was found to be 16.2 kcal/mol. The  $E_a$  value in inhibited acid thus varied and depended upon the ability of the inhibitor to reduce the corrosion rate. According to Putilova et al [18] the  $E_a$  value is higher in inhibited solutions and can be compared with unstable catalyst poisons whose adsorption fall off appreciably with rise in temperature and indicate physical adsorption on the metal surface. The extent of inhibition is likely to decrease with increasing temperature because of desorption of the inhibitor which would expose larger surface areas to the corrosion solution.

At 0.8% inhibitor concentration, weight losses were determined at 35°C, 45°C, 55°C and 65°C for an immersion period of 30 minutes. In plain acid the loss of metal due to corrosion increased from 1120 mg/dm<sup>2</sup> at 35°C to 7608 mg/dm<sup>2</sup> at 65°C (Table-3). In inhibited acid also the weight loss due to corrosion was found to increase with temperature but as compared to uninhibited acid it was much less upto 65°C, and the inhibition efficiencies were found to be 99.3% at 35°C and 98.8% at 65°C in ANPMB. However, when the inhibitor is present in sufficient amount it can confer ~ 98% to 99% protection in the temperature range 35° - 65°C.

**Table-2 :** Thermodynamic parameters :

Inhibitor (%)	Temp (°C)	2.0M HCl		
		$\Delta G_A^\circ$ (kcal mol <sup>-1</sup> )	$\Delta S_A^\circ$ (cal mol <sup>-1</sup> )	$Q_A$ (kcal mol <sup>-1</sup> ) (35°-65°C)
0.8	35	-7.5	36.1	-3.6
	45	-7.8	35.9	
	55	-7.8	35.0	
	65	-7.9	34.1	

Table : 3 Activation Energy and effect of temperature.

Inhibitor concentration (%)		Weight loss (mg/dm <sup>2</sup> ) at a temperature of				Energy of activation, E <sub>a</sub> (kcal/mol) 35° - 65°C
		35°C	45°C	55°C	65°C	
Nil (HCl only)	1	1072	2410	4980	7682	14.3
	2	1104	2453	4932	7562	
	3	1184	2335	4817	7581	
	avg.	1120	2399	4910	7608	
0.8	1	8	13	37	85	16.2
	2	8	19	48	74	
	3	8	16	43	104	
	avg.	8 (99.3%)	16 (99.3%)	43 (99.1%)	88 (98.8%)	

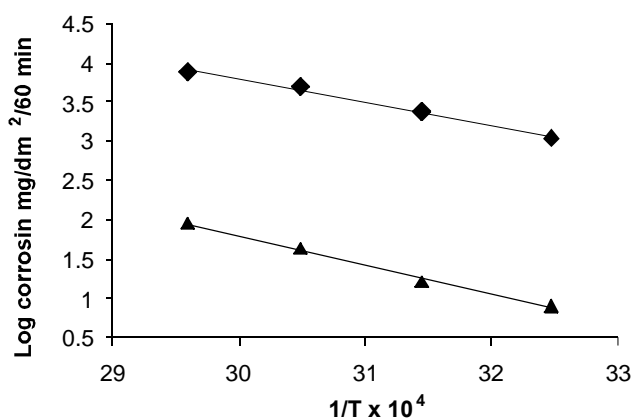


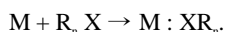
Fig.2 : Arrhenius plots for Al-Mg alloy in 2.0 M hydrochloric acid in the presence and absence of inhibitor ANPMB.

◆...◆ 2.0 M hydrochloric acid alone

▲...▲ inhibitor ANPMB (0.8%) in 2.0 M hydrochloric acid.

### Mechanism of inhibition

Organic compounds containing one or more polar units, which may be regarded as the reaction centre/centres for the chemisorption process function as corrosion inhibitors. The adsorption bond strength is determined by the electron density on the atom (e.g., N, S, O, etc.) acting as the reaction centre and by the polarisability of the unit. Thus, organic corrosion inhibitors are adsorbed on the bulk metal, M, forming a charge transfer complex between their polar atoms and the metal;



The size, shape and orientation of the molecule, and the electronic charge on the molecule determine the degree of adsorption and that way the effectiveness of the inhibitor.

The structure of the inhibitor shows that it is having three anchoring site (one iminic group  $>C=N-$ , and two aromatic rings, among the one having methoxy  $-OCH_3$  group attached) and they show good inhibitive power when present in sufficient amounts. It is assumed that the compound form onium ions in acidic media and move to the cathodic regions, then adsorption will take place through the iminic nitrogen ( $>C=N-$ ) and also through the delocalized  $\pi$ -electrons of the benzene moiety, and gives good protection.

The results show that ANPMB is the effective inhibitor and this may be traced to the fact that the  $-OCH_3$  group (+R, -I)

supplies electron density to the aromatic benzaldehydic ring and thus the delocalized  $\pi$ -electrons of this ring help in the chemisorption of the compound with stronger bonds and gives better protection.

### CONCLUSION

- 1) ANPMB confers 98-99% protection to Al-Mg alloy in hydrochloric acid at 0.8% inhibitor concentration.
- 2) The adsorption follows Langmuir isotherm.
- 3) The heat of adsorption and free energy of adsorption are negative while the entropy of adsorption is positive. The free energy of adsorption are more negative in the case of very good inhibitor. The positive values of the entropy of adsorption suggest that the adsorption is a spontaneous process.
- 4) Activation energy is higher in the presence of inhibitor compared to that in plain acid.

The presence of iminic group ( $>C=N-$ ) and methoxy group ( $-OCH_3$ ) in the molecule, appeared to be the main factor enhancing chemisorption of an inhibitor.

### REFERENCES

- [1] Obot, I.B., Ohi-Egbedi, N.O. and Umoren, S.A. (2009) Antifungal drugs as corrosion inhibitors for aluminium in 0.1 M HCl, 51: 1868-1875.
- [2] Greenwood, N.N. and Earnshaw, A. (1997) *Chemistry of Elements* (2<sup>nd</sup> Edn.) Butterworth & Heinemann, Oxford, pp-224.
- [3] Vargel, C. (2004) *Corrosion of Aluminium*, Elsevier publishing house, Oxford, pp-3.
- [4] Binger, W.W. (1963) *Corrosion Resistance of Metals and alloys*, Reinhold publ. Corp., New York, pp-183.
- [5] Godard, H.P., Jepson, W.B., Bothwell, M.R. and Kane, R.L. (1967) *The Corrosion of Light Metals*, John Wiley & Sons. Inc., New York, pp-20.
- [6] Winston, Revie. R. (2000) *Uhlig's Corrosion Handbook* (2<sup>nd</sup> Edn.), John Wiley & Sons. Inc., New York, pp-685.
- [7] Desai, M.N., Desai, M.B. (1984) Carbonyl compounds as corrosion inhibitors for mild steel in HCl solutions, *Corrosion Science*, 24: 649-660.
- [8] Desai, M.N., Desai, M.B., Shah, C.B. and Desai, S.M. (1986) Schiff bases as corrosion inhibitors for mild steel in hydrochloric acid solutions, *Corrosion Science*, 26: 827.
- [9] Mudaliar, G.V. (2007) *Organic Corrosion Inhibitors*, Ph.D. Thesis, Gujarat University, Ahmedabad, India.

- [10] Jaeger, F.M. (1920) Some condensation products of aromatic aldehydes and amines, *Proceedings of Acad. Sci., Amsterdam*, 23 : 74-83.
- [11] Pearson, R.G. (1968) Hard and Soft acids and bases, HSAB, Part-1 fundamental principles, *J. Chemical. Ed.*, 45 : 581.
- [12] Brubaker, G.R., Beverley, P. and Phipps, P. (1979) Corrosion Chemistry, Am. Chem. Soc., Washington, pp-281.
- [13] Trivedi, P.T. (2009) *Inhibition of the Corrosion of Aluminium - Magnesium Alloy in Hydrochloric Acid*, Ph.D. Thesis, Gujarat University, Ahmedabad, India.
- [14] Hoar, T.P., Holiday and R.P. (1953) The inhibition by quinoline and thioureas of the acid dissolution of mild steel, 3 : 502-513.
- [15] Abdel, A.M.S. and Saiyed, A.El. (1981) Inhibiting effects of some organic onium compound on the corrosion of zinc in perchloric acid solutions, *Trans. SAEST.*, 16 : 197-207.
- [16] Lavine, I.N. (1988) *Physical Chemistry*, McGraw-Hill, New York, pp. 539.
- [17] Atkins, P.W. (1996) *The Elements of Physical Chemistry*, Oxford University Press, Oxford, pp. 282.
- [18] Putilova, I.N., Balezin, S.A., Barnnik, V.P. (1960) *Metallic Corrosion Inhibitors*, Pergamon Press, New York, pp. 27.



## GRAFTING OF BUTYL ACRYLATE ONTO SODIUM SALT OF PARTIALLY CARBOXYMETHYLATED GUAR GUM USING CERIC IONS

J.H. Trivedi\*, T.A. Bhatt<sup>1</sup> and H.C. Trivedi

Department of Chemistry, Sardar Patel University, Vallabh Vidynagar-388 120, Gujarat State, INDIA

<sup>1</sup>Department of Chemistry, M. S. University of Baroda, Vadodara

### ABSTRACT

The graft copolymerization of butyl acrylate (BA) onto sodium salt of partially carboxymethylated guar gum (Na-PCMGG,  $\overline{DS} = 0.497$ ) has been carried out using ceric ammonium nitrate (CAN) as a redox initiator in an aqueous medium. The optimal reaction conditions have been evaluated by successively varying reaction conditions viz. amount of the backbone, concentrations of initiator, nitric acid and monomer as well as reaction time and temperature. The influence of various reaction conditions on the grafting yields have also been discussed. The experimental results have been analyzed according to the kinetics scheme of graft copolymerization proposed earlier and results are found to be in very good agreement. The reactivity of butyl acrylate toward graft copolymerization has been compared with that of literature data reported in the case of other vinyl monomers and plausible explanation has been furnished. TGA/DSC techniques have been used to study the thermal behaviour of Guar Gum, Na-PCMGG,  $\overline{DS} = 0.497$ , Na-PCMGG-g-PBA and PBA samples and the results are discussed. The spectroscopic (IR) and Scanning Electron Microscopy (SEM) methods have been used to prove grafting.

**Key words:** Sodium salt of Partially Carboxymethylated Guar Gum, Butyl Acrylate, Graft Copolymerization, Infrared Spectroscopy (IR), Thermogravimetric Analysis (TGA), Differential Scanning Calorimetry (DSC) and SEM

### INTRODUCTION

Grafting reactions provide a potential route for significantly altering the physical and the chemical properties of a substrate polymer to specific end uses. Modification of guar gum properties by graft copolymerization of vinyl monomers using different initiating systems have been the subject of research for the last decade [1-6]. However, the data on grafting of vinyl monomers onto sodium salt of partially carboxymethylated guar gum (Na-PCMGG) are scanty. As a part of our comprehensive research programme we have, therefore, successfully carried out the modification of Sodium salt of Partially Carboxymethylated Guar Gum (Na-PCMGG,  $\overline{DS} = 0.497$ ) by grafting of methyl acrylate (MA) [7], acrylonitrile (AN) [8], methyl methacrylate (MMA) [9] and ethyl methacrylate (EMA) [10] using ceric ammonium nitrate (CAN) as a redox initiator. We have also used CAN as a photoinitiator and successfully grafted MMA onto Na-PCMGG ( $\overline{DS} = 0.291$ ) [11]. Recently, we have also compared the reactivity of different vinyl monomers towards grafting [12] and studied the effects of substrate structure and liquor ratio on percentage grafting [13] using the optimum reaction conditions established for affording maximum percentage of grafting of different vinyl monomers onto Na-PCMGG ( $\overline{DS} = 0.497$ ).

In the present investigation, we report the evaluation of the optimal reaction conditions for affording maximum percentage of grafting in the case of grafting of butyl acrylate (BA) onto Na-PCMGG ( $\overline{DS} = 0.497$ ) using CAN as a redox initiator and the results regarding characterization of the graft copolymer sample by IR, SEM and TGA/DSC techniques. This has been done not only to arrive at a good understanding of the kinetics and mechanism of grafting but also to obtain the basic information needed for the improvement of the products.

### EXPERIMENTAL

#### Materials

Guar Gum (GG) was kindly supplied by H.B. Gum Industries Pvt. Ltd.; Kalol (Gujarat/India). The method of preparation and purification as well as the measurement of degree of substitution ( $\overline{DS}$ ) of the Na-PCMGG were followed as described earlier [14-15]. The  $\overline{DS}$  of Na-PCMGG sample was

found to be 0.497. Butyl acrylate (BA) (Chiti-Chem. Corpn; Baroda, Gujarat State, India) was purified by extracting with aqueous sodium hydroxide solution and dried over sodium sulfate. The stabilizer free monomer was distilled and the middle fraction was used. Ceric Ammonium Nitrate and analar grade nitric acid (both Qualigens, Glaxo India Ltd.) were used without further purification. All other reagents and solvents used in the present work were of reagent grade. The nitrogen gas was purified by passing through fresh pyrogallol solution. The low conductivity water was used for the preparation of solutions as well as for polymerization reactions.

#### Graft Copolymerization

A 500 mL three-necked flask equipped with mechanical stirrer, reflux condenser and a glass inlet-system was immersed in a constant temperature bath for grafting reactions. In a typical reaction, varying amount (0.5g to 3.0g, dry basis) of Na-PCMGG ( $\overline{DS} = 0.497$ ) was dissolved in low conductivity water (100 mL) with constant stirring and bubbling a slow stream of nitrogen gas for 1h at the desired temperature (15°C to 50°C). Freshly prepared 10 mL solution of CAN ( $1.0 \times 10^{-2}$  M to  $8.0 \times 10^{-2}$  M) in nitric acid (nil to 0.8 M) was added and stirred for 20 min. Nitrogen gas was continuously passed through the reaction solution and freshly distilled BA (0.075 M to 0.70 M) was added. The grafting reactions were carried out for varying time intervals (0.5h to 10h). After the completion of the reaction, the mixture was immediately poured into excess of methanol. The crude copolymer product was filtered, repeatedly washed with nitric acid as well as 95% methanol and finally washed with pure methanol. The crude copolymer thus obtained was dried to constant weight in a vacuum oven at 40°C.

#### Extraction of Homopolymer

The coprecipitated ungrafted homopolymer, was extracted with acetone, in a soxhlet apparatus, for 48h to extract polybutylacrylate (PBA) from the crude graft copolymer. After complete removal of homopolymer, the pure graft copolymer was dried at 40°C under vacuum to a constant weight.

#### Isolation of Grafted Chains

The graft copolymer of Na-PCMGG ( $\overline{DS} = 0.497$ ) containing PBA was hydrolyzed by refluxing it for 12h in 1N

\*Corresponding author: drjignesh2575@yahoo.co.in

HCl as suggested by Brockway [16]. After all the Na-PCMGG went into the solution, resinous mass was obtained which was characterized by IR spectroscopy as PBA.

#### IR Spectroscopy

IR spectra of Guar Gum, Na-PCMGG ( $\overline{DS} = 0.497$ ), Na-PCMGG-g-PBA and PBA were taken in KBr pellets using Nicolet Impact 400 D Fourier Transform Infra Red Spectrophotometer.

#### Thermogravimetric Analysis (TGA)

The thermal behavior of Guar Gum, Na-PCMGG ( $\overline{DS} = 0.497$ ), Na-PCMGG-g-PBA and BA has been examined in an inert atmosphere at a heating rate of  $10^{\circ}\text{C}/\text{min}$  with the help of the Dupont 951 thermogravimetric analyzer.

#### Differential Scanning Calorimetry (DSC)

The DSC scans of Guar Gum, Na-PCMGG ( $\overline{DS} = 0.497$ ), Na-PCMGG-g-PBA and PBA have been recorded in nitrogen atmosphere at a scan rate of  $10^{\circ}\text{C}/\text{min}$  on DSC 2920 TA instrument.

#### Scanning Electron Microscopy (SEM)

Model ESEM TMP + EDAX, Philips make has been used to obtain the micrographs of Guar Gum, Na-PCMGG ( $\overline{DS} = 0.497$ ) and Na-PCMGG-g-PBA.

#### Grafting Yields and Kinetic Parameters

The grafting yields viz. percentage of grafting (%G) and percentage grafting efficiency (%GE) as well as the kinetic parameters viz. the rates of polymerization ( $R_p$ ), graft copolymerization ( $R_g$ ) and homopolymerization ( $R_h$ ) were evaluated by using expressions as reported earlier [17].

### RESULTS AND DISCUSSION

In the study of ceric ion-induced grafting of butyl acrylate (BA) onto Na-PCMGG ( $\overline{DS} = 0.497$ ), various reaction conditions were used to discover those optimum for grafting. The reaction conditions studied included amount of Na-PCMGG, concentrations of ceric ammonium nitrate (CAN), nitric acid ( $\text{HNO}_3$ ) and monomer (BA) as well as reaction time and temperature.

#### Effect of Backbone concentration

The influence of backbone concentration on the grafting yields is represented in Fig. 1. It can be seen from this figure that %G consistently decreases with the increasing amount of Na-PCMGG but the value of %GE remains almost constant over the whole range of Na-PCMGG studied. The observed variation in %G could be attributed to the fact that even though with the increase in Na-PCMGG concentration the weight of the grafted side chains may increase but the decrease in the monomer-to-backbone ratio lowers %G. In addition to this, large number of Na-PCMGG macroradicals interact with each other to terminate the reaction as a result of which the termination rate of graft copolymerization becomes faster compared to that of initiation thereby also lowering %G. Similar results are also reported in

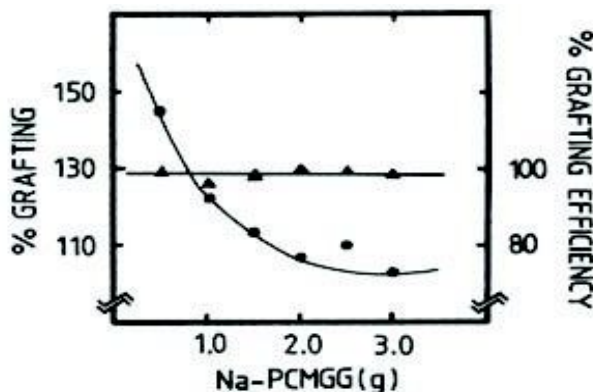


Figure 1: Effect of amount of Na PCMGG on :  
 (●) - %G and (▲) - %GE

the case of grafting of butyl acrylate onto gelatin [18], acrylonitrile onto sodium alginate [19] as well as onto sodium salt of partially carboxymethylated guar gum [8].

#### Effect of Initiator Concentration

Fig. 2 shows the influence of the initiator concentration on the grafting yields. The value of %G increases with increasing ceric-ion concentration and reaches a maximum value of 186.38 at  $[\text{Ce}^{+4}] = 0.06 \text{ mol/L}$  but with further increase in  $[\text{Ce}^{+4}]$ , %G decreases. However, the value of %GE remains almost constant over the whole range of initiator concentration studied. The observed increase in %G within the initiator concentration range of 0.01-0.06 mol/L may be due to the fact that within this concentration range the increasing concentration of ceric ions results in an increase in the total number of the complex Na-PCMGG-ceric ions which decompose to give more active sites on the backbone upon which grafting of BA takes place. Beyond  $[\text{Ce}^{+4}] = 0.06 \text{ mol/L}$ , the observed decrease in %G is attributed to the fact that at higher concentration of the initiator the complex formation between the monomer and ceric ion assumes predominance over that between Na-PCMGG and ceric ion leading to the formation of homopolymer at the cost of grafting. Similar results are also observed in the literature [10, 19-21].

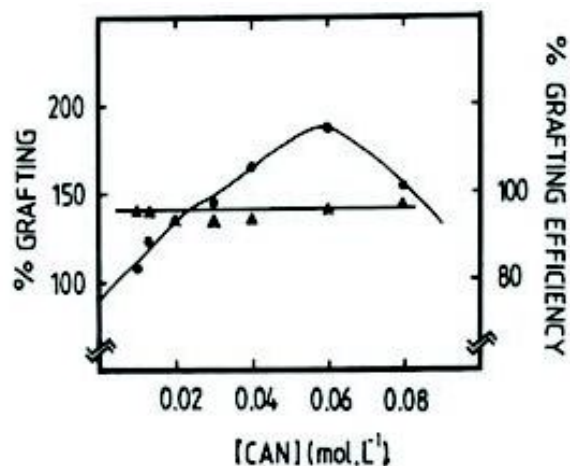


Figure 2: Effect of ceric ammonium nitrate concentration on :  
 (●) - %G and (▲) - %GE

#### Effect of Nitric acid Concentration

The effect of nitric acid concentration on the grafting yields is shown in Fig. 3. Even at the zero concentration of nitric acid interestingly higher value of grafting is observed which is due to the fact that even in the absence of acid in an aqueous medium Na-PCMGG swells to a greater extent making the functional groups of Na-PCMGG more accessible towards grafting. As seen from this figure there exists an optimum concentration of  $[\text{HNO}_3] = 0.2 \text{ M}$ . Beyond this optimum value, the value of %G decreases and approaches the value which is even lower than in the absence of acid. The ceric-ion exists as  $\text{Ce}^{+4}$ ,  $[\text{Ce}(\text{OH})_3]^{+3}$  and  $[\text{Ce-O-Ce}]^{+6}$  in an aqueous solution and the concentrations of these species vary with the concentration of acid. The species like  $\text{Ce}^{+4}$  and  $[\text{Ce}(\text{OH})_3]^{+3}$  having smaller sizes facilitate the formation of a complex with Na-PCMGG resulting in an increase in %G as observed in Fig. 3. However, beyond the optimum concentration in addition to these species, an abundance of hydrogen protons which are generated at higher acid concentration accelerate the termination of growing grafted chains resulting in a decrease in %G as evidenced in Fig. 3. Moreover, ceric ion leads to the oxidative termination of the growing monomeric chains as per the following reaction [22-25]:



as a result of which also the decrease in %G is observed beyond the optimum concentration.

**Effect of Monomer Concentration**

The effect of butyl acrylate concentration on the grafting yields is shown in Fig. 4. It can be seen from this figure that with an increase in the monomer concentration the value of percentage grafting increases and reaches a maximum value of 128.44% at [BA] = 0.3 mol/L. However, further increase in monomer concentration leads to a decrease in %G. On the other hand the value of %GE decreases very slowly upto the optimum concentration of the monomer and remains almost constant with further increase in the monomer concentration. The observed decrease in %G with increasing monomer concentration could be ascribed to the greater availability of grafting sites to monomer. However, the decreasing trend of %G beyond [BA] = 0.3 mol/L is due to the competition between the homopolymerization and grafting where the former prevails over the latter at higher monomer concentration. In addition to this the excess monomer will also shield the graft copolymer radicals which are formed leading to inhibition of the rate of graft copolymerization. Similar results are also reported in the case of grafting of MMA onto silk fibers [26] as well as onto sodium salt of partially carboxymethylated guar gum [9].

**Effect of Reaction Time**

The results of Fig. 5 show the effect of the reaction time on the grafting yields. It can be observed from this figure that a value of 104.68% has been obtained for percentage grafting during first half an hour but thereafter the value increases up to a maximum of 125.36% within 2h. The increase in %G is due to the increase in the number of grafting sites on the Na-PCMGG backbone as reaction progresses. However, beyond the optimum value of reaction time i.e.2h, the value of %G decreases which is attributed to the depletion of monomer and initiator as well as shortage of

the available grafting sites. When the reaction progresses, as observed from this figure the %G increases, even though the value of %GE decreases upto 2h because homopolymer is still forming. However, after 2h it is found to be increased up to 3h beyond which it almost levels off.

Fig. 6 represents the plot of log%G versus log(time) from which it can be seen that %G increases linearly for the first 2h, beyond which it decreases indicating that 2h is the optimum time for grafting.

**Effect of Temperature**

Fig. 7 represents the results regarding the influence of temperature on the grafting yields. As it can be seen from this

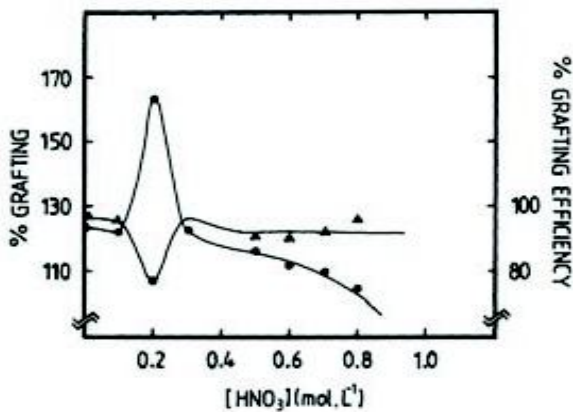


Figure 3: Effect of nitric acid concentration on :  
 (●) - %G and (▲) - %GE

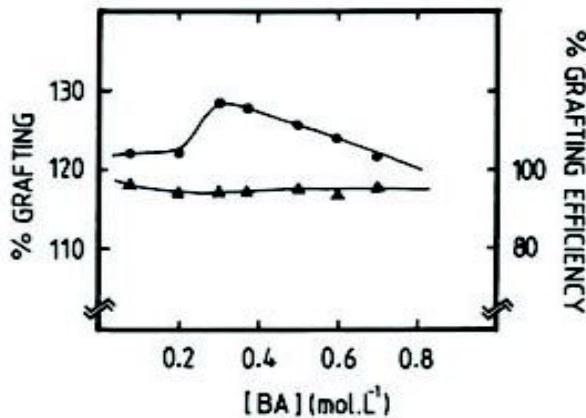


Figure 4: Effect of Butyl Acrylate (BA) concentration on:  
 (●) - %G and (▲) - %GE

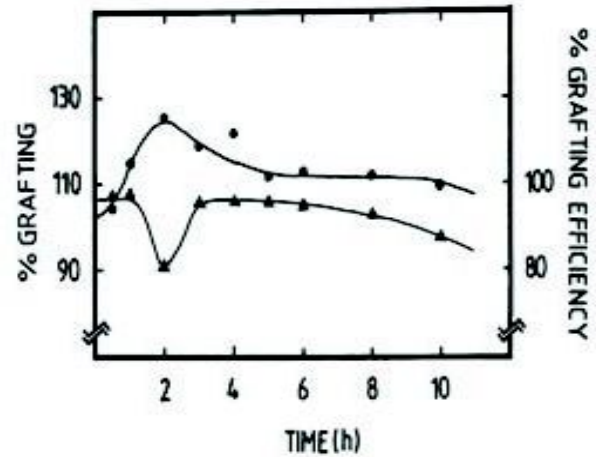


Figure 5: Influence of reaction time on :  
 (●) - %G and (▲) - %GE

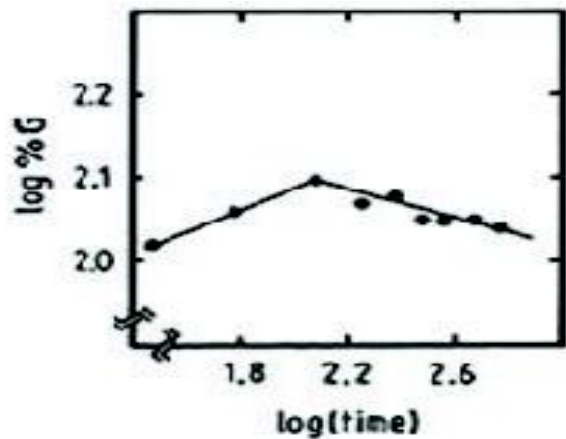


Figure 6: Plot of log %G versus log (time)

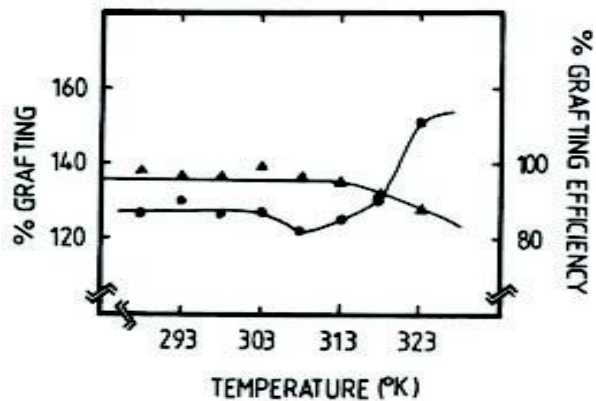


Figure 7: Influence of temperature on :  
 (●) - %G and (▲) - %GE

figure that %G remains almost constant up to 30°C and then decreases slowly up to 35°C beyond which it increases continuously up to 50°C. On the other hand %GE remains almost constant from the very beginning up to 40°C and then decreases very slowly with further rise in temperature. The observed increase in percentage grafting beyond 35°C can be attributed to the faster decomposition of Na-PCMGG-Ceric complex so that more active sites are generated on the backbone leading to the increase in the rates of initiation and propagation of grafting. However, the observed decrease in %GE beyond 40°C could be ascribed to the fact that at higher temperature graft copolymerization occurs with poor selectivity.

#### Effect of Liquor Ratio

The results regarding the influence of liquor ratio on %G are tabulated in Table 1. It can be observed from this table that there is a continuous increase in %G from 102.50% to 144.68%, at a slower rate with the increase in the liquor ratio from 50 to 300 ml. soln./g. Na-PCMGG, except for the liquor ratio value 75. This observation can be explained on the basis of the fact that as the value of the liquor ratio decreases, the viscosity of medium increases which, in turn, hinders the movement of free radicals thereby decreasing %G. Thus, from the above discussion the optimized reaction conditions evaluated in the graft copolymerization of BA are : Na-PCMGG ( $\overline{DS} = 0.497$ ) = 2.0 g (dry basis); [CAN] = 0.06 mol/L; [HNO<sub>3</sub>] = 0.20 mol/L; [BA] = 0.30 mol/L; Time = 2h; Temperature; = 40°C; Volume of Water = 133.55 ml; and Total Volume = 150 mL.

**Table 1 :** Effect of Liquor ratio on % grafting of butyl acrylate (BA) onto Sodium salt of Partially Carboxymethylated Guar Gum (Na-PCMGG),

Liquor ratio mL soln./g, Na -PCMGG	%Grafting (%G)
300 : 1	144.68
150 : 1	121.99
100 : 1	113.07
75 : 1	106.52
60 : 1	109.84
50 : 1	102.50

<sup>a</sup>mL solution per g Na-PCMGG = Varied as shown; [CAN] = 0.013 mol/L; [HNO<sub>3</sub>] = 0.10 mol/L; [BA] = 0.075 mol/L; Time = 4 h; Temperature = 35°C; Volume of Water = 138.40 mL; Total Volume = 150 mL.

#### KINETICS AND MECHANISM

The hydroxyl groups and carboxylate anions which are present in Na-PCMGG form a complex with ceric-ions and the complex may dissociate giving rise to free radicals onto Na-PCMGG. The mechanism of free radical graft copolymerization of BA onto Na-PCMGG ( $\overline{DS} = 0.497$ ) is expected to proceed according to the scheme, which has been proposed earlier by us [27]. The present experimental results, as tabulated in Tables 2 and 3, have been treated in light of the proposed kinetic scheme and accordingly the plot of  $R_g$  versus  $[CAN]^{0.5}$  should be linear at lower [CAN]. Such type of typical plot obtained in the present case is shown in Fig. 8 which is found to be linear at lower [CAN], indicating that termination takes place by recombination of double radicals.

However, the plot deviates from linearity at higher initiator concentration further indicating that the termination occurs by single radical leading to the decrease in the rate of graft copolymerization. The influence of the concentration of the monomer (BA) as well as that of the initiator (CAN) on the overall rate of polymerization ( $R_p$ ) as expected from the relationship derived earlier [27] is exemplified in Fig. 9. As evident, the plots of  $R_p$  versus  $[M]^2$  and  $R_p$  versus  $1/[Ce^{4+}]$  are

found to be linear for the present case, supporting the proposed kinetic scheme [27].

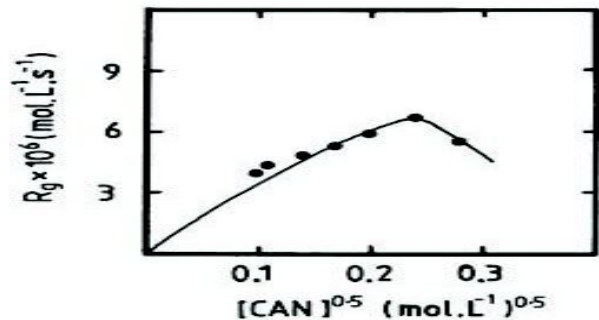


**Figure 8:** Plot of (●)  $R_g \times 10^6$  versus  $[CN]^{0.5}$

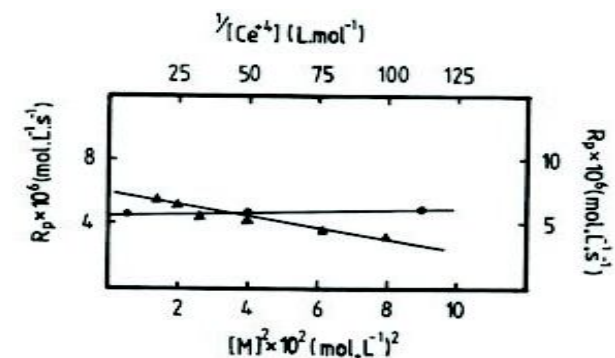


**Figure 9:** Plots of (●)  $R_p \times 10^6$  versus  $[M]^2$  and (▲)  $R_p \times 10^6$  versus  $1/[Ce^{4+}]$

**Table 2 :** Rates of graft copolymerization ( $R_g$ ) and polymerization ( $R_p$ ) for grafting of BA onto Na-PCMGG ( $\overline{DS} = 0.497$ ) at various initiator concentrations<sup>a</sup>.

[CAN] X 10 <sup>3</sup> (mol.L <sup>-1</sup> )	$R_p \times 10^6$ (mol.L <sup>-1</sup> .s <sup>-1</sup> )	$R_g \times 10^6$ (mol.L <sup>-1</sup> .s <sup>-1</sup> )
10.0	4.06	3.90
13.0	4.57	4.41
20.0	5.19	4.88
30.0	5.56	5.26
40.0	6.31	5.96
60.0	7.00	6.73
80.0	5.71	5.54

<sup>a</sup>Na-PCMGG ( $\overline{DS} = 0.497$ ) = 1.0 g (dry basis), [CAN] = Varied as shown; [HNO<sub>3</sub>] = 0.10 mol/L; [BA] = 0.075 mol/L; Time = 4h; Temperature = 35°C; Volume of water = 138.40 mL and Total volume = 150 mL.

**Table 3:** Rate of polymerization ( $R_p$ ) for grafting of BA onto Na-PCMGG ( $\overline{DS} = 0.497$ ) at various monomer concentrations<sup>a</sup>.

[BA] (mol.L <sup>-1</sup> )	$R_p \times 10^6$ (mol.L <sup>-1</sup> .s <sup>-1</sup> )
0.075	4.57
0.200	4.71
0.300	4.93

<sup>a</sup>Na-PCMGG ( $\overline{DS} = 0.497$ ) = 1.0 g (dry basis), [CAN] = 0.013 mol/L; [HNO<sub>3</sub>] = 0.10 mol/L; [BA] = Varied as shown; Time = 4h; Temperature = 35°C; Volume of water = 138.40 mL and Total volume = 150 mL.

### REACTIVITY OF VINYL MONOMERS

The maximum values of the grafting yields evaluated in the present case, under the evaluated optimum reaction conditions as discussed above, are tabulated in Table 4 along with those obtained in the case of grafting of MA and MMA onto Na-PCMG (DS= 0.497) earlier [7, 9] with a view to compare the reactivity of different vinyl monomers towards grafting. The perusal of the results of Table 4 shows the reactivity of different vinyl monomers varies towards grafting as per the following order:



With MMA, the extra  $-\text{CH}_3$  at the vinylic position probably offers some more steric hindrance than MA and this is why MMA is found to be less reactive than MA. In the case of BA, the butyl group attached to the ester moiety offers greater steric hindrance making it less reactive than MMA towards grafting onto Na-PCMG (DS=0.497).

### EVIDENCE OF GRAFTING

IR spectra of Na-PCMG (DS = 0.497) and its graft copolymer, Na-PCMG-g-PBA (not shown) have been compared to ascertain grafting. The IR spectrum of Na-PCMG-g-PBA showed absorption bands of Na-PCMG as well as an additional strong absorption band at  $\sim 1730 \text{ cm}^{-1}$  assigned to C=O stretching of ester group ( $-\text{COOCH}_3$ ), characteristic of the methacrylates. Moreover, the graft copolymer was hydrolyzed in order to isolate grafted PBA chains and the IR spectrum (not shown) of it showed the presence of C=O stretching at  $\sim 1730 \text{ cm}^{-1}$  indicating that hydrolysis of the graft copolymer gives back butyl acrylate. This also provides a substantial evidence of grafting of BA onto Na-PCMG (DS=0.497).

Fig. 10 and 11 represent the scanning electron micrographs of Na-PCMG (DS = 0.497) and Na-PCMG-g-PBA respectively. Upon comparison of the scanning electron micrograph of Na-PCMG-g-PBA (Fig. 11) with that of the ungrafted sample (Fig. 10) it is clearly evident that the grafted chains (PBA) have drastically changed the topology of the sample Na-PCMG indicating that grafting has taken place.

**Table 4 :** Maximum values of the grafting yields obtained in the case of grafting of different vinyl monomers onto Sodium salt of Partially Carboxymethylated Guar Gum (Na-PCMG, DS = 0.497) under the optimum reaction conditions<sup>acc</sup>.

Monomer	%Grafting (%G)	%Grafting Efficiency (%GE)	Reference
MA	206.00	85.99	7
MMA	172.38	97.15	9
BA	150.15	82.51	Present Work

Optimum Reaction Conditions for :

- MA :**  
Na-PCMG (DS = 0.497) = 0.5 g (dry basis), [CAN] = 0.06 mol/L; [HNO<sub>3</sub>] = 0.40 mol/L; [MA] = 0.147 mol/L; Time = 3h; Temperature = 30°C; Volume of water = 138 mL and Total volume = 150 mL.
- MMA :**  
Na-PCMG (DS = 0.497) = 1.0 g (dry basis), [CAN] = 0.03 mol/L; [HNO<sub>3</sub>] = 0.20 mol/L; [MMA] = 0.222 mol/L; Time = 4h; Temperature = 25°C; Volume of water = 136.45 mL and Total volume = 150 mL.
- BA :**  
Na-PCMG (DS = 0.497) = 2.0 g (dry basis), [CAN] = 0.06 mol/L; [HNO<sub>3</sub>] = 0.20 mol/L; [BA] = 0.30 mol/L; Time = 2h; Temperature = 40°C; Volume of water = 133.55 mL and Total volume = 150 mL.

### Thermogravimetric Analysis (TGA)

Fig. 12 represents the primary thermograms for Guar Gum and Na-PCMG (DS = 0.497), obtained at a scan rate of 10°C/min in an inert atmosphere. The overall degradation of Guar Gum (Fig. 12) involves only single step. The sample begins to decompose at 175°C, rapidly loses 60% of its weight up to 285°C. Beyond 285°C, the weight loss is slow and gradual up to about 700°C, leaving 16% residual weight. In the temperature range 285°C-700°C, the sample loses 24% of its original weight. The maximum rate of weight loss occurs at 275°C. It can be further seen from this figure that the single step degradation of Na-PCMG sample begins at 160°C and proceeds at a faster rate up to 270°C and the sample loses 45% of its original weight at this temperature. However, beyond this temperature degradation proceeds at a very slow rate up to 570°C. This temperature range (i.e. 270-570°C) involves about 18% weight loss. With further increase in temperature, the degradation is found to occur at a relatively fast rate up to 700°C, compared to the degradation found to be proceeded in the earlier temperature range. The temperature at which the maximum rate of weight loss occurs is 265°C. The overall degradation leaves about 14.5% residue. Figure 13 represents the primary thermograms obtained for Na-PCMG (DS = 0.497), Na-PCMG-g-PBA (%G = 150.15) and PBA at a scan rate of 10°C/min in an inert atmosphere. It is evident from this figure that the overall degradation of Na-PCMG-g-PBA exhibits two steps. The sample begins to



**Figure 10 :** Scanning Electron Micrograph of Na-PCMG (DS = 0.497) (400X)

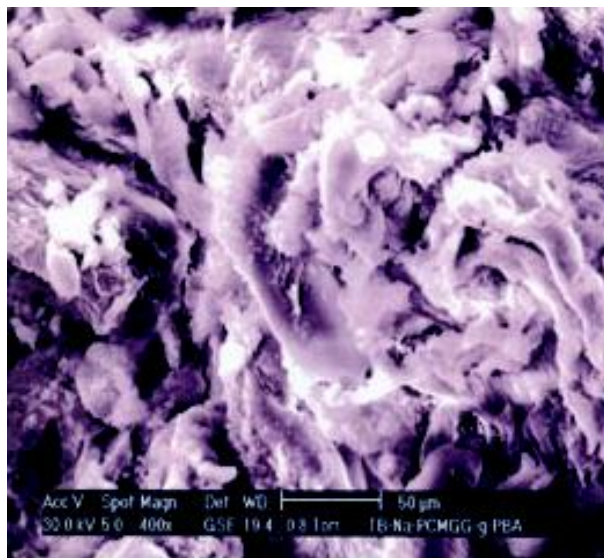


**Figure 11 :** Scanning Electron Micrograph of Na-PCMG-g-PBA (%G = 150.15%) (400X)

decompose at about 130°C and loses its weight very rapidly up to 310°C during which the sample loses 45% of its weight. The second decomposition step is immediately followed and found to be proceeded with a slow rate up to 420°C involving about 31% weight loss. The maximum rates of weight loss for the first and second decomposition steps are 245°C and 350°C respectively. The degradation is completed at about 420°C leaving behind about 23% residual weight. On the other hand in the case of PBA, the overall degradation exhibits only single step which commences from 180°C, followed by a very slow decrease in weight upto 315°C. Beyond 315°C, there is a steep weight loss involving about 69% upto 375°C, with a maximum rate of weight loss at 345°C. With further increase in temperature beyond 375°C, the degradation proceeded slowly up to 490°C. The sample leaves about 4.5% char yield.

The temperature characteristic values as well as the Integral Procedural Decomposition Temperature (IPDT) values of Guar Gum, Na-PCMGG ( $\overline{DS} = 0.497$ ), Na-PCMGG-g-PBA (%G = 150.15) and PBA are tabulated in Table 5. The examination of IPDT values indicates that the overall thermal stability of Guar Gum has been increased upon its carboxymethylation which may be due to the introduction of the polar groups into guar gum leading to the increased intermolecular and intra-molecular interactions which ultimately imparts higher thermal stability to it. However, the observed decrease in the thermal stability of the graft copolymer i.e. Na-PCMGG-g-PBA compared to Na-PCMGG ( $\overline{DS} = 0.497$ ) is attributed to the tendency of the polyacrylates to undergo depolymerization upon pyrolysis [28].

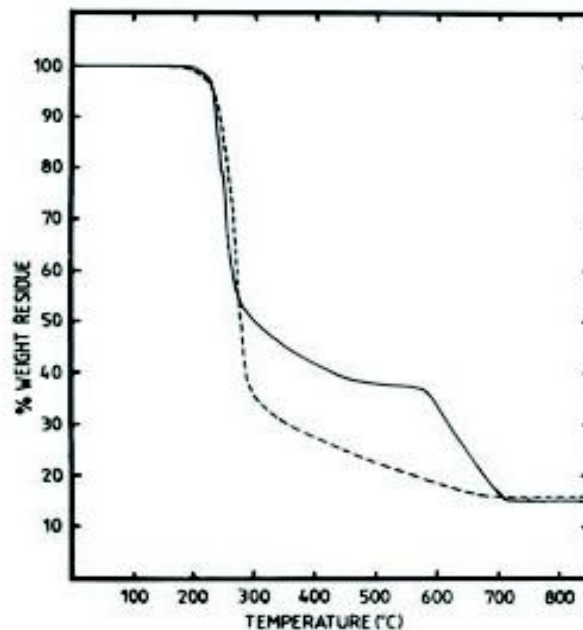


Figure 12 : TG thermograms for (---) Guar Gum and (-) Na-PCMGG ( $\overline{DS} = 0.497$ )

Table 5 : Thermal Analysis of Guar Gum, Na-PCMGG ( $\overline{DS} = 0.497$ ), Na-PCMGG-g-PBA (%G = 150.15) and PBA samples.

Sample	Thermogravimetric Analysis Data							Transition Data from DSC	
	$T_i$ °C (IDT)	$T_f$ °C (FDT)	$T_{max}$		$T_{10}$ (°C)	$T_{50}$ (°C)	IPDT (°C)	$T_1$ (°C)	$T_2$ (°C)
			Step 1	Step 2					
Guar Gum	175	700	275	-	240	275	401.33	145.15 (endo)	308.44 (exo)
Na-PCMGG	160	700	265	-	230	295	436.75	177.50 (endo)	282.18 (exo)
Na-PCMGG -g-PBA (%G = 150.15)	130	420	245	350	215	315	271.95	133.70 (endo)	269.44 (exo)
PBA	180	490	345	-	305	345	314.29	-	-

### Differential Scanning Calorimetry

The transition temperature data of Guar Gum, Na-PCMGG ( $\overline{DS} = 0.497$ ), Na-PCMGG-g-PBA (%G = 150.15) and PBA samples obtained from their respective DSC thermograms (not shown) are also tabulated in Table 5. It can be observed from the results of this table that Guar Gum shows an endothermic peak at 145.15°C and an exothermic peak at 308.44°C. The observed endothermic peak may be due to the melting of guar gum and the exothermic peak is due to the decomposition of it. On the other hand for the case of Na-PCMGG sample the endothermic transition appeared at 177.50°C and the exothermic transition observed at 282.18°C are attributed respectively to the melting and the decomposition of the sample. The endothermic peak observed at 133.70°C and the exothermic transition appeared at 269.44°C in the case of the Na-PCMGG-g-PBA sample is attributed to the gross melting and the decomposition of the sample. It is interesting to note that the DSC studies in comparison with TGA results also confirm the decrease in the thermal stability of Na-PCMGG due to grafting of BA onto it.

### CONCLUSIONS

The optimized reaction conditions have been evaluated successfully in the case of grafting of butylacrylate onto Na-PCMGG ( $\overline{DS} = 0.497$ ) using CAN as a redox initiator. The effect of various reaction conditions on the grafting yields has been discussed. The experimental results are found to be in very

good agreement with the kinetic scheme proposed earlier. The reactivity of BA towards grafting has been compared with other monomers and the plausible explanation has been furnished. TGA/DSC techniques have been used to characterize Guar Gum as well as Na-PCMGG ( $\overline{DS} = 0.497$ ) and its graft copolymer (Na-PCMGG-g-PBA) and the results are discussed. The overall thermal stability of Guar Gum has been increased upon its carboxymethylation but it is decreased upon grafting of BA onto Na-PCMGG ( $\overline{DS} = 0.497$ ). DSC studies also confirm about the decrease in the thermal stability of Na-PCMGG upon grafting of BA onto it. The evidence of grafting has been successfully ascertained by the spectroscopic (IR) and SEM techniques.

### ACKNOWLEDGEMENT

The authors thank Prof. Dr. Yong Huang, Deputy Director of Technical Institute of Physics & Chemistry, CAS and Director of National Research Center for Engineering Plastics, Beijing, China for the constructive and valuable suggestions for the preparation of this manuscript.

### References

- [1] Bihari, K., Tripathi, M. and Taunk, K. (1999)  $Cu^{2+}$ /mandelic acid redox pair initiated graft copolymerization acrylamide onto guar gum. *Journal of Applied Polymer Science*, **71**: 739-745.

- [2] Bihari, K., Tripathi, M., Taunk, K. and Kumar, R. (2000) Studies of graft copolymerization of acrylamide onto guar gum using peroxydiphosphate–metabisulphite redox pair. *Polymer International*, **49**: 153-157.
- [3] Srivastava, A. and Bihari, K. (2007) Synthesis, Characterization and Study of Metal Ion Sorption Capacity and Water Swelling Behavior of Xanthan Gum-g-N,N'-Dimethylacrylamide. *Journal of Macromolecular Science, Part A: Pure and Applied Chemistry*, **44**: 453-462.
- [4] Taunk, K. and Behari, K. (2000) Graft copolymerization of acrylic acid onto guar gum. *Journal of Applied Polymer Science*, **77**: 39-44.
- [5] Bihari, K., Kumar, R., Tripathi, M. and Pandey, P. (2001) Graft Copolymerization of Methacrylamide onto Guar Gum using a Potassium Chormate/Malonic Acid Redox Pair *Macromolecular Chemistry and Physics*, **202**: 1873-1877.
- [6] Chowdhury, P., Samui, S., Kundu, T. and Nandi, M. (2001) Graft polymerization of methyl methacrylate onto guar gum with ceric ammonium sulfate/dextrose redox pair. *Journal of Applied Polymer Science*, **82**: 3520-3525.
- [7] Trivedi, J., Kalia, K., Patel, N. and Trivedi, H. (2005) Modification of Sodium salt of Partially Carboxymethylated Guar Gum by Graft Copolymerization with Methyl Acrylate. *Polymers and Polymer Composites*, **13**: 301-312.
- [8] Trivedi, J., Kalia, K., Patel, N. and Trivedi, H. (2005) Ceric-Induced Grafting of Acrylonitrile onto Sodium salt of Partially Carboxymethylated Guar Gum. *Carbohydrate Polymers*, **60**: 117-125.
- [9] Trivedi, J., Kalia, K., Patel, N. and Trivedi, H. (2005) Graft Copolymerization of Sodium Salt of Partially Carboxymethylated Guar Gum with Methyl Methacrylate: An examination of Reaction Variables. *Journal of Applied Polymer Science*, **96**: 1855-1864.
- [10] Trivedi, J., Kalia, K., Patel, N. and Trivedi, H. (2008) Grafting of Ethyl Methacrylate onto Sodium salt of Partially Carboxymethylated Guar Gum by Tetravalent Cerium Ion. *Journal of Polymer Materials*, **25**: 541-555.
- [11] Thakar, M. and Trivedi, H. (2005) Ultraviolet-radiation-induced graft copolymerization of methyl acrylate onto the sodium salt of partially carboxymethylated guar gum. *Journal of Applied Polymer Science*, **97**: 1977-1986.
- [12] Trivedi, J., Kalia, K., Patel, N. and Trivedi, H. (2005) Grafting of Vinyl Monomers onto Sodium salt of Partially Carboxymethylated Guar Gum: Comparison of Their Reactivity. *Polymer- Plastics Technology & Engineering*, **44**: 407-425.
- [13] Trivedi, J., Kalia, K., Patel, N. and Trivedi, H. (2005) Ceric-Induced Grafting of Vinyl Monomers onto Sodium salt of Partially Carboxymethylated Guar Gum: Effects of Substrate Structure and Liquor Ratio. *Journal of Pure & Applied Sciences-“PRAJNA” (Sardar Patel University Journal)*, **13**: 44-55.
- [14] Joshi, K., Sinha, V., Patel, C. and Trivedi, H. (1995) Ceric-Induced Grafting of Acrylonitrile onto Sodium Salt of Partially Carboxymethylated Starch. *Journal of Macromolecular Science, Pure and Applied Chemistry*, **A32**: 133-146.
- [15] Trivedi, H., Patel, C. and Patel, R. (1978) Polarographic studies of ion binding, I. Cadmium carboxymethylcellulose. *Die Angew Makromol Chemie*, **70**: 39-48.
- [16] Brockway, C. and Seaberg, P. (1967) Grafting of polyacrylonitrile to granular corn starch. *Journal of Polymer Science Part A-1: Polymer Chemistry*, **5**: 1313-1326.
- [17] Vijaykumar M., Reddy, C. and Joseph, K. (1985) Grafting of poly(glycidyl methacrylate) onto alginic acid. *European Polymer Journal*, **21**: 415-419.
- [18] Chong, Li, Fong, Fu., Huang, M. and Lian, N. (1988) Graft Copolymerization of Butyl Acrylate onto Gelatin in the Presence of Ceric Ion. *Journal of Macromolecular Science, Part A: Pure and Applied Chemistry*, **25**: 1487-1513.
- [19] Shah, S., Patel C. and Trivedi, H. (1992) Ceric-induced Grafting of Acrylonitrile onto Sodium Alginate. *High Performance Polymers*. **4**: 151-159.
- [20] Egboh, S. and Jinadu, B. (1988) Modification of starch by graft copolymerization with methyl methacrylate. *Die Angew Makromol Chemie*. **163**: 93-99.
- [21] Shah, S., Patel, C. and Trivedi, H. (1994) Ceric-induced grafting of ethyl-acrylate onto sodium alginate. *Die Angew Makromol Chemie*. **214**: 75-89.
- [22] Collision, E. and Dainton, F. (1956) Termination of Chains in Vinyl Polymerization by Metal Salts. *Nature*, **177**: 1224-1225.
- [23] Collision, E., Dainton, F. and McNaughton, G. (1957) The effect of acrylamide on the X- and  $\gamma$ -ray yields of hydrogen peroxide from de-aerated water. *Transactions of the Faraday Society*, **53**: 357-362.
- [24] Kantouch, A., Hebeish, A. and Bendak, A. (1971) Ce<sup>IV</sup> initiated graft polymerization of methyl methacrylate on wool fibres. *European Polymer Journal*, **7**: 153-163.
- [25] Saha, S. and Chaudhari, A. (1971) Effect of amines on the ceric ion-initiated polymerization of vinyl monomers I. Polymerization of acrylonitrile by ceric ion-triethylamine catalyst system. *Journal of Polymer Science Part A-1: Polymer Chemistry*, **9**: 1505-1516.
- [26] Mohanty, N., Pradhan, B., Mohanta, M. and Das, H. (1983) Grafting vinyl monomers on silk fibres—I. Graft copolymerization of methyl methacrylate on silk by tetravalent cerium ion. *European Polymer Journal*, **19**: 415-418.
- [27] Patel, B., Sinha, V. and Trivedi, H. (1991) Graft copolymerization of sodium salt of partially carboxymethylated amylose with acrylonitrile. *Journal of Polymer Materials*, **8**: 321-328.
- [28] Varma, D. and Sadhir, R. (1979) Radiation induced graft copolymerization of methyl methacrylate on natural and modified wool III. Thermal Behaviour. *Die Angew Makromol Chemie*, **81**: 179-191.



## SIMULTANEOUS EQUATION AND ABSORBANCE RATIO METHODS FOR ESTIMATION OF FLUOXETINE HYDROCHLORIDE AND OLANZAPINE IN TABLET DOSAGE FORM

Vijaykumar K. Parmar<sup>a,\*</sup>, Uday H. Thorat<sup>b</sup>, Girish K. Jani<sup>b</sup> and Laxman M. Prajapati<sup>c</sup>

<sup>a</sup>Department of Pharmaceutical Sciences, Sardar Patel University, Vallabh Vidyanagar – 388 120, INDIA

<sup>b</sup>SSR College of Pharmacy, Silvassa – 396 230, UT of Dadara and Nagar Haveli, INDIA

<sup>c</sup>Shri B. M. Shah College of Pharmaceutical Education and Research, College Campus, Modasa – 383 315, INDIA

### ABSTRACT

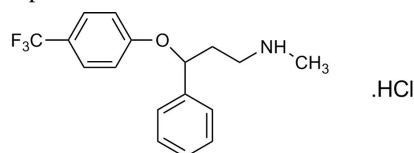
Fluoxetine hydrochloride (FH) and Olanzapine (OZ) combined tablet dosage form is used for the treatment of depressive episodes associated with bipolar disorder, called as manic depressive illness. Two spectrophotometric procedures for simultaneous estimation of FH and OZ from two component tablet dosage form have been developed. In the present investigation an attempt has been made to develop rapid and cost-effective procedures for simultaneous estimation of FH and OZ in pharmaceutical formulation. The first method is based on Vierodt's simultaneous equation method in which selected wavelengths are 225 nm and 258 nm, the wavelength maxima of FH and OZ, respectively. Additivity principle for the absorbances of FH and OZ at these selected wavelengths was validated. The second method is absorbance ratio method, wherein selected wavelengths are 236 nm and 258 nm, iso-absorptive point of both drugs and wavelength maximum of OZ, respectively. The adherence to Beer's law for both the drugs was checked by validating the linearity range at the selected wavelengths. The proposed methods were successfully applied to the estimation of FH and OZ in tablet formulations. The results suggested that the proposed procedures can be used for routine quality control of tablets containing FH and OZ.

**Key words:** simultaneous equation, absorbance ratio, fluoxetine hydrochloride, olanzapine, tablets

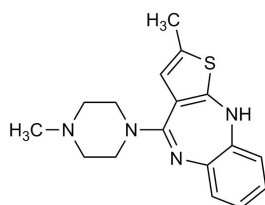
### 1. INTRODUCTION

Fluoxetine hydrochloride (FH) is a selective serotonin reuptake inhibitor which is one of the commonly prescribed drugs for treating depression [1]. Chemically, it is d,l-N-methyl-3-phenyl-3-[ $\alpha,\alpha,\alpha$ -trifluoro-p-tolyl]oxy]propyl amine hydrochloride. A survey of literature revealed that spectrophotometric[2,3], spectrofluorimetric[4,5], electrochemical[6], gas chromatography[7] and liquid chromatography [8-10] methods are reported for determination of FH from pharmaceutical formulation. Olanzapine (OZ), 2-methyl-4-(4-methyl-1-piperazinyl)-10H[2,3-b][1,5]benzodiazepine, is an antipsychotic medicine[11]. Spectrophotometric[12-16], linear voltametric[15], HPLC[15-17], capillary zone electrophoresis[16] methods are reported for determination of OZ from pharmaceutical dosage form. The chemical structures of FH and OZ are shown in Figure 1.

**Figure 1 :** Chemical structures of fluoxetine hydrochloride and olanzapine



Fluoxetine hydrochloride



Olanzapine

FH in combination with OZ is used in treatment of depressive episodes associated with bipolar disorder[18]. This combination of FH and OZ produce robust and sustained increases of extracellular levels of dopamine and norepinephrine, which were significantly greater than with either drug alone[19]. This combination drugs are available in tablet dosage form in the market. The combination of FH and OZ is not official in any pharmacopoeia. HPLC[20-23] and HPTLC[22,23] methods were reported in the literature for simultaneous determination of FH and OZ from combined dosage forms. However, the methods reported for simultaneous determination of these two drugs are found to be comparatively expensive and time consuming. No spectrophotometric method has been reported for the simultaneous determination of FH and OZ from combined dosage form. In the present investigation an attempt has been made to develop rapid and cost-effective procedures for simultaneous determination of FH and OZ in tablet dosage forms. The developed procedures are based on Vierodt's simultaneous equation and absorbance ratio methods. The proposed procedures were successfully applied for simultaneous determination of FH and OZ in tablet formulations that are available in market.

### 2. EXPERIMENTAL

#### 2.1 Instrumentation

A double beam HELIOS  $\alpha$  UV/Visible spectrophotometer with two matched quartz cells of 1 cm path length was used for spectral measurements.

#### 2.2 Chemicals and reagents

Fluoxetine hydrochloride (gift sample from Cadila Healthcare Pvt. Ltd., Ahmedabad, INDIA) and olanzapine (gift sample from Mangalam Organic Pvt. Ltd., Vapi, INDIA), hydrochloric acid (AR Grade, Finar Chemicals (India) Pvt. Ltd., Ahmedabad, India) and distilled water were used for the present study.

#### 2.3 Preparation of stock solutions

FH powder (100 mg) was accurately weighed and transferred to a 100 mL volumetric flask. It was dissolved and

\*Corresponding author: vijaykparmar@gmail.com

diluted to 100 mL with 0.1 N hydrochloric acid solution to obtain a stock solution of FH with final concentration of 1 mg/mL.

OZ powder (100 mg) was accurately weighed and transferred to a 100 mL volumetric flask. It was dissolved and diluted to 100 mL with 0.1 N hydrochloric acid solution to obtain a stock solution of OZ with final concentration of 1 mg/mL.

#### 2.4 Preparation of working standard solutions

Stock solution of FH (10 mL) was transferred to a 100 mL volumetric flask and diluted to 100 mL with 0.1 N hydrochloric acid solution to obtain working standard solution of FH with final concentration of 100 µg/mL.

Stock solution of OZ (10 mL) was transferred to a 100 mL volumetric flask and diluted to 100 mL with 0.1 N hydrochloric acid solution to obtain working standard solution of OZ with final concentration of 100 µg/mL.

#### 2.5 Procedure I – Simultaneous equation method

##### 2.5.1 Wavelength selection

The standard solutions of FH (10 µg/mL) and OZ (2.5 µg/mL) were scanned in the range of 200 to 400 nm to record the spectra. The wavelength maxima of FH and OZ were determined from the spectra recorded.

##### 2.5.2 Calibration curve for FH

Aliquots of working standard solution of FH (4, 8, 16, 24 and 30 mL) were transferred to series of 100 mL volumetric flask. The volume was made up to the mark with 0.1 N hydrochloric acid solution to obtain final concentration of 4, 8, 16, 24 and 30 µg/mL, respectively. The absorbance of each resulting solution was measured at 225 nm against 0.1 N hydrochloric acid solution. Calibration curve was constructed by plotting absorbance of FH against respective concentration. Regression equation for FH was calculated from calibration curve of FH.

##### 2.5.3 Calibration curve for OZ

Aliquots of working standard solution of OZ (1, 2, 4, 8 and 12 mL) were transferred to series of 100 mL volumetric flask. The volume was made up to the mark with 0.1 N hydrochloric acid solution to obtain final concentration of 1, 2, 4, 8 and 12 µg/mL, respectively. The absorbance of each resulting solution was measured at 258 nm against 0.1 N hydrochloric acid solution. Calibration curve was constructed by plotting absorbance of OZ against respective concentration. Regression equation for OZ was calculated from calibration curve of OZ.

##### 2.5.4 Validation of additivity principle

Working standard solutions of FH (16, 20, 24, 16, 20 and 24 mL) and OZ (4, 5, 6, 8, 10 and 12 mL) were transferred in series of 100 mL volumetric flasks, respectively. The mixture was shaken for 2 min and volume was made up to mark with 0.1 N hydrochloric acid solution. The absorbance of the resulting solutions was measured at 225 nm and 258 nm against 0.1 N hydrochloric acid solution. The observed values of absorbance were compared with values calculated from regression equations derived from calibration curves of FH and OZ at 225 and 258 nm, respectively.

#### 2.6 Procedure II – Absorbance ratio method

##### 2.6.1 Wavelength selection

The zero order spectra of FH and OZ were overlaid in spectrum SCAN mode. The iso-absorptive point was determined using TRACK function.

##### 2.6.2 Calibration curve for FH

Aliquots of working standard solution of FH (8, 16, 20, 24 and 30 mL) were transferred to series of 100 mL volumetric flask. The volume was made up to the mark with 0.1 N hydrochloric acid solution to obtain final concentration of 8, 16, 20, 24 and 30 µg/mL, respectively. The absorbance of each resulting solution was measured at 236 and 258 nm against 0.1 N hydrochloric acid solution. Calibration curve was constructed by plotting absorbance of FH at selected wavelengths against respective concentration. Regression equations for FH were calculated from calibration curves of FH at 236 and 258 nm.

##### 2.6.3 Calibration curve for OZ

Aliquots of working standard solution of OZ (2, 4, 8, 12 and 16 mL) were transferred to series of 100 mL volumetric flask. The volume was made up to the mark with 0.1 N hydrochloric acid solution to obtain final concentration of 2, 4, 8, 12 and 16 µg/mL, respectively. The absorbance of each resulting solution was measured at 236 and 258 nm against 0.1 N hydrochloric acid solution. Calibration curve was constructed by plotting absorbance of OZ at selected wavelengths against respective concentration. Regression equations for OZ were calculated from calibration curves of OZ at 236 and 258 nm.

#### 2.7 Analysis of sample

Twenty tablets were accurately weighed and finely powdered. Tablet powder equivalent to 5 mg of OZ was accurately weighed and transferred to 100 mL volumetric flask and 20 mL of 0.1 N hydrochloric acid solution was added. The mixture was sonicated for 30 min, diluted to 100 mL with 0.1 N hydrochloric acid solution and filtered through Whatman filter paper No. 41. The absorbance of resulting solution was measured at 225 and 258 nm for simultaneous equation method and at 236 and 258 nm for absorbance ratio method. The concentration of FH and OZ were found by fitting values of absorbance in the corresponding equations of simultaneous equation method and absorbance ratio method.

### 3. RESULTS AND DISCUSSION

#### 3.1 Simultaneous equation method

In this method, both the components (FH and OZ) were quantified using simultaneous equation to resolve the interference due to spectral overlapping of two components.

##### 3.1.1 Wavelength selection

Wavelength maxima ( $\lambda_{max}$ ) of FH and OZ in 0.1 N hydrochloric acid solution was selected for generation of simultaneous equation. The  $\lambda_{max}$  of FH and OZ were found to be 225 and 258 nm, respectively (Figure 2).

##### 3.1.2 Linearity of FH and OZ

The linearity of FH at 225 nm was found to be in the range of 4-30 µg/mL. The co-relation co-efficient was found to be

**Table 1 :** Linearity data for FH at 225 nm and OZ at 258 nm (n=5)

FH			OZ		
Concentration (µg/mL)	Absorbance (Mean± S.D.)	% C.V.	Concentration (µg/mL)	Absorbance (Mean± S.D.)	% C.V.
4	0.165±0.005	2.68	1	0.081±0.006	4.82
8	0.319±0.004	1.15	2	0.153±0.008	4.00
16	0.616±0.005	0.84	4	0.299±0.006	1.88
24	0.919±0.003	0.31	8	0.593±0.007	1.11
30	1.135±0.003	0.31	12	0.849±0.003	0.32

**Table 2 :** Results of checking additivity principle for FH and OZ at 225 and 258 nm (n=5)

Concentration ( $\mu\text{g/mL}$ )		Observed absorbance		Calculated absorbance	
FH	OZ	At 225 nm	At 258 nm	At 225 nm	At 258 nm
16	4	0.759	0.349	0.767	0.360
20	5	0.941	0.437	0.959	0.450
24	6	1.128	0.512	1.151	0.540
16	8	0.991	0.635	0.979	0.667
20	10	1.246	0.814	1.224	0.834
24	12	1.495	0.962	1.469	1.001

**Table 3. Absorption coefficients of FH and OZ**

Absorption coefficient ( $\epsilon$ )	In $\text{Lmol}^{-1}\text{cm}^{-1}$	In $\text{mLg}^{-1}\text{cm}^{-1}$
$\epsilon$ at 225 nm for FH	12000.77	347.00
$\epsilon$ at 236 nm for FH	4244.86	122.76
$\epsilon$ at 258 nm for FH	1152.89	33.30
$\epsilon$ at 225 nm for OZ	16582.50	530.60
$\epsilon$ at 236 nm for OZ	17585.16	562.83
$\epsilon$ at 258 nm for OZ	24000.00	768.00

0.9999. The linearity of OZ at 258 nm was found to be in the range of 1-12  $\mu\text{g/mL}$ . The co-relation co-efficient was found to be 0.9996. The average linear regressed equations for the corresponding curves were  $y=0.0373x+0.0183$  (FH) and  $y=0.0703x+0.0153$  (OZ). The linearity data for FH at 225 nm and OZ at 258 nm are shown in Table 1.

### 3.1.3 Additivity principle

Validation of additivity principle for the absorbances of FH and OZ at 225 nm and 258 nm was performed by measuring the absorbances of mixed solution of FH and OZ in the concentration ranges of 16-24  $\mu\text{g/mL}$  and 4-12  $\mu\text{g/mL}$ , respectively. The observed absorbances were found to be closer to the calculated value (Table 2).

### 3.1.4 Simultaneous equation

Absorption coefficients were calculated for FH and OZ at 225 and 258 nm, the wavelength maxima of FH and OZ, respectively (Table 3). The simultaneous equations derived for determination of concentration of FH and OZ are (Equation-1)  $\text{CFH} = (\epsilon\text{OZ1} \times \text{A225} - \epsilon\text{OZ2} \times \text{A258}) / (\epsilon\text{FH2} \times \epsilon\text{OZ1} - \epsilon\text{FH1} \times \epsilon\text{OZ2})$  and (Equation-2)  $\text{COZ} = (\epsilon\text{FH2} \times \text{A225} - \epsilon\text{FH1} \times \text{A258}) / (\epsilon\text{FH2} \times \epsilon\text{OZ1} - \epsilon\text{FH1} \times \epsilon\text{OZ2})$ , respectively, where, CFH = Concentration of FH in mol/lit, COZ = Concentration of OZ in mol/lit, A225 = Absorbance of mixture at 225 nm, A258 = Absorbance of mixture at 258 nm,  $\epsilon\text{FH1}$  = Absorption coefficient of FH at 225 nm,  $\epsilon\text{FH2}$  = Absorption coefficient of FH at 258 nm,  $\epsilon\text{OZ1}$  = Absorption coefficient of OZ at 225 nm,  $\epsilon\text{OZ2}$  = Absorption coefficient of OZ at 258 nm.

**Table 4 :** Linearity data for FH at 236 nm and 258 nm (n=5)

Concentration ( $\mu\text{g/mL}$ )	FH at 236 nm		FH at 258 nm	
	Absorbance (Mean $\pm$ S.D.)	% C.V.	Absorbance (Mean $\pm$ S.D.)	% C.V.
8	0.099 $\pm$ 0.003	3.096	0.020 $\pm$ 0.003	4.782
16	0.195 $\pm$ 0.004	2.065	0.040 $\pm$ 0.002	4.330
20	0.245 $\pm$ 0.006	2.388	0.051 $\pm$ 0.002	4.035
24	0.296 $\pm$ 0.004	1.472	0.065 $\pm$ 0.004	6.153
30	0.367 $\pm$ 0.006	1.680	0.078 $\pm$ 0.003	3.846

**Table 5 :** Linearity data for OZ at 236 nm and 258 nm (n=5)

Concentration ( $\mu\text{g/mL}$ )	OZ at 236 nm		OZ at 258 nm	
	Absorbance (Mean $\pm$ S.D.)	% C.V.	Absorbance (Mean $\pm$ S.D.)	% C.V.
2	0.115 $\pm$ 0.006	4.702	0.140 $\pm$ 0.005	4.052
4	0.227 $\pm$ 0.004	2.018	0.278 $\pm$ 0.002	0.903
8	0.449 $\pm$ 0.005	1.225	0.552 $\pm$ 0.005	1.028
12	0.659 $\pm$ 0.005	0.888	0.810 $\pm$ 0.009	1.172
16	0.898 $\pm$ 0.003	0.340	1.102 $\pm$ 0.008	0.726

### 3.2 Absorbance ratio method

In Absorbance ratio method, absorbances were measured at the iso-absorptive wavelength and maximum absorption wavelength of one of the drugs.

#### 3.2.1 Wavelength selection

The iso-absorptive point, wavelength at which FH and OZ show similar absorbance, was found to be 236 nm (Figure 2). The wavelength maximum of OZ, 258 nm, was selected as another wavelength for spectral measurement in absorbance ratio method.

**Figure 2 :** Overlain spectra of FH and OZ

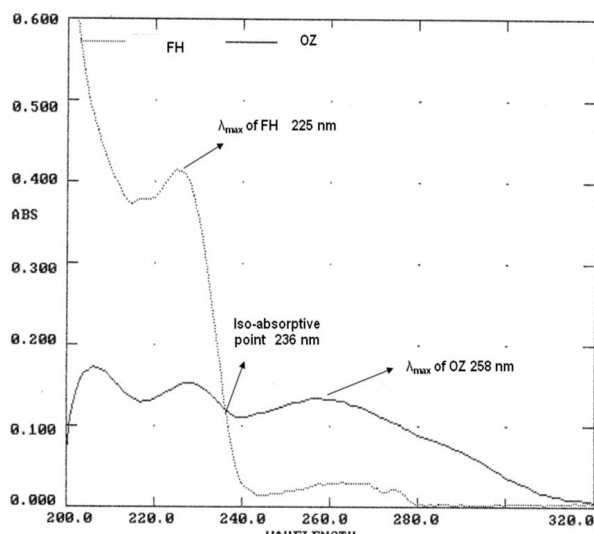


**Table 6 :** Assay of FH and OZ from combined tablet formulations

Tablet Formulation	Labeled value (mg)		Content of FH (% Label claim)		Content of OZ (% Label claim)	
	FH	OZ	SE <sup>#</sup>	AR <sup>\$</sup>	SE	AR
OLEANZ®PLUS	20	5	103.21	97.59	100.95	98.27
OLEANZ®FORTE	20	10	101.95	99.87	101.46	97.24
OLAPADPLUS	20	5	98.64	97.64	100.33	98.64

#SE = Simultaneous equation method

\$AR = Absorbance ratio method

### References

- [1] Risley, D.S. and Bopp, R.J. (2005) *Fluoxetine. In Analytical profiles of drug substances (Ed. Florey, K.), Academic Press, New York, 19, pp. 193-219.*
- [2] Naik, M.T., Rokad, M.D. and Dhadke, P.M. (1999) Extractive spectrophotometric estimation of fluoxetine hydrochloride in pharmaceutical formulations. *Indian J PharmSci*, **61**: 156.
- [3] Mandrioli, R., Pucci, V., Visini, D., Varani, G. and Raggi, M.A. (2002) Rapid methods for determination of fluoxetine in pharmaceutical formulations. *J Pharm Biomed Anal*, **29**: 1127.
- [4] Prabhakar, A.H., Patel, V.B. and Giridhar, R. (1999) Spectrophotometric determination of fluoxetine hydrochloride in bulk and in pharmaceutical formulations. *J Pharm Biomed Anal*, **20**: 427.
- [5] Berzas, J.J., Alañón, A. and Lázaro, J.A. (2002) Cyclodextrin enhanced spectrofluorimetric determination of fluoxetine in pharmaceuticals and biological fluids. *Talanta*, **58**: 301.
- [6] da Silva, A.R., Lima, J.C., Oliva Teles, M.T. and Oliveira Brett, A.M. (1999) Electrochemical studies and square wave adsorptive stripping voltammetry of the antidepressant fluoxetine. *Talanta*, **49**: 611.
- [7] Berzas Nevado, J.J., Berzas Nevado, M.J., Contento Salcedo, A.M. and Aguas Nuevo, E.J. (2000) Determination of Fluoxetine, Fluvoxamine, and Clomipramine in Pharmaceutical Formulations by Capillary Gas Chromatography. *Chromatogr Sci*, **38**: 200.
- [8] El-dawy, M.A., Mokhtar, M.M. and El-dawy, F.A. (2002) Liquid chromatographic determination of fluoxetine. *J Pharm Biomed Anal*, **30**: 561.
- [9] United States Pharmacopoeia 30, NF 25 (2007) United States Pharmacopoeial Convention, Rockville, MD. pp. 2165-2170.
- [10] British Pharmacopoeia (2007) Stationery Office, London. Vol. III, pp. 2593-2594.
- [11] Howland, R.D. and Mycek, M. J. (2005) *Lippincott's illustrated reviews – Pharmacology*. B. I. Publication Pvt. Ltd., London, pp. 150-153.

### 3.2.2 Linearity of FH and OZ at selected wavelength

Regression analysis for the Absorbance ratio method was carried out and the linearity of the calibration graph and adherence of the method to Beer's law was validated for FH and OZ at selected wavelengths (236 nm and 258 nm). The linearity data for FH at 236 nm and 258 nm are shown in Table 4. The correlation co-efficient was found to be 0.9999 and 0.9979, respectively. The linearity data for OZ at 236 nm and 258 nm are shown in Table 5. The co-relation co-efficient was found to be 0.9998 and 0.9998, respectively.

### 3.2.3 Absorbance ratio equation

The absorptivity coefficients of each at both wavelengths were determined (Table 3). The concentration of each drug in laboratory mixture and tablet formulation was determined by substituting the absorbance and absorptivity coefficients in following equations: Equation 3:  $C_x = (Q_m - Q_y) A / (Q_x - Q_y) A_{x1}$  and Equation 4:  $C_y = (Q_m - Q_x) A / (Q_y - Q_x) A_{y1}$ , where,  $C_x$  = concentration of FH,  $C_y$  = concentration of OZ,  $Q_m$  = ratio absorbance of sample at 236 and 258 nm wavelengths,  $Q_x$  = ratio of absorptivity coefficient of FH,  $Q_y$  = ratio of absorptivity coefficient of OZ,  $A_{x1}$  = absorptivity coefficient of FH at 236nm,  $A_{y1}$  = absorptivity coefficient of OZ at 236nm.

### 3.3 Analysis of Marketed Formulations

Quantitative determination of FH and OZ in tablets using proposed methods, simultaneous equation and absorbance ratio method, was performed and the results were in good agreement with the labeled amount of FH and OZ in (Table 6).

## 4. CONCLUSION

The proposed two procedures were developed and validated for quantitative determination of fluoxetine hydrochloride and olanzapine in tablets. The developed methods were found to be simple, rapid and economical. Results obtained for the analysis of marketed combined dosage forms were in good agreement with the labeled claim. The proposed methods can be utilized for the routine analysis of FH and OZ in tablet dosage form.

- [12] Basavaiah, K., Zenita, O., Tharpa, K., Nagaraju, R., Anilkumar, U.R., Hiriyana, S.G. and Vinay, K.B. (2009) Iodimetric assay of olanzapine in pharmaceuticals using iodate and Nile blue as reagents. *Chem Ind Chem Eng Quarterly*, **15**: 95.
- [13] Krebs, A., Starczewska, B., Puzanowska-Tarasiewicz, H. and Sledz, J. (2006) Spectrophotometric determination of Olanzapine by its Oxidation with N- Bromosuccinimide and Cerium(IV)sulfate. *Anal Sci*, **22**: 829.
- [14] Jasińska, A. and Nalewajko, E. (2004) Batch and flow-injection methods for the spectrophotometric determination of olanzapine. *Anal Chim Acta*, **2**: 165.
- [15] Biryol, I. and Erk, N. (2003) Voltammetric, spectrophotometric, and high performance liquid chromatographic analysis of olanzapine. *Anal Lett*, **36**: 2497.
- [16] Raggi, M.A., Casamenti, G., Mandrioli, R., Izzo, G. and Kenndler, E. (2000) Quantitation of olanzapine in tablets by HPLC, CZE, derivative spectrometry and linear voltammetry. *J Pharm Biomed Anal*, **23**: 973.
- [17] Prameela, R.A. and Bala, S.C. (2009) Development of HPLC method for the determination of Olanzapine in bulk and dosage forms. *Int J Pharm Tech Res*, **1**: 654.
- [18] Tohen, M., Vieta, E., Calabrese, J., Ketter, T.A., Sachs, G., Bowden, C., Mitchell, P.B., Centorrino, F., Risser, R., Baker, R.W., Evans, A.R., Beymer, K., Dube, S., Tollefson, G.D. and Breier, A. (2003) Efficacy of Olanzapine and Olanzapine-Fluoxetine Combination in the Treatment of Bipolar I Depression. *Arch Gen Psychiatry*, **60**: 1079.
- [19] Zhang, W., Perry, K.W., Wong, D.T., Potts, B.D., Bao, J., Tollefson, G.D. and Bymaster, F.P. (2000) Synergistic Effects of Olanzapine and Other Antipsychotic Agents in Combination with Fluoxetine on Norepinephrine and Dopamine Release in Rat Prefrontal Cortex. *Neuropsychopharmacology*, **23**: 250.
- [20] Reddy, B.V., Reddy, S., Sreeramulu, J. and Kanumula, G.V. (2007) Simultaneous Determination of Olanzapine and Fluoxetine by HPLC. *Chromatographia*, **66**: 111.
- [21] Phatak, A. and Rajput, S.J. (2009) Development of a stability-indicating HPLC method for simultaneous determination of olanzapine and fluoxetine in combined dosage forms. *J Chromatogr Sci*, **47**: 605.
- [22] Shah, C.R., Shah, N.J., Shuagia, B.N. and Patel, N. (2007) Simultaneous assay of olanzapine and fluoxetine in tablets by column high-performance liquid chromatography and high-performance thin-layer chromatography. *JAOAC Int*, **90**: 1573.
- [23] Patel, S. and Patel, N.J. (2009) Simultaneous RP-HPLC and HPTLC estimation of fluoxetine hydrochloride and olanzapine in tablet dosage forms. *Indian J Pharm Sci*, **71**: 477.



## BOOTSTRAPPING OF PHONE MODELS FOR A LARGE VOCABULARY CONTINUOUS SPEECH RECOGNITION FOR GUJARATI

Himanshu N. Patel\* and Paresh V. Virparia<sup>1</sup>

\*Anand Institute of Information Science, Anand, Gujarat, India

<sup>1</sup>G. H. Patel Dept. of Computer Science, Sardar Patel University, V. V. Nagar, Gujarat, India

### ABSTRACT

**In the bootstrapping approach, an already existing acoustic model of a speech recognition system for a different language is used to obtain initial phone models for a new language. There are primarily two approaches used for bootstrapping. We explain these approaches using English as the base language and Gujarati as the new or target language:**

**In this paper we present a technique that has been used to build a large-vocabulary continuous Gujarati speech recognition system. We present a technique for fast bootstrapping of initial phone models of a Gujarati language. The training data for the Gujarati language is aligned using an existing speech recognition engine for English language. This aligned data is used to obtain the initial acoustic models for the phones of the Gujarati language. Following this approach requires less training data.**

*Keywords: bootstrapping, acoustic model, phone set mapping, LVCSR*

### INTRODUCTION

An automatic speech recognition (ASR) system consists of two main components—an acoustic model and a language model. The acoustic model of an ASR system models how a given word or “phone” is pronounced.

The language model of an ASR system predicts the likelihood of a given word sequence appearing in a language. The most common technique used for this purpose is an N-gram language model. By using both the acoustic model and the language model, the combined likelihood of the word is computed.

In order to train the acoustic model, a phonetically aligned speech database and acoustic models are required in order to automatically align a speech database. One possible method is to manually align the speech database; however, manually aligning a large speech database is very time-consuming and error-prone. Obtaining preliminary phone models for a new language is thus a demanding job. In [1], Byrne et al. have suggested techniques to create phone models for languages which do not have a lot of training data available. They have used knowledge-based and automatic phone mapping methods to create phone models for the target language, using phone models of other languages. Previous approaches [2, 3] to generate initial phone models include bootstrapping from a multilingual phone set and the use of codebook lookup.

A codebook specifies the mapping to be used while performing the bootstrapping. The generation of this codebook requires linguistic knowledge of the languages. The technique mentioned in [2] requires a system already trained in the languages. On the other hand, the method in [3] requires labeled and segmented data in the language for which the system is to be trained. Authors in [4] describe various methods of generating the Chinese phone models by mapping them to the English phone models.

This requires the collection of specific utterances of isolated monosyllabic data that is difficult for a language such as Gujarati. Moreover, it may not be the best means for initializing the phone models that are to be used in large vocabulary continuous speech recognition tasks. Cross lingual use of recognition systems is also seen in [5], where the aim is to generate a crude alignment of words that do not belong to the language of the recognition system.

In this paper, we propose an approach for building good initial phone models through bootstrapping. We make use of the existing acoustic models of another language for bootstrapping. Following the approach proposed in [1], we define a phone

mapping between the two languages to obtain an initial alignment of the target language speech data. However, in the case of Gujarati, we have special acoustic classes, e.g., nasalized vowels and stressed plosives, which require more than one phone from the base language (English) for bootstrapping. We use this aligned data to obtain initial phone models of the target language. While segmenting the aligned data for target language phones, we use a module called a lexeme context comparator, which helps in differentiating phones in the target language which were mapped to same phone in the base language. The proposed approach requires relatively lower amounts of speech data for the new language to build initial phone models.

For training the acoustic model, baseforms for the training words are required along with the initial phone models. These baseforms are also required during recognition for each word in the vocabulary. Researchers have used a pure rule-based technique for baseform builders for phonetic languages [6]. The advantage of this technique is that once all of the rules are accounted for, the accuracy is very high; however, this requires deep linguistic knowledge that may be difficult to obtain [7]. While pronunciation rules can be extracted from existing online dictionaries, existing online dictionaries for Gujarati are not exhaustive in their word coverage or on pronunciations. Additionally, each such online dictionary for Gujarati requires a specific format in which the Gujarati characters are encoded, thus making them even more difficult to use. It is easy to capture the general linguistic nature of phonetic languages, but their idiosyncrasies and exceptions are difficult to capture by rules. On the other hand, using pure statistical techniques requires a large amount of training data that is not easily available for a new language.

Different statistical approaches have been tried for baseform builders. Decision trees [8–11], machine learning techniques [12], delimiting, and dynamic time warping (DTW) [13] are a few of the techniques that have been studied. All of the statistical techniques require a large amount of training data for respectable accuracy. Moreover, their performance is compromised for “unknown words,” typically proper nouns [9]. In order to improve the statistical techniques, other knowledge sources such as acoustics are used in conjunction with the spellings to obtain better results [14]. Pure acoustic-based baseform builders have also been built [15]. However, the techniques that use acoustics are restricted in their usage, since they require a recognition engine for the language and are better used for generating speaker-dependent pronunciations.

In this paper we present a hybrid approach that combines rule-based and statistical techniques in a novel two-step fashion. We use a rule-based technique to generate an initial set of baseforms

\*Corresponding author: hnp.aiis@gmail.com, patel\_himanshu6@gtu.edu.in

and then modify them using a statistical technique. We show that this approach is extremely useful for phonetic languages such as Gujarati. The phonetic nature of the language can be exploited to a greater extent by using the rule-based approach, while the statistical technique can be used to improve on this. We experimented with two different techniques as the statistical component of our hybrid system—one of them uses modification probabilities, while the other uses context-dependent decision trees.

**BOOTSTRAPPING OF PHONE MODELS**

In the bootstrapping approach, an already existing acoustic model of a speech recognition system for a different language is used to obtain initial phone models for a new language. In the literature [2, 4], there are primarily two approaches used for bootstrapping. We explain these approaches using English as the base language and Gujarati as the new or target language:

**1) BOOTSTRAPPING THROUGH ALIGNMENT OF TARGET LANGUAGE SPEECH DATA**

In the first approach, phonetic transcription of the target language text is written using the phone set of the base language. This is achieved by using a mapping defined between the two phone sets, which are detailed in the subsection on phone set mapping. The speech data in the target language is aligned using

the speech recognition system of the base language. Initial phone models for the target language can then be built from the aligned speech data. The Gujarati phone set is presented in **Figure 1**.

For example,  
 BHARAT –/BHAARAXTX/ (actual);  
 BHARAT –/B AARAXTH/  
 (using English phone set)

In this case, the phones /BH/ and /B/ in the target language are both mapped to phone /B/ in the base language. Hence, to initially obtain the aligned data for /BH/, the data aligned with /B/ is randomly distributed between /BH/ and /B/. Phone /TX/ in the target language is mapped to phone /TH/ in the base language.

**2) BOOTSTRAPPING THROUGH ALIGNMENT OF BASE LANGUAGE SPEECH DATA**

In the second approach, speech data of the base language itself is aligned using its speech recognition system. The aligned speech data of the base language is used as the aligned speech data for the target language using the mapping between the two phone sets. For example, BAR –/B AAR/.

The aligned data for /B/ is randomly distributed to obtain the aligned data for /BH/ and /B/.

Gujarati phone (Y)	Gujarati alphabet	h(Y)	p(Y)	Gujarati phone (Y)	Gujarati alphabet	h(Y)	p(Y)	Gujarati phone (Y)	Gujarati alphabet	h(Y)	p(Y)	Gujarati phone (Y)	Gujarati alphabet	h(Y)	p(Y)
AA	Aɸ	AA	AA	DH	v\$	DH	DH	JH	S>	JH	JH	S	k	S	S
AAN	Aɸ,	AA	AA+N	DHH	^	DH	DH+H H	JHH	T	JH	JH+HH	SH	i	SH	SH
AE	Aj	AE	AE	DN	Z	DX	DX+N	K	L\$	K	K	T	v\$	T	T
AEN	Aç	AE	AE+N	DXH	Y\$	DX	DX+H H + R	KH	M	KD	KD+H H	TH	'	TH	TH
AW	Aɸi	AW	AW	EY	A#	EY	EY	L	g	L	L	THH	v\$	TH	TH+H H
AWN	Aɸç	AW	AW+N	EYN	Aç	EY	EY+N	M	d	M	M	TX	s	TH	TH
AX	A	AX	AX	F	a	F	F	N	"	N	N	UH	D	UH	UH
AXN	A,	AX	AX+N	G	N	G	G	OW	Aɸi	OW	OW	UHN	E	UH	UH+N
B	b	B	B	GH	O	GD	GD+H H	OWN	Aɸç	OW	OW+N	UW	D	UW	UW
BH	c	BD	BD+H H	HH	I	HH	HH	P	'	P	P	UWN	J	UW	UW+N
CH	Q	CH	CH	IH	B	IH	IH	PD	'	PD	PD	v	h	v	v
CHH	R>	CH	CH+H H	IY	C	IY	IY	PH	a	P	PD+H H	y	e	y	y
D	X\$	D	D	IYN	I	IY	IY+N	R	f	R	R	Z	S>	Z	Z

**Figure-1:** Gujarati phonemes for characters in Gujarati. Mappings are shown using an English phone set. A mapping  $h(y)$  is from a Gujarati to English phone and  $p(y)$  is aligned phone set.

**3) PROPOSED APPROACH**

We have proposed a new technique for bootstrapping which provides more accurate initial phone models for the target language. We have modified the first approach as described above, so that the aligned speech data for two similar phones in the target language can be easily separated, for example for phones /BH/ and /B/. We propose to use both the phone sets, i.e., the phone sets of base and target languages, to avoid the

confusion between the phones in the target language which are mapped to the same phone in the base language.

Figure 2 shows the technique that is used to align Gujarati speech by using an English speech recognition system. A mapping  $h()$  from a Gujarati phone set denoted by  $\Gamma$  to an English phone set denoted by  $\pi$  is used to generate the pronunciation of Gujarati words by the English phone set.

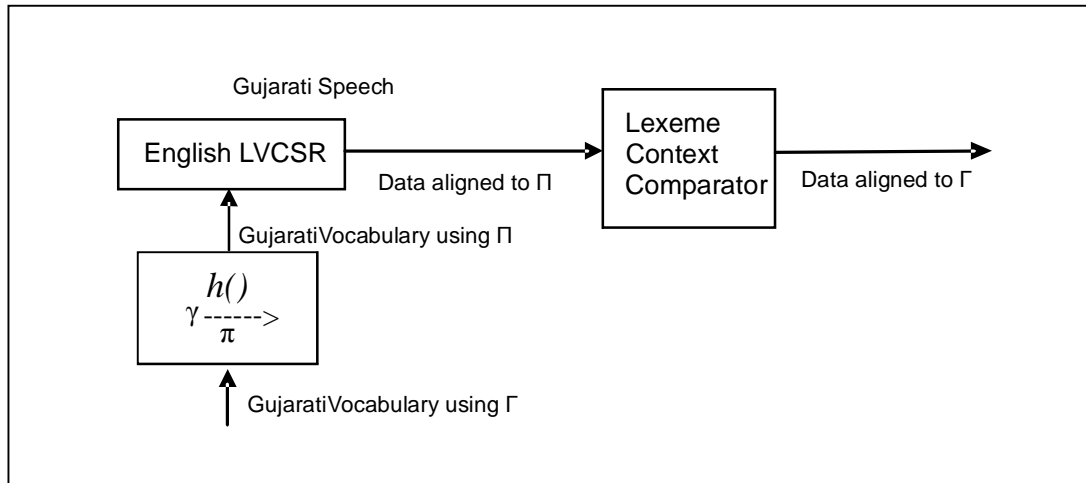


**Figure-2:** Alignment of the target language data. (LVCSR: large-vocabulary continuous speech recognition.)

Using linguistic knowledge, this mapping is based on the acoustic closeness of the two phones. The mapping is such that each phone  $\gamma \in \Gamma$  is mapped to one and only one phone in  $\Pi$ . A vocabulary created by such a mapping is used to align Gujarati speech data. Since more than one element in  $\Gamma$  may map to a single element in  $\Pi$ ,  $h(\cdot)$  is a many-to-one mapping in general and hence cannot always be used in reverse to obtain  $\gamma$  from  $\pi$ . Therefore, in order to recreate the alignment labels with Gujarati phones, an inverse mapping  $h^{-1}(\cdot)$  will not be feasible. A lexeme context comparator is used to generate the correct labels from  $\pi \in \Pi$ . This uses the context to resolve the ambiguity which arises from the one-to-many mapping  $h^{-1}(\cdot)$ .

To illustrate the requirement of a lexeme context comparator, we take the example of two Gujarati words,  $\text{Cjfs}$  and  $\text{bl}^0$ . The base forms for these words are shown in Table 1. For both words, the alignment would be generated for the phone /B/. However, this /B/ must be replaced by /BH/ if the word is and by /B/ if the word is  $\text{Cjfs}$ . This information is not available by using the mapping  $h^{-1}(\cdot)$ . Therefore, a lexeme comparator is used to examine the lexemes of the words and disambiguate for such cases.

Gujarati Word	Gujarati Baseform	English Baseform
$\text{Cjfs}$	BH AAR AX TD	B AAR AX TD
$\text{bl}^0$	B AX HH UH	B AX HH UH

**Table-1:** Baseforms for two Gujarati words.

The algorithm can be stated in the steps mentioned below:

- For a feature vector labeled with a phone  $\pi \in \Pi$ , form a subset  $\Psi \in \Gamma$  using the inverse mapping  $h^{-1}(\cdot)$  [since  $h^{-1}(\cdot)$  is a one-to-many mapping in general].
- If  $\Psi$  is a singleton, change the label of the feature vector to the element  $\gamma \in \Psi$ .
- If not, from the lexeme context of the feature vector, compare the two phonetic spellings of the two lexemes (one written with phones in  $\Pi$  and other with phones in  $\Gamma$  to which this vector belongs. Using this information, handle the disambiguate and choose the phone from  $\Psi$  that satisfies the mapping  $h^{-1}(\cdot)$  for the lexeme—for example, /B/ and /BH/.

This technique would generate the aligned Gujarati speech corpus without the need for a Gujarati speech recognizer. Although this alignment may not provide exact phone boundaries, it would serve the purpose of building the initial phone models. The inaccurate phone boundaries are a result of phonetic space differences in the two languages owing to the

different acoustic characteristics of the languages. This depends on the two languages; if the languages are acoustically similar, we can have accurate phone boundaries using the above technique. It should be noticed that using the phone set of the target language in the lexeme context comparator not only separates the aligned data for /B/ and /BH/ but also provides the right context information for other phones in the aligned speech corpus. This context information would otherwise have been abused because of the many-to-one phone mapping from target language to base language.

#### 4) PHONE SET MAPPING

The International Phonetic Association (IPA) [16] has defined phone sets for labeling speech databases for sounds of a large number of languages, including Gujarati. However, there are some sounds in Gujarati which are not included in the IPA phone set but are important when building phone models that are to be used for the purpose of automatic speech recognition. In continuous speech recognition tasks, the purpose of defining a phonetic space is to form well-defined, non-overlapping clusters for each phoneme in the acoustic space. This clustering makes it easier for the system to recognize the phone to which an input utterance of speech belongs. For the same number of data and phoneme models, a better phone set is one that gives a higher classification rate and is able to distinguish the words present in the vocabulary of the language. We define a Gujarati phone set which can cover all the different sounds that occur in Gujarati. This phone set takes into consideration the fact that even though Gujarati is a phonetic language, from an acoustic point of view some phones such as plosives have different acoustic properties when they occur at the end of the word. Taking these into account, we have constructed a Gujarati phone set consisting of 61 phones (including the inter-word silence  $D\$$  and long pause silence  $X$ ) to represent the sounds in Gujarati. It is seen that of these 61 phones, 39 are already present in English. Figure 1 shows the corresponding characters as written in Gujarati script. In the figure,  $h(\gamma)$  represents the mapping of Gujarati phones to the corresponding English phones for aligning the Gujarati data using English acoustic models, and  $p(\gamma)$  represents the mapping to obtain the initial phone models for the Gujarati phones from English data. In addition to ten English vowels, Gujarati has nine nasalized vowels (AAN, AEN, AWN, AXN, EYN, IYN, OWN, UHN, UWN). Each plosive phone (B, D, K, P, T) has an additional phone (BD, DD, KD, PD, TD) to represent the acoustic dissimilarity when they occur at the end of a word. The bootstrapping approach described in the preceding subsection requires a mapping from the phones of the base language to the phones of the target language. A phone set mapping is defined using the linguistic knowledge of the two languages. We define three categories of mapping as follows:

- *Exact mapping* Some of the phones may be common to both the base and the target language. For example, many vowels

such as /AX/, /AA/, and /IY/ are common to English and Gujarati, and they have an exact mapping from one language to the other. The mappings  $h()$  and  $p()$  are the same for such phones.

- **Merging** Some of the phones in the target language may have sounds from more than one phone in the base language. For example, Gujarati has some nasalized vowels such as /AAN/ and /EYN/, which are a combination of the corresponding vowel and nasal sound /N/. For these phones, one-to-many mapping is defined from such Gujarati phones to their English counterparts. For example, the Gujarati phone /GH/ is a combination of the English phones /GD/ and /HH/ while creating the mapping  $p()$ . The mapping for such phones differs in the case of  $h()$  and  $p()$ .
- **Approximation** Some of the phones in the target language may not be present in the base language at all. Such phones are simply mapped to the closest phone in the base language. For example, phone /TX/ in Gujarati (CpfS - BH AAR AX TX) is mapped to phone /TH/ in English (B AAR AX TH). The mappings  $h()$  and  $p()$  are the same for such phones.

### 5) REFINING PHONE SET MAPPING

We now present a method that is used to improve the initial phone set mapping  $p()$ . This method is based on a measure of phonetic similarity between the phones in  $\Gamma$  and the phones in  $\Pi$ . One possible measure of similarity is the distance between the phones in the MFCC domain. Each phone of  $\Pi$  is modeled by a normal distribution, and the phonetic distance of a phone  $\gamma \in \Gamma$  from a phone  $\pi \in \Pi$  is defined as

$$D(\gamma, \pi) = \sum_{v_i \in \gamma} \frac{(v_i - m_\pi)^2}{\|\Gamma\|}$$

Where  $v_i$  represents a 24-dimensional MFCC vector belonging to  $\gamma$  and  $m_\pi$  is the mean vector corresponding  $\pi$ . However, we used a distance measure based on the log likelihood of the phone models in  $\Pi$  for each test vector in  $\gamma \in \Gamma$ . The mean of log likelihoods is taken as the measure of acoustic similarity between the phones in the two languages. This measure is calculated for each phone  $\gamma \in \Gamma$  over all of the phones in  $\Pi$  that are considered to be close to  $\gamma$ . The mapping  $p()$  is refined if the acoustic similarity measure shows that a phone  $\gamma$  is closer to some phone  $\pi'$  than it is to  $\pi$ , to which it was initially mapped. The log-likelihood-based distance measure produces better results. As a result of the refinement, we changed the mapping of /DDN/ from /DD + HH/ to /DD + R/ and of /DXH/ from /DD + HH/ to /DD + HH + R/.

### CONCLUSION

In this paper we have presented novel technique that can be used to build a continuous large-vocabulary Gujarati speech recognition system. A new technique for fast bootstrapping the initial phone models has been presented.

### REFERENCES

[1] W. Byrne, P. Beyerlein, J. M. Huerta, S. Khudanpur, B. Marthi, J. Morgan, N. Peterek, J. Picone, D. Vergyri, and W. Wang, (2000) Towards Language Independent Acoustic Modeling, *Proceedings of the International Conference on Acoustics, Speech and Signal Processing*, Istanbul, pp. 1029–1032.

[2] J. Kohler, (1996) Multi-Lingual Phoneme Recognition Exploiting Acoustic-Phonetic Similarities of Sounds, *Proceedings of the International Conference on Spoken Language Processing*, Atlanta, pp. 2195–2198

[3] O. Anderson, P. Dalsgaard, and W. Barry, (1994) On the Use of Data-Driven Clustering Technique for Identification of Poly- and Mono-Phonemes for Four European Languages, *Proceedings of the International Conference on Acoustics, Speech and Signal Processing*, Adelaide, Australia, pp. 121–124

[4] M. C. Yuen and P. Fung, (1998) Adapting English Phoneme Models for Chinese Speech Recognition, *Proceedings of the International Conference on Spoken Language Processing*, Sydney, Australia, pp. 80–82

[5] T. A. Faruque, C. Neti, N. Rajput, L. V. Subramaniam, and A. Verma, (2000) Translingual Visual Speech Synthesis, *Proceedings of the IEEE International Conference on Multimedia and Expo (ICME)*, New York, pp. 1089–1092.

[6] M. Choudhury, Rule-Based Grapheme to Phoneme Mapping for Gujarati Speech Synthesis, (2003) presented at the 90th Indian Science Congress of the International Speech Communication Association (ISCA), Bangalore.

[7] M. Choudhury and A. Basu, (2002) A Rule Based Schwa Deletion Algorithm for Gujarati, *Proceedings of the International Conference on Knowledge Based Computer Systems*, Mumbai, pp. 343–353

[8] E. Fosler-Lussier, (1999) Multi-Level Decision Trees for Static and Dynamic Pronunciation Models, *Proceedings of the Eurospeech Conference*, Budapest, pp. 459–462

[9] A. W. Black, K. Lenzo, and V. Pagel, (1998) Issues in Building General Letter to Sound Rules, *Proceedings of the 3<sup>rd</sup> European Speech Communication Association (ESCA)*, pp. 77–80.

[10] A. K. Keinappel and R. Kneser, (2001) Designing Very Compact Decision Trees for Grapheme-to-Phoneme Transcription, *Proceedings of the Eurospeech Conference*, Scandinavia, pp. 1911–1914

[11] J. Suontausta and J. Hakkinen, (2000) Decision Tree Based Text-to-Phoneme Mapping for Speech Recognition, *Proceedings of the International Conference on Spoken Language Processing*, Beijing, pp. 199–202

[12] F. Mana, P. Massimino, and A. Pacchiotti, (2001) Using Machine Learning Techniques for Grapheme to Phoneme Transcription, *Proceedings of the Eurospeech Conference*, Scandinavia, pp. 1915–1918.

[13] R. W. P. Luk and R. I. Damper, (1992) Inference of Letter-Phoneme Correspondences by Delimiting and Dynamic Time Warping Techniques, *Proceedings of the International Conference on Acoustics, Speech and Signal Processing*, San Francisco, pp. 61–62

[14] L. R. Bahl, S. Das, P. V. deSouza, M. Epstein, R. L. Mercer, B. Merialdo, D. Nahamoo, M. A. Picheny, and J. Powell, (1991) Automatic Phonetic Baseform Determination, *Proceedings of the International Conference on Acoustics, Speech and Signal Processing*, Toronto, pp. 173–176.

[15] B. Ramabhadran, L. R. Bahl, P. V. deSouza, and M. Padmanabhan, (1998) Acoustics-Only Based Automatic Phonetic Baseform Generation, *Proceedings of the International Conference on Acoustics, Speech and Signal Processing*, Seattle, pp. 309–312.

[16] J. Wells and J. House, (1995) *The Sounds of the IPA*, Department of Phonetics and Linguistics, University College London.

[17] L. R. Bahl, P. V. deSouza, P. S. Gopalakrishnan, D. Nahamoo, and M. A. Picheny, (1991) Decision Trees for Phonological Rules in Continuous Speech, *Proceedings of the International Conference on Acoustics, Speech and Signal Processing*, Toronto, pp. 185–188.

[18] N. Mukherjee, N. Rajput, L. V. Subramaniam, and A. Verma, (2000) On Deriving a Phoneme Model for a New Language, *Proceedings of the International Conference on Spoken Language Processing*, Beijing, pp. 850–852



NATURAL LANGUAGE INTERFACE FOR STUDENT INFORMATION SYSTEM (NLSIS)

Amisha Shingala\*, Rinku Chavda and Paresh Virparia<sup>1</sup>

\*Department of MCA, SVIT, Vasad, Gujarat, India

<sup>1</sup>G. H. Patel Computer Science Department, Sardar Patel University, Vallabh Vidyanagar, Gujarat, India

ABSTRACT

Any computer system that interacts with user has a high utility value and ease. Natural Language Interface is a concept for making computer interface with a user who wants to retrieve the information from a computer database with its own language rather than learning a specialized language. The challenges in Natural language arise due to difficulty in correct interpretation, disambiguation and context resolution.

We present our work in designing and implementing the Natural Language Interface for querying Student Information System. It semantically parses the natural language question and built corresponding structured query from the database. The data which is to be retrieved can be in the form of a spreadsheet or database. The system is developed in Java using JDBC for Student Information System.

Keywords: Language, Database Interface, Structured Query Language, Data Retrieval

INTRODUCTION

The computer era has began from last few years and the phase of bringing awareness into different walks of society regarding use and benefits of computer increased successfully. Not only industry but educational institute, service sectors, manufacturing sectors etc are using computers to store, process and update the information. The huge amount of data are stored in repository called database and in order to query or retrieve information from a database by general public, a Natural Language (English) will provide correct and precise information without knowing the depth of SQL query language. The idea of using Natural language with database prompted the development of new type of processing method called Natural Language Interface to Database.

Some of the earlier attempts in providing Natural Language Interface are given below:

- 1) MASQUE/SQL by Androutopoulos et al [4] and Anuxeree, P [5] can answer English question by generating SQL code.
- 2) LUNAR [13] that answered questions about rock samples back from the moon.
- 3) LIFER/LADER describe by Hendrix [9] was designed as a natural language interface to database about US Navy ships.
- 4) Warren et al's CHAT-80[12] and Auxerre et al's transform written English questions into prolog queries which are executed against Prolog database.

Information related to overview of various Natural Language Interfaces and the difference between Natural Language Interface and Question Answering could be found in reference [1]. The approach used in most of the recent systems is to handle the entire query as one entity for transformation to SQL

either through conversion to intermediate representation or directly. We had overcome many limitations which were given by earlier researchers [11].

MODEL AND METHODOLOGY OF NATURAL LANGUAGE STUDENT INFORMATION SYSTEM (NLSIS)

The following goals were set for the proposed NLSIS:

- **Fault Tolerance**– An algorithm [2] is developed for tolerating spelling errors, which uses degree of phonetic match and degree of spelling match to correct misspelled words. Since the semantics of the query for purpose of conversion to SQL statement within a limited domain does not use the grammatical structure of sentence formation, it is implicitly tolerated. However, use of grossly, inappropriate words (particularly prepositions e.g. using “by” in place of “of”, etc and interrogative pronouns) may lead to wrong or failed interpretation of the user query.
- **Better Context Resolution and Disambiguation** – We first partition the query into intermediate language and then to SQL clause. A part of query with associate SQL along with domain-specific lexicon leads to an improved context resolution and disambiguation.
- **Multiple database tool support:** A tool is developed which can covert data from spreadsheet to database and database to relational database.
- **History Log Maintenance:** The query once asked, was stored in separate log which can be help in retrieving the same information again without processing whole algorithm.

Domain-Specific Ontology

Figure A present below ontology of Student Information System (SIS) domain.

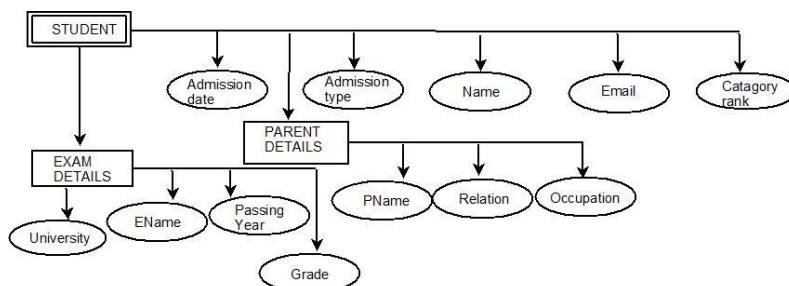


Figure A: Domain ontology for Student Information System

\*Corresponding author : am\_bt@yahoo.com

A. The **Linguistic model** consists of Lexical Analysis, Parser and Semantic representation as shown in figure B which is explained below:

*Lexical Analysis:* Here the natural language sentence is divided into smaller fragments called tokens. The elements in natural language query are words or special characters. This process is performed by following function:

- i. Token analyzing function: It is used to generate the token which is treated as a single unit.
- ii. Spell checker function: It makes sure that the user inputted query with correct word.
- iii. Ambiguity reduction: It reduces ambiguity of sentence and simplified the task of parser by substituting multiple words or symbols with base word. E.g. Comma considered as AND, co-occurring word as single word etc. Also, we try to find out that the expected answer would be named entity or not. Figure C represent hierarchy of named entity [7]

**Architecture of system**

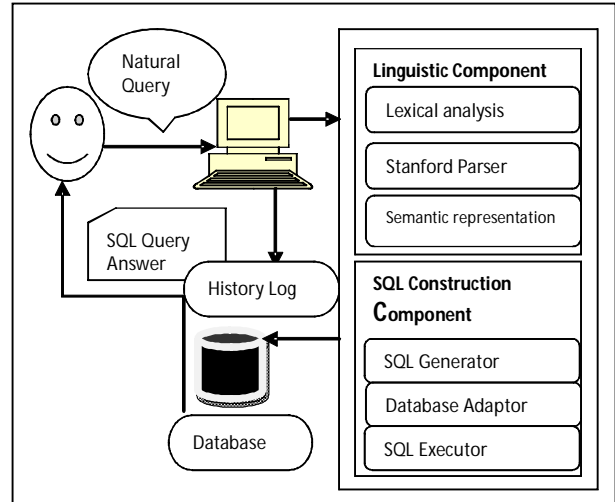


**Figure B:** Architecture of NLSIS

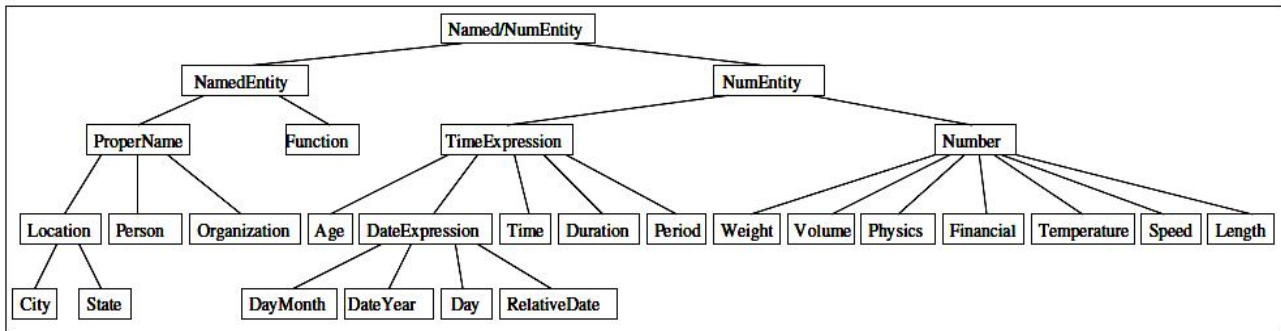


**Figure C :** Hierarchy of Named Entity

*Stanford Parser:* The Stanford Parser is a probabilistic parser which uses the knowledge of language gained from hand-parsed sentences to try to produce the *most likely* analysis of new sentences as shown in figure D. This package is a Java implementation of probabilistic natural language parsers.

The Stanford dependencies provide a representation of grammatical relations between words in a sentence for any user who wants to extract textual relationships [3]. The dependency obtained from Stanford parser can be mapped directly to graphical representation in which words in a sentence are nodes in the graph and grammatical relationships are edge labels [6]. In our system, we use the POS tagger and Typed Dependency for an inputted query or sentences.

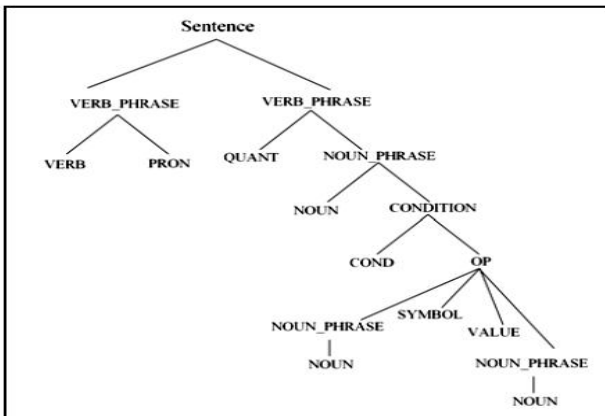


**Figure D:** Hierarchical structure of Stanford Parser

*Semantic Representation:* We had used two types of lexicon semantic representation in the form of grammar for terminal words, non terminal words and terminal symbols.

**Table 1:** Example of Terminal Words

Terminal Words	Semantics/Base Word
girls, girl, female, madam	Female
Percentage above 70	Distinction

**Table 2:** Example of NonTerminal Words

NonTerminal Words	Semantics/Base Word
Greater than or equal to	>=
Less, lower or lesser	<

**Table 3:** Example of Terminal Symbols

Terminal Symbols	Semantics/Base Word
Greater, larger, bigger, biggest	Greater
Equal to, Like, equals, same	Equal

**B. SQL Constructing Component**

This component consists of SQL generator, Database Adaptor and SQL execution.

*SQL Generator:* The task is to map element of the Natural Language sentence into an actual element of SQL. We consider

only SELECT as a statement to view the data in various forms. We used BNF form of SQL grammar [10]

<select query> ::= <select> [UNION [ ALL | DISTINCT ] <select query>]

<select> ::= SELECT [ ALL | DISTINCT ] <select list> <from clause>

[ <where clause> ]

<select list> ::= '\*' | <column element> [ {',' <column element> }... ]

<column element> ::= <column> | <aggregate function> '(' <column> ')'

<from clause> ::= FROM <table reference> [ {',' <table reference> }... ]

<table reference> ::= <table schema> [[AS ] <correlation name>] | <table reference>

[INNER | LEFT | RIGHT] JOIN <table reference> ON <search conditions>

<where clause> ::= WHERE <search conditions>

The <search condition> is a logical predicate composed of logical conditions with AND and OR operator. The <aggregate functions> like max, min, sum, average and count transforms set of rows into scalar statement. The <condition> is a expression in form  $X_R Y$  where X and Y are the set of values representing column, aggregate function, constant or NULL and R can be operated like {<, <=, >=, !=, ==}.

*Database Adaptor:* The data repository can be in the form of a spreadsheet or database. Our algorithm converts these data into MySQL database and retrieve the answer from MySQL database tool.

*SQL Executor:* The task is to map the SQL generated query to Database Adaptor and retrieve the relevant information or answer by connecting to the appropriate database tool.

**3. Algorithm for NLSIS**

- (i) Read statement or user query S
- (ii) Search S from History Log H
  - If found, call query generate algorithm and retrieve the query Q
  - Execute the Query Q and Display the answer Ans.
- (iii) If S not successful, perform all the steps from step iv.
- (iv) For each word  $W_i$  from S do
  - If  $W_i$  base word then
  - Add  $W_i$  to symbol table ST
  - End if
  - Endfor
- (v) For each  $W_i$  from ST do
  - Add  $W_i$  to Parse tree
  - End for
- (vi) Display POS tagger and Typed dependency and get relationship between words PDR
- (vii) For each PDR do
  - If metadata = PDR then
  - Add table name, attribute and condition to OUT
  - Endif
  - Endfor

- (viii) For each OUT do
  - Generate the SQL query Q1
  - Call Data conversion algorithm
  - Execute SQL query Q
  - End for
- (ix) Display SQL query Ans.

**RESULTS and DISCUSSION**

The software has been subjected to test with a number of volunteers phrasing the queries differently. In around 70% cases, the system could correctly interpret and process the query. Currently, the system fails in some cases to handle very complex queries coupled with fuzzy terms. We had paraphrased different queries in the form of simple query, condition query, order by query and join query. Figure E shown implemented version of the system.

**Table 4: List of normal Queries.**

<i>Input or Query</i>	<i>SQL Query generated</i>
Display details of all students	Select * from students;
Who are our students ? show me list of all students ?	Select * from students;
Show me all branches	Select * from branch
Display various branches	Select bnm from branch

**Table 5: List of Conditional Queries**

<i>Input Sentence or Query</i>	<i>SQL query generated</i>
List of all female students or Display details of girls students	Select studnm from student where gender = 'F'
List of students who live in Baroda	Select studnm from student where city = 'VADODARA'
Details of Monalisa?	Select * from student where studnm = 'monalisa'
Give me hsc% of aryan or display 12 <sup>th</sup> percentage of Aryan	Select hscper from student where studnm = '%aryan%'

**Table 6: List of Aggregate function Queries**

<i>Input Sentence or Query</i>	<i>SQL query generated</i>
How many students are in semester 6	Select count(*) from students where sem =6;
List youngest student in sem 1	Select min(age) from students where sem =1;
How many students we have ?	Select count(*) from students

**Table 7: List of Order by Queries**

<i>Input Sentence or Query</i>	<i>SQL query generated</i>
Display student record in ascending order of their rollnos	Select * from students order by studid;
Display male students in descending order of their age	Select studnm, age from students where gender = 'm' order by age

**Table 8: List of Simple join Queries**

<i>Input Sentence or Query</i>	<i>SQL query generated</i>
Display branch in which rima study	Select bnm from branch natural join student

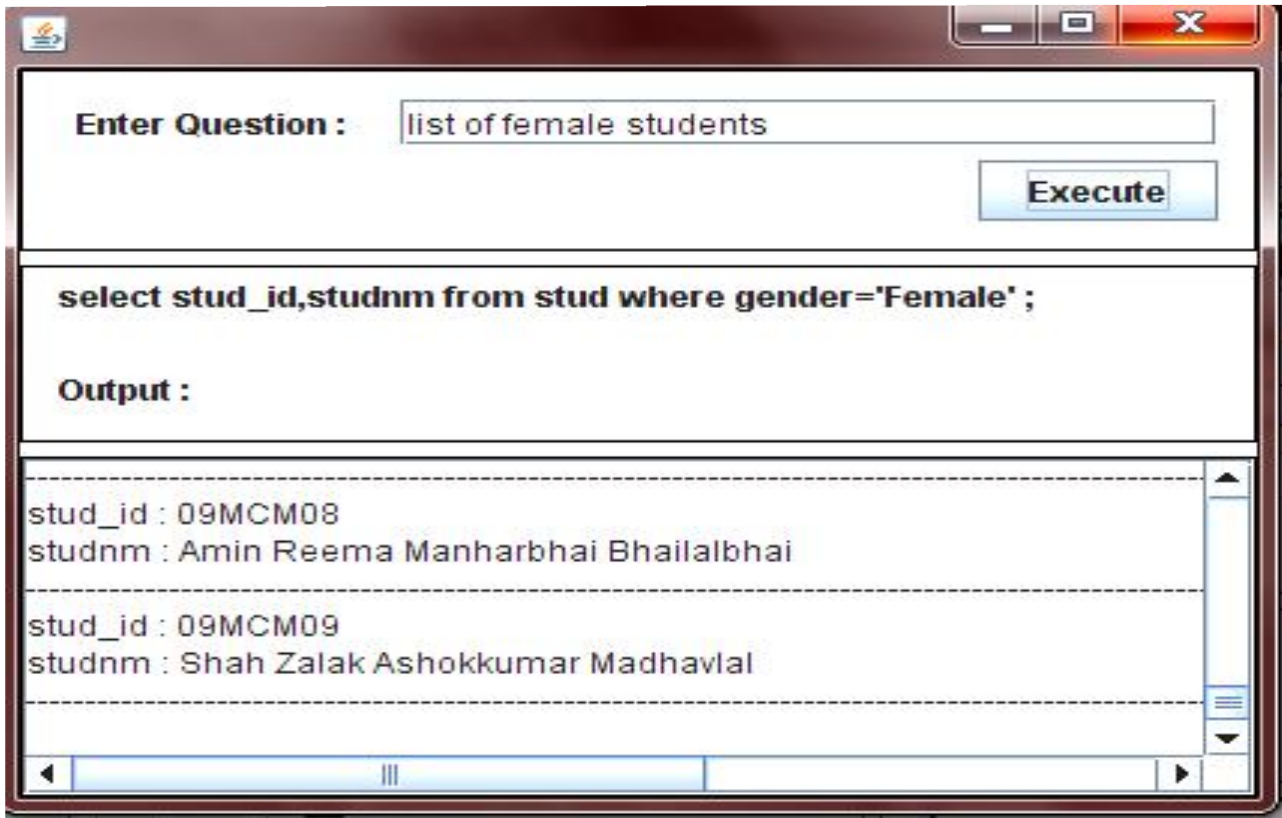


**Figure E:** A sample screen shot of the system

#### CONCLUSION AND FUTURE WORK

The degree of correct interpretation and processing of Natural Language Queries relies on the extent of exhaustiveness of domain-specific lexicon. Despite of some limitations, the proposed system provides a robust tool to handle Natural Language Queries allowing fault-tolerance to some degree. The work can be further extended by providing multilingual (Gujarati or Hindi language) query to SQL conversion.

#### REFERENCES

- [1] Amisha Shingala & Paresh Virparia, (2011) A Survey of Natural Language Interface, International Journal of RESEARCH@ICT: International Journal of Information and Computing Technology, Volume 2 , ISSN: 0976 – 5999.
- [2] Amisha Shingala & Sanjay Vij (2007) Manage and Access Information and Knowledge through Natural Language Queries, Fifth AIMS International conference.
- [3] Anjali Ganesh Jivani, Amisha Shingala & Paresh Virparia (2011) The Multi-Liaison Algorithm, International Journal of Advanced Computer Science and Applications, Volume 2 Issue, ISSN 2156-5570 (Online)
- [4] Androutsopoulos, I, Ritchie & Thanisch P (1993), MASQUE/SQL- An efficient and portable Natural Language Query Interface for Relational Database, Proc. of Sixth International Conference on Industrial & Engineering Applications of AI & Expert System, Edinburgh.
- [5] Anuxerre, P & Inter R (1993) MASQUE Modular Answering System for Queries in English - User's Manual, AI Applications Institute, Univ. of Edinburgh.
- [6] Faraj A. El-Mouadib, Zakaria S. Zubi, Ahmed A. Almagrous, and Irdess S. El-Feghi (2009) Generic Interactive Natural Language Interface to Databases (GINLIDB), International Journal of Computers, Issue 3, Volume 3.
- [7] Ferret, B. Grau, M. Hurault-Plantet, G. Illouz, How NLP can improve Question Answering, Limsi-cnrs, BP Orsay Cedex
- [8] F.Siasar djahantighi, M.Norouzifard, S.H.Davarpanah, M.H.Shenassa (2008) Using Natural language processing in order to create SQL queries, Proceedings of the International Conference on Computer and Communication Engineering, Kuala Lumpur, Malaysia
- [9] Hendrix, C.G; Sacerdoti, E.D; Sangalowicz, D; Slocum J (1978) Developing a natural language interface to complex data “, ACM Trans on Database Systems, 3(2), pp. 105-147.
- [10] M<sup>a</sup> José Suárez-Cabal (2009) Structural Coverage Criteria for Testing SQL Queries, *Journal of Universal Computer Science*, vol. 15.
- [11] Niculae Stratica (2002) *Natural language interface for querying Cindi*, Thesis, Master of Computer Science, Concordia university, Quebec, Canada.
- [12] Warren D and F. Pereira (1982) An Efficient Easily Adaptable System for Interpreting Natural Language Queries, Computational Linguistics, pp.110-122
- [13] Woods, W.A. (1973) Progress in Natural Language Understanding: An Application to Lunar Geology, AFIPS Conf. Proc. 42, pp. 141-450.



## A MATHEMATICAL MODEL FOR A GROWTH CURVE OF RICE CROP

R. Lakshmi<sup>1\*</sup> and V. Ravichandran<sup>2</sup>

<sup>1</sup>Department of Mathematics (PG), PSGR Krishnammal College for Women,  
Coimbatore-641004, Tamil Nadu, India

<sup>2</sup>Department of Rice, Tamil Nadu Agricultural University,  
Coimbatore-641003, Tamil Nadu, India

### ABSTRACT

In this study, a mathematical model is described for a growth curve of rice crop. The parameters of the growth equations are related to the plant. This modeled growth curve is interpreted for growth data from experiments using rice plant of different varieties and the results are reported for conclusion. Here this growth curve also describes the plant dry weight data over a whole season.

**Key words:** Mathematical model, rice crop, growth curve, varieties

### INTRODUCTION

Growth is one of the important properties of living organisms. Changes in a phenotype during the growth period can be modeled via growth curves, such as generalized logistic, logistic or Gompertz growth curves [1]. Behavior of the growth curves can change according to living organisms, the phenotype to be studied and environment to which it is exposed [2]. To evaluate growth data properly, it is required to select a suitable growth curve and its parameters should be interpreted biologically [3]. This study reports on a comparison of logistic growth curve of plant dry weight of three rice varieties that are commonly grown in Tamil Nadu. The aims of this study are: 1) to determine a logistic growth curve for plant dry weight data; and 2) to compare plant dry weight of rice varieties via the growth curve. This study was carried out during 2010. The experiment is conducted at the Tamil Nadu Agricultural University, Coimbatore. Rice varieties namely IR 64, Jaya, Tulasi, which are widely grown in India are used. The field plots used was allocated in a randomized block design (RBD) with five replicate plots per variety. Rice plants dry weights are recorded in every weeks starting from emergence. Measurements are used for five plants given each plot and each variety.

Changes in the plant dry weight of three varieties are modeled through logistic growth curve and are given in mathematical formulation.

### MATHEMATICAL FORMULATIONS

The problem is to find a growth curve which will give a good description of plant dry weight data over a whole season. The parameters of the growth equation are physiologically meaningful, and are related either to the environment or to the plant. This growth equation is used to summarize data, and possibly to interpret growth data from experiments using plants of different varieties or with different environmental treatments.

#### ASSUMPTIONS

- (i) The plant is completely defined by its dry weight  $W$ . The system is described by a single state variable. The variable  $W$  is a dependent variable, and varies with time  $t$  where  $t$  is an independent variable.
- (ii) Growth occurs at the expense of a single substrate  $S$ .
- (iii) The rate of the growth reaction is linearly proportional to the substrate level  $S$ , and also to the plant dry weight  $W$ , so that the growth is autocatalytic. The rate of the growth reaction is  $kWS$  where  $k$  is a constant.

### MATHEMATICAL EQUATION

As a consequence of assumption (iii), it follows that

$$\frac{dW}{dt} = kSW \quad (1)$$

This first-order differential equations cannot be solved, because the substrate level  $S$  will vary as growth proceeds. If  $W$  and  $S$  are measured in the same units, and there is no loss of material when converting  $S$  into  $W$  by the growth reaction, then

$$dW = -dS \quad (2)$$

This equation states that an increment in dry weight is exactly matched by a loss in substrate. Equation (2) can be written as  $d(W+S) = 0$ , which on integration gives

$$W + S = W_i + S_i = \text{constant}, \quad (3)$$

Where  $W_i$  and  $S_i$  are the values of  $W$  and  $S$  at time  $t = 0$ , and denote the initial conditions. Equations of (2) or (3) simply express the conservation of matter. Since  $W$  and  $S$  are not allowed to be negative (such values would be physiologically meaningless), it is clear from (3) that  $W$  will have its maximum and final value when there is no substrate left, and  $S = 0$ . Equation (3) may be re written as

$$W + S = W_f = W_i + S_i \quad (4)$$

Where  $W_f$  is the maximum value of  $W$ . Substituting for  $S$  from Equation (4), Equation (1) becomes

$$\frac{dW}{dt} = k(W_f - W)W \quad (5)$$

This equation is a statement of the model in differential form. As the system has only one state variable, only one equation is needed.

Equation (5) is of the variables – separable type, and can be re-arranged in the form

$$\int_{W_i}^W \frac{dW}{(W_f - W)W} = \int_0^t k dt \quad (6)$$

The left side is split up into its component partial fractions

$$\int_{W_i}^W \frac{1}{W_f} \left( \frac{1}{W_f - W} + \frac{1}{W} \right) dW = \int_0^t k dt \quad (7)$$

and on integration gives

$$\frac{1}{W_f} \left[ \ln \left( \frac{W}{W_i} \right) + \ln \left( \frac{W_f - W_i}{W_f - W} \right) \right] = kt \quad (8)$$

This becomes

\*Corresponding author: rfluxmath@gmail.com

$$W = \frac{W_i W_f e^{W_f k t}}{W_f - W_i + W_i e^{W_f k t}} \tag{9}$$

For low values of  $t$   $W \approx W_i e^{W_f k t}$  as  $t \rightarrow \infty$ ,  $w \rightarrow W_f$ .

Where

$W_i$  is the initial plant dry weight,

$W_f k$  is the maximum specific growth rate achieved by the plant in early growth when there is no substrate limitation; and

$W_f$  is the final plant weight which is determined [through equation (4)] by the initial amount of substrate available per plant and the initial plant dry weight.

Model fitting and parameter estimation are performed via MATLAB 7 procedure [4] of computing solution to crop growth model.

Results from growth curve fitting of Logistic curve to plant dry weights data and the observed results are summarized in Table 1. The computed plant dry weights and observed values via logistic curve for rice varieties are shown in Fig 1 and Fig 2.

**Table 1:** Total plant dry weight (Tones/hectare) of rice crop varieties

Total plant dry weight (Tones/hectare)					
IR 64		Jaya		Thulasi	
Observed	Computed	Observed	Computed	Observed	Computed
3.5	3.5000	3.8	3.8000	2.7	2.7000
5.7	5.7126	6.6	6.6945	4.2	4.2864
7.5	7.5613	8.9	8.9993	5.8	5.8031
8.6	8.6430	10.1	10.1773	6.0	6.8873
9.3	9.3612	10.6	10.6455	7.5	7.5116
9.4	9.4458	10.8	10.8132	7.8	7.8273
9.4	9.4790	10.8	10.8701	7.9	7.9764
9.4	9.4929	10.8	10.8901	8.0	8.0445
9.4	9.4968	10.8	10.8967	8.0	8.0752
9.4	9.4988	10.8	10.8989	8.0	8.0890
9.4	9.4995	10.8	10.8996	8.0	8.0951
9.4	9.4949	10.8	10.8999	8.0	8.0978
9.4	9.4979	10.9	10.9000	8.0	8.0990
9.4	9.5000	10.9	10.9000	8.1	8.0996
9.5	9.5000	10.9	10.9000	8.0	8.0998
9.5	9.5000	10.9	10.9000	8.1	8.0999
9.5	9.5000	10.9	10.9000	8.1	8.1000
9.5	9.5000	10.9	10.9000	8.0	8.1000

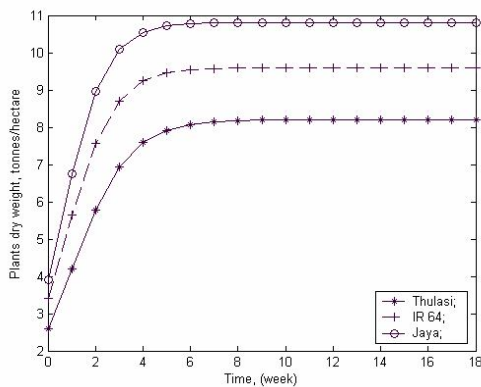


**Fig.1:** Growth curves of three varieties of rice crop – (Computed)

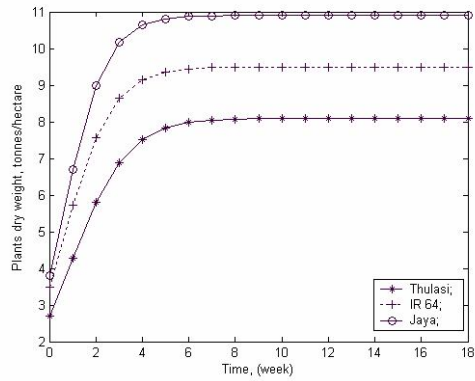


**Fig.2:** Growth curves of three varieties of rice crop – (Observed)

**CONCLUSION**

In this study, growth curve is described for plant dry weight of three varieties of rice crop by Mathematical modeling and it is found that the Jaya variety has more dry weight and has good agreement with the observed results.

**ACKNOWLEDGMENT**

Authors are highly thankful to anonymous referee for valuable comments and kind suggestions.

**REFERENCES**

- [1] Thornely, J.H.M and France, J. (2007) *Mathematical Models in agriculture: Quantitative methods for plant, animal and ecological sciences*, London, UK, pp.1-887.
- [2] Wang, E. and Smith, C. (2004) Modeling the growth and water uptake function of plant root system: a review. *Aust. J. Agric. Res.* **55** : 501–523.
- [3] Christopher Teh (2006) *Introduction to mathematical Modeling of crop growth: How the equation are derived and assembled into a computer Program*. Brown Walker press, Boca Raton, pp. 1-280.
- [4] Chapra, S. C (2007) *Applied Numerical Methods with MATLAB for Engineers and Scientist*, Tata McGraw-Hill publishing company limited, New Delhi, pp. 1-588.



## ON A NEW SEQUENCE OF FUNCTIONS DEFINED BY A GENERALIZED RODRIGUES FORMULA

J.C. Prajapati\*<sup>1</sup>, N.K. Ajudia<sup>1</sup> and A.K. Shukla<sup>2</sup>

<sup>1</sup>Department of Mathematical Sciences, Faculty of Applied Sciences (P. D. Patel Institute of Applied Sciences),  
 Charotar University of Science and Technology, Changa, Anand-388 421

<sup>2</sup>Department of Applied Mathematics and Humanities, S.V.National Institute of Technology, Surat- 395 007

### ABSTRACT

**In present paper, an attempt is made to provide an elegant unification of several classes of polynomials. Introduced sequence of the functions  $\{V_n^{(\alpha, \beta)}(x, a, k, s) / n = 0, 1, 2, \dots\}$  by means of generalized Rodrigues formula (7), which involves Mittag-Leffler function  $E_\alpha(z)$  and other two similar kind of class of polynomials (5), (6). Some generating relations and finite summation formulae have also been obtained for (7).**

**Keywords:** Mittag-Leffler function, generating relations, finite summation formulae.

AMS (2000) subject Classification: 33E10, 33E12, 33E99, 44A45.

### INTRODUCTION:

In 1971, Srivastava and Singhal [8] introduced general class of polynomial  $G_n^{(a)}(x, r, p, k)$  by employing the operator  $x^{k+1} D$ , defined as

$$G_n^{(a)}(x, r, p, k) = 1/n! x^{-a-kn} \exp(px^r) (x^{k+1} D)^n [x^a \exp(-px^r)] \quad (1)$$

Mittal [2] proved a Rodrigues formula for a class of polynomials  $T_{kn}^{(a)}(x)$  is given by

$$T_{kn}^{(a)}(x) = 1/n! x^{-a} \exp\{p_k(x)\} \times D_x^n [x^{a+n} \exp\{-p_k(x)\}] \quad (2)$$

where  $p_k(x)$  is a polynomial in  $x$  of degree  $k$ . Mittal [2] also proved the following relation

$$T_{kn}^{(a+s-1)}(x) = 1/n! x^{-a-n} \exp\{p_k(x)\} \times (T_s)^n [x^a \exp\{-p_k(x)\}] \quad (3)$$

where,  $T_s \equiv x(s + xD)$ .

In 1979, Srivastava and Singh [7] introduced a general sequence of functions  $V_n^{(a)}(x; a, k, s)$  by employing the operator  $\theta \equiv x^a(s + xD)$  where  $a$  and  $s$  are constants, defined as

$$V_n^{(a)}(x; a, k, s) = 1/n! x^{-a} \exp\{p_k(x)\} \theta^n [x^a \exp\{-p_k(x)\}] \quad (4)$$

where  $p_k(x)$  is a polynomial in  $x$  of degree  $k$ .

The new sequences of functions introduced in this paper are defined by (5) and (6) in the generalized form of (1) and (2) respectively as:

$$G_n^{(\alpha, \beta)}(x; r, p, k) = 1/n! x^{-\beta-kn} E_\alpha(px^r) (x^{k+1} D)^n [x^\beta 1/E_\alpha(px^r)], \quad (5)$$

$$T_{kn}^{(\alpha, \beta+s-1)}(x) = 1/n! x^{-\beta-n} E_\alpha\{p_k(x)\} \times (T_s)^n [x^\beta 1/E_\alpha\{p_k(x)\}] \quad (6)$$

In this paper, authors also introduced one more new sequence of functions  $\{V_n^{(\alpha, \beta)}(x; a, k, s) / n=0, 1, 2, \dots\}$  by means of generalized Rodrigues formula (7)

$$V_n^{(\alpha, \beta)}(x; a, k, s) = 1/n! x^{-\beta} E_\alpha\{p_k(x)\} \theta^\alpha [x^\beta 1/E_\alpha\{p_k(x)\}] \quad (7)$$

where,  $\theta \equiv x^a(s + xD)$ ;  $a, s$  are constants and  $\alpha \geq 0$ ,  $\alpha$  and  $\beta$  are real or complex numbers;  $n = 0, 1, 2, \dots$ ,  $k$  is finite and non-negative integer,  $p_k(x)$  is a polynomial in  $x$  of degree  $k$  with

$x \in (0, \infty)$

The Mittag-Leffler function [1] defined as:

$$E_\alpha(z) = \sum_{n=0}^{\infty} \frac{z^n}{\Gamma(\alpha n + 1)} \quad (8)$$

where  $z$  is a complex variable and  $\Gamma(s)$  is a gamma function,  $\alpha \geq 0$ . The Mittag-Leffler function is direct generalization of the hypergeometric function  $\frac{1}{1-z}$  and exponential function  $e^z$  to which it reduces for  $\alpha=0$  and  $\alpha=1$ , i.e.  $E_0(z) = \frac{1}{1-z}$  and  $E_1(z) = e^z$ . Its importance is realized during the last two decades due to its direct involvement in the problems of physics, chemistry, biology, engineering and applied sciences. Mittag-Leffler function naturally occurs as the solution of fractional order differential equation or fractional order integral equations. Therefore, it is obvious that (1), (2) and (4) are special cases of (5), (6) and (7) respectively for  $\alpha=1$ .

In the present paper, the generating relations and finite summation formulae obtained for sequence of functions (7) as these are obviously more powerful sequence of functions than (5) and (6). The technique discussed in this paper will certainly apply for sequence of functions (5) and (6).

To obtain generating relations and finite summation formulae, the properties of the differential operators  $\theta \equiv x^a(s + xD)$  and  $\theta_1 \equiv x^a(1 + xD)$ , where  $D \equiv \frac{d}{dx}$  used on the based of work (Mittal [3], Patil and Thakare [5]).

In the fourth section, the relations between (7) with some well-known polynomials (9) and (10) also have been discussed.

**Hermite polynomials** (Rainville [6]) defined as:

$$H_n(x) = (-1)^n \exp(x^2) D^n [\exp(-x^2)] \quad (9)$$

**Konhauser polynomials of first kind** (Srivastava [9]) defined as:

$$Y_n^\alpha(x; k) = \frac{x^{-kn-\alpha-1} e^x}{k^n n!} (x^{k+1} D)^n [x^{\alpha+1} e^{-x}] \quad (10)$$

### GENERATING RELATIONS:

We obtained some generating relations of (7) as,

$$\sum_{n=0}^{\infty} x^{-an} V_n^{(\alpha, \beta)}(x; a, k, s) t^n = (1-at)^{-\left(\frac{\beta+\alpha}{\alpha}\right)} \frac{E_\alpha[p_k(x)]}{E_\alpha[p_k(x(1-at)^{\frac{1}{\alpha}})]} \quad (11)$$

$$\sum_{n=0}^{\infty} x^{-an} V_n^{(\alpha, \beta-an)}(x; a, k, s) t^n = (1+at)^{\frac{\beta+\alpha-1}{\alpha}} \frac{E_\alpha[p_k(x)]}{E_\alpha[p_k(x(1+at)^{\frac{1}{\alpha}})]} \quad (12)$$

\*Corresponding author: jyotindraprajapati.maths@charusat.ac.in

$$\sum_{n=0}^{\infty} x^{-an} \binom{m+n}{n} V_n^{(\alpha, \beta)}(x; a, k, s) t^n = (1-at)^{-\left(\frac{\beta+s}{a}\right)} \frac{E_a\{p_k(x)\}}{E_a\{p_k\{x(1-at)^{-\frac{1}{a}}\}\}} \times V_n^{(\alpha, \beta)}\{x(1-at)^{-\frac{1}{a}}; a, k, s, \} \tag{13}$$

**Proof of (11):**

From (7), we consider

$$\sum_{n=0}^{\infty} V_n^{(\alpha, \beta)}(x; a, k, s) t^n = x^{-\beta} E_a\{p_k(x)\} e^{\theta} x^{\beta} \left[ \frac{1}{E_a\{p_k(x)\}} \right]$$

above equation reduces to

$$\sum_{n=0}^{\infty} V_n^{(\alpha, \beta)}(x; a, k, s) t^n = x^{-\beta} E_a\{p_k(x)\} x^{\beta} (1-ax^a t)^{-\left(\frac{\beta+s}{a}\right)} \times \frac{1}{E_a\{p_k\{x(1-ax^a t)^{-\frac{1}{a}}\}\}}$$

and replacing  $t$  by  $tx^{-a}$ , which gives (11).

**Proof of (12):**

From (7), we consider

$$\sum_{n=0}^{\infty} x^{-an} V_n^{(\alpha, \beta-an)}(x; a, k, s) t^n = x^{-\beta} E_a\{p_k(x)\} e^{\theta} \left[ x^{\beta-an} \frac{1}{E_a\{p_k(x)\}} \right]$$

and simplifying the above equation, we get

$$\sum_{n=0}^{\infty} x^{-an} V_n^{(\alpha, \beta-an)}(x; a, k, s) t^n = x^{-\beta} E_a\{p_k(x)\} x^{\beta} (1+at)^{\frac{\beta+s}{a}-1} \times \frac{1}{E_a\{p_k\{x(1+at)^{\frac{1}{a}}\}\}}$$

which proves (12).

**Proof of (13):**

writing (7) as

$$\theta^n [x^{\beta} E_a\{-p_k(x)\}] = n! x^{\beta} \frac{1}{E_a\{p_k(x)\}} V_n^{(\alpha, \beta)}(x; a, k, s)$$

or

$$e^{\theta} (\theta^n [x^{\beta} E_a\{-p_k(x)\}]) = n! e^{\theta} \left[ x^{\beta} \frac{1}{E_a\{p_k(x)\}} V_n^{(\alpha, \beta)}(x; a, k, s) \right]$$

above equation can be written as

$$\begin{aligned} \sum_{m=0}^{\infty} \frac{t^m \theta^{m+n}}{m!} [x^{\beta} E_a\{-p_k(x)\}] &= n! x^{\beta} (1-ax^a t)^{-\left(\frac{\beta+s}{a}\right)} \times \\ &\frac{1}{E_a\{p_k\{x(1-ax^a t)^{-\frac{1}{a}}\}\}} \times \\ &V_n^{(\alpha, \beta)}\{x(1-ax^a t)^{-\frac{1}{a}}; a, k, s, \} \\ &= \sum_{m=0}^{\infty} \frac{1}{m! n!} (m+n)! x^{\beta} \frac{1}{E_a\{p_k(x)\}} \times \\ &V_{m+n}^{(\alpha, \beta)}(x; a, k, s) t^m \\ &= x^{\beta} (1-ax^a t)^{-\left(\frac{\beta+s}{a}\right)} \frac{1}{E_a\{p_k\{x(1-ax^a t)^{-\frac{1}{a}}\}\}} \times \\ &V_n^{(\alpha, \beta)}\{x(1-ax^a t)^{-\frac{1}{a}}; a, k, s, \} \end{aligned}$$

and above expression reduces to

$$\begin{aligned} \sum_{m=0}^{\infty} \binom{m+n}{n} V_{m+n}^{(\alpha, \beta)}(x; a, k, s) t^m &= (1-ax^a t)^{-\left(\frac{\beta+s}{a}\right)} \frac{E_a\{p_k(x)\}}{E_a\{p_k\{x(1-ax^a t)^{-\frac{1}{a}}\}\}} \times \\ &V_n^{(\alpha, \beta)}\{x(1-ax^a t)^{-\frac{1}{a}}; a, k, s, \} \end{aligned}$$

replacing  $t$  by  $tx^{-a}$ , which leads to (13).

**FINITE SUMMATION FORMULAE:**

We obtained two finite sum formulae for (7) as

$$V_n^{(\alpha, \beta)}(x; a, k, s) = \sum_{m=0}^n \frac{1}{m!} (ax^a)^m \binom{\beta}{a}_m V_{n-m}^{(\alpha, 0)}(x; a, k, s) \tag{14}$$

$$V_n^{(\alpha, \beta)}(x; a, k, s) = \sum_{m=0}^n \frac{1}{m!} (ax^a)^m \binom{\beta-\gamma}{a}_m V_{n-m}^{(\alpha, \gamma)}(x; a, k, s) \tag{15}$$

**Proof of (14):**

We can write (7) as,

$$V_n^{(\alpha, \beta)}(x; a, k, s) = \frac{1}{n!} x^{-\beta} E_a\{p_k(x)\} \theta^n \left[ x x^{\beta-1} \frac{1}{E_a\{p_k(x)\}} \right]$$

we get,

$$\begin{aligned} V_n^{(\alpha, \beta)}(x; a, k, s) &= \frac{1}{n!} x^{-\beta} E_a\{p_k(x)\} x \times \\ &\sum_{m=0}^n \binom{n}{m} \theta^{n-m} \left[ \frac{1}{E_a\{p_k(x)\}} \right] \theta^m (x^{\beta-1}) \end{aligned}$$

which yields

$$\begin{aligned} V_n^{(\alpha, \beta)}(x; a, k, s) &= \frac{1}{n!} x^{-\beta+1} E_a\{p_k(x)\} \sum_{m=0}^n \frac{n!}{m!(n-m)!} \times \\ &x^a (n-m) [(s+xD)(s+a+xD)(s+2a+xD) \\ &\dots (s+(n-m-1)a+xD)] \left[ \frac{1}{E_a\{p_k(x)\}} \right] \\ &\times x^{am} [(1+xD)(1+a+xD)(1+2a+xD) \\ &\dots (1+(m-1)a+xD)] x^{\beta-1} \\ &= E_a\{p_k(x)\} \sum_{m=0}^n \frac{1}{m!(n-m)!} x^{an} \times \\ &\prod_{i=0}^{n-m-1} (s+ia+xD) \left[ \frac{1}{E_a\{p_k(x)\}} \right] a^m \binom{\beta}{a}_m \tag{16} \end{aligned}$$

Putting  $\beta = 0$  and replacing  $n$  by  $n-m$  in (7) then equation reduces to

$$\begin{aligned} V_{n-m}^{(\alpha, 0)}(x; a, k, s) &= \frac{1}{(n-m)!} E_a\{p_k(x)\} \theta^{n-m} \left[ \frac{1}{E_a\{p_k(x)\}} \right] \end{aligned}$$

thus, we have

$$\begin{aligned} \frac{1}{(n-m)!} \theta^{n-m} \left[ \frac{1}{E_a\{p_k(x)\}} \right] &= \frac{1}{E_a\{p_k(x)\}} V_{n-m}^{(\alpha, 0)}(x; a, k, s) \end{aligned}$$

we get,

$$\begin{aligned} \frac{1}{(n-m)!} \prod_{i=0}^{n-m-1} (s+ia+xD) \left[ \frac{1}{E_a\{p_k(x)\}} \right] &= \frac{x^a (n-m)}{E_a\{p_k(x)\}} V_{n-m}^{(\alpha, 0)}(x; a, k, s) \tag{17} \end{aligned}$$

use of (17) and (16), which immediately leads (14).

**Proof of (15):**

From (7) we consider,

$$\sum_{n=0}^{\infty} V_n^{(\alpha, \beta)}(x; a, k, s) t^n = x^{-\beta} E_a\{p_k(x)\} e^{\theta} \left[ x^{\beta} \frac{1}{E_a\{p_k(x)\}} \right]$$

above equation reduces to,

$$\begin{aligned} \sum_{n=0}^{\infty} V_n^{(\alpha, \beta)}(x; a, k, s) t^n &= (1-ax^a t)^{-\left(\frac{\beta+s}{a}\right)} \frac{E_a\{p_k(x)\}}{E_a\{p_k\{x(1-ax^a t)^{-\frac{1}{a}}\}\}} \\ &= x^{-\beta} E_a\{p_k(x)\} x^{\beta} (1-ax^a t)^{-\left(\frac{\beta+s}{a}\right)} \times \\ &\frac{1}{E_a\{p_k\{x(1-ax^a t)^{-\frac{1}{a}}\}\}} \end{aligned}$$

which yields

$$\sum_{n=0}^{\infty} V_n^{(\alpha, \beta)}(x; a, k, s) t^n = (1 - ax^a t)^{-\left(\frac{\gamma+s}{a}\right)} \sum_{m=0}^{\infty} \left(\frac{\beta - \gamma}{a}\right)_m \frac{(ax^a t)^m}{m!} \times \frac{E_\alpha [p_k(x)]}{E_\alpha [p_k \{x(1 - ax^a t)^{-\frac{\gamma}{a}}\}]}$$

by using (11),

$$\begin{aligned} \sum_{n=0}^{\infty} V_n^{(\alpha, \beta)}(x; a, k, s) t^n &= \sum_{m=0}^{\infty} \left(\frac{\beta - \gamma}{a}\right)_m \frac{(ax^a t)^m}{m!} x^{-\gamma} \times \\ &E_\alpha \{p_k(x)\} e^{\theta} \left[ x^\gamma \frac{1}{E_\alpha \{p_k(x)\}} \right] \\ &= \sum_{m=0}^{\infty} \sum_{n=0}^{\infty} \left(\frac{\beta - \gamma}{a}\right)_m \frac{(ax^a)^m t^{n+m}}{m! n!} x^{-\gamma} \times \\ &E_\alpha \{p_k(x)\} \theta^n \left[ x^\gamma \frac{1}{E_\alpha \{p_k(x)\}} \right] \\ &= \sum_{n=0}^{\infty} \sum_{m=0}^n \left(\frac{\beta - \gamma}{a}\right)_m \frac{(ax^a)^m t^n}{m! (n-m)!} x^{-\gamma} \times \\ &E_\alpha \{p_k(x)\} \theta^{n-m} \left[ x^\gamma \frac{1}{E_\alpha \{p_k(x)\}} \right] \end{aligned}$$

by equating the coefficients of  $t^n$ , we get

$$V_n^{(\alpha, \beta)}(x; a, k, s) = \sum_{m=0}^n \frac{1}{m!} (ax^a)^m \left(\frac{\beta - \gamma}{a}\right)_m \frac{x^{-\gamma}}{(n-m)!} \times E_\alpha \{p_k(x)\} \theta^{n-m} \left[ x^\gamma \frac{1}{E_\alpha \{p_k(x)\}} \right]$$

and use of (7), we get (15).

**SPECIAL CASES:**

In this section, we have obtained some special cases and relations of sequence of functions  $V_n^{(\alpha, \beta)}(x; a, k, s)$ , in the connection of (4), (9) and (10): Putting  $\alpha = 1$  and replacing  $\beta$  by  $\alpha$  in (7) then

$$V_n^{(1, \alpha)}(x; a, k, s) = V_n^{(\alpha)}(x; a, k, s) \tag{18}$$

Therefore, we can say that (4) is a particular case of (7).

If  $\alpha = 1$ , replacing  $\beta$  by  $\alpha + 1, \alpha = 1, p_k(x) = p_l(x) = x$ , and  $s = 0$ , then (7) reduces to

$$V_n^{(1, \alpha+1)}(x; 1, 1, 0) = x^n Y_n^\alpha(x; 1) \tag{19}$$

if  $\alpha = 1, \beta = 0, p_k(x) = p_2(x) = x^2$ , and  $s = 0$ , then (7) reduces to  $\alpha = -1$  and  $s = 0$  then (7) gives  $V_n^{(1, 0)}(x; -1, 2, 0) = \frac{(-1)^n}{n!} H_n(x)$  20

**CONCLUSION:**

The new sequence of functions (5), (6) and (7), introduced in the section 1, the results obtained in sections 2, 3 and 4 seem to be new and quite interesting.

**ACKNOWLEDGMENT:**

Authors are grateful to the referee/s for carefully reading the manuscript and suggesting a way of improvement.

**REFERENCES**

- [1] Mittag – Leffler G.M. (1903): Sur la nouvelle fonction  $E_\alpha(x)$  *C.R. Acad. Sci. Paris* **137**, 554 – 558.
- [2] Mittal, H. B. (1971) A generalization of Laguerre polynomials, *Publ. Math. Debrecen* **Vol. 18**, pp. 53-88.
- [3] Mittal, H. B. (1971) Operational representations for the generalized Laguerre polynomial, *Glasnik Mat. Ser III* **Vol. 6(26)**, pp. 45-53.
- [4] Mittal, H. B. (1977) Bilinear and Bilateral generating relations, *American J. Math.* **Vol. 99**, pp. 23-45.
- [5] Patil, K. R. and Thakare, N. K. (1975) Operational formulas for a function defined by a generalized Rodrigues formula-II, *Sci. J. Shivaji Univ.* **Vol. 15**, pp.1-10.
- [6] Rainville, E. D. (1960) *Special functions*, The Macmillan Company, New York.
- [7] Srivastava, A. N. and Singh, S. N. (1979) Some generating relations connected with a function defined by a Generalized Rodrigues formula, *Indian J. Pure and Appl. Math* **Vol. 10(10)**, pp. 1312-1317.
- [8] Srivastava, H. M. and Singhal J. P. (1971) A class of polynomials defined by generalized Rodrigues formula, *Ann. Mat. Pure Appl* **Vol. 4**, pp.75-85.
- [9] Srivastava, H. M. (1982) Some biorthogonal polynomials suggested by the Laguerre polynomials, *Pacific J. Math.* **Vol. 98(1)**, pp. 235-250.



**Editorial Note:** This paper is a corrected version of the paper published earlier as PRAJNA - Journal of Pure and Applied Sciences, Vol. 18: 115 -116 (2010). In the earlier version inadvertently the Statement of Theorem 2.3 was left out and Illustration 2.2 was misplaced. We regret for this and for a complete academic record, we publish this corrected version.

## MEAN LABELING FOR SOME NEW FAMILIES OF GRAPHS

S.K. Vaidya\*<sup>1</sup> and Lekha Bijukumar <sup>2</sup>

<sup>1</sup>Department of Mathematics, Saurashtra University, Rajkot-360005, Gujarat, India

<sup>2</sup>Shanker Sinh Vaghela Bapu Institute of Technology, Gandhinagar, Gujarat, India

### ABSTRACT

Some new families of mean graphs are investigated. We prove that the step ladder graph, total graph of path  $P_n$  are mean graphs. In addition to this we derive that two copies of cycle  $C_n$  sharing a common edge admits mean labeling.

**Key words:** Mean labeling, Mean graph, Step ladder graph, Total graph

**AMS Subject classification number (2010):** 05C78

### INTRODUCTION

We begin with simple, finite, connected and undirected graph  $G = (V(G), E(G))$  with  $p$  vertices and  $q$  edges. For all other standard terminology and notation we follow Harary [1]. We will provide brief summary of definitions and other information which serve as prerequisites for the present investigations.

**Definition 1.1** Let  $P_n$  be a path on  $n$  vertices denoted by  $(1,1), (1,2), \dots, (1,n)$  and with  $n-1$  edges denoted by  $e_1, e_2, \dots, e_{n-1}$  where  $e_i$  is the edge joining the vertices  $(1,i)$  and  $(1,i+1)$ . On each edge  $e_i$ ,

$i = 1, 2, \dots, n-1$  we erect a ladder with  $n-(i-1)$  steps including the edge  $e_i$ . The graph obtained is called a *step ladder graph* and is denoted by  $S(T_n)$ , where  $n$  denotes the number of vertices in the base.

**Definition 1.2** The vertices and edges of a graph are called its elements. Two elements of a graph are neighbours if they are either incident or adjacent. The *total graph* of a graph  $G$  is denoted by  $T(G)$  is a graph with vertex set  $V(G) \cup E(G)$  and two vertices are adjacent in  $T(G)$  whenever they are neighbors in  $G$ .

**Definition 1.3** If the vertices are assigned values subject to certain conditions then it is known as *graph labeling*. Graph labeling is one of the fascinating areas of graph theory with wide ranging applications. An enormous body of literature has grown around in graph labeling in last five decades. A systematic study of various applications of graph labeling is carried out in Bloom and Golomb [3]. According to Beineke and Hegde [2] graph labeling serves as a frontier between number theory and structure of graphs. For detailed survey on graph labeling we refer to A Dynamic Survey of Graph Labeling by Gallian [4].

**Definition 1.4** A function  $f$  is called a *mean labeling* of graph  $G$  if  $f: V(G) \rightarrow \{0, 1, 2, \dots, q\}$  is injective and the induced function  $f^*: E(G) \rightarrow \{1, 2, \dots, q\}$  defined as

$$f^*(e = uv) = f(u) + f(v)/2 \quad \text{iff } f(u) + f(v) \text{ is even}$$

$$= f(u) + f(v) + 1/2 \quad \text{iff } f(u) + f(v) \text{ is odd}$$

is bijective. The graph which admits mean labeling is called a *mean graph*.

The mean labeling is introduced by Somasundaram and Ponraj [5] and they proved the graphs  $P_n, C_n, P_n \times P_m, P_m \times C_n$  etc. admit

mean labeling. The same authors in [6] have discussed the mean labeling of subdivision of  $K_{1,n}$  for  $n \leq 3$  while in [7] they proved that the wheel  $W_n$  does not admit the mean labeling for  $n \leq 4$ . Mean labeling in the context of some graph operations is discussed by Vaidya and Lekha [8]. In the present work three new results corresponding to mean labeling and some new families of mean graphs are investigated.

### MAIN RESULTS

**Theorem-2.1:** The step ladder graph  $S(T_n)$  is a mean graph.

**Proof:** Let  $P_n$  be a path on  $n$  vertices denoted by  $(1,1), (1,2), \dots, (1,n)$  and with  $n-1$  edges denoted by  $e_1, e_2, \dots, e_{n-1}$  where  $e_i$  is the edge joining the vertices  $(1,i)$  and  $(1,i+1)$ . The step ladder graph  $S(T_n)$  has vertices denoted by  $(1,1), (1,2), \dots, (1,n), (2,1), (2,2), \dots, (2,n), (3,1), (3,2), \dots, (3,n-1), \dots, (n,1), (n,2)$ . In the ordered pair  $(i,j)$ ,  $i$  denotes the row (counted from bottom to top) and  $j$  denotes the column (from left to right) in which the vertex occurs.

Define  $f: V(S(T_n)) \rightarrow \{0, 1, 2, \dots, q\}$  as follows.

$$f(i,1) = (n^2 + n - 2) - (i - 1); \quad 1 \leq i \leq n$$

$$f(1,j) = (n^2 + n - 2) - \sum_{k=1}^{j-1} (n-k) - \sum_{k=2}^j [(n+k) - (j-1)]; \quad 2 \leq j \leq n$$

$$f(i,j) = (n^2 + n - 2) - \sum_{k=1}^{i-1} (n-k) - \sum_{k=2}^j [(n+k) - (j-1)] - (i-1); \quad 2 \leq i, j \leq n \& j \neq n+2-i$$

$$f(i, n+2-i) = i^2 - 2; \quad 2 \leq i \leq n$$

In view of the above defined labeling pattern  $f$  is a mean labeling for the step ladder graph  $S(T_n)$ . That is,  $S(T_n)$  is a mean graph.

**Illustration 2.2:** The Figure 1 shows the labeling pattern for  $S(T_6)$ .

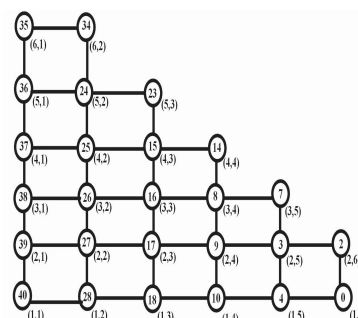


**Fig. 1**

\*Corresponding author: samirkvaidya@yahoo.co.in

**Theorem-2.3:** The total graph of path  $P_n$  that is,  $T(P_n)$  is a mean graph.

Proof: Let  $v_1, v_2, \dots, v_n$  be the vertices of path  $P_n$  with  $n-1$  edges denoted by  $e_1, e_2, \dots, e_{n-1}$ . According to the definition of total graph and two vertices are adjacent in  $T(P_n)$  if they are neighbors in  $P_n$ . Define  $f: V(T(P_n)) \rightarrow \{0, 1, 2, \dots, q\}$  as follows.

$$\begin{aligned}
 f(v_i) &= 0 \\
 f(v_i) &= 4(i-2)+2; & \text{for } 2 \leq i \leq n \\
 f(e_j) &= 4j; & \text{for } 1 \leq j \leq n-2 \\
 f(e_j) &= 4j-1; & \text{for } j = n-1
 \end{aligned}$$

Thus  $f$  provides a mean labeling for  $T(P_n)$ . That is,  $T(P_n)$  is a mean graph.

**Illustration 2.4:** The labeling pattern of  $T(P_5)$  is given in Fig. 2.

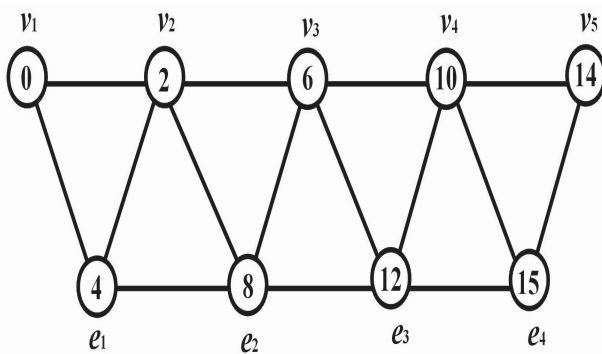


Fig. 2

**Theorem-2.5:** Two copies of cycle  $C_n$  sharing a common edge admit mean labeling.

**Proof:** Let  $v_1, v_2, \dots, v_n$  be the vertices of cycle  $C_n$ . Consider two copies of cycle  $C_n$ . Let  $G$  be the graph for two copies of cycle sharing a common edge in which  $v_1, v_2, \dots, v_n$  is a spanning path. Then  $V(G) = 2n-2$  and  $E(G) = 2n-1$ .

To define  $f: V(G) \rightarrow \{0, 1, 2, \dots, q\}$  the following two cases are to be considered.

**Case 1:**  $n$  is odd.

Without loss of generality assumes that  $e = \frac{v_{\frac{n+1}{2}} v_{\frac{3n-1}{2}}}$  be the common edge between two copies of  $C_n$ .

$$\begin{aligned}
 f(v_i) &= 2(i-1); & \text{for } 1 \leq i \leq n+1/2 \\
 f(v_i) &= 2i-1; & \text{for } n+3/2 \leq i \leq n \\
 f(v_i) &= 2(2n-2-i)+4; & \text{for } n+1 \leq i \leq 3n-3/2 \\
 f(v_i) &= 2(2n-2-i)+3; & \text{for } 3n-1/2 \leq i \leq 2n-2
 \end{aligned}$$

**Case 2:**  $n$  is even.

Without loss of generality assume that  $e = \frac{v_{\frac{n+2}{2}} v_{\frac{3n}{2}}}$  be the common edge between two copies of  $C_n$ .

$$\begin{aligned}
 f(v_i) &= 2(i-1); & \text{for } 1 \leq i \leq n+2/2 \\
 f(v_i) &= 2i-1; & \text{for } n+4/2 \leq i \leq n \\
 f(v_i) &= 2(2n-2-i)+4; & \text{for } n+1 \leq i \leq 3n-2/2 \\
 f(v_i) &= 2(2n-2-i)+3; & \text{for } 3n/2 \leq i \leq 2n-2
 \end{aligned}$$

Then the above defined function  $f$  provides mean labeling for two copies of cycle sharing a common edge.

**Illustration 2.6:** The Fig. 3 shows the mean labeling pattern for two copies of  $C_{10}$  sharing an edge.

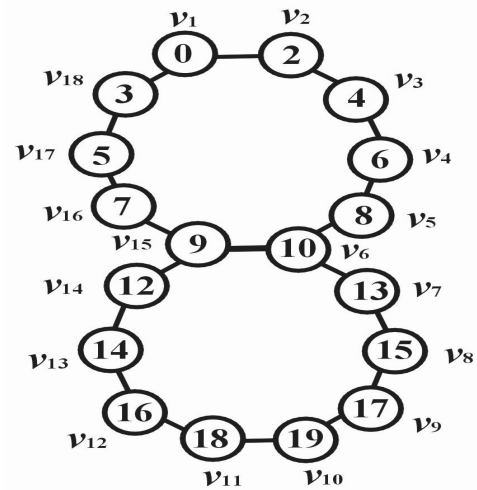


Fig. 3

**CONCLUDING REMARKS AND FURTHER SCOPE**

As all graphs are not mean graphs it is very interesting to investigate graphs which admit mean labeling. Here we contribute three new families of mean graphs. It is possible to investigate similar results for other graph families and in the context of different labeling techniques.

**ACKNOWLEDGMENT**

Authors are highly thankful to anonymous referee for valuable comments and kind suggestions.

**REFERENCES**

- [1] Harary, F. (1972) *Graph Theory*, Addison Wesley, Reading, Massachusetts.
- [2] Beineke, L. W. and Hegde, S. M. (2001), Strongly multiplicative graphs. *Discuss. Math. Graph Theory*, **21**: 63-75.
- [3] Bloom, G. S. and Golomb, S. W. (1977) Applications of numbered undirected graphs, *Proceedings of IEEE*, **65**(4): pp. 562-570.
- [4] Gallian, J. A. (2009) A dynamic survey of graph labeling, *The Electronic Journal of Combinatorics*, **16** DS6.
- [5] Somasundaram, S. and Ponraj, R. (2003) Some results on mean graphs, *Pure and Applied Mathematical Sciences*, **58**: 29-35.
- [6] Somasundaram, S. and Ponraj, R. (2004) On mean graphs of order  $< 5$ . *J. Decision and Mathematical Sciences*, **9**: 47-58.
- [7] Somasundaram, S. and Ponraj, R. (2003) Non existence of mean labeling for a wheel. *Bulletin of Pure and Applied Sciences*, **22E**: 103-111.
- [8] Vaidya, S. K. and Lekha, B. (2010) Mean labeling in the context of some graph operations, *Int. Journal of Algorithms, Comp. and Math.* **3**(1): 1-8.



## CORRELATIONS AMONG ATOMIC PROPERTIES AND ESTIMATES ON EXOTIC ATOMS

**Pooja Bhowmik, <sup>1</sup>Ramji H. Patel and K.N. Joshipura**

*Department of Physics, Sardar Patel University, Vallabh Vidyanagar – 388 120*

*<sup>1</sup>R. P. Arts, K. B. Commerce & Smt. B. C. J. Science College, Khambhat – 388 620*

### ABSTRACT

**In this paper we first examine and propose the relationships between the first ionization energy ( $I_0$ ), polarizability ( $\alpha_0$ ) and orbital radius specifically for inert gas-atoms. These are known in general over a range of atomic number  $Z$ . This paper reports linear relation between  $I_0$  and  $\alpha_0$  especially for the inert gas atoms and predicts the properties of super- heavy inert gas atom  $Z = 118$ . The correlation study is extended to lesser known regime of ions on one hand and meta-stable atomic species on the other.**

### INTRODUCTION

First ionization energy ( $I_0$ ) of atoms is one of the most well known experimental as well as theoretical quantity. This property is known to correlate strongly with another important atomic property i. e., electric dipole polarizability  $\alpha_0$  and this was shown for selected atomic species by Fricke [1]. The quantity  $\alpha_0$  is a measure for the response of an atomic system to an external electric field. While  $I_0$  corresponds to transitions in continuum,  $\alpha_0$  corresponds to virtual excitations. Correlation between  $\alpha_0$  and  $I_0$ , as well as  $\alpha_0$  and the average atomic radius  $\langle r \rangle$  were discussed by Dimitrieva & Plindov [2]. Hatti & Dutta [3] have also reported the same correlation using a semi-empirical approach. In earlier studies [4, 5] a relationship between  $\alpha_0$  and atomic volume was also established. Politzer et al [6] also showed relation between local ionization energy and polarizability in his recent publication. Considerable work has been reported in this field till date for atoms in their usual ground state. A number of empirical correlations between polarizabilities and volumes have also been reported [7- 9]. In this paper, we bring out a relationship between the quantities  $I_0$  and  $\alpha_0$  by equations which are exact for 1 electron atoms. We feel that for many - electron atoms it is more appropriate to make this type of generalization on the basis of periodic table groups, and this has been attempted in the present work. Thus we propose semiempirical equations for the important properties of the inert gas atoms. Comparisons of our generated or estimated values are made with available experimental data.

As an outcome of the correlations studied it has been possible to estimate or predict microscopic properties of exotic species like a super-heavy atom on one hand and meta-stable atoms on the other. The importance of present study lies in our quantitative conclusion about these special kinds of atoms for which very little knowledge exists at present.

### THEORETICAL ASPECTS

It is well known that polarizability and ionization energies have periodic property. Also, it has been established that atomic polarizabilities are dependent on size of the atoms. The graph of first ionization energy and polarizability in log scale for 88 elements was first plotted by Fricke [1]. The linear relationship between ionization energy and polarizability was extrapolated [1] to estimate the polarizability of heavier atom of a periodic group. To understand the reason for such behavior we can start with a prototype example of hydrogen atom.

Since early days of Quantum Mechanics the exact knowledge

\*Corresponding author: pujabhowmik@gmail.com

about 1- electron (hydrogenic atoms) exists. The ionization energy ( $I_0$ ) for hydrogen atom [10] is given as follows.

$$I_0 = \frac{13.6}{n^2} eV = \frac{1}{2n^2} \text{ au} \quad (1)$$

And the corresponding expectation value of s-electron radius is given by

$$\langle r \rangle = 3/2 a_0 \quad (2)$$

Where ground state value corresponds to  $n=1$ . Under the influence of infinitely massive nucleus the average or expectation value of the hydrogenic radius becomes

$$\langle r \rangle = 3/2 \text{ au} \\ I_0 = 1/\langle r \rangle \text{ or } I_0 = \delta / \langle r \rangle \quad (3)$$

With  $\delta$  as a constant, this correlates the atomic size i. e., average radius with ionization energy [10]. Now, it can be seen from [4 - 8] that the atomic dipole polarizability  $\alpha_0$  is proportional to  $\langle r \rangle^3$ , so that

$$\alpha_0 \propto \frac{1}{I_0^3} \text{ or } \alpha_0 = \frac{\beta}{I_0^3} \quad (4)$$

Here  $\beta$  is a constant. A similar relation was reported in other works [2, 3, 6]. Dimitrieva & Plindov [2] have deduced a similar dependence via a statistical model, as follows

$$\alpha_0(N, Z) = (Z - N + 1)^3 I_0^{-3}(N, Z) f(N, Z) \quad (5)$$

These authors [2] used experimental data for 34 neutral atoms to demonstrate that  $f(N, Z)$  is slowly varying function of the nuclear charge, the correlation coefficient for fitting these data was 0.97 which is quite good. But, both the ionization energy and the polarizability cannot be expected to correlate strongly in such a general way as in equation (4) for all atoms, because the structure of the valence shell of each atom is different. But systematic variations are expected over a group in the periodic table. Thus it is more reasonable to search for correlations within a group in the periodic table.

In view of the above discussion, we can generalize and propose an equation connecting  $\alpha_0$  and  $1/I_0^3$  in the following linear expression

$$\alpha_0 = A/I_0^3 + B \quad (6)$$

Here slope A and intercept B are parameters for a periodic group and their value varies from one group to another group. This means that these values essentially depend on outer electron configuration or number of electrons and other parameters of atoms in the group. Parameters A and B in a group are obtained by the standard linear least square fitting. Thus we find that for the inert gas group, the linear equation becomes

$$\alpha_0 = 7036.01/I_0^3 - 0.1934 \quad (7)$$

The correlation coefficient for this fitting is 0.99593, which is better than that in [2].

Let us also consider the cations  $\text{Li}^+$ ,  $\text{Na}^+$ ,  $\text{K}^+$ ,  $\text{Rb}^+$ ,  $\text{Cs}^+$  and  $\text{Fr}^+$  which are respectively isoelectronic with the nearby inert gas atom. Therefore, the relation between  $\alpha_0$  &  $I_0$  is expected to be as per equation (6) with a different set of A and B. We have also attempted here a similar correlation between  $\alpha_0$  &  $I_0$  for the metastable atoms  $\text{He}^*(2^3S_1)$ ,  $\text{Ne}^*(^3P_2)$ ,  $\text{Ar}^*(^3P_2)$ ,  $\text{Kr}^*(^3P_2)$ ,  $\text{Xe}^*(^3P_2)$ . The parameters A and B in each of the above three categories of atomic systems are exhibited in table 1.

**Table- 1** Linear fitting parameters A and B for equation (6)

Group of atoms	A	B	Correlation coefficient
Noble gases (ground state)	7036.01	-0.193	0.995
Group IA (cations)	33720.75	-0.172	0.994
Noble gas (Metastable states)	3434.99	1.5123	0.991

## RESULT AND DISCUSSION

In the present theoretical study, we have proposed a linear relation between  $\alpha_0$  and  $1/I_0^3$  as given in equation (6), for three different atomic systems, viz., noble gases, noble-gas like positive ions and meta-stable atomic states. These are discussed separately below.

### Noble gas atoms

We find that there is excellent correlation over the inert gas group. Let us (Fig. 1) take the advantage of the excellent correlation of 99% and extrapolate the graph in figure 1 to super-heavy inert gas atom of  $Z = 118$ , called EKARADON, Uuo. For this purpose the first ionization potential for this exotic super-heavy atom is taken from [11]. The value of  $I_0$  is 8.92 eV, when supplied to equation (7) brings out the value of polarizability to be  $9.72 \text{ \AA}^3$ . However some physical insight also can be made by using semi-quantum mechanical arguments.

The radius of a particular electronic shell is defined as the distance at which the electron charge density  $e|\Psi|^2$  is maximum. Denoting this by  $R_{\text{max}}$  we find from Hirshfelder et al [7] and also from Bransden and Joachain [10] that,

$$R_{\text{max}} = \frac{n^{*2}}{Z-s} \quad (8)$$

Where  $n^*$  is effective principal quantum number and  $(Z-s)$  is effective nuclear charge, which can be calculated using the Slater rules as stated in Hirschfelder [7].

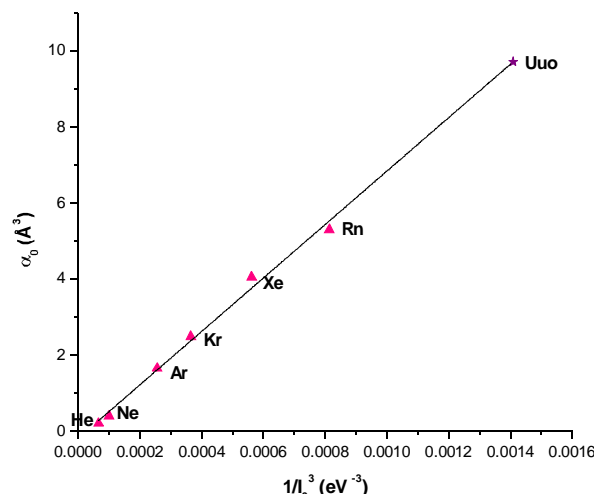


**Fig. 1** Fitting of  $\alpha_0 \rightarrow 1/I_0^3$  for ground state noble gas atoms.

Thus, the ionization energy corresponding to  $n^*$  may be considered as,

$$I_0 \propto \frac{1}{n^{*2}} \quad (9)$$

We first calculate  $R_{\text{max}}$  for  $Z=118$  using equation (8), while  $(Z-s)$  is calculated using Slater's rules. The value of  $R_{\text{max}}$  obtained in this case is  $2.35 a_0$ . From this we find that the ionization potential is 9.83 eV. Now, again from this  $I_0$  and equation (7), we obtain the value of polarizability to be  $7.21 \text{ \AA}^3$ , which is comparable to  $9.72 \text{ \AA}^3$  as reported earlier in this section.

### Noble Gases and respective iso-electronic ions

Consider now a set of singly charged alkali positive ions  $\text{Li}^+$ ,  $\text{Na}^+$ ,  $\text{K}^+$ ,  $\text{Rb}^+$ ,  $\text{Cs}^+$  and  $\text{Fr}^+$  having electronic configuration of the respective (iso-electronic) noble gas atoms. Studying the correlation between  $\alpha_0$  and  $I_0$  for these cations, we find excellent correlation coefficient for the fitting equation (6). The values of A and B of this atomic system are different from that of noble gases. This is due to the nature of the tightly bound cations, resulting into high  $I_0$  and small  $\langle r \rangle$  as well as  $\alpha_0$ .

From Figure 2 we can obtain a fitting relation as predicted by our model with the help of which we can estimate the polarizability of an atom whose ionization energy is known. The fitting parameters along with their respective correlation coefficient are mentioned in Table 3. Whereas Table 2 displays the estimated values of polarizability obtained from the fitting relation. The unphysical negative but small value of  $\alpha_0$  of  $\text{Li}^+$  generated by the fitting equation, wide a Table 2, indicates very small polarizability arising out of very tight binding of this

**Table 2** ionization potential and polarizability for noble gas-like positive alkali ions

Sr. No	Ion (no. of electrons)	Ionization potential $I_0$ (eV)	Electric dipole polarizability $\alpha_0$ ( $\text{\AA}^3$ )	Calculated $\alpha_0$ ( $\text{\AA}^3$ ) From (6)
1	$\text{Li}^+$ (2)	75.64	0.03	-0.09
2	$\text{Na}^+$ (10)	47.28	0.14	0.14
3	$\text{K}^+$ (18)	31.63	0.79	0.89
4	$\text{Rb}^+$ (36)	27.28	1.41	1.48
5	$\text{Cs}^+$ (54)	23.15	2.42	2.54
6	$\text{Fr}^+$ (86)	22.40	3.02	2.82

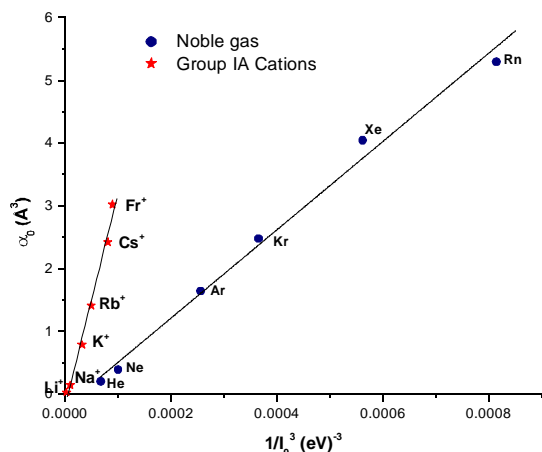


**Fig. 2** Fitting of  $\alpha_0 \rightarrow 1/I_0^3$  for Alkali metal ions, along with noble gas atoms. The values of ionization energy  $I_0$  and polarizability are taken from References 11 - 14.

One can also think of a similar fitting of  $\alpha_0 \rightarrow I_0^{-3}$  for the group VII A negative ions, F, Cl, Br and I whose electron configuration also corresponds to the noble gases. However, preliminary study does not indicate a good linear relation between  $\alpha_0 \rightarrow I_0^{-3}$  in this case. The F particularly differs considerably from the other three anions. Therefore, these results are not exhibited here.

#### Metastable atoms

Metastable states are electronically excited states of atoms or molecules having longer life time in view of the dipole selection rules. Metastable states exhibit characteristics like large size, larger polarizability and lower ionization potentials. Ionization energies of these states can be determined easily, but there is lack of data on polarizability of these species. This is because of difficulties arising in experimental techniques and complicated method of calculating the polarizability tensors. So, we extend the present correlation study to the metastable excited states, where the plot of  $\alpha_0$  as a function of  $1/I_0^3$  again gives a linear relation between the two quantities as shown in the Figure 3.

**Table 3** ionization potential and polarizability of meta-stable states of noble gas-atoms.

Sr. No	Metastable Atom	Ionization potential $I_0$ (eV)	Electric dipole Polarizability $\alpha_0$ ( $\text{\AA}^3$ )	Calculated $\alpha_0$ ( $\text{\AA}^3$ ) From eq (6)
1	He*( $2^3S_1$ )	4.77	44.66	33.24
2	Ne*( $^3P_2$ )	4.94	27.79	30.01
3	Ar*( $^3P_2$ )	4.21	47.89	47.44
4	Kr*( $^3P_2$ )	4.09	50.70	51.71
5	Xe*( $^3P_2$ )	3.81	63.59	63.43

We note the special behavior of He\* with respect to Ne\* in the graphical plot of Figure 3. The data values and the generated values of  $\alpha_0$  show a good matching as shown in Table 3.

#### Conclusions

Thus, this paper presents our semi-empirical studies on the linear relations of  $\alpha_0$  as a function of  $1/I_0^3$  in several atomic cases. Searching for general trend and correlations among the physical properties has been a passion with physicists. Several attempts have been done, as highlighted in the Introduction section, to find the equations relating the atomic first ionization threshold

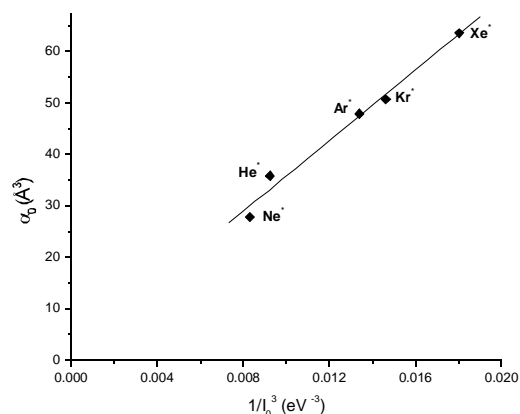


**Fig.3** of Fitting  $\alpha_0 \rightarrow 1/I_0^3$  for metastable excited states of noble gas atoms. The values of ionization energy  $I_0$  and polarizability are taken from References 15 - 20.

and the polarizability, and the present equation (6) is a yet another effort. We focus on a periodic table group rather than choosing a range of continuous Z values, and this is reasonable. The present study can be extended to other groups as well. Further, interesting correlations can also be found among the static properties  $I_0$  and  $\alpha_0$ , and a dynamic quantity viz., electron impact ionization cross section peak, at a given incident energy. This work is underway. Finally correlations between  $I_0$  and  $\alpha_0$  can also exist for atoms under extreme conditions, say in dense plasma or under high pressure.

#### References

- [1] Fricke B., (1986) On the correlation between electric polarizabilities and the ionization potential of atoms *J. Chem. Phys.* **84**: 862 - 866
- [2] Dmitreiva I. K. and Plindov G. I., (1983) Dipole polarizability, radius and ionization potential for Atomic systems *Phys. Scr.* **27**, 402-406
- [3] Hati S. and Datta D., (1996) At the most, only one electron can be added to a free atom in Gas phase *J. Phys. Chem.* **100**: 4828 - 4830
- [4] Condon E. U. and Odishaw H. (1958) *Handbook of Physics*, McGraw-Hill, New York
- [5] Politzer P., Jin P. and Murray J., (2002), Atomic polarizability, volume and ionization energy *J. Chem. Phys.* **117**: 8197 - 8202
- [6] Politzer P., Murray J. and Bulat F. (2010), Average local ionization energy: A review *J Mol Model* **16**: 1731 - 1742
- [7] Hirschfelder J. O., Curtiss C. F. and Bird R. B. (1954), *Molecular Theory of Gases and Liquids*, Wiley, New York
- [8] Brinck T., Murray J., Politzer P. (1993) Polarizability and volume *J. Chem. Phys.* **98**: 4035 - 4036
- [9] Chandrakumar K.R.S, Ghanty T. and Ghosh S. (2004) Relationship between ionization potential, polarizability and softness: A case study of Lithium and Sodium metal clusters, *J. Phys. Chem.* **108**: 6661 - 6666
- [10] Bransden B. H. and Joaichain C. J. (1983), *Physics of Atoms and Molecules*, Longman Group Ltd. New York

- [11] Pershina V., Boeschevsky A., Eliav E. and Kaldor U. (2008) Adsorption of inert gases including element 118 on noble metal and inert surfaces from ab initio Dirac-Coulomb atomic calculations *J. Chem. Phys.* **129**: 144106–9
- [12] Lide D. R. (2003), *CRC Handbook of Chemistry and Physics*, CRC Press LLC, Boca Raton FL
- [13] Coker H. (1976), Empirical free ion polarizabilities of the alkali metal, alkaline earth metal and halide ions *J Phys Chem.* **80**: 2078–2084
- [14] Pearson R.G.(1988), Absolute Electronegativity and hardness: Application to inorganic chemistry *Inorg Chem* **27**: 734-740
- [15] Nesbet R.K. (1977) Atomic polarizabilities for ground and excited states of C, N and O. *Phys. Rev A* **16**: 1-5
- [16] Molof R.W, Schwartz H.L, Miller T.M. and Bederson B. (1974) Measurement of electric dipole polarizabilities of the alkali-metal atoms and the metastable noble-gas atoms. *Phys. Rev A* **10**: 1131 - 1140
- [17] Corsby D.A. (1977) Dipole polarizability of  $2^3S_1$  and  $2^1S_0$  metastable helium measured by the electric deflection time-of-flight method. *Phys. Rev A* **16**: 488 - 491
- [18] Asgar M. and Stone P.M. (2008) Electron impact ionization of metastable rare gases: He, Ne and Ar. *Int. J Mass Spec* **271**: 51- 57
- [19] Kim Y.K and Descaulx J.K (2002) Ionization of carbon, nitrogen and oxygen. *Phys. Rev A* **66**: 012708 - 12
- [20] Ton-That D. and Flannery M.R. (1977) Cross sections for ionization of metastable rare-gas atoms ( $Ne^*$ ,  $Ar^*$ ,  $Kr^*$ ,  $Xe^*$ ) and of metastable  $N_2^*$ ,  $CO^*$  molecules by electron impact. *Phys. Rev A* **15**: 517–526



## CRYSTAL QUARTZ WINDOWS FOR FAR-INFRARED INTERFEROMETER OF SST-1

Asha Adhiya\* and Rajwinder Kaur

*Institute for Plasma Research, Bhat, Gandhinagar- 382 428, Gujarat*

### ABSTRACT

This paper presents the estimation of power transmission through optical windows for three (vertical, lateral and tangential) views of the far infrared (FIR) interferometer operating at 118.8 $\mu\text{m}$  and 432.6 $\mu\text{m}$  for plasma density measurement in steady-state superconducting tokamak-1 (SST-1). The lateral and tangential views have fan of beams incident on the optical windows at different angles of incidence. Crystal quartz has been selected as the window material owing to its good optical properties in Far infrared region, in addition to high melting point and very high physical strength. Ordinary and extraordinary modes of propagation inside crystal quartz cuts for incident s and p-polarized light beams have been investigated. z-cut crystal quartz has been selected to get maximum power transmission and reduce the effect of birefringence. The reflectivity of windows for the ordinary mode propagation has been calculated using resonant effect by Fresnel equations for all probing beams and the thicknesses have been optimized corresponding to maximum transmission through the windows. The power transmission of incident beams taking absorption coefficient into account has been given.

**Keywords:** *Crystal Quartz, Ordinary and extraordinary modes, Quartz cuts, Resonant effect and Fresnel equation*

### INTRODUCTION

Interferometry is the principle diagnostics method for density measurement in tokamak plasmas [1-7]. Radiation of suitable wavelength, decided by beam refraction and mechanical stability of the interferometer support structure, is used to probe the plasma. SST-1 is a modest size ( $R\sim 1.1\text{m}$ ,  $a\sim 0.2\text{m}$ ,  $\kappa\sim 1.7-2$ ,  $\delta\sim 0.4-0.7$ ,  $B_T\sim 3\text{T}$ ,  $I_p\sim 220\text{kA}$ ) steady state superconducting tokamak designed to operate for stable long pulse duration of 1000 sec. SST-1 plasma will have D-shaped cross-section which limits diagnostics access due to presence of stabilizer and divertor plates. The loss of circular symmetry requires multiview, multichannel density measurements. Optically pumped FIR lasers operating at 118.8 $\mu\text{m}$  and 432.6 $\mu\text{m}$  have been selected as radiation sources for three views of interferometer being developed for SST-1 tokamak [7]. Far infrared laser beams enter the plasma column through vacuum windows mounted on machine ports.

This paper discusses the criteria for the selection of diagnostic window material for vertical, lateral and tangential viewing of FIR interferometers for SST-1 tokamak. Based on various considerations, crystalline quartz has been found to be the material preferred for vacuum windows in the present case. Section 2 describes lines of sight of vertical, lateral and tangential view FIR interferometers and their orientation at window surface. The selection of window material and possible modes of propagation inside crystal quartz are presented in section 3. The selection of window thickness that corresponds to maximum power transmission through windows for above-mentioned views of the FIR interferometer for SST-1 is presented in section 4. The concluding remarks are made in section 5.

### LINES OF SIGHT

In SST-1 tokamak, the density distribution will be measured using a single channel vertical, five channel lateral and six channel tangential view FIR interferometers (Fig.1). For vertical viewing, the beam waist  $d_0\sim 7\text{mm}$  is placed at the midplane and expands to  $d_{\text{win}}\sim 8\text{mm}$ . The window aperture has been kept to be 63mm to accommodate the refraction due to transverse density gradient as well as to avoid diffraction losses.

The lateral and tangential views of the FIR interferometer employ fan beam geometries to cover the plasma cross-section [5]. The pivot points in both the views are kept at window surfaces.

Owing to the fan beam geometries, the laser beams are incident on the windows at different angles. Fig.1b shows five probing beams ( $l_1-l_5$ ) of the lateral view interferometer and the corresponding incidence angles are  $9^\circ$ ,  $4^\circ$ ,  $0^\circ$ ,  $-4^\circ$  and  $-8^\circ$ . The beam diameter is  $d_{\text{win}}\sim 32\text{mm}$  at the window for lateral viewing and the corresponding clear aperture of the window is taken to be 100mm. Fig.1(c) shows six probing beams ( $t_1-t_6$ ) of the tangential view interferometer covering whole of the plasma cross-section (plasma major radius  $R = 0.9-1.3\text{m}$ ) at the equatorial plane. The incidence angles of these beams at the window surface are  $4.32^\circ$ ,  $2.9^\circ$ ,  $1.46^\circ$ ,  $1.48^\circ$ ,  $2.99^\circ$  and  $4.52^\circ$ . The Gaussian beam waist  $d_0\sim 24\text{mm}$  is located at the retroreflectors mounted on the outside wall of vessel and expands to  $d_{\text{win}}\sim 26\text{mm}$  at the vacuum window. The 63mm clear aperture of the window ensures negligible diffraction losses. The transmissivity of windows will be different for different channels since their angles of incidence are different. The thicknesses of windows have been chosen to maximize power transmission for all lines of sight.

### SELECTION OF VACUUM WINDOW

The selected windows should have high transmission in the far infrared region and good optical properties in the visible region for easy alignment with visible light. In addition, the mechanical strength of window material should be sufficient to withstand differential pressure and high baking temperature [8]. The window material should satisfy all these critical requirements. The materials that are transparent at far infrared wavelengths include sapphire, crystal quartz, TPX, polyethylene, mica etc [6]. Plastics are not acceptable for high-vacuum devices; therefore, TPX and polyethylene cannot be used to make vacuum windows. Mica has very high physical strength but its melting point is low, hence cannot survive at high baking temperature. Crystal quartz and sapphire seem to be best suited [5,6] for diagnostics windows of FIR interferometers in

\*Corresponding author: adhiya@ipr.res.in

SST-1. We have preferred to use crystal quartz due to its lower absorption coefficient than sapphire.

The vacuum windows for FIR interferometer of SST-1 are plane parallel plates of quartz made from its crystalline form by cutting it at precise orientations with respect to its crystallographic axes. Crystal quartz is an optically active and birefringent medium, i.e., the normal eigen modes for arbitrary angle of incidence (with respect to optic axis) are elliptically polarized. It exhibits optical activity for propagation along optic axis and linear birefringence for propagation perpendicular to optic axis. Hence modes of propagation inside crystalline quartz and the state of polarization of transmitted beam depend on orientation of E-vectors of the incident beam with respect to optic axis. The propagation modes inside quartz crystal with cut parallel to optic axis (x & y -cut) are shown in Fig.2(a) and with cut perpendicular to optic axis (z-cut) are shown in Fig.2(b). For single mode propagation inside above-mentioned crystallographic cuts, the E-vectors of incident beam must be oriented exactly parallel or perpendicular to the optic axis, which, in practice, is nearly impossible to achieve.

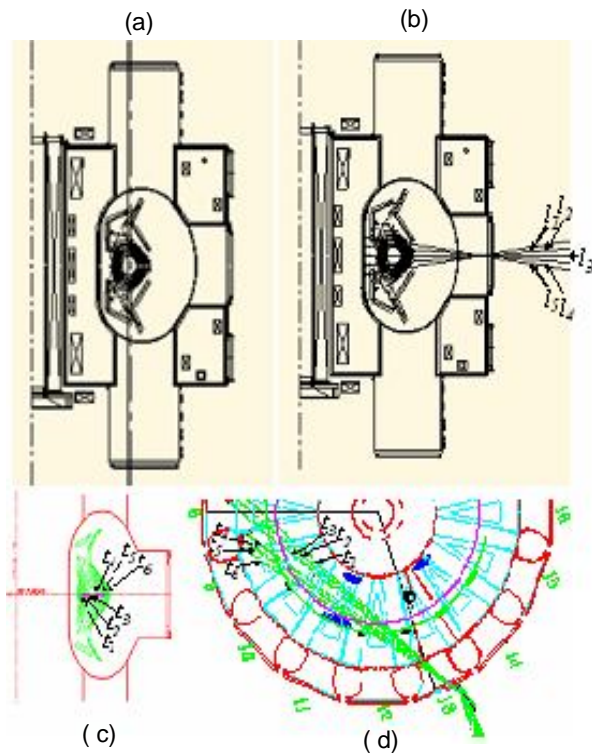


Fig. 1 (a) Vertical (b) lateral (c) tangential probe beams shown in the Cross-section of SST-1 and (d) tangential probing beams shown in the plan of SST-1.

We have selected z-cut quartz crystal for the vacuum windows for all the views of interferometer. The incident beams are arranged such that each fan of beams lies in single incident planes, with E-vectors oriented normal to this plane. This ascertains that the plane of polarization of the incident laser beams is aligned normal to the optic axis (s-polarization), thereby ensuring ordinary mode propagation inside all the crystal quartz windows. The optic axis is further aligned normal to the toroidal magnetic field of SST-1. This arrangement has an advantage that it introduces lesser ellipticity than x & y cuts in the transmitted beams.

RESULTS AND DISCUSSION

The thickness of window is calculated to withstand the atmospheric pressure and minimize reflection losses. The window apertures for vertical and tangential viewing are 76mm and lateral viewing is 114mm. Based on mechanical considerations, the rough estimates of window thickness  $d = (1.1PD^2/MR)^{1/2}$ , P = differential pressure, D = window diameter & MR = modulus of rupture ~ 6000 psi for crystal quartz) are made. Keeping the safety factor of 1.5-2, the window thicknesses are estimated to be 9.9mm and 6.5mm respectively for lateral and vertical/tangential viewing of FIR interferometer.

Further, a precise calibration of window thickness has been done by considering resonant effect between waves reflected by the parallel surfaces of etalon [9].

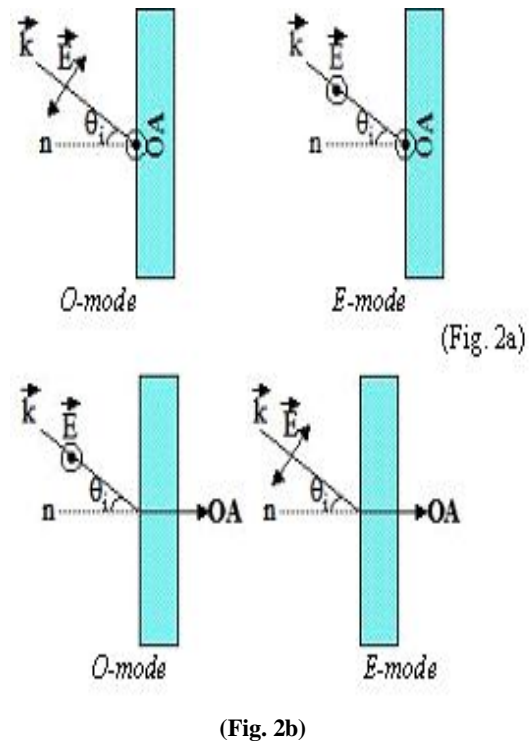


Fig. 2 Propagation modes (ordinary mode: O-mode & extraordinary mode: E-mode) inside (a) x or y-cut and (b) z-cut crystal quartz with incident planes perpendicular to the window surface.

The refractive index ( $n = 2.10748$  for 432.6mm and  $n = 2.12033$  for 118.8mm) and absorption coefficient ( $\alpha = 0.1$  for 432.6 $\mu\text{m}$  and  $\alpha = 0.55$  for 118.8 $\mu\text{m}$ ) are interpolated from the table given by Russel and Bell [10]. The reflectivity of window has been calculated from [11].

$$\frac{I_r}{I_o} = \frac{4R \sin^2 \frac{\delta}{2}}{(1-R)^2 + \left(4R \sin^2 \frac{\delta}{2}\right)} \tag{1}$$

where,  $\delta$  is the phase difference caused due to passage through the windows:

$$\delta = \frac{4\pi}{\lambda} nd \cos\theta_r \tag{2}$$

d is the window thickness,  $\theta$  is the angle of refraction and n is the refractive index of crystal quartz for the selected mode of propagation inside the window.

$$r_s = -\frac{\sin(\theta_i - \theta_r)}{\sin(\theta_i + \theta_r)} \quad R = |r_s|^2 \quad (3)$$

The reflectivity of z-cut quartz windows has been calculated as function of window thicknesses for vertical, lateral and tangential view interferometers. The reflectivity varies sinusoidally with its thickness at a given incidence angle and for a given wavelength.

Taking power absorption ( $P = P_o (1 - \exp(-\alpha d \cos \theta r))$ ,  $P_o =$  incident power) inside the window into consideration, the power transmissivity of these windows is calculated for all the channels.

The window thickness of 76mm aperture for vertical and tangential viewing of 118.8 $\mu$ m interferometer is 6.502 $\pm$ 0.002mm and 114mm aperture for lateral viewing of 432.6 $\mu$ m interferometer is 9.967 $\pm$ 0.002mm. The incidence angle for vertical viewing is 3 $^\circ$  to eliminate reflection of the He-Ne laser beam [12,13]. The corresponding transmissivity of the window for single pass through two windows is 1.55dB. For double pass lateral and tangential viewing, transmissivity through the windows is plotted in fig.3 as function of window thickness for all channels.

**CONCLUSIONS**

The vacuum windows chosen for various views of far infrared interferometer are made up of crystalline quartz due to double advantage of having low absorption coefficient and being transparent to both far-infrared and visible radiation. Further, it has high melting point to withstand baking temperature of 250 $^\circ$ C. z-cut crystal quartz should be preferred to get maximum power transmission and reduce ellipticity. The thickness, 6.502 $\pm$  0.002 mm for vertical/tangential and 9.967  $\pm$  0.002 mm for lateral viewing minimizes reflection losses and can withstand atmospheric pressure. The above-mentioned thicknesses provide maximum transmission for all the 12 channels of vertical, lateral and tangential view interferometers.

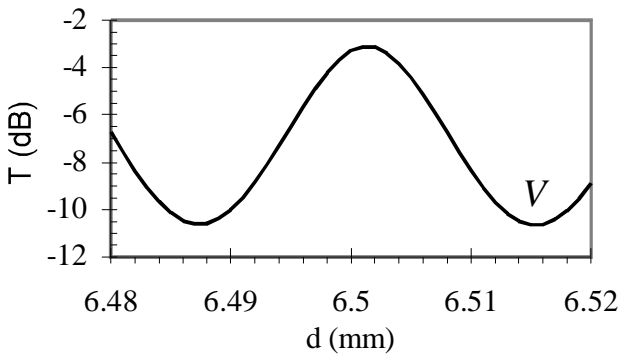


Fig. 3(a)

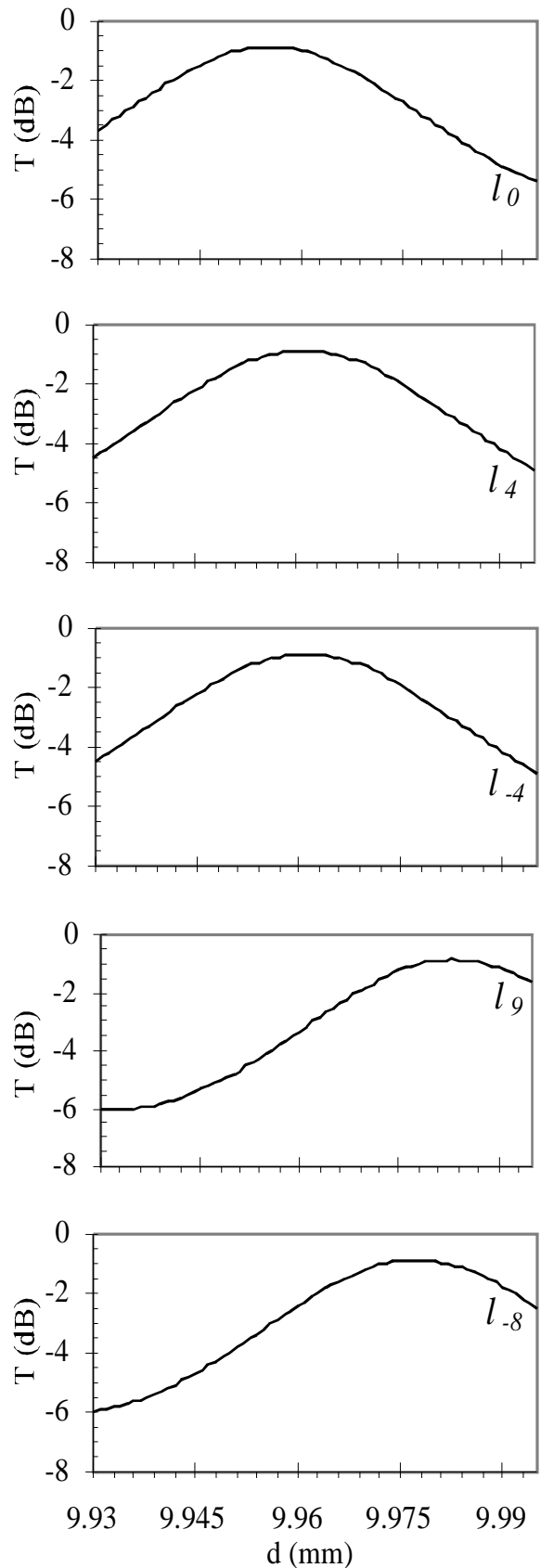


Fig. 3(b)

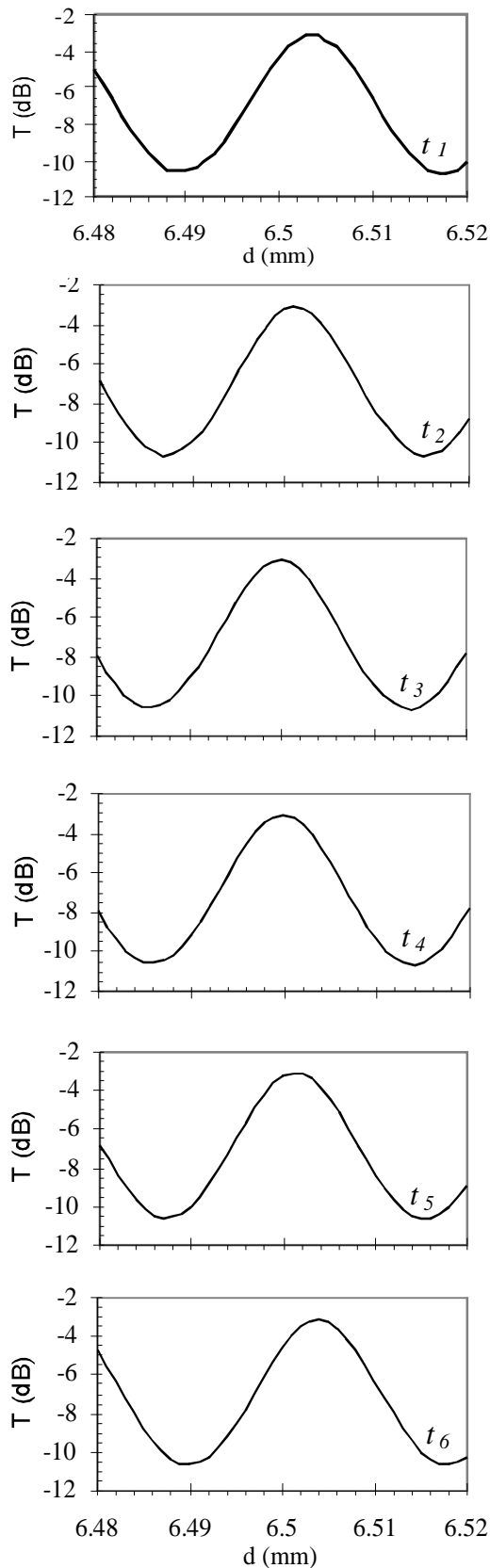


Fig. 3(c)

Fig.3 Transmissivity as function of thickness for (a) single channel vertical (V), (b) five channel lateral ( $l_0, l_d, l_p, l_g$  &  $l_s$ ) and (c) six channel tangential ( $t_1, t_2, t_3, t_4, t_5$  &  $t_6$ ) viewing.

REFERENCES

- [1] Donne A J H, Barth C J & Weisen H, *Fusion Science And Technology*, **53** (2008) 397.
- [2] Zhou Y, Deng Z, Liu Z, Yi J, Tang Y, Gao B, Tian C, Li Y & Ding X, *Rev. Sci. Instrum*, **78** (2007) 113503.
- [3] Murari A, Zabeo L, Boboca A, Mazon D & Riva M, *Rev. Sci. Instrum*, **77** (2006) 073505.
- [4] Cheon M S, Nam Y U, Ha J H & Hwang Y S, *Rev. Sci. Instrum*, **75** (2004) 3402.
- [5] Kaur R, Chaturvedi S & Mattoo S K, Conceptual Design Report of a Far Infrared Interferometer for SST-1, *Design report*, (1995) ST-51.
- [6] Veron D, *Infrared and Millimeter Waves Academic Press*, New York, Volume **2**, 1979, pp.69-135.
- [7] Okajima S, Nakayama K, Tazawa H, Kawahata K, Tanaka K, Tokuzawa T, Ito Y & Mizuno K, *Rev. Sci. Instrum*, **72** (2001) 1094.
- [8] Mozeleski M A & Lewin G (1981), Bakable Optical Windows for the Tokamak Fusion Test Reactor, *9th symp. on eng. problems of fusion research*, Chicago, pp.26-29.
- [9] Naylor D A, Boreiko R T & Clark T A, *Appl. Opt*, **17** (1978) 1055.
- [10] Russel E R and Bell E E, *J. Opt. Soc. Am.*, **57** (1979) 341.
- [11] Born M and Wolf E, *Principles of Optics*, Cambridge University Press, New York, 6th Edn, 1980, pp.327.
- [12] Yasunori K, Akira N, Katsuhiko T, So-ichi G & Takaki H, *J. Pla. Fus. Res*, **73** (1997) 870.
- [13] Veron D, Certain J & Crenn J P, *J. Opt. Soc. Am.*, **67** (1977)



## DECAY WIDTHS OF $B_c \rightarrow J/\Psi \pi^+$ IN CPP $\nu$ MODEL

Arpit Parmar<sup>1</sup>, Kaushal Thakkar<sup>2</sup>, Bhavin Patel<sup>3</sup> and P.C. Vinodkumar<sup>1</sup>

<sup>1</sup>Department of Physics, Sardar Patel University, Vallabh Vidyanagar-388120

<sup>2</sup>Department of Applied Physics, SVNIT, Surat

<sup>3</sup>Department of Physical Sciences, P. D. Patel Institute of Applied Sciences, CHARUSAT, Changa

### ABSTRACT

The non leptonic properties of  $B_c$  meson in the final  $J/\Psi$  state have been studied in the general framework of non relativistic potential models. The Schrodinger equation corresponding to  $B_c$  ( $\bar{b} c$ ) and  $Q\bar{Q}$  ( $c, b$ ) is solved numerically using the Coulomb plus power potential with varying index of the potential ranging from 0.1 to 2.0 as the quark- antiquark interaction. We employ the experimental quarkonia masses to fix the quark masses and the corresponding potential parameters. The ground state mass of the  $B_c$  meson is predicted with no additional parameters. The resultant masses and their radial wave functions obtained here are used to compute the decay widths for  $B_c \rightarrow J/\Psi \pi^+$  channel. The predicted mass is found to be in accordance with the experimental data for the choices power of the potential,  $\nu \approx 0.5$  for  $B_c$  meson and  $\nu \approx 0.5$  for  $J/\Psi$  meson. The non leptonic decay width is found to occur at relatively weaker interquark potential compared to that responsible to form the bound state.

**Keywords:** non leptonic decay, quarkonia, potential models

### INTRODUCTION

$B_c$  meson is of particular interest amongst the heavy flavoured mesons because of its uniqueness of being only open flavoured heavy meson. The spectroscopy and decay properties of  $B_c$  meson have been predicted by various theoretical models [1-9]. Study on the decay properties of  $B_c$  meson in final state  $J/\Psi$  is of particular interest for experimentalists, because  $J/\Psi$  can be observed with the high precision in the leptonic mode  $J/\Psi \rightarrow l^+ l^-$ . Contrary to the semileptonic modes, the nonleptonic decay mode  $B_c \rightarrow J/\Psi \pi^+$  is outstanding in reconstructing the  $B_c$  vertex by detecting charged particle tracks and the  $B_c$  mass can be measured.

### NON LEPTONIC DECAY WIDTHS

The estimation of the decay widths  $B_c \rightarrow J/\Psi \pi^+$  has been carried out by various theoretical models [4, 5, 10]. However, the potential models are assumed to give more precise prediction about the decay width due to the fact that the transition form-factors are determined by the overlapping integrals of the decaying and the produced mesons. For the present study we follow the non relativistic formalism given by [10] according to which the total decay width for the  $B_c \rightarrow J/\Psi \pi^+$  channel can be given by,

$$\Gamma(B_c \rightarrow J/\Psi \pi^+) = G_F^2 |V_{cb}|^2 \frac{128\pi\alpha_s^2}{81} f_{B_c}^2 f_{J/\Psi}^2 f_{\pi}^2 \left( \frac{M_{B_c} + M_{J/\Psi}}{M_{B_c} - M_{J/\Psi}} \right)^3 \frac{M_{B_c}^2}{(M_{B_c} - M_{J/\Psi})^2 M_{J/\Psi}^2} \quad (1)$$

In Eqn. 1,  $f_{B_c}$  and  $f_{J/\Psi}$  are the decay constants and are obtained by parameterizing the matrix elements of weak current between the corresponding mesons and the vacuum as,

$$\langle 0 | Q J^{\mu} Q | P_{\mu}(k) \rangle = i f_P k^{\mu} \quad (2)$$

$$\langle 0 | Q J^{\mu} Q | P_{\mu}(k) \rangle = f_P M_P \epsilon^{\mu} \quad (3)$$

The decay constants appeared in Eqn. 1 can be computed in the nonrelativistic formalism by incorporating first order QCD correction to the Van Royen-Weiskopff formula as,

$$f_{P/V} = \sqrt{\frac{3}{\pi M_{P/V}}} |R_{nP/V}(0)| \left( 1 + \frac{\alpha_s}{\pi} \left[ \frac{m_q - m_{\bar{q}}}{m_q + m_{\bar{q}}} \right] \ln \frac{m_Q}{m_{\bar{q}}} - \delta^{P/V} \right) \quad (4)$$

\*Corresponding author: p.c.vinodkumar@gmail.com

Here,  $\delta^p = 8/3$  and  $\delta^v = 2$ . Hence, by knowing about the spectroscopic parameter and behavior of the wave function at origin we can calculate the decay width for  $B_c \rightarrow J/\Psi \pi^+$ .

### THE PHENOMENOLOGY AND EXTRACTION OF THE SPECTROSCOPIC PARAMETERS

For the description of the quark-antiquark bound states, we adopt the phenomenological Coulomb plus power potential (CPP) expressed as [11, 12]

$$V(r) = -\frac{4}{3} \frac{\alpha_s}{r} + Ar^{\nu} \quad (5)$$

Here,  $A$  is the confinement strength of the potential and  $\alpha_s$  is the running strong coupling constant which is computed as,

$$\alpha_s(\mu^2) = \frac{4\pi}{(11 - \frac{2}{3}n_f) \ln \frac{\mu^2}{\Lambda^2}} \quad (6)$$

where  $n_f$  is the number of flavors,  $\mu$  is the renormalization scale related to the constituent quark mass and  $\Lambda$  is the QCD scale which is taken as 0.150 GeV by fixing  $\alpha_s = 0.118$  at the  $Z$ -boson mass (91 GeV) [13].

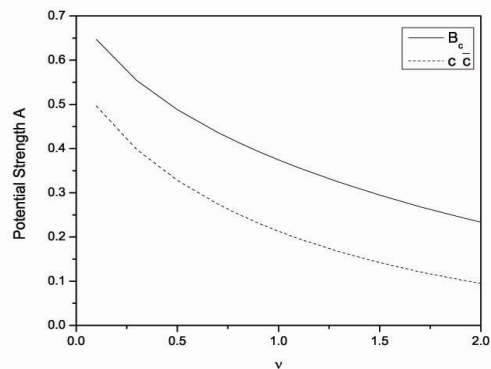


**Fig. 1** Potential Strength  $A$  (in  $\text{GeV}^{-\nu}$ ) obtained from ground state spin average mass against the choices of potential index,  $\nu$  ( $0.1 \leq \nu \leq 2.0$ )

The potential parameter, A of Eqn.4 is similar to the string strength  $\sigma$  of the Cornell potential. We particularly chose to vary  $\nu$  in our study as very different interquark potentials can provide fairly good description of the mass spectra, while the transitions and other decay properties are very sensitive to the wave functions. And the wave functions vary differently with different choices of interquark potential. Thus in the present study, we vary the potential index  $\nu$  in the range  $0.1 \leq \nu \leq 2.0$ . It can also provide significant understanding of the quark-antiquark interaction in the mesonic states while they undergo a transition or decay through annihilation channels. The different choices of  $\nu$  here then correspond to different potential forms. So, the potential parameter A expressed in  $\text{GeV}^{\nu+1}$  can be different for each choices of  $\nu$ . The model potential parameter A and the mass parameter of the quark/antiquark ( $m_1, m_2$ ) are fixed using the known ground state center of weight (spin average) mass and the hyperfine splitting ( $M_{3s_1} - M_{1s_0}$ ) of the ground state  $c\bar{c}$  and  $b\bar{b}$  systems respectively. The spin average mass for the ground state is computed for the different choices of  $\nu$  in the range  $0.1 \leq \nu \leq 2.0$ . The spin average or the center of weight mass,  $M_{\text{CW}}$  is calculated from the known experimental/theoretical values of the pseudoscalar ( $J=0$ ) and vector ( $J=1$ ) mesonic mass as

$$M_{\text{m,cw}} = \frac{\sum_j (2j+1) M_{\Pi_j}}{\sum_j (2j+1)} \quad (7)$$

The Schrodinger equation is numerically solved using the mathematica notebook of the Runge-Kutta method [14]. For computing the mass difference between different spin degenerate mesonic states, we consider the spin dependent part of the usual one gluon exchange potential (OGEP) given by [15-19]. Accordingly, the spin dependent part,  $V_{\text{SD}}(r)$  for the angular quantum number  $l=0$  contains only the spin-spin hyperfine interaction given by

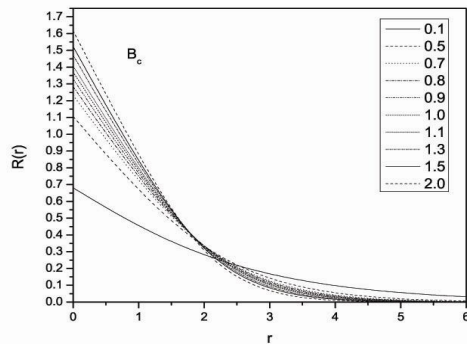


Fig. 2 Behaviour of wave function for different choices of potential index  $\nu$  for  $B_c$  meson.

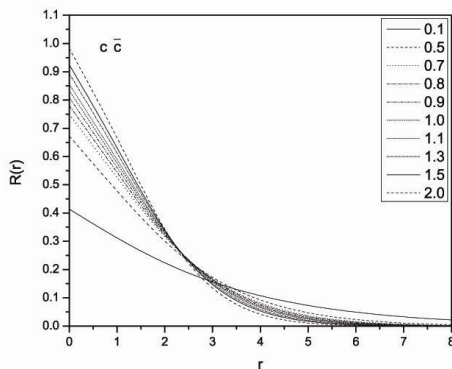


Fig. 3 Behaviour of wave function for different choices of potential index  $\nu$  for  $c\bar{c}$  meson

$$V_{\text{SD}}(r) = V_{\text{SS}}(r) \left[ S(S+1) - \frac{3}{2} \right] \quad (8)$$

The coefficient of this spin-dependent term of Eqn.7 is given by the usual one gluon exchange (OGE) interaction as [17]

$$V_{\text{SS}}(r) = \frac{16\pi\alpha_s}{9 m_1 m_2} \delta^{(3)}(\vec{r}) \quad (9)$$

The computed masses of the  $B_c$  and  $c\bar{c}$  states are listed in Table 1. The spectroscopic parameters thus correspond to the fitted quark masses, the potential strength A, the potential index,  $\nu$  and the corresponding radial wave functions. The fitted mass parameters are  $m_c = 1.28 \text{ GeV}/c^2$ ,  $m_b = 4.4 \text{ GeV}/c^2$  while the potential strength A for each choices of  $\nu$  are shown in Fig. 1. The numerical solution for the radial wavefunctions thus obtained for the different choices of the potential index,  $\nu$  are plotted in Fig. 2 and in Fig. 3 in the case of  $B_c$  and  $c\bar{c}$  systems respectively.

Table-1 Masses (in GeV) of  $B_c$  and  $J/\psi$  mesons and decay widths of  $B_c \rightarrow J/\psi \Pi^+$

$\nu$	$M_{B_c}$ GeV	$M_{j/\psi}$ GeV	$f_{B_c}$ GeV	$F_{j/\psi}$ GeV	$B_c \rightarrow J/\psi \Pi^+ \times 10^{-15}$ GeV
0.1	6.305	3.076	0.264	0.231	0.21
0.5	6.279	3.088	0.428	0.376	1.48
0.7	6.268	3.093	0.477	0.420	2.31
0.8	6.264	3.095	0.497	0.437	2.74
0.9	6.26	3.097	0.515	0.453	3.16
1.0	6.256	3.099	0.530	0.467	3.57
1.1	6.253	3.100	0.544	0.480	3.97
1.3	6.246	3.103	0.568	0.501	4.75
1.5	6.241	3.106	0.588	0.519	5.47
2.0	6.321	3.111	0.624	0.552	7.04
Expt[20]	6.277	3.097			
[21]	6.27	3.096			
[4]	6.356				1.22
[5]	6.302				1.06
[10]					2.0

RESULTS AND DISCUSSIONS

The computed mass spectra and decay constants for  $B_c$  and  $J/\psi$  mesons and the decay widths for  $B_c \rightarrow J/\psi \Pi^+$  channel with different choices of potential index  $\nu$  are shown in Table 1. Our computed mass parameter agrees with the experimental data [20] for the  $\nu \approx 0.5$  for  $B_c$  meson and  $\nu \approx 0.9$  for  $J/\psi$  mesons. As experimental results are still awaited for the decay channel  $B_c \rightarrow J/\psi \pi^+$ . We find our results in the range of potential index  $0.1 \leq \nu \leq 0.8$  are in accordance with other theoretical model predictions. It is being observed that the nonleptonic weak decays of  $B_c$  meson occur at relatively weaker interquark potential than that corresponds to form a bound state. Such a behavior as seen from the present study is in accordance with our understanding that weak interaction is smaller than strong interaction range.

ACKNOWLEDGMENT:

Part of this work is carried out under the UGC grant with ref no. F.40-457/2011(SR).

REFERENCES

[1] Ivanov M A, Korner J G and Santorelli P, (2006) Semileptonic decays of  $B_c$  mesons into charmonium

- states in a relativistic quark model. *Phys. Rev. D* **71** 094006.
- [2] Ebert D, Faustov R N and Galkin V (2003) Weak decays of  $B_c$  meson to Charmonium and D mesons in relativistic quark model. *Phys. Rev. D* **68** 094020.
- [3] Chang C H, Chen Y Q, Wang G L and Zong H S, (2002) Weak decays of the Bc meson to charmonium and D mesons in the relativistic quark model. *Phys. Rev. D* **65** 014017.
- [4] HadyAbd El, Munoz J H and Vary J P, (2000) Semileptonic and nonleptonic Bc decays. *Phys. Rev. D* **62** 014019
- [5] Liu J F and Chao K T, (1997) Bc meson weak decays and CP violation. *Phys. Rev. D* **56** 4133
- [6] Kiselev V V, Likhoded A K and Onishchenko A I, (2000) Semileptonic Bc-meson decays in sum rules of QCD and NRQCD. *Nucl.Phys. B* **569** 473.
- [7] Colangelo P and Fazio F DE, (2000) Using heavy quark spin symmetry in semileptonic Bc decays. *Phys. Rev. D* **61** 034012.
- [8] Anisimov A Y, Kulikov P Y, Narodetsky I M and Ter-Martirosian K A, (1999) Exclusive and Inclusive Decays of B<sub>c</sub> meson in the Light-Front ISGW Model. *Yad. Fiz.* **62** 1868.
- [9] Sanchis-Lozano M A, (1995) Weak decays of doubly heavy hadrons. *Nucl.Phys. B* **440** 251.
- [10] Kiselev V V, (1996) Hard-soft factorization in  $B_c^+ \rightarrow \psi \pi^+$  decay. *Phys.Lett.B* **37** 2326.
- [11] Rai A K, Pandya J N and Vinodkumar P C, (2005) Decay rates of quarkonia and potential models. *J. Phys. G :Nucl. Part. Phys.* **31** 1453.
- [12] Rai A K, Pandya J N and Vinodkumar P C, (2008) Decay rates of quarkonia with NRQCD formalism using spectroscopic parameters of potential models. *Eur. Phys. J. A* **38** 77 arXiv:0901.1546[hep-ph].
- [13] Amsler C et al., (Particle Data Group), (2008) Review of Particle Physics. *Phys. Lett. B* **667** 1.
- [14] Lucha W and Shoberl F, (1999) Solving the Schroedinger equation for bound states with Mathematica 3.0. *Int. J. Mod. Phys. C* **10**, arXiv:hep-ph[9811453].
- [15] Branes T, Godfrey S and Swanson E S, (2005) Properties of the charmed P-wave mesons. *Phys.Rev. D* **72** 054029
- [16] Lakhina Olga and Swanson Eric S, (2006) Dynamic properties of charmonium. *Phys. Rev. D* **74** 014012 [arXiv:hep-ph/0603164].
- [17] Voloshin M B, (2008) Charmonium. *Prog. Part. Nucl. Phys.* **61** 455 arXiv:hep-ph/0711.4556.
- [18] Eichten E, Godfrey S, Mahlke H and Rosner J L, (2008) Quarkonia and their transitions. *Rev. Mod. Phys.* **80** 1161.
- [19] Gershtein S S, Kiselev V V, Likhoded A K and Tkabladze A V, (1995) Bc spectroscopy. *Phys. Rev. D* **51** 3613
- [20] Nakamura K et al., (2010) Review of Particle Physics. *J. Phys. G* **37** 075021.
- [21] Ebert D, Faustov R N and Galkin V O, (2003) Properties of heavy quarkonia and Bc mesons in the relativistic quark model. *Phys. Rev. D* **67** 014027



## DFT STUDIES ON ELECTRONIC STRUCTURE AND ELASTIC PROPERTIES OF CoN: ZINCBLENDE AND ROCKSALT STRUCTURES

Jameson Maibam<sup>1</sup>, B. Indrajit Sharma<sup>1\*</sup>, Ramendu Bhattacharjee<sup>1</sup>,  
R.K. Thapa<sup>2</sup> and R.K. Brojen Singh<sup>3</sup>

<sup>1</sup>Department of Physics, Assam University, Silcher-788011, Assam

<sup>2</sup>Department of Physics, Mizoram University, Tanhril, Aizawl-796 009

<sup>3</sup>Centre for Interdisciplinary Research in Basic Sciences, Jamia Millia Islamia, New Delhi-110 025

### ABSTRACT

We have calculated *ab initio* the electronic, structural and elastic properties of CoN in rocksalt (RS) and zincblende (ZB) structures using full potential linearised augmented plane wave method with generalised gradient approximation as exchange correlation. Of these two phases, the ZB-CoN is more stable. The density of states show no band gap indicating the compound is metallic. The second order elastic constants have been calculated and other related quantities such as Zener anisotropy factor, Poisson's ratio, Young's modulus, Kleinman parameter, Debye temperature, sound velocities have also been determined.

**Key words:** DFT; electronic structure; DOS; elastic constants

### Introduction

Transition metal nitrides are well known for possessing a number of extreme properties that are of scientifically interest and technologically important [1]. They show a rich variety of properties ranging from high  $T_c$  superconductivity to very hard surface coatings and heterogeneous catalysis. In view of these properties, a large number of theoretical investigations were carried out in the last few decades [2-4]. The aim of this paper is to present the result of a theoretical investigation of the structural, electronic and elastic properties of CoN in both rocksalt and zincblende structures. The calculations were done using the full-potential linearised augmented plane wave (FP-LAPW) method [5-7] based on the density functional theory. Recently CoN has been synthesized by Suzuki et al in zincblende structure [8]. In addition, Taylor et al. [9] reported the existence of CoN in zincblende structure. Schmit-Dumont et al.[10] synthesized CoN in rocksalt structure. However, Shimizu's [4] theoretical calculation using LDA claimed that rock salt structure is more stable. While Wang Hong Bo et al.[11], using GGA, have shown that ZB-CoN is more stable. From the earlier comparisons [12-14] of the computational works using LDA and GGA, it is well known that GGA yields good agreement with experiments. Therefore, in this study, GGA is applied. The rest of the paper is organised as follows. In sec. 2 we describe the details of the *ab initio* method used. In sec. 3 we report the structure of two different phases of CoN studied band structure, density of states and elastic constants of RS-CoN and ZB-CoN as results and discussion. Overall conclusion is given in sec.4.

### Computational details

The calculation of cobalt nitrides in the rock salt and zincblende structures were performed with the FP-LAPW within the framework of the density functional theory with GGA-PBE for the exchange correlation potential [5]. We have employed the scalar relativistic hybrid full potential (linearized) augmented plane waves plus local orbitals (FP-LAPW+lo) method as implemented in the WEIN2k code.[15]. This method has been extensively tested and is among the most accurate methods for performing electronic structure calculations of crystals. In this method, the unit cell is divided into non-overlapping atomic

spheres whose centre is at atomic position and interstitial region. Inside the muffin tin region the potential is a product of radial function and spherical harmonics. For the interstitial region, i.e., outside the muffin tin sphere, the potential are expanded in plane waves. Muffin-tin spheres for metal atoms, carbon atoms and nitrogen atoms are listed in table 1. For every case the wave functions inside the MT spheres which are expanded into spherical harmonics are up to  $l=9$  and the  $RK_{max}=10$ . The number of k points used for the integration procedure is 7000 which reduces to 222 irreducible k points inside the Brillion zone including five high symmetry points W, L,  $\Gamma$ , X and K. The calculations were performed at the equilibrium lattice constants, which are determined from the plot of total energy against the unit cell volume by fitting to the Murnaghan equation of state [16].

### Results and Discussion

We investigated two different phases of CoN, namely, the rock salt structure (space group F-43m) and zincblende structure (space group Fm-3m). The equilibrium lattice parameter, bulk modulus, and its pressure derivative have been computed by minimizing the crystal total energy calculated for different values of the lattice constants by means of Murnaghan's equation of state (EOS) [16] and are shown in Fig 1 (a)-(b). The results are listed in Table 1 along with other experimental and theoretical values. It is found that zincblende (ZB-CoN) phase has lower energy and is more stable structure. This result is not in agreement with the other theoretical work by Shimizu et al. which claimed that RS-CoN is more stable than ZB-CoN. The lattice parameters are found to be 4.00 Å for RS-CoN and 4.24 Å for ZB-CoN. It indicates that the unit cell of RS-CoN is smaller than that of ZB-CoN, which is in agreement with the experimental result. The lattice parameter of ZB-CoN differs from that of experimental by an amount of 0.04 Å to 0.05 Å, indicating the accuracy of our work. The calculated bulk moduli fo RS-CoN and ZB-CoN are 3.09 Mbar and 2.58 Mbar respectively which are in agreement with other theoretical work by Wang Hong-Bo et al [11]. The band structure of CoN in both structures are shown in Fig.2(a)-(b). It can be seen that there are many bands crossing the Fermi level in the band structures of

\*Corresponding author: indraofficial@rediffmail.com

both structures. It clearly indicates that RS and ZB structure of CoN exhibits metallic in nature. The total and partial density of states (DOS) are shown in Fig. 3 (a-f). The metal 3d states and the N 2p states are strongly hybridized in total DOS in both the structures. The lowest band in the band structure is mainly nitrogen 2s orbital. They do not contribute to the bonding. Above this band, there lies the 2p non-metal and 5d metal states. These bands overlap and mixed in  $\Delta$ . According to Hund's rule, the d band is further decomposed to  $d-t_{2g}$  and  $d-e_g$ . This is observed in band structure as the 3d metal state decomposes to  $d-t_{2g}$  and  $d-e_g$  originating at  $\Gamma$ . The bands near the Fermi level are mainly contributed by Co-d and N-p.

From the valence electron density plot along the 100 planes in Fig.4 (a) and Fig. 4(b), it seems that the bond between the Co and N in RS-CoN has more covalent nature whereas ZB-CoN shows more ionic nature. This may be the cause of difference in stability and other physical properties such as hardness etc. The covalency/ionicity nature in the compound can also be explained from charge transfer analysis.

The difference in the electronic charge inside the atomic sphere between the crystal (LAPW) value  $Q_{\text{crystal}}^{\text{sphere}}$  and the superimposed atomic value  $Q_{\text{crystal}}^{\text{sphere}}$  which is the quantity for studying charge transfer in a compound are given in table 2. From this table we can observe that in ZB-CoN there is a charge transfer of about two electrons from the metal to the non-metal. While in RS-CoN the charge transfer is about half an electron. Therefore one can conclude that ionic nature is more in ZB-CoN where as covalent nature is more in RS-CoN.

In this study, to compute the elastic constants  $C_{ij}$ , we use the 'volume conserving' technique [17]. For cubic crystal structures such as those of ZB-CoN or RS-CoN, the necessary condition for mechanical stability is given by [18]  $(C_{11}-C_{12}) > 0$ ,  $(C_{11}+2C_{12}) > 0$ ,  $C_{11} > 0$ ,  $C_{44} > 0$ . The findings are listed in Table 1. These values satisfy all the stability conditions. Thus we have concluded that both ZB-CoN and RS-CoN are mechanically stable which favours the experimental results [8-10].

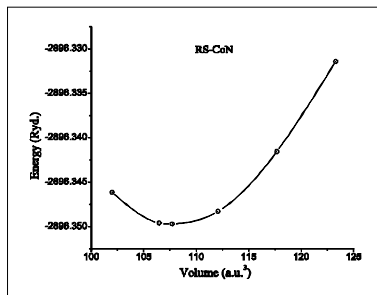


Fig.1 (a) Total energy of RS-CoN as a function of volume. The circles are the calculated points and the curve is fitted to Murnaghan's equation of state.

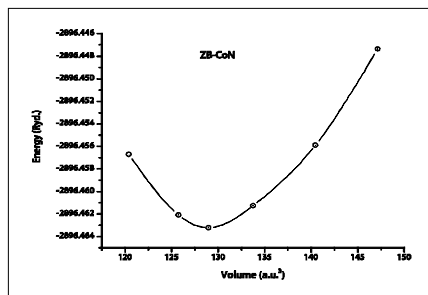


Fig. 1(b) Total energy of ZB-CoN as a function of volume. The circles are the calculated points and the curve is fitted to Murnaghan's equation of state.

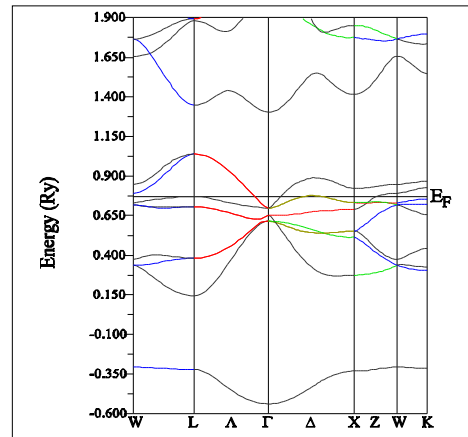


Fig.2. (a) Electronic band structure of RS-CoN

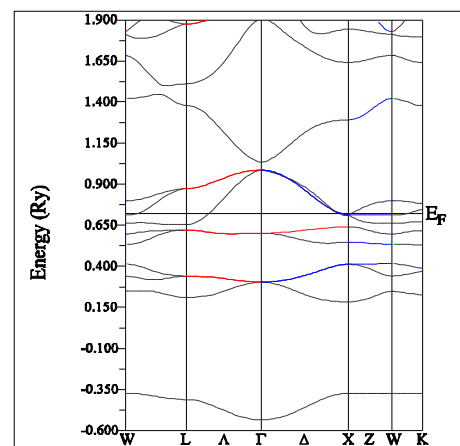


Fig.2. (b) Electronic band structure of ZB-CoN

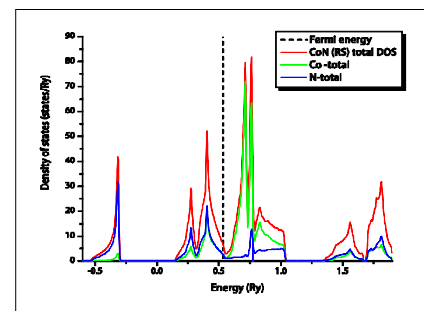


Fig. 3. (a) Total density of states of RS-CoN

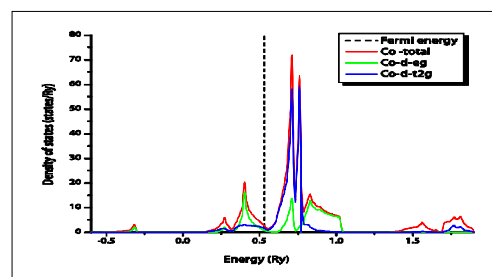


Fig. 3. (b). Partial density of states of Co in RS-CoN

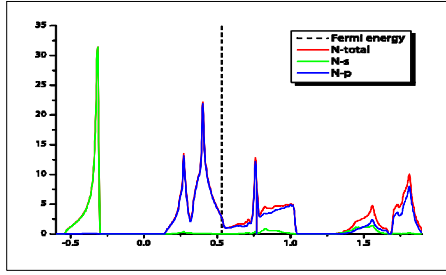


Fig. 3 (c) Partial density of states of N in RS-CoN.

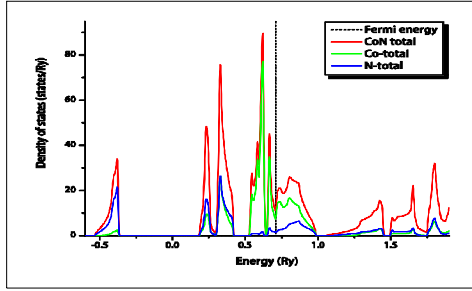


Fig. 3 (d) Total density of states of ZB-CoN

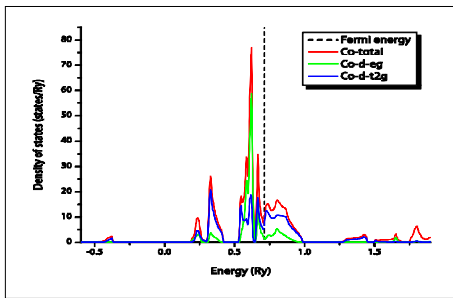


Fig. 3 (e) Partial density of states of Co in ZB-CoN

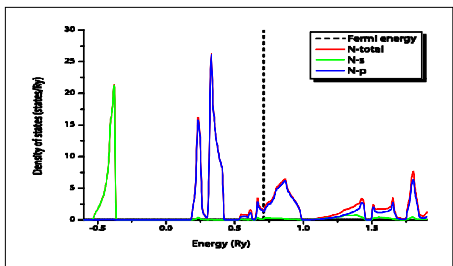


Fig. 3. (f) Partial density of states of N in ZB-CoN.

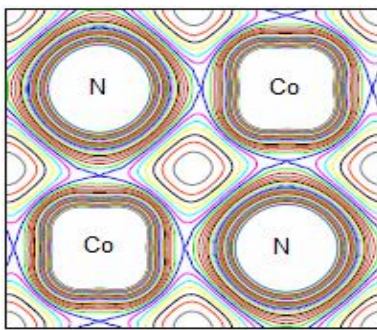


Fig. 4. (a) Total valence charge density of RS-CoN in 100 plane.

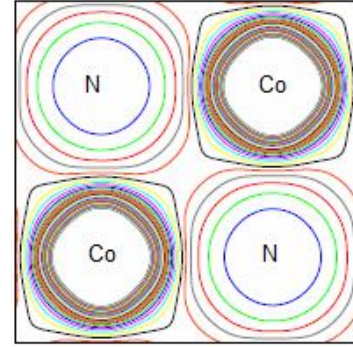


Fig. 4. (b) Total valence charge density of ZB-CoN in 100 plane

**Table 1.** Calculated and experimental lattice constant ( $a_0$ ), bulk modulus (B), and the pressure derivative of bulk modulus ( $B'$ ), Zener anisotropy factor (A), Poisson's ratio ( $\nu$ ), Kleinman parameter ( $\zeta$ ), Young's modulus (Y), and shear modulus ( $C'$ ), longitudinal, transverse, average elastic wave velocities ( $v_l, v_t, v_m$ ) and the Debye's temperature ( $\theta_D$ ) of RS-CoN and ZB-CoN.

Parameters	Rock salt structure	Zincblende structure
$a_0$ Å	4.00 <sup>a</sup> , 4.05 <sup>b</sup> , 3.90 <sup>c</sup> , 4.27 <sup>d</sup>	4.24 <sup>a</sup> , 4.29 <sup>b</sup> , 4.20 <sup>e</sup> , 4.296 <sup>f</sup> , 4.428 <sup>g</sup>
B Mbar	3.09 <sup>a</sup> , 2.93 <sup>b</sup> , 4.82 <sup>c</sup>	2.58 <sup>a</sup> , 2.56 <sup>b</sup> , 2.45 <sup>c</sup>
$B'$	4.51 <sup>a</sup>	8.06 <sup>a</sup>
$C_{11}$ Mbar	4.36 <sup>a</sup>	2.77 <sup>a</sup>
$C_{12}$ Mbar	2.87 <sup>a</sup>	2.08 <sup>a</sup>
$C_{44}$ Mbar	0.99 <sup>a</sup>	1.45 <sup>a</sup>
A	1.34 <sup>a</sup>	4.19 <sup>a</sup>
$\nu$	0.37 <sup>a</sup>	0.36 <sup>a</sup>
$\zeta$	0.75 <sup>a</sup>	0.82 <sup>a</sup>
Y(Mbar)	2.43 <sup>a</sup>	2.22 <sup>a</sup>
$C'$ (Mbar)	0.74 <sup>a</sup>	0.34 <sup>a</sup>
$v_l$ (m/s)	10620.50 <sup>a</sup>	10764.12 <sup>a</sup>
$v_t$ (m/s)	4840.97 <sup>a</sup>	5086.85 <sup>a</sup>
$v_m$ (m/s)	5456.72 <sup>a</sup>	5724.03 <sup>a</sup>
$\theta_D$ (K)	644.93 <sup>a</sup>	637.34 <sup>a</sup>

a Present work, b Ref. [11], c Ref. [4], d Ref. [9], e Ref. [22], f Ref. [8]

**Table 2** LAPW partial charge difference for RS- CoN and ZB-CoN

Inside the atomic spheres	RS- CoN		ZB-CoN	
	Co	N	Co	N
$Q_{crystal}^{in}$	25.016	6.568	24.432	5.654
$Q_{atomic}^{in}$	25.061	6.225	26.431	5.653
$Q_{crystal}^{in} - Q_{atomic}^{in}$	-0.448	0.343	-1.999	0.001

The Zener anisotropy factor A, Poisson's ratio  $\nu$ , shear modulus  $C'$ , and Young's modulus Y are calculated using the relations given by Mayer et al. [19].

$$A = \frac{2C_{44}}{C_{11}C_{12}} \quad \nu = \frac{1}{2} \left[ \frac{B - \frac{1}{2}G}{B + \frac{1}{3}G} \right], \quad Y = \frac{9GB}{G + 3B}$$

Where,  $G = G_v + G_r/2$  is the isotropic shear modulus,  $G_v$  is Voigt's shear modulus corresponding to the upper bound of  $G$  values, and  $G_r$  is Reuss's shear modulus corresponding to the lower bound of  $G$  values. They can be expressed as

$$G_v = \frac{(C_{11} - C_{12} + 3C_{44})}{5}$$

$$\frac{5}{G_r} = \frac{4}{(C_{11} - C_{12})} + \frac{3}{C_{44}}$$

The Kleinman parameter  $\zeta$  which describes the relative positions of the cation and anion sub lattices under volume conserving strain distortions for which positions are fixed by symmetry. We use the following relations

$$\zeta = \frac{C_{11} + 8C_{12}}{7C_{11} + 2C_{12}}$$

for Kleinman parameter and

$$C' = (C_{11} - C_{12})/2$$

for the shear modulus [20]. The calculated value of density  $\rho$ , Zener anisotropy factor  $A$ , Poisson's ratio  $\nu$ , Kleinman parameter  $\zeta$ , Young's modulus  $Y$ , and shear modulus  $C'$  of RS-CoN and ZB-CoN are listed in table 1. Following common relation given in Ref. [21], the Debye temperature  $\theta_D$  is calculated from the elastic constants data using the average sound velocity  $v_M$ , by the relation

$$\theta_D = \frac{h}{k} \left[ \frac{3n}{4\pi} \left( \frac{N_A \rho}{M} \right) \right]^{1/3} v_M$$

where  $h$  is Planck's constant,  $k$  is the Boltzmann's constant,  $N_A$  is Avogadro's number,  $n$  is the number of atoms per formula unit,  $M$  is the molecular mass per formula unit,  $\rho$  ( $=M/V$ ) is the density, and  $v_M$  is given as [23]

$$v_M = \left[ \frac{1}{3} \left( \frac{2}{v_l^3} + \frac{1}{v_t^3} \right) \right]^{1/3}$$

where  $v_l$  and  $v_t$  are the longitudinal and the transverse elastic wave velocities, respectively, which are obtained from Navier's equations [24]

$$v_l = \sqrt{\frac{3B + 4G}{3\rho}} \quad v_t = \sqrt{\frac{G}{\rho}}$$

The calculated values of the longitudinal, transverse and average sound velocities along with the Debye temperature are given in Table 1.

## Conclusion

To conclude, we have studied the structure, elastic properties, and lattice stability of CoN in rock salt and zinblende phase. The calculation reveals that with two structures, the ground state energy of zinblende phase of CoN is higher as compare to rock salt CoN phase. The calculated band structure shows that these materials are metallic in nature. The density of states for both structures indicate that the metal Co 3d state intensely hybridize with the N 2p. The bonding nature of RS-CoN can be described as covalent due to hybridization of N and Co states, but there is also some ionic character with the electron transfer from the metal atoms to nitrogen atoms as well as obvious metallic

character. The bonding nature of RS-CoN is seems to be dominated by covalent nature and that of ZB-CoN is dominated by ionic nature.

## Acknowledgments

Financial support under the Fast Track Project (SR/FTP/PS-33/2006 dt.06.05.2008) from Department of Science and Technology (DST), Government of India is gratefully acknowledged.

## References

- [1] Toth, L. E., (1971) *Transition Metal Carbides and Nitrides*, Academic Press, New York.
- [2] Hardy, G. F. and Hulm, J. K., (1954) The Superconductivity of Some Transition Metal Compounds. *Phys. Rev.*, **93**:1004-1016.
- [3] Dismukes, J. P., Yim, W. M. and Ban, V. S., (1972) Epitaxial growth and properties of semiconducting ScN. *J. Cryst. Growth*, **13/14**:365-370.
- [4] Shimizu, H., Shirai, M. and Suzuki, N., (1997) Electronic, Structural and Magnetic Properties of Transition Metal Mononitrides. *J. Phys. Soc. Jpn.*, **66**:3417-3152.
- [5] Perdew, J. P., Burke, S. and Ernzerhof, M., (1996) Generalized Gradient Approximation Made Simple. *Phys. Rev. Lett.*, **77**:3865-3868.
- [6] Singh, D. J., (1994) *Plane Waves, Pseudopotentials and the LAPW Method*, Kluwer Academic, Boston.
- [7] Blaha, P., Schwarz, K. and Sorantin, P., (1990) Full-potential, linearized augmented plane wave programs for crystalline systems. *Comput. Phys. Commun.*, **59**:399-415.
- [8] Suzuki, K., Kaneko, T., Yoshida, H., Morita, H. and Fujimori, H., (1995) Crystal structure and magnetic properties of the compound CoN. *J. Alloys Compounds*, **224(2)**:232-236.
- [9] Taylor, B., Joyner, B. and Verhoek, F. H., (1961) Products of the Thermal Decomposition of Some Cobalt Ammine Azides. *J. Am. Chem. Soc.*, **83(5)**:1069-1072.
- [10] Schmitz-Dumont, O. and Kron, N., (1955) Cobalt Nitrides from the Thermal Decomposition of Co Amide. *Angew. Chem.*, **67**:231-232.
- [11] Hong-Bo, W. and De-Sheng, X., (2004) Electronic Structures and Magnetic Properties of CoN, NiN and CuN. *Chin. Phys. Lett.*, **21(8)**:1612.
- [12] Kohn, W., Becke, A. D. and Parr, R. G., (1996) Density Functional Theory of Electronic Structure. *J. Chem. Phys.*, **100**:12974-12980.
- [13] Ernzerhof, M., Perdew, J. P. and Berke, K., (1996) Topics in Current Chemistry: *Theory I Density Functional*, Springer, Berlin, Vol. **180**, p1.
- [14] Stamp, C., Mannstadt, W., Asahi, R. and Freeman, A. J., (2001) Electronic structure and physical properties of early transition metal mononitrides: Density-functional theory LDA, GGA, and screened exchange LDA FLAPW calculations. *Phys. Rev. B*, **63**:155106-155116.
- [15] Blaha, P., Schwarz, K., Madsen, G. K. H, Kvasnicka, D. and Luitz, J., (2001) *WIEN2k An Augmented Plane Wave + Local Orbitals Program for Calculating Crystal Properties*, Karlheinz Schwarz, Techn. Universitat Wien, Austria.

- [16] Murnaghan, F. D., (1944) The Compressibility of Media under Extreme Pressures, *Proceedings Natl. Acad. Sci., USA*, **30(9)**:244-247.
- [17] Brich, F. J., (1938) The Effect of Pressure Upon the Elastic Parameters of Isotropic Solids, According to Murnaghan's Theory of Finite Strain. *Appl. Phys.*, **9**:279-289.
- [18] Wallace, D. C. (1972) *Thermodynamics of crystals*, Wiley, New York.
- [19] Mayer, B., Anton, H., Bott, E., Methfessel, M., Sticht, J. and Schmidt, P. C., (2003) Ab-initio calculation of the elastic constants and thermal expansion coefficients of Laves phases. *Intermetallics*, **11**: 23-32.
- [20] Harisson, W. A. (1989) *Electronic structures and properties of solids*, Dover, New York.
- [21] Johnston, I., Keeler, G., Rollins, R. and Spicklemeire, S. (1996) Solid State Physics Simulations, *The Consortium for Upper-Level Physics Software*, Wiley, New York.
- [22] Li, M. K., Li, C. B., Liu, C. S., Fan, X. J., Fu, D. J., Shon, Y. and Kang, T. W., (2004) Cathodoluminescence and Magnetic Properties of Mn<sup>+</sup> Implanted AlN. *Chin. Phys. Lett.*, **21(2)**: 393-395.
- [23] Anderson, O. L. (1963) A simplified method for calculating the Debye temperature from elastic constants. *Phys. Chem. Solids*, **24**:909-917.
- [24] Schreiber, E., Anderson, O. L. and Soga, N., (1973) *Elastic Constants and Their Measurements*, McGraw-Hill, New York.



## ELECTRICAL TRANSPORT PROPERTIES OF TUNGSTEN DITELLURIDE (WTe<sub>2</sub>) CRYSTALS

Priyanka Desai\*, D.D. Patel, D.N. Bhavsar and A.R. Jani

Department of Physics, Sardar Patel University, Vallabh Vidyanagar- 388120

### ABSTRACT

Tungsten Ditelluride (WTe<sub>2</sub>) crystals having a layer structure grown by chemical vapour transport technique (CVT) using iodine as transporting agent are studied here. The electrical resistivity and thermoelectric power (TEP) of these crystals were carried out within the range 313K to 573K. The crystals were found to exhibit semiconducting nature in this range. The activation energy, Seebeck coefficient and scattering parameters were calculated for these crystals. The Hall coefficient, carrier concentration and Hall mobility were determined from Hall Effect measurements at room temperature. Also the measurement of Thermal conductivity and Electrical conductivity of WTe<sub>2</sub> crystals along the chain axis were carried out. The implications of the results have been discussed.

**Key words :** Tungsten Ditelluride, thermoelectric power, Seebeck co-efficient, scattering parameter, thermal conductivity, electrical conductivity.

### INTRODUCTION

W and Te are the members of groups VIB and VIA respectively, which possesses layered structure. Tungsten Ditelluride constitutes a well defined family of compounds which crystallize in a layer type structure. The layered tungsten dichalcogenides also exhibits superconducting behavior when intercalated with alkali. The crystal structure of WTe<sub>2</sub> is orthorhombic with space group P<sub>mm</sub> 21 having lattice parameters a=3.38Å, b=6.27Å and c=14.16Å. The study of electrical properties of the layered compounds of the group IV-VI has aroused a widespread interest and attention of the material scientists all over the world during the last few decades [1-8]. Most of the semiconductor applications are governed by the electrical properties of the materials. Hence, electrical properties like resistivity, Hall coefficient, thermoelectric power, thermal conductivity and electrical conductivity along the chain axis were carried out on the WTe<sub>2</sub> crystals. The study of thermo electric power provides an independent way to determine the charge carrier sign, density and position of Fermi level in semiconductors.

### EXPERIMENTAL

Crystals of Tungsten Ditelluride (WTe<sub>2</sub>) grown by [9] chemical vapour transport method using iodine as the transporting agent are studied here. In this report we present results on electrical resistivity and thermoelectric power measured in temperature range 313K to 573K and also on hall parameters, electrical conductivity and thermal conductivity[3,5].

### RESISTIVITY MEASUREMENTS

In the present study, resistivity has been measured perpendicular to c-axis (along the chain axis).

Two- probe method and four- probe method are used for resistivity measurement.

### TWO-PROBE METHOD

In the present study resistance has been measured along the cleavage plane with the help of multimeter (model 2700, Make: KEITHLEY). The measurements were carried out in the temperature range from 313K to 573K at an interval of 5K. The

resistivity ( $\rho$ ) of the samples was calculated by using the formula

$$\rho = RA/l \quad (1)$$

Where A is the cross sectional area of the specimen in the direction of measurement, R is the resistance of the specimen and l is the length of specimen.

From the slopes of  $\log \rho$  Vs  $1000/T$  plots the values of activation energies were calculated using the formula,

$$E_a = 2.303 X k_b X 10^3 X \text{slope (eV)} \quad (2)$$

Where  $k_b = 8.602 X 10^{-5}$  eV/K

### FOUR-PROBE METHOD

Electrical resistivity measurements along chain axis of WTe<sub>2</sub> single crystals were performed by four- probe method. Measurements were performed in the temperature range from 303K to 483K using the set up made in our laboratory. Expressions for resistivity and activation energy are same as two-probe method.

### MEASUREMENT OF HALL PARAMETERS

Hall Effect measurement was performed along the cleavage plane of crystals of WTe<sub>2</sub> in order to determine the type of conductivity, mobility and carrier concentration. Ohmic nature of the contacts taken (by silver conducting adhesive) for these measurement was confirmed by I-V characteristics measurement using Van der Pauw technique. Knowing the value of difference in resistance (R), magnetic field (B) and thickness of the sample t, the mobility of charge carriers is evaluated using the relation

$$\mu_H = \frac{t}{\Delta B} \times \frac{\Delta R}{\rho} \quad (3)$$

The Hall coefficient ( $R_H$ ) and carrier concentration (n) are evaluated using the following formula;

$$R_H = \mu_H \times \rho \quad (4)$$

$$n = 1/R_H \times e \quad (5)$$

### THERMOELECTRIC POWER MEASUREMENT

The measurements of the thermoelectric power with temperature were carried out in the temperature range 313 K to 573 K. For the study of temperature dependent thermoelectric power S of a p-type semiconductor the expression is given by

\*Corresponding author: priyanka13desai@gmail.com

$$S = \frac{k}{e} \left[ A + \frac{E_{FV}}{kT} \right] \tag{6}$$

Where k is Boltzmann constant, e is the electronic charge,  $E_{FV} = E_F - E_V$  is the separation of the fermi level from the top of the valence band and A is the constant determined by the scattering process.

**THERMAL CONDUCTIVITY**

A simple method known as the divided bar method for thermal conductivity measurement is used. Here, thermal conductivity is measured at 100°C. Assuming that the loss of heat by radiation from the surfaces is negligible compared to the heat transferred and the heat flowing through the metal block and the crystal, we get,

$$K_m A (dT/dX)_m = K_c A (dT/dX)_c \tag{7}$$

$$K_c = K_m (dT/dX)_m / (dT/dX)_c \tag{8}$$

Here,  $K_m$ ,  $K_c$ , are co-efficient of thermal conductivity of metal and crystal respectively and  $(dT/dX)_m$  and  $(dT/dX)_c$  are thermal gradients of metal and crystal respectively[5].

**ELECTRICAL CONDUCTIVITY**

Electrical conductivity ( $\sigma$ ) is given by

$$\sigma = 1/\rho \tag{9}$$

Where, resistivity,

$$\rho = R \times A/l \tag{10}$$

Here, electric conductivity is also measured at 100°C.

**RESULTS AND DISCUSSION**

Variations of  $\log \rho$  versus  $1000/T$  for  $WTe_2$  crystals for two-probe method and four-probe method are shown in Figures 1 and 2 respectively. The resistivity along the cleavage plane decreases with increase in the temperature which indicates the semiconducting behavior of these crystals. From the high temperature resistivity measurements we get the activation energy of  $WTe_2$  crystals which is presented in Table 1. Variation of thermoelectric power (S) with an inverse of temperature for  $WTe_2$  crystals is shown in Figure 3. From the variation of thermoelectric power with temperature gives the value of scattering parameter and fermi energy are given in Table 3. All the results obtained from the Hall Effect measurements are given in Table 2. Current-voltage characteristic of  $WTe_2$  crystal is shown in Figure 4. Using Wiedemann–Franz law, we can find the Lorentz number of  $WTe_2$  crystal which is the relation between thermal conductivity and electrical conductivity. The values of thermal conductivity, electrical conductivity and Lorenz number (L) are given in the table 4.

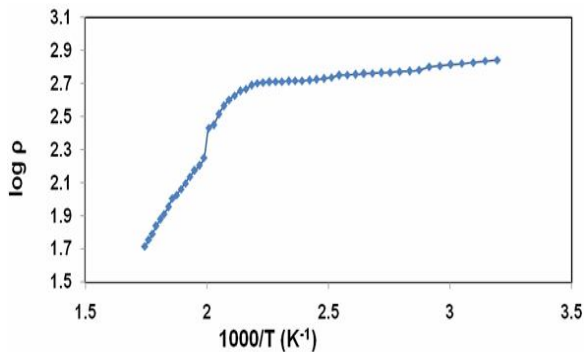


**Fig. 1** Variation of  $\log \rho$  vs  $1000/T$  for  $WTe_2$  crystal for two probe method

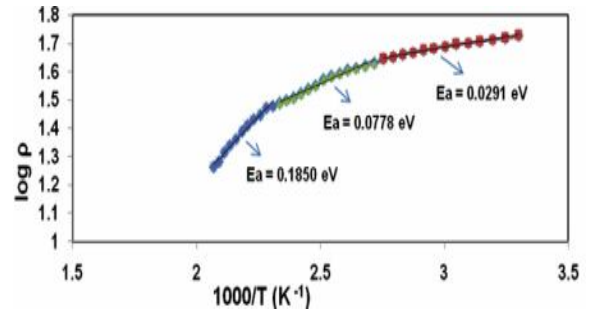


**Fig. 2** Variation of  $\log \rho$  vs  $1000/T$  for  $WTe_2$  crystal for four probe method

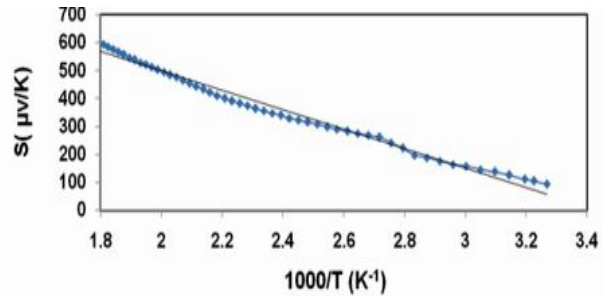


**Fig. 3** Variation of thermoelectric power (S) with an inverse of temperature for  $WTe_2$  crystals.

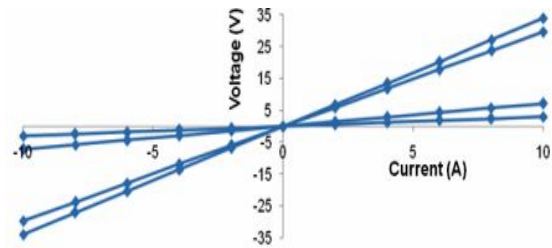


**Fig. 4** Current-Voltage curve for  $WTe_2$  crystal

**Table - 1** Activation energies determined by high temperature resistivity measurement for  $WTe_2$  crystals

Sample (method)	Temperature (K)	Activation Energy (eV)
$WTe_2$ (Two- Probe)	313-573	0.2542
$WTe_2$ (Four -Probe)	303-363	0.0291
$WTe_2$ (Four- Probe)	368-428	0.0778
$WTe_2$ (Four- Probe)	433-483	0.1850

**Table-2** Hall parameters for  $WTe_2$  crystals

Sample	Resistivity $\rho(\Omega\cdot m)$	Conductivity $\sigma(\Omega\cdot m)^{-1}$	Hall coefficient $R_H (m^3/C)$	Mobility $\mu^2 (m^2/V\cdot s)$	Carrier concentration $N_c \times 10^5 (m^{-3})$
$WTe_2$	3.11	0.32	621	239	$2.44 \times 10^{16}$

**Table -3** Parameters A,  $E_{FV}$  and s for  $WTe_2$  crystals

Sample	A	Scattering parameters	$E_{FV}$ (eV)
$WTe_2$	1.1970	1.3030	0.3480

**Table- 4** Value of electrical conductivity, thermal conductivity and Lorentz number for WTe<sub>2</sub> crystals

Electrical conductivity	Thermal conductivity	Lorenz number
$1.7288 \times 10^{-3} (\text{? cm})^{-1}$	0.03134 W/cm K	0.048 W <sup>2</sup> K <sup>-2</sup>

### CONCLUSIONS

The resistivity along the basal plane decreases with increase in the temperature which indicates the semiconducting nature of these crystals and also we can use this material as a lubricant at high temperature. The positive values of the Hall coefficient and the Seebeck co-efficient of the crystals of WTe<sub>2</sub> indicate that all crystals are *p*-type in nature and majority charge carriers in them are holes. The values of thermal conductivity, electrical conductivity and Lorenz number confirmed that the crystal of WTe<sub>2</sub> has semiconductor nature.

### REFERENCES

- [1] Clemen, C., Saldhana, X.I., Munz P. and Bucher E. (1978), Photovoltaic properties of some Semiconducting layer structures *J. Phys. Status Solidi*, **A49**: 437-443.
- [2] Brixner, L. H. (1962), Preparation and the properties of the single crystalline AB<sub>2</sub> -type selenides and tellurides of niobium, tantalum, molybdenum and tungsten. *J. Inorg Nucl. Chem.*, **24**: 257-263.
- [3] Brixner, L. H. (1963) ,X-ray Study and Thermoelectric Properties of the W<sub>x</sub>Ta<sub>1-x</sub>Se<sub>2</sub> System. *J. Electrochem. Soc.*, **110**: 289-293.
- [4] Static, V., Pierre, A. C., Etsall, T. H. and Mikula, R. J. (1997), Preparation of tungsten sulfides by sol-gel processing. *J. Non-Cryst Solid*, **220**: 58-62.
- [5] Troadec, J. P., Bideau, D. and Guyon, E. (1981), Transport properties of conducting and semiconducting anisotropic mixtures. *J. Phys. C: Solid State Phys.* **14**:4807-4819.
- [6] Revolinsky, E. and Beerntsen, D. (1964), Electrical Properties of the MoTe<sub>2</sub>-WTe<sub>2</sub> and MoSe<sub>2</sub>-WSe<sub>2</sub> Systems. *J. Appl. Phys.*, **35**: 2086-2089.
- [7] Malliaris, A., and Turner, D. T. (1971), Influence of Particle Size on the Electrical Resistivity of Compacted Mixtures of Polymeric and Metallic Powders *J. Appl. Phys.*, **42**: 614-618.
- [8] Upadhyayula, L., Loferski, J., Wold, A., Girit, W. and Kershaw, R. (1968), Semiconducting Properties of Single Crystals of n- and p- Type Tungsten Diselenide (WSe<sub>2</sub>) *J. Appl. Phys.*, **39**: 4736-4740.
- [9] Dave, M., Vaidya, R. and Patel, S. G. (2003), X-Ray Diffraction Studies for WTe<sub>2</sub> single Crystals. *J. Pure and Appl. Sciences – Prajna*, **12**: 83-87.



## ELECTRON IMPACT TOTAL CROSS SECTIONS FOR ETHYLENE OXIDE

Avani Y. Barot<sup>1</sup>, Minaxi Vinodkumar<sup>1</sup> and Bobby Antony<sup>2\*</sup>

<sup>1</sup>V P & R P T P Science College, Vallabh Vidyanagar – 388 120, Gujarat, India

<sup>2</sup>Dept. of Applied Physics, Indian School of Mines, Dhanbad – 826004, JH, India

### ABSTRACT

Present paper reports various total cross sections viz. total elastic, total inelastic, total ionization and total cross sections for ethylene oxide on electron impact from ionization threshold to 2 keV. We have employed the well established Spherical Complex Optical Potential (SCOP) formalism to compute total elastic and total inelastic cross sections. While total (complete) and total ionization cross sections are derived from these cross sections. There is only one measurement for total (complete) cross sections and a BEB (Binary - encounter Bethe) calculation by the same group for total ionization cross sections. In the present case, both cross sections are derived from the same formalism and hence we are quite confident that these results are consistent. Also, the results give an overall good agreement with other data in both cases.

**Key words :** ethylene oxide; Total cross section; Spherical Complex Optical Potential; Complex Optical Potential ionization contribution

### INTRODUCTION

Ethylene oxide (C<sub>2</sub>H<sub>4</sub>O) is an organic compound composed of two alkyl groups attached to an oxygen atom in a cyclic shape. Because of its special molecular structure, ethylene oxide easily participates in the addition reaction, opening its cycle, and thus forming polymers [1,2]. Electron impact studies on these molecules are very important since they find applications in varied fields [3-5]. Its principle use lies in the manufacture of ethylene glycol and higher alcohols which find important applications in automotive antifreeze, explosives, cellophane, polyester resins, synthetic fibers and rubbers, and hydraulic fluids. Moreover ethylene oxide in mixture with carbon dioxide and halogenated propellants find utility as a fumigant, fungicide and sterilizing agent [6]. The local chemistry in all these cases is dependent on the reactive nature of these chemicals and their radicals formed by the scattering by electrons. Hence, electron impact scattering and ionization is very important to characterize the nature of reactions possible in such cases.

Electron impact studies with organic targets gained prominence after the study of Boudaiffa et al [7]. They pointed out that secondary electrons produced by energetic radiations are responsible for single and double strand breaks in DNA. Moreover systematic and detailed knowledge of cross sections resulting from electron collisions with simple organic systems can help us to understand the behavior of more complex biomolecules. Despite its importance very little attempts were made in this direction. The only measurement of electron impact total cross sections is performed by Szmytkowski et al [8]. They have also reported total ionization cross section using BEB formalism. To the best of our knowledge, no other experimental and/or theoretical cross section data is available for this molecule in the present energy range.

### THEORETICAL METHODOLOGY

In our Spherical Complex Optical Potential (SCOP) formalism [9], the electron-molecule system is represented by a complex potential given by,

$$V(r, E_i) = V_R(r, E_i) + i V_I(r, E_i) \quad (1)$$

such that

$$V_R(r, E_i) = V_{st}(r) + V_{ex}(r, E_i) + V_p(r, E_i) \quad (2)$$

represents various real potentials arising from the electron target interaction namely, static, exchange and polarization respectively. To evaluate these potentials we use spherically averaged molecular charge-density  $\rho(r)$ , determined from the constituent atomic charge densities given by Cox and Bonham [10]. Since the molecule dealt here is quite large, we have adopted a group additivity method to represent the charge density. In this method the molecular charge density is partitioned depending on the bond length and various groups associated with the molecule. For ethylene oxide, the C<sub>2</sub>H<sub>2</sub>- and O were treated as separate groups and then the charge density is formulated by expanding it at the centre of mass of each group in the molecule [11]. Later the charge densities corresponding to these groups are added together and renormalized incorporating the covalent bonding to get the complete picture. The exchange potential may be derived from the static potential thus obtained employing Hara's parameter free and energy dependent 'free electron gas exchange model' [12]. The polarization potential is of Zhang et al [13]. Finally, the imaginary part  $V_I$  of the complex potential is derived from the well-known non-empirical quasi-free model form given by Staszeweska et al. [14],

$$V_{abs}(r, E_i) = -\rho(r) \sqrt{\frac{T_{loc}}{2}} \cdot \left( \frac{8\pi}{10k_F^3 E_i} \right) \theta(p^2 - k_F^2 - 2\Delta) \cdot (A_1 + A_2 + A_3) \quad (3)$$

The local kinetic energy of the incident electron is given by,

$$T_{loc} = E_i - (V_{st} + V_{ex} + V_{pol}) \quad (4)$$

Where,  $A_1$ ,  $A_2$  and  $A_3$  are dynamic functions (defined in ref [14]) depends differently on  $\theta(x)$ ,  $I$ ,  $\Delta$  and  $E_p$ , where  $I$  is the ionization threshold of the target,  $p^2 = 2E_i$  and  $k_F = [3\pi^2\rho(r)]^{1/3}$  is the Fermi wave vector. Further,  $\theta(x)$  is the Heaviside unit step-function and  $\Delta$  is the energy parameter which determines a threshold below which  $V_{abs} = 0$ , where the ionization or excitation is prevented energetically. We have modified the original model by considering  $\Delta$  as a slowly varying function of  $E_i$  around  $I$  as,

$$\Delta(E_i) = 0.8I + \beta(E_i - I) \quad (5)$$

$\beta$  is obtained by requiring that  $\Delta = I$  (eV) at  $E_i = E_p$ , and also beyond  $E_p$  it is held constant equal to  $I$ . This is done to include excitations at low energies and inner shell ionization at high

\*Corresponding author: bka.ism@in.com

energies. After generating the full complex potential given in Eq. (2), we solve the Schrödinger equation numerically using partial wave analysis to obtain complex phase shifts which are then used to find cross sections  $Q_{inel}$  and  $Q_{el}$  [15]. Using these cross sections, the total cross section is obtained through,

$$Q_t = Q_{inel} + Q_{el} \quad (6)$$

Since  $Q_{inel}$  cannot be measured directly and the measurable  $Q_{ion}$  is of more practical importance, we extract  $Q_{ion}$  contained in the  $Q_{inel}$ . Hence, to obtain  $Q_{ion}$ ,  $Q_{inel}$  is partitioned as,

$$Q_{inel}(E_i) = \sum Q_{exc}(E_i) + Q_{ion}(E_i) \quad (7)$$

Where, the first term is the sum over total excitation cross sections for all accessible electronic transitions. The second term is the total cross sections of all allowed ionization processes induced by the incident electrons. In order to extract  $Q_{ion}$  from  $Q_{inel}$ , a reasonable approximation can be evoked by using a dynamic ratio function,

$$R(E_i) = \frac{Q_{ion}(E_i)}{Q_{inel}(E_i)} \quad (8)$$

Such that,  $0 < R \leq 1$ . We assign three physical conditions to this ratio. It is apparent that when the incident energy is less than or equal to the ionization threshold of the target, this ratio is zero as the ionization process has not started. Also, at very high energy, the only dominant process is the ionization and hence the ratio approaches almost 1. Thus,

$$\begin{aligned} R(E_i) &= 0 \text{ for } E_i \leq I \\ &= R_p \text{ at } E_i = E_p \\ &\approx 1 \text{ for } E_i \gg E_p \end{aligned} \quad (9)$$

$R_p$  is the value of  $R$  at  $E_i = E_p$ . The general observation is that, at energies close to peak of ionization, the contribution of  $Q_{ion}$  is about 70–80% of the total inelastic cross sections  $Q_{inel}$ . This behavior is attributed to the smaller values of  $\sum Q_{exc}$  compared to  $Q_{ion}$  with the increase in energy beyond  $E_p$  value. However the choice of  $R_p$  in Eq. (9) is not rigorous and introduces uncertainty in the final results. It has been by now tested for large number of atoms and molecules and it is observed that the proposed uncertainty is found to be less than 10% [9]. For calculating the  $Q_{ion}$  from  $Q_{inel}$  we use the following analytical form.

$$R(E_i) = 1 - C_1 \left( \frac{C_2}{U+a} + \frac{\ln(U)}{U} \right) \quad (10)$$

Here,  $U = E_i / I$ . At low and intermediate energies the first term dominates and gives reasonable energy dependence at this range. However, when the energy increases further, the second term catches up and defines the ratio quite adequately here. The reason for such variation is due to the fact that initially the contribution to electron excitation is high, the contribution to the ionization channel is just picking up. However, as the energy is increased further, ionization contribution rises and the discrete excitation decreases rapidly. Consequently, we need to use the above functional form to attribute this behavior. It is quite evident that the conditions (as shown in Eq. 9) to find the parameters  $C_1$ ,  $C_2$ , and  $a$  used in Eq. (10) will depend on the properties of the target under investigation [9,16,17]. The method given above to extract  $Q_{ion}$  from  $Q_{inel}$  is called the Complex Scattering Potential–ionization contribution (CSP-ic) [9]. Once  $Q_{ion}$  is obtained,  $\sum Q_{exc}$  can easily be evaluated by eqn (7).

The values of  $Q_{el}$ ,  $Q_{inel}$  and  $\sum Q_{exc}$  for ethylene oxide are not reported here, but are available with the authors. We note that in view of the approximations made here, no definitive values are claimed, but by and large our results fall within the experimental error limits in most of the cases

## RESULTS AND DISCUSSION

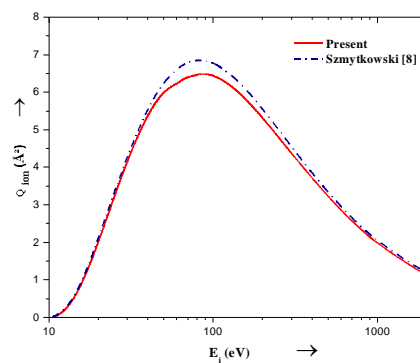
The theoretical approach of SCOP along with CSP-ic method discussed above offers the determination of the total cross sections  $Q_t$ ,  $Q_{el}$  and  $Q_{ion}$  along with a useful estimation of electronic excitations in terms of the summed total cross section  $\sum Q_{exc}$ . Various important target parameters used for the present calculation are the best available from the literature [18].

The main advantage of the present work is that it covers all the major TCSs on electron impact of Ethylene oxide under the same formalism of SCOP along with CSP-ic. The present values of the total elastic, total inelastic, total ionization and total cross sections for  $C_2H_4O$  for the impact of electrons from threshold to 2 keV are tabulated in Table 1.

**Table 1** Numerical values of ionization cross section ( $Q_{ion}$ ) and total cross section ( $Q_t$ ) in  $\text{\AA}^2$  for  $C_2H_4O$

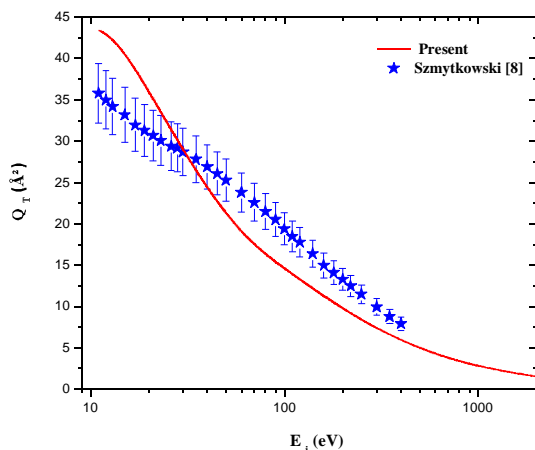
$E_i$ (eV)	$Q_{ion}$	$Q_t$	$E_i$ (eV)	$Q_{ion}$	$Q_t$
11	0.024	43.456	65	6.338	18.282
12	0.121	42.969	70	6.405	17.559
13	0.274	42.269	75	6.437	16.912
14	0.472	41.423	80	6.472	16.367
15	0.701	40.523	85	6.486	15.878
16	0.951	39.590	90	6.484	15.430
17	1.215	38.654	95	6.468	15.013
18	1.484	37.746	100	6.442	14.630
19	1.752	36.828	110	6.363	13.932
20	2.017	35.965	120	6.262	13.293
21	2.276	35.132	130	6.151	12.729
22	2.528	34.346	140	6.034	12.214
23	2.768	33.579	150	5.912	11.738
24	2.999	32.842	160	5.790	11.297
25	3.219	32.136	170	5.667	10.884
26	3.427	31.458	180	5.547	10.884
27	3.625	30.809	190	5.429	10.504
28	3.813	30.186	200	5.315	9.806
30	4.157	29.032	225	5.047	9.064
32	4.463	27.958	250	4.803	8.428
34	4.736	26.970	275	4.578	7.877
36	4.976	26.069	300	4.374	7.391
38	5.189	25.225	400	3.713	5.955
40	5.377	24.446	500	3.229	4.999
42	5.541	23.734	600	2.860	4.321
44	5.684	23.067	700	2.568	3.805
46	5.805	22.446	800	2.334	3.410
48	5.909	21.877	900	2.139	3.090
50	5.994	21.340	1000	1.977	2.830
55	6.145	20.142	1500	1.437	1.997
60	6.226	19.105	2000	1.128	1.545

Present results are also shown graphically along with available comparison in Figures 1 and 2. We have also presented the mutual comparison of various total cross sections using bar chart in Figure 3.



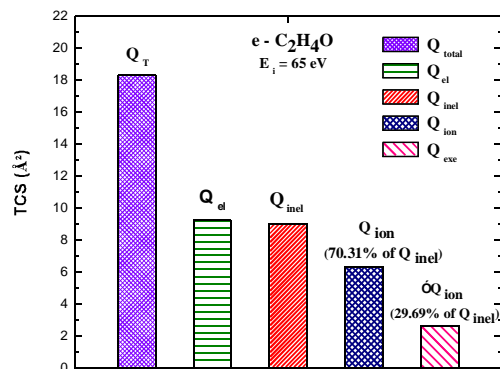
**Figure 1:** Total ionization cross section of  $C_2H_4O$ . Solid line represents present data and dash dot line represents the BEB

Figure 1 shows comparison of electron impact total ionization cross section for  $e - C_2H_4O$  scattering. Present results are in excellent agreement with theoretical results of Szmytkowski et al [8]. They have employed BEB method for computation of total ionization cross section. There is no other theoretical or experimental data available in the literature for this molecule.



**Fig. 2** Total cross section of  $e - C_2H_4O$ . Solid line represents present data and stars gives the experimental values from Szmytkowski et al [8].

Figure 2 shows comparison of total cross section for  $e - C_2H_4O$  scattering. Present results are in overall agreement with measured values of Szmytkowski et al [8]. At low energies present results are slightly higher than Szmytkowski et al [8]. This may be due to the fact that we have employed group additivity approach which will overestimate at low energies. There are no other theoretical or experimental results available to best of our knowledge.



**Fig. 3** Bar Chart of various total cross sections at incident energy  $E_i=65$  eV.

Figure 3 shows bar chart for various total cross sections for  $e - C_2H_4O$  scattering at 65 eV. Bar chart gives us pictorial comparison of mutual contribution of various cross sections to total cross section. At 65 eV, total elastic and total inelastic cross sections are almost 50%. Also total ionization cross section is 70% of total inelastic cross section while total ionization cross section is 30% of total inelastic cross section.

## CONCLUSION

We have calculated total and ionization cross section for ethylene oxide molecule within the 11 - 2000 eV incident energy range. The method employed here is the Spherical Complex Optical Potential method and Complex Scattering Potential – ionization contribution method. These methods are well

established for obtaining cross section with reasonable accuracy. The present total ionization cross section obtained shows a maximum centred near 85eV which is very well replication by the theoretical values of Szmytkowski et al [8]. The comparison is quite good throughout the energy range. We have also calculated the total cross section and at the intermediate and high impact energies up to 2 keV. This is in reasonable agreement with the experimental cross section by Szmytkowski et al [8]. The slight variation in the cross section may be due to the fact the group additivity method adopted here might overestimate the cross section at low energies. Further, the inconsistencies present in the total cross section may be rectified once more theoretical and experimental works will be available in the future. We are quite sure that present work will inspire other researchers to look into this less studied, but very important molecule, ethylene oxide.

## ACKNOWLEDGEMENT:

MVK thanks Department of Science and Technology, New Delhi for financial support through Project Grant No: SR/S2/LOP-26/2008 and BKA thanks UGC, New Delhi for financial support through project Grant No: 39-119/2010(SR) for major research projects under which part of this work is done.

## REFERENCES

- [1] Matsumoto K and Kanitani M (2003), "High-speed ethylene oxide plasma sterilization system without toxic residuals" IEEE Conf. Record-Abstracts: 30th Int. Conf. on Plasma Science (Jeju, Korea) p 285.
- [2] <http://www.nist.gov/chemistry-portal.cfm>
- [3] Christophorou L. G. and Olthoff J. K. (2004), "Fundamental Electron Interactions with Plasma Processing Gases" (New York: Kluwer).
- [4] Sanche L. (2005), "Low energy electron - driven damage in biomolecules." *Eur. J. Phys. D*, **35**: 367–90.
- [5] Greenberg J. M. (2002), "The tritrophic trinity a source of pollutant degrading enzymes and its implications for phytoremediation." *Surf. Sci.*, **500**: 793–822.
- [6] [http://www.c-f-c.com/specgas\\_products/ethyleneox.htm](http://www.c-f-c.com/specgas_products/ethyleneox.htm)
- [7] Boudaiffa B., Cioutier P., Hunting D., Hules M. A. and Sanche L. (2000), "Resonant formation of DNA strand breaks by low – energy (3 to 20 eV) electrons." *Science*, **287**: 1658.
- [8] Szmytkowski Cz., Domaracka A., Mozejko P., Ptasin ska -Denga E. (2008), "Electron collisions with ethylene oxide molecules", *J. Phys. B: At. Mol. Opt. Phys.*, **41**: 065204.
- [9] Vinodkumar M., Korot K. and Bhutadia H. (2010), "Calculations of total and ionization cross sections on electron impact for alkali metals (Li, Na, K) from threshold to 2keV." *Int. J. Mass Spectrom.*, **294**: 54.
- [10] Cox H. L. and Bonham R. A. (1967), "Elastic electron scattering amplitudes for natural atoms calculated using the partial wave method at 10,40,70, and 100 kV for  $Z = 1$  to  $Z = 54$ ." *J. Chem. Phys.*, **47**: 2599.
- [11] Vinodkumar M., Limbachiya C., Antony B. K. and Joshipura K. N. (2007), "Calculation of elastic, ionization and total cross sections for inert gases upon electron impact: threshold to 2keV." *J. Phys. B: At. Mol. Opt. Phys.*, **40**: 3259.
- [12] Hara S. (1967), "The scattering of slow electrons by hydrogen molecules.", *J. Phys. Soc. Japan*, **22**: 710.

- [13] Zhang X., Sun J. and Liu Y. (1992), "A new approach to the correlation potential- low- energy electron elastic scattering by He – atoms.", *J. Phys. B: At. Mol. Opt. Phys.*, **25**: 1893.
- [14] Staszewska G., Schewenke D. W., Thirumalai D. and Truhlar D. G. (1983), "Quasifree-scattering model for the imaginary part of the optical potential for electron scattering", *Phys. Rev. A*, **28**: 2740.
- [15] Joachain C. J. (1983), "Quantum Collision Theory" (Amsterdam: North-Holland).
- [16] Vinodkumar M., Joshipura K. N., Limbachiya C. and Mason N. J. (2006), "Theoretical calculations for the total and ionization cross section for electron impact on some simple biomolecules." *Phys. Rev. A*, **74**: 022721.
- [17] Vinodkumar M., Dave R., Bhutadia H., Antony B. K. (2010), " Electron impact total ionization cross section for halogens and their hydrides." *Int. J. Mass Spectrom.* **292**: 7.
- [18] Lide R. (2003), "CRC Handbook of Chemistry and Physics" (Boca Raton, FL: CRC Press).



## INFRARED SPECTRA OF CHARGE TRANSFER COMPLEXES OF PROTEOGLYCAN

Pravinsinh I. Rathod, Vishal Patel and A.T. Oza

Department of Physics, Sardar Patel University, Vallabh Vidyanagar – 388120, Gujarat, India

### ABSTRACT

The FTIR spectra of charge transfer complexes of an important biomolecule called proteoglycan (PG) with acceptors such as TCNQ, TCNE, DDQ, chloranil and iodine have been studied. Proteoglycan-TCNQ shows features corresponding to strongly ionic nature of complex and stacks of  $\text{TCNQ}^-$  and  $\text{TCNQ}^=$  ions. Proteoglycan-chloranil spectrum shows oscillations in the density of states along chloranil stacks. Proteoglycan-TCNQ, proteoglycan-chloranil and proteoglycan-iodine (I<sub>2</sub>) spectra reveal forbidden indirect transitions across the band gaps while proteoglycan-TCNE forbidden direct transition.

**Key words:** Proteoglycan, Charge transfer complexes, Infrared spectra, Nature of transition, Gaussian distribution

### INTRODUCTION

Proteoglycan is an important molecule which is combination of protein and polysaccharides. Proteoglycan has a branched core structure. The branches are polypeptide chains. Each polypeptide chain has sub-branches made up of glycosaminoglycans. If the polysaccharides are dominant in proteoglycan in content, it is called proteoglycan [1]. If protein content dominates, it is called glycoprotein. Here we study proteoglycan. It has structure suggested in Little's model of high temperature superconductivity [2]. Therefore, we selected proteoglycan in the present study.

### EXPERIMENTAL DETAILS

Proteoglycan was a white powder obtained from Sigma chemical company, USA. Proteoglycan was mixed with acceptors such as TCNE (tetracyano-p-ethylene), DDQ (2,3-dichloro-5,6-dicyano-pbenzoquinone), TCNQ (7,7,8,8-tetracyano-p-quinodimethane), Chloranil (2,3,5,6-tetrachloro-p-benzoquinone) and iodine (I<sub>2</sub>) in 1:1 molecular weight proportion. The mixtures were grinded in a mortar till the CT (charge transfer) complexes were formed. These CTCs (charge transfer complexes) were further grinded with 95% of dry spectrograde KBr powder till dispersed homogeneously. Circular discs which were semitransparent prepared using a die and a manual compressing machine. The discs were placed in a dark chamber of spectrophotometer.

### RESULTS AND DISCUSSION

The FTIR spectrum of proteoglycan is shown in Figure 1. The material is transmitting in the range of  $1800\text{cm}^{-1}$  to  $3000\text{cm}^{-1}$ , which shows that it does not have any band gap in IR (infrared) range. Various vibrational bands particularly corresponding to outer periphery of large molecule of proteoglycan are observed in FTIR (fourier transform infrared spectroscopy) spectrum. No background absorption has developed indicating that it is an insulator. The FTIR spectrum of proteoglycan-TCNQ is also shown in Figure 2. Here TCNQ being a large molecule as compared with other acceptors used in the present study. It forms segregated stacks and absorbs being  $\text{TCNQ}^-$  or  $\text{TCNQ}^=$  radical-ions. No bands of proteoglycan are pronounced in IR range. Bands of  $\text{TCNQ}^-$  and  $\text{TCNQ}^=$  dominate the full IR spectrum which shows presence of TCNQ stacks and ionic nature of the compound. The spectrum is

similar to those of hemoglobin-TCNQ and myoglobin-TCNQ where TCNQ goes into the cavity of hemoglobin in the place of diphosphoglycerate enzyme. The bands of  $\text{TCNQ}^-$  and  $\text{TCNQ}^=$  dominate the spectra of hemoglobin-TCNQ and myoglobin-TCNQ. Here a similar spectrum is observed indicating that TCNQ goes into the cavity of proteoglycan molecules. The IR spectrum is mainly governed by the vibrational levels of  $\text{TCNQ}^-$  and  $\text{TCNQ}^=$  organic radical-anions. This special interaction is due to  $\pi$ -character of TCNQ.

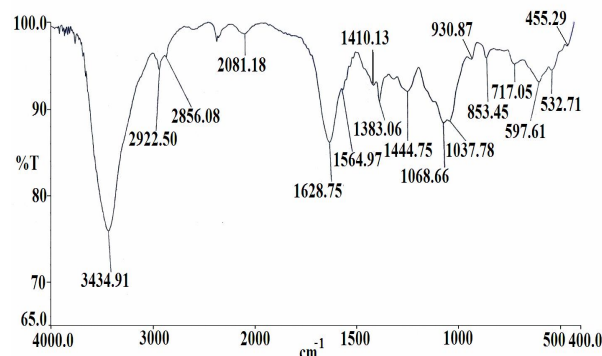


Fig. 1 The FTIR spectrum of proteoglycan only

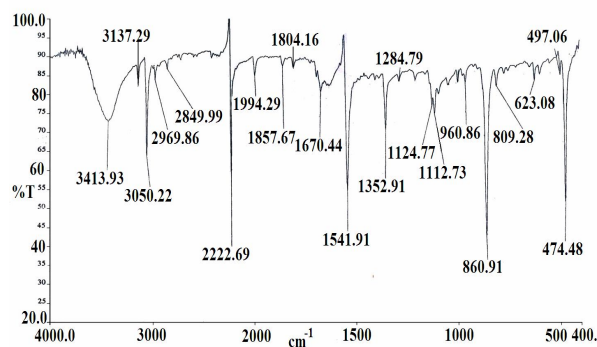
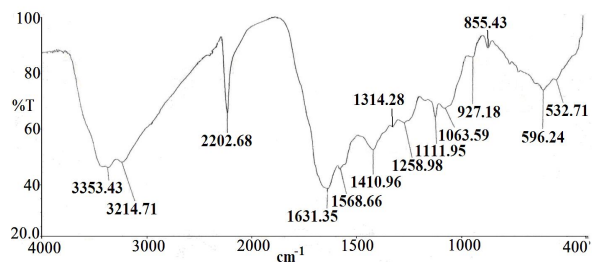


Fig. 2 FTIR spectrum of proteoglycan-TCNQ charge transfer complex.

\*Corresponding author: rathod.pravinsinh@gmail.com

The FTIR spectrum of proteoglycan-TCNE is shown Figure 3. Here TCNE interacts as an acceptor with various vibrational levels of proteoglycan. The spectrum is different from that of proteoglycan alone. There is development of absorption in the range of  $3000\text{cm}^{-1}$  to  $1800\text{cm}^{-1}$ . This can be ascribed to electronic transition across the band gap as found normally in all CT complexes. The nature of transition is analyzed to be a forbidden direct transition [3, 4] obeying  $A_{hv} = B(h\nu - E_g)^{3/2}$  with a graph of  $(A_{hv})^{2/3}$  vs  $h\nu$  which shown in Figure 4. Other background absorptions developed around  $1630\text{cm}^{-1}$  and  $596\text{cm}^{-1}$  can be assigned to imperfect nesting. When imperfect nesting occurs, a distorted and asymmetric triangular distribution is observed.



**Fig. 3** The FTIR spectrum of proteoglycan-TCNE charge transfer complex.

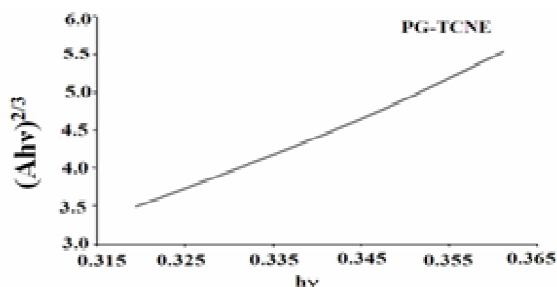


**Fig. 4** The nature of transition of proteoglycan-TCNE charge transfer complex

The Other important compound is proteoglycan-DDQ whose spectrum is shown in below figure 5. A nature of transition range is found in a small range of  $2800\text{cm}^{-1}$  to  $2000\text{cm}^{-1}$ . The absorption in this range is analyzed and it is found that it is a forbidden indirect transition obeying  $A_{hv} = B(h\nu - E_g \pm E_p)^3$  by plotting  $(A_{hv})^{1/3}$  vs  $h\nu$  Figure 6. Apart from this, two Gaussians, one broad and other sharp are observed in the mid-IR range of  $1000\text{cm}^{-1}$  to  $1800\text{cm}^{-1}$ . Both the Gaussians are fitted which obey  $\alpha = \alpha_0 \exp(-(k-k_0)^2/2m^2)$  where  $\alpha_0$  is maximum value of absorption,  $k_0$  is the central wave number and  $m^2$  is the second moment of the distribution. These fits are shown in which  $\ln \alpha$  vs  $(k-k_0)^2$  are plotted as in figure 7 and figure 8. The proteoglycan-chloranil shows a completely different spectrum shown in figure 9. Here the transition across the band gap leads to development of absorption in the range of  $3000\text{cm}^{-1}$  to  $1750\text{cm}^{-1}$ . The transition is found to be of forbidden indirect type upon analysis and fitted as shown in figure 10 i.e. it obeys  $A_{hv} = B(h\nu - E_g)^3$ . Rest of the spectrum of proteoglycan-chloranil complex shows repeated structures below  $1700\text{cm}^{-1}$ . Three repeated structures with only little damping are observed. These structures can be assigned to the oscillations in the density of states. The shape of each structure is governed by square-root singularity unique for one-dimensional systems of lattice vibrations. There is strong electron-phonon interaction through which these lattice vibrations become infrared active. The system acts as a

molecular multivibrator. This is a special state in molecular electronics. Multivibrator has non-sinusoidal periodic structures. Here it is also a non-sinusoidal type vibration. This is found in other chloranil complexes too. It is not know why chloranil complexes many times reveal oscillations in the density of states. Biolytin-chloranil, hemoglobin-chloranil and myoglobin-chloranil have also similar property [5].

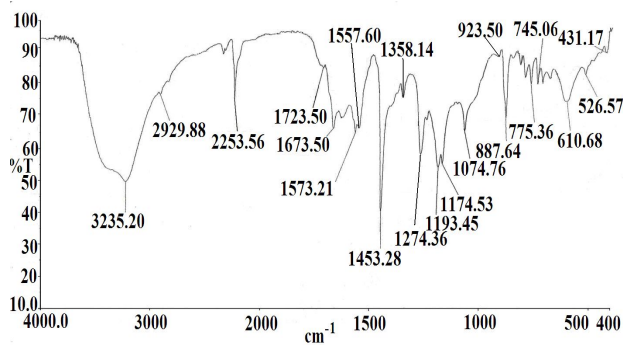


**Fig. 5** The FTIR spectrum of proteoglycan-DDQ charge transfer complex

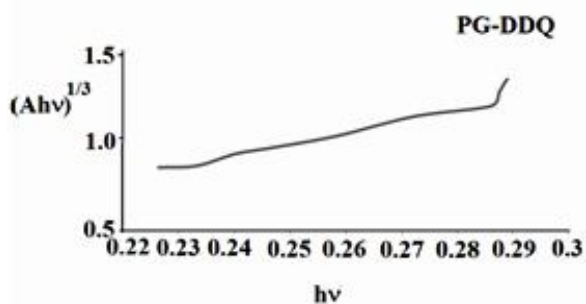


**Fig. 6** The nature of transition in proteoglycan-DDQ charge transfer complex

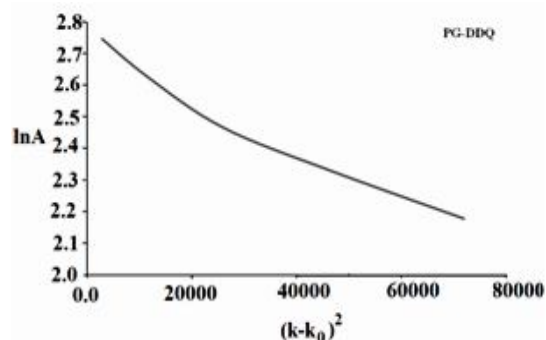


**Fig. 7** Broad Gaussian Fitted in mid-IR range in proteoglycan-DDQ charge transfer complex

The FTIR spectrum of proteoglycan-iodine is shown as below figure 11. It shows a range in which transition across a band gap occurs and two broad Gaussians in other lower frequency ranges. The nature of transition is analyzed to obey  $A_{hv} = B(h\nu - E_g \pm E_p)^3$  revealing a forbidden indirect type transition which shown in figure 12. There are weak and a broad Gaussian distribution in absorption around  $1380\text{cm}^{-1}$  and  $595\text{cm}^{-1}$ . Also there is comparatively stronger gaussian band around  $595\text{cm}^{-1}$ .

Both of these Gaussian bands are fitted by plotting  $\ln A$  vs  $(k-k_0)^2$  which are shown in Figure 13 and Figure 14.

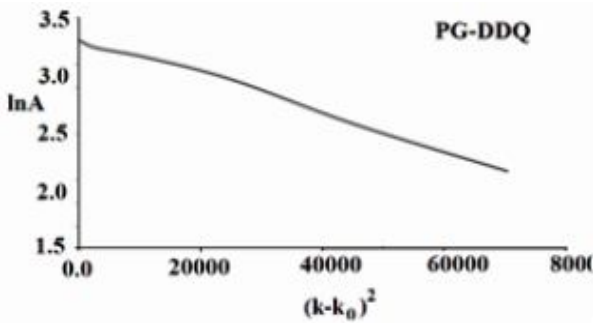


Fig. 8 Sharp Gaussian Fitted in mid-IR range in proteoglycan-DDQ charge transfer complexes

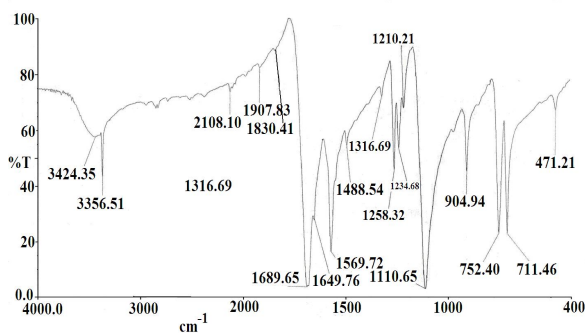


Fig. 9 The FTIR spectrum of proteoglycan-Chloranil charge transfer complex

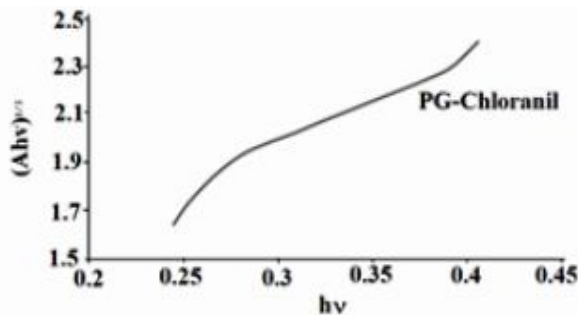


Fig. 10 The nature of transition of proteoglycan-Chloranil charge transfer complex

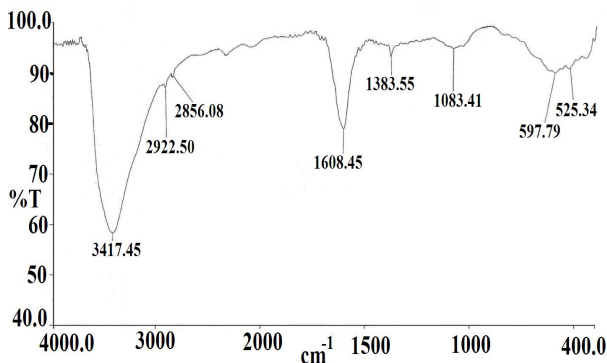


Fig. 11 The FTIR spectrum of proteoglycan-iodine charge transfer complex

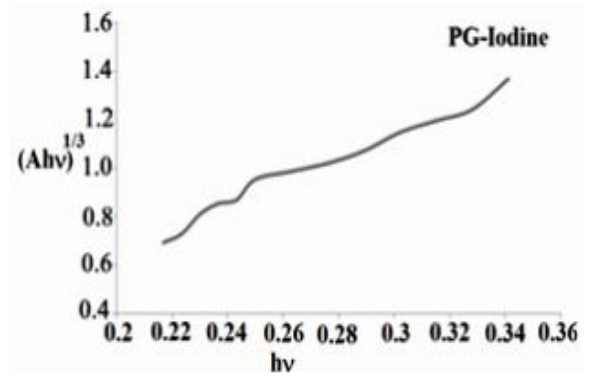


Fig. 12 Nature of transition of proteoglycan-iodine charge transfer complex

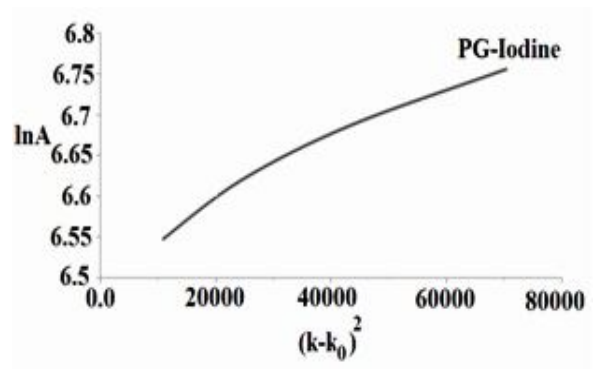


Fig. 13 Gaussian band fitted around 1380  $\text{cm}^{-1}$  of proteoglycan-iodine charge transfer complex

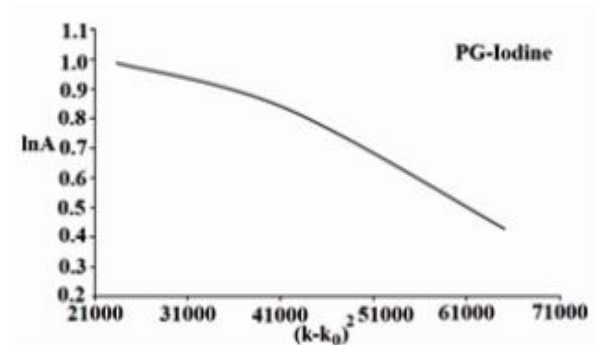


Fig. 14 Gaussian band fitted around 595  $\text{cm}^{-1}$  of proteoglycan-iodine charge transfer complex

Table - 1 Parameter of gaussian distribution in the different proteoglycan complexes.

Name of the complex	$\alpha_{\text{max}}$ (%) Peak value	$K_{\text{max}}$ ( $\text{cm}^{-1}$ ) Central wave number	FWHM ( $\text{cm}^{-1}$ )
PG-DDQ			
(1)	84.412	1392.5	301
(2)	73.24	1032.25	408.5
PG-I <sub>2</sub>			
(1)	96.928	1102	510
(2)	92.496	455.56	276.27

**Table - 2** Nature of transitions in proteoglycan charge transfer complexes.

Name of the complex	Absorption function	Values of band gap(eV) (Forbidden direct)
PG-TCNE	$A_{hv} = \beta(h\nu - E_g)^{3/2}$	0.32 eV
PG-DDQ	$A_{hv} = \beta(h\nu - E_g \pm E_p)^3$	0.23 eV
PG-Chloranil	$A_{hv} = \beta(h\nu - E_g \pm E_p)^3$	0.25 eV
PG-I <sub>2</sub>	$A_{hv} = \beta(h\nu - E_g \pm E_p)^3$	0.21 eV

**CONCLUSION**

Proteoglycan forms charge transfer complexes with organic acceptors and iodine. The spectra of CTCs are very much different from the spectrum of proteoglycan alone which shows

presence of charge transfer interaction. Four complexes reveal transition across a band gap in IR range and subsequent (resultant) development of absorption. Proteoglycan–TCNQ spectrum reveals absorptions due to TCNQ<sup>-</sup> and TCNQ<sup>•-</sup> ions and therefore indicates ionic nature of the complex. Proteoglycan–chloranil shows oscillations in the density of states with repeated structures which are almost undamped.

**REFERENCE**

- [1] A L Lenhinger (1987) *Principles of Biochemistry*, CBS Publishers and Distributors, New Delhi, **pp 296**
- [2] W.A.Little (1964) Possibility of synthesizing an organic superconductors, *Phys. Rev.* 134, **A1416–1424**
- [3] J I Pankove (1971) *Optical Process in Semiconductors*, Prentice Hall Inc, Englewood Cliff, New Jersey
- [4] P S Kireev (1975) *Semiconductor Physics*, Mir Publishers Moscow.
- [5] Ashvin B. Padhiyar, Ph.D. Thesis (2011) *Spectroscopic study of charge transfer complexes of some biomolecules*, Sardar Patel University, Vallabh Vidyanagar.



## OPTICAL PROPERTIES OF TIN MONOSULPHIDE AND TIN MONOSELENIDE SINGLE CRYSTALS

**B.B. Nariya\*, A.K. Dasadia and A.R. Jani**

*Department of Physics, Sardar Patel University, Vallabh Vidyangar-388 120, Gujarat, India*

### ABSTRACT

**Optical absorption in SnS and SnSe single crystals has been measured at room temperature in the spectral range 550nm-2500nm. Absorption near the fundamental edge was found to be due to direct allowed transition and the optical band gap corresponding to this transition has also been determined. By using the values obtained from optical absorption measurements optical absorption coefficient, extinction coefficient, refractive index and real and imaginary parts of complex dielectric constant are calculated.**

**Keywords :** *Optical absorption, Optical Constants, Tin monosulfide and Tin monoselenide*

### INTRODUCTION

Among the IV-VI semiconductor compounds, tin sulphide (SnS), tin selenide (SnSe), germanium sulphide (GeS) and germanium selenide (GeSe) have the layered orthorhombic structure with eight atoms per unit cell forming biplanar layers normal to the largest c axis [1-3]. In unit cell of SnS and SnSe, atoms in a single layer are joined to three nearest neighbors by covalent bond which forms zigzag chains along the b axis while there is only Van der Waals bonding between the layers. This material shows a wide variety of interesting anisotropic optical and electrical properties, which make them interesting materials intermediate between two dimensional and three-dimensional semiconductors. These compounds have attracted considerable attention because of their optoelectronic properties [5], useful in applications like holographic recording systems [5,6], electronic switching [7,8] and infrared production and detection.

### EXPERIMENTAL

Single crystals of SnS and SnSe have been grown by direct vapour transport method. For the growth process, the charge was transferred into thoroughly cleaned quartz ampoule. This ampoule with charge of material was evacuated at 10-5 torr and sealed. The ampoule was then inserted into a two-zone horizontal furnace. The front zone (reaction zone) of the furnace was maintained at 1073 K while the back zone (growth zone) was kept at 1023 K for the growth of SnS and SnSe single crystals. The room temperature absorption spectra of SnS and SnSe of thickness 100µm have been taken using UV-VIS-NIR spectrophotometer (Make: Perkin Elmer, lambda-19) in the wavelength range of 550nm-2500nm with the incident beam normal to the basal plane of as grown crystals i.e along c-axis of the grown crystals.

### RESULTS AND DISCUSSION

Figures 1 and 2 show the absorption, reflectance and transmission spectrum of SnS and SnSe single crystals. A careful study of these spectra reveals the presence of an absorption edge in the spectral range 815nm to 905nm for SnS and 1190nm to 1250nm for SnSe. To analyze the results in the vicinity of the absorption edge on the basis of three dimensional models, value of  $\alpha$  were determined at step of 1 nm.

The interpretation of experimental results, in terms of the direct and indirect transition is most often performed with the help of the following equation

$$\alpha h\nu = A(h\nu - E_g)^r \quad (1)$$

for direct transition and

$$\alpha h\nu = \sum_j B_j (h\nu - E_g \pm E_{pj}) \quad (2)$$

for indirect transition.

Figures 3 and 4 show the spectral variation of  $(\alpha h\nu)^2$  and the value of direct band gap obtained from the extrapolation of the straight line portion [9-10]. Obtained values of direct band gap of SnS and SnSe are shown in Table 1 while Figures 4 to 8 display the variation of extinction coefficient, refractive index, real and imaginary part of complex dielectric constant with wavelength for SnS and SnSe single crystals. Using the value obtained from optical absorption, reflectance and transmittance measurements optical absorption coefficient is calculated using the formula

$$T = (1 - R)^2 e^{(-\alpha d)} \quad (3)$$

The extinction coefficient (K) and refractive index (n) have been calculated using relations

$$K = \alpha \lambda / 4\pi \quad (4)$$

$$R = \frac{(n-1)^2 + K^2}{(n+1)^2 + K^2} \quad (5)$$

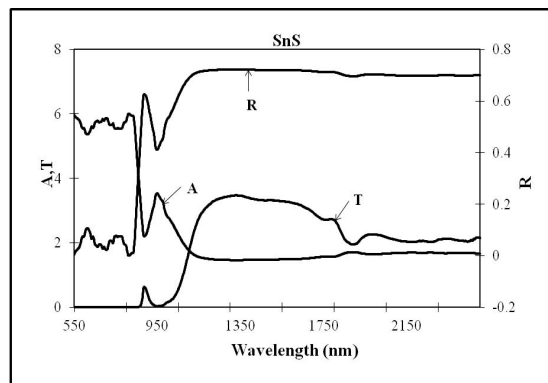


**Fig. 1** Optical absorption, transmittance and reflectance spectrum of SnS single crystals.

\*Corresponding author: bbnariya@gmail.com

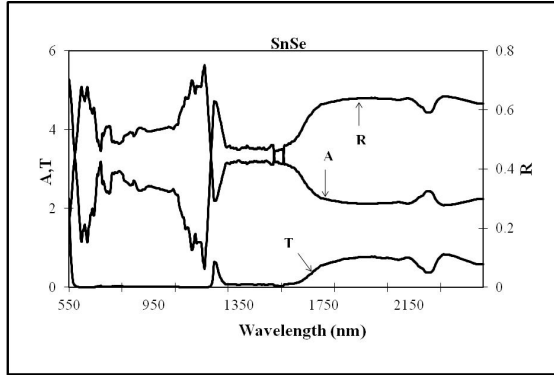


Fig. 2 Optical absorption, transmittance and reflectance spectrum of SnSe single crystals.

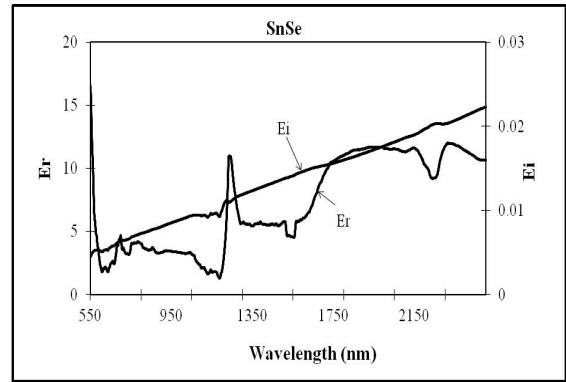


Fig. 6 Wavelength dependence of real and imaginary part of complex dielectric constant for SnSe.

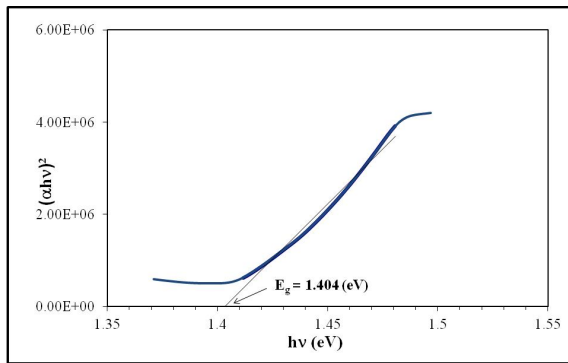


Fig. 3 Plot of  $(ahv)^2$  Vs  $h\nu$  of SnS single crystals.

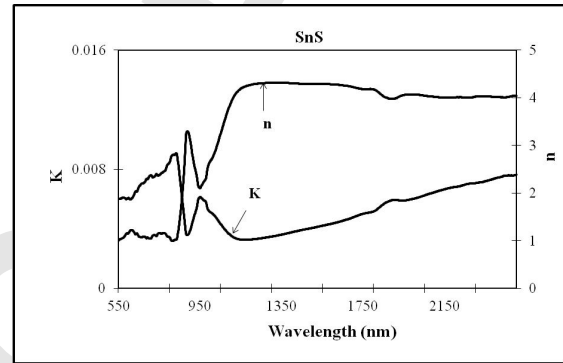


Fig. 7 plot of  $k, n$  Vs wavelength for SnS single crystals.

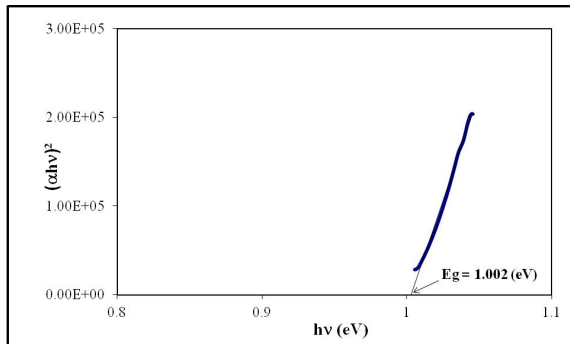


Fig. 4 Plot of  $(ahv)^2$  Vs  $h\nu$  of SnSe single crystals.

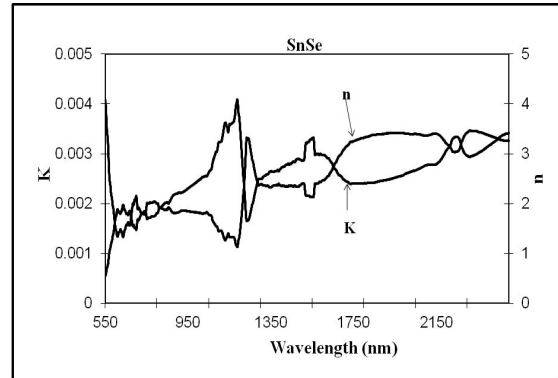


Fig. 8 Plot of  $k, n$  Vs wavelength for SnSe single crystals

Furthermore, real and imaginary parts of complex dielectric constant are determined through the following equations

$$\epsilon_r = n^2 - K^2; \quad \epsilon_i = 2nK \quad (6)$$

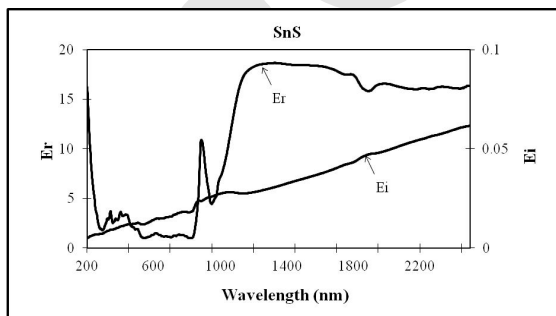


Fig. 5 Wavelength dependence of real and imaginary part of complex dielectric constant for SnS.

Table 1 Value of direct band gap for SnS and SnSe single crystals.

Direct band gap	SnS	SnSe
	1.404 (eV)	1.002 (eV)

### CONCLUSIONS

Single crystals of SnS and SnSe have been grown by direct vapour transport method. It is found that crystals studied in present case show direct symmetry allowed transitions leading to a good account of the optical absorption edge in SnS and SnSe single crystals. The band gap of nearly 1.4 eV for SnS is quite promising for it to be used as a solar material. Nearly flat response of both SnS and SnSe above 1400 nm may make them useful for optical coating.

## REFERENCES

- [1] Okazaki (1958) The crystal structure of germanium selenide, *J. Phys. Soc. Japan*, **13**: 1151-1155.
- [2] Logothetidis, S. and Polatoglou, H. M. (1987) Ellipsometric studies of the dielectric function of SnSe and a simple model of the electronic structure and the bands of the orthorhombic IV-VI compounds, *Phys. Rev.*, **B36**: 7491-7499.
- [3] Valiukonis, G., Gussienova, D. A., Krivaite, G. and Sileika, A. (1986) Optical spectra and energy band structure of layer-type AIV-BVI compounds, *Phys. Stat. Solidi (b)*, **135**: 299-307.
- [4] Parentau, M. and Carlone, M. (1990) Influence of temperature and pressure on the electronic transitions in SnS and SnSe semiconductors, *Phys. Rev.*, **B41**: 5227-5234.
- [5] Bletskan, D.I., Taran, V.I. and Sichka, M. YU. (1976) Switching effect in layered IV-VI crystals, *Ukr. Fiz. Zh.*, **21**: 1436-1441.
- [6] Singh, J.P. and Bedi, R.K. (1990) Tin selenide films grown by hot wall epitaxy, *J. Appl. Phys.*, **68**: 2776-2779.
- [7] Lofersky, J.J (1956) Theoretical considerations governing the choice of optimum semiconductor for photovoltaic solar energy conversion, *J. Appl. Phys.*, **27**: 777-784.
- [8] Lofersky, J.J (1963) Recent research on photovoltaic solar energy converters, *Proc. I.E.E.E.*, **51**: 667-674.
- [9] Elkorashy, A. M. (1986) Optical absorption in Tin monoselenide single crystals, *J. Phys Chem.Solids*, **47**: 497-500.
- [10] Dholakiya, A. D., Solanki, G. K., Patel, S. G. and Agarwal, M. K. (2001) Two and Three dimensional models for analysis of optical absorption in Tungsten disulfide single crystals, *Bull. Mater. Sci.*, **24** (3): 291-296.



## STRUCTURAL CHARACTERIZATION AND TRANSPORT PROPERTIES OF CVT GROWN ZrSe<sub>3</sub> AND ZrS<sub>3</sub> CRYSTALS

A.K. Dasadia\*, B.B. Nariya and A.R. Jani

Department of Physics, Sardar Patel University, Vidyanagar-388 120, Gujarat, India

### ABSTRACT

Single crystals of ZrSe<sub>3</sub> and ZrS<sub>3</sub>, are family of materials with low symmetry structure were grown by chemical vapour transport technique using iodine as a transporting agent. The grown crystals were characterized by energy dispersive analysis of X-ray (EDAX) for confirmation of stoichiometric proportion of constituent elements and structure of grown crystals was determined by X-ray diffraction (XRD) technique. The resistivity and thermoelectric power measurements were carried out in the temperature range 308 K to 573 K. The Hall coefficient, carrier concentration and Hall mobility were determined from Hall Effect measurements at room temperature.

**Key words:** Monoclinic structure, Hall coefficient, Carrier concentration, Hall mobility and Thermoelectric power

### INTRODUCTION

Layered transition metal dichalcogenides have been studied in past years [1-2] but few data are available for transition metal trichalcogenides. This is due to the difficulty of growing large size and good quality crystals of the MX<sub>3</sub> compounds. Transition metal trichalcogenides, MX<sub>3</sub>, (M is a transition metal of group IVB, VB and VIB where X is a chalcogen) constitute structurally well defined family of compounds. These trichalcogenides are thin fibrous ribbons and offer several interesting phenomena originating from their strong anisotropy. Zirconium triselenide and zirconium trisulphide have a chain-like structure belonging to space group P2<sub>1</sub>/m [3]. Trisulphides and triselenides of Zirconium constitute a family of structurally related solids and form MX<sub>3</sub> trigonal prisms that share opposite faces resulting in MX<sub>3</sub> chains. The rich variety of physical properties of the various members of this family arises from variation of X-X and M-M bonds. Transition metal trichalcogenides of ZrSe<sub>3</sub> and ZrS<sub>3</sub> family belong to the first group possessing a single type of MX<sub>3</sub> chains [4] and have been, for over a decade, the subject of intense interest related to their anisotropic character. [5-10]. These crystals have a monoclinic-type structure with a symmetry described by the C<sub>2h</sub><sup>2</sup> point group. As shown in fig.1 metal ions are located in the center of distorted trigonal prisms which share trigonal faces forming, parallel to the b axis, chains that are linked together in two-dimensional slabs by the metal-chalcogene bonds. The layers are bound by sulphure-sulphure Van der-Waals interactions. Figure 1 shows the basic structure of unit cell for the ZrSe<sub>3</sub>, in which MX<sub>3</sub> trigonal prisms are formed. Here columns run parallel to the crystallographic b-direction and displaced from the neighboring columns by one half of the unit cell and ZrS<sub>3</sub> have same monoclinic crystal structure like ZrSe<sub>3</sub>.

Cleavage plane

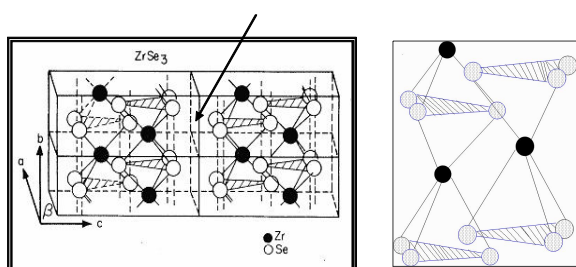


Fig. 1 Crystallographic structure of ZrSe<sub>3</sub>-type compound.

\*Corresponding author: abhi4physix@yahoo.com

Resistivity measurements and Hall Effect measurements were performed in order to determine resistivity, conductivity, mobility and carrier concentration along the basal plane of as grown ZrSe<sub>3</sub> and ZrS<sub>3</sub> crystals. The thermo electric effect offers a distinctive advantage over other methods because the measured thermoelectric voltage is directly related to the carrier concentration, which makes the thermo electric measurements simpler even for high mobility materials. The study of thermo electric power provides an independent way to determine the carrier sign, density and position of Fermi level in semiconductors. In this paper we present results on thermoelectric power measured in temperature range 313K-573K.

### EXPERIMENTAL

With a view to allowing effective and faster transport of constituent to produce the necessary super saturation for crystal growth in a vapour phase system, the chemical vapour transport method was employed. For preparation of starting material from available powders of zirconium (99.9% purity, Alfa Aesar), sulphur (99.9% purity, Alfa Aesar) and selenium (99.9% purity, Alfa Aesar) corresponding to a stoichiometric charge of 10 g was introduced into a thoroughly cleaned quartz ampoule and sealed at a pressure of 10-5 mbar. In the sealed ampoule, the constituent element in the powder form was then distributed uniformly all over the length and kept in the horizontal furnace co-axially in the centre. The temperature was slowly increased at a rate of 2K/min. In the present case, the required temperature was 1073 K. The ampoule was kept at this constant temperature for 18 hrs. After this period, the furnace was slowly cooled down to room temperature at the same rate 2 K/min and then switched off. As a result fine free flowing; shiny homogenous polycrystalline material was obtained for both compounds. Now once we

Table-1: Growth parameters for ZrSe<sub>3</sub> and ZrS<sub>3</sub> single crystals.

Crystal	Temperature distribution		Growth Period (hrs)
	Reaction Zone (K)	Growth Zone (K)	
ZrSe <sub>3</sub>	1173	1073	76
ZrS <sub>3</sub>	1153	1003	87



The magnetic field modifies the path of the electrons producing Hall voltage. Knowing the value of difference in resistance (R), magnetic field (B) and thickness of the sample t, the mobility of charge carriers is evaluated using the relation

$$\mu_H = \frac{t}{\Delta B} \times \frac{\Delta R}{\rho} \quad (1)$$

The Hall coefficient ( $R_H$ ) and carrier concentration ( $n$ ) are evaluated using the following formula;

$$R_H = \mu_H \times \rho \quad (2)$$

$$\eta = \frac{1}{R_H \cdot e} \quad (3)$$

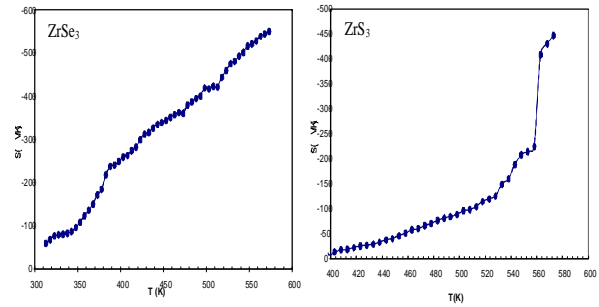


Fig. 5 The variation of thermoelectric power (S) with temperature (T) for ZrSe<sub>3</sub> and ZrS<sub>3</sub> single crystals.

Table - 3 Various electrical properties of ZrX<sub>3</sub> (X=S, Se) single crystals.

Sample	Resistivity $\rho(\Omega\text{m})$	Conductivity $\sigma(\Omega\text{m})^{-1}$	Hall coefficient $R_H$	Mobility $\mu$ ( $\text{m}^2/\text{Vs}$ )	Carrier concentration $N_c \times 10^5 (\text{m})^{-3}$
ZrSe <sub>3</sub>	2.62	0.38	-760	290	$8.22 \times 10^{15}$
ZrS <sub>3</sub>	18.74	0.05	-895	48	$0.66 \times 10^{15}$

The variation of thermoelectric power (S), with temperature (T) for single crystals of ZrX<sub>3</sub> (X=S, Se) are shown in Figures 5. For the study of temperature dependent thermoelectric power S of a semiconductor the expression is given [11] as;

$$S = \pm \frac{k}{e} \left[ A + \frac{E_{FV}}{kT} \right] \quad (4)$$

## CONCLUSION

The work described in this paper attempt to provide some explanation of unit cell structural information as well as some electrical properties of ZrSe<sub>3</sub> and ZrS<sub>3</sub> crystals. Unit cell of ZrX<sub>3</sub> (X=S, Se) possess MX<sub>6</sub> trigonal prisms in which centre of this prism metal ions are located and three chalcogen ions are attached at the upper and lower part of the metal ions. This kind of arrangement of metal chalcogen ions forms columns or chains of distorted prisms in the monoclinic b-direction. Here columns run parallel to the crystallographic b-direction and displaced from the neighboring columns by one half of the unit cell. Both of have same monoclinic crystal structure which is confirmed by X-ray diffraction analysis. The resistivity along the basal plane decreases with increase in the temperature which indicates the semiconducting nature of the grown crystals. The negative values of the Hall coefficient and the TEP measurement of the single crystals of ZrX<sub>3</sub> (X=S, Se) indicate that all crystals are n-type in nature and majority charge carriers in them are electrons. The variation of TEP with respect to temperature shows that the charge impurity scattering predominates in ZrX<sub>3</sub> (X=S, Se) single crystals.

## REFERENCES

- [1] Okazaki (1958), The crystal structure of germanium selenide, *J. Phys. Soc. Japan*, **13**: 1151-1155.
- [2] Logothetidis, S. and Polatoglou, H. M. (1987), Ellipsometric studies of the dielectric function of

SnSe and a simple model of the electronic structure and the bands of the orthorhombic IV-VI compounds, *Phys. Rev.*, **B36**: 7491-7499.

- [3] Valiukonis, G., Gussienova, D. A., Krivaite, G. and Sileika, A. (1986), Optical spectra and energy band structure of layer-type AIV-BVI compounds, *Phys. Stat. Solidi (b)*, **135**: 299-307.
- [4] Parentau, M. and Carlone, M. (1990), Influence of temperature and pressure on the electronic transitions in SnS and SnSe semiconductors, *Phys. Rev.*, **B41**: 5227-5234.
- [5] Bletskan, D.I., Taran, V.I. and Sichka, M. YU. (1976), Switching effect in layered IV-VI crystals, *Ukr. Fiz. Zh.*, **21**: 1436-1441.
- [6] Singh, J.P. and Bedi, R.K. (1990), Tin selenide films grown by hot wall epitaxy, *J. Appl. Phys.*, **68**: 2776-2779.
- [7] Lofersky, J.J (1956), Theoretical considerations governing the choice of optimum semiconductor for photovoltaic solar energy conversion, *J. Appl. Phys.*, **27**: 777-784.
- [8] Lofersky, J.J (1963), Recent research on photovoltaic solar energy converters, *Proc. I.E.E.E.*, **51**: 667-674.
- [9] Elkorashy, A. M. (1986), Optical absorption in Tin monoselenide single crystals, *J. Phys Chem. Solids*, **47**: 497-500.
- [10] Dholakiya, A. D., Solanki, G. K., Patel, S. G. and Agarwal, M. K. (2001), Two and Three dimensional models for analysis of optical absorption in Tungsten disulfide single crystals, *Bull. Mater. Sci.*, **24** (3): 291-296.
- [11] Static, V., Pierre, A. C., Etsall, T. H. and Mikula, R. J. (1997), Preparation of Tungsten Sulfides by sol gel processing, *J Non-Cryst Solid*, **220**: 58-62.



## THEORETICAL CALCULATION OF ELECTRON IMPACT TOTAL CROSS SECTIONS FOR HCl MOLECULE OVER A WIDE RANGE OF IMPACT ENERGIES (0.1 eV – 2000 eV)

Mayuri Y. Barot\*, Harshad Bhutadia<sup>1</sup>, Minaxi Vinodkumar\*

<sup>\*</sup>V P & R P T P Science College, Vallabh Vidyanagar – 388 120, Gujarat, India

<sup>1</sup>Government Engineering College, Patan-384 265, Gujarat, India

### ABSTRACT

Total cross sections  $Q_T$  for electron impact on hydrochloric acid molecule is reported over a wide energy range from circa 0.1 eV through 2 keV. An *ab initio* calculation method, R-Matrix is employed using Quantemol- N software below the ionization threshold of the target and beyond which Spherical Complex Optical Potential (SCOP) calculations are performed. The two methods show consistency at the transition energy and in general good agreement is observed with the available data.

**Key Words:** Spherical Complex Optical Potential, R matrix method, Total cross section

### INTRODUCTION

Electron impact collision data are in ever increasing demand for many decades. This is the consequence of their utility in various fields of applied physics. Hence considerable progress has been made on electron- atom/molecule collision studies both theoretically as well as experimentally. Looking to the theoretical side, with the availability of high performing computers and development of more accurate theories like R-matrix, computation of reliable cross sections are now possible. The accurate method e.g. R-matrix [1, 2] is feasible for low impact energies (energy insufficient to ionize the target), whereas beyond this energy the cross sectional data is obtained using theories like Spherical Complex Optical Potential formalism (SCOP) [3, 4]. SCOP formalism is used by many research groups [5, 6, 7] across the world and has been successfully utilized for varieties of targets [8, 9, 10]. The total cross section data is important at low, intermediate and high energy for their appropriate usage in various applications. Hence in the present work our attempt is to compute the total cross sections over wide range of impact energies from meV to keV for HCl.

Owing to enormous applications of HCl, it is highly attended molecule both by experimentalists as well as theoreticians. The first measurement of electron impact total cross sections was done by Bruche in 1926 [11] on a Ramsauer type apparatus for impact energies 4 - 30 eV. Radle et al [12] indirectly obtained the total cross sections from differential cross sections for impact energies 0.5 - 10 eV. Very recently Hamada and Sueoka [13] measured total cross sections using linear transmission type time of flight apparatus. On the theoretical front Itikawa and Takayanagi [14], Padial et al [15, 16], Pfingst et al [17] and Jain and Baluja [18] performed computation of electron impact total cross section for HCl in different energy regimes.

In this paper we present electron impact total cross sections,  $Q_T$  for HCl over a wide range of impact energies from 0.1 eV to 2 keV. Below the ionization threshold of the target the total cross section,  $Q_T$ , is obtained as a sum of the elastic and electronic excitation cross sections and in this energy regime we have employed UK molecular R-Matrix code through the Quantemol-N software package, while cross sections at energies beyond the ionization threshold are determined using the SCOP formalism. The two methods are found to be consistent at the transition energy. The present results are, in general, found to be in good agreement with previous experimental and theoretical results

(wherever available) and thus the present results can serve as a benchmark for the cross sections over a wide range of energy.

### THEORETICAL METHODOLOGY

This paper reports low energy (0.1eV to about 15 eV) *ab-initio* calculations using Quantemol- N [19] employing UK molecular R-matrix code [20] while the SCOP method is used for calculating total (elastic plus inelastic) cross sections beyond ionization threshold up to 2 keV [21]. These two (SCOP & R-matrix) being different approaches, we will discuss them separately in two subsections. Before going to the details of theoretical methods we discuss the target model employed for the present systems.

#### Target Model

HCl is a linear molecule with bond length of 2.409 atomic units (au). We have used a double zeta plus polarization (DZP) Gaussian basis set for target wave function representation. The double zeta basis set is important as it allows us to treat each orbital separately when we conduct the Hartree-Fock calculation. This gives us more accurate representation of each orbital. HCl has  $C_{\infty v}$  point group symmetry but we have considered  $C_{2v}$  point group symmetry of the order 4. We have chosen  $C_{2v}$  point group because it reduces the computational efforts that are required to generate the target wave function. The ground state Hartree-Fock electronic configuration is  $1a_1^2, 2a_1^2, 3a_1^2, 1b_1^2, 1b_2^2, 4a_1^2, 5a_1^2, 1b_2^2, 2b_2^2$ . Out of 18 electrons we have frozen 10 electrons in  $1a_1, 2a_1, 3a_1, 1b_1, 1b_2$  molecular orbitals while remaining 8 electrons are kept free in active space of  $4a_1, 5a_1, 6a_1, 7a_1, 2b_1, 2b_2$  molecular orbitals. Total 14 target states are represented by 298 configuration state functions (CSF's) for the ground state. A channel is a possible mode of fragmentation of the composite system (target + projectile) during the collision process and here the number of channels included in the calculation is 46. The R-matrix radius is taken as  $10 a_0$  while R- matrix calculation is propagated up to  $100.1 a_0$ . The GAUSPROP and DENPROP modules of Quantemol-N generate target properties. DENPROP constructs the transition density matrix from the target eigenvectors obtained from the CI calculation. From this it then computes the multipole transition moments required for solving the outer region coupled equations, the dipole polarisability  $\alpha_0$  and where possible the diagonalised tensor components  $\alpha_{xx}, \alpha_{yy}$  and  $\alpha_{zz}$ . These are computed using second-order perturbation theory and the property integrals evaluated by GUASPROP. Only multipole moments up to and including  $l=2$  are computed.

\*Corresponding author: barot\_mayuri@yahoo.com

The GAUSPROP and DENPROP modules [22] yield the ground state energy of HCl as  $-460.07$  Hartree. There is no theoretical or experimental data available for comparison to best of our knowledge. The first electronic excitation energy is  $8.168$  eV which is probably reported here for first time. The present computed dipole moment is  $0.544$  au which is good agreement with theoretical value of  $0.478$  au [17]. The present rotational constant of  $10.592$   $\text{cm}^{-1}$  is in very good agreement with theoretical value  $10.593$   $\text{cm}^{-1}$  reported in [23].

All the computed target parameters for this system are reported in Table 1 with available comparisons. Notably there is no experimental data available for comparison for various target parameters.

**TABLE-1** Target Properties: Ground state energy (Hartree), Dipole moment (au), First electronic excitation energy (eV) and Rotational constant ( $\text{cm}^{-1}$ ).

Target	Ground state energy (Hartree)		Dipole moment (au)		First excitation energy $E_i$ (eV)			Rotational Constant (B) ( $\text{cm}^{-1}$ )	
	Present	Theo	Present	Theo	Present	Theo	Exp	Present	Theo
HCl	-460.72	---	0.5438	0.4782 [17]	8.1684	---	8.317[24] 8.318[25]	10.592	10.59 [23]

The electronic excitation thresholds for HCl are listed in Table 2. HCl has 14 electronic excitation states.

**Table - 2** Vertical excitation energies in eV.

HCL	
State	Energy(eV)
$^1A_1$	0.0
$^3B_1$	8.168
$^3B_2$	8.168
$^1B_1$	8.884
$^1B_2$	8.884
$^3A_1$	10.859
$^1A_1$	15.028
$^3B_1$	20.965
$^3B_2$	20.965
$^3A_2$	21.308
$^1B_1$	22.167
$^1B_2$	22.167
$^1A_2$	22.987
$^3A_1$	23.329

Low energy formalism (0.01 ~ 15 eV)

The crux idea behind the R-matrix formulation [22] lies in dividing the complete configuration space into two regions called inner region having R-matrix radius 'a' which is usually 10 au and the outer region extending to the radius of 100 au. The splitting of R-matrix configuration space into these two regions relies mostly on the size of the target and also on the stability of the results obtained in the inner region and outer region calculations. This distribution is the consequence of electronic charge distribution around the centre of mass of the system. Presently we have considered R-matrix radius as 10 au for HCl which was found to give consistent results.

In the inner region the total wave function for the system is written as [20],

$$\psi_k^{N+1} = A \sum_I \psi_I^N(x_1, \dots, x_N) \sum_j \zeta_j(x_{N+1}) a_{Ijk} + \sum_m \chi_m(x_1, \dots, x_{N+1}) b_{mk} \quad (1)$$

where A is the anti-symmetrization operator,  $x_N$  is the spatial and spin coordinate of the  $n^{\text{th}}$  electron,  $\zeta_j$  is a continuum orbital spin-coupled with the scattering electron and  $a_{Ijk}$  and  $b_{mk}$  are variational coefficients determined in the calculation. The first summation runs over the target states used in the close-coupled expansion. The second summation runs over configurations  $\chi_m$ , where all electrons are placed in target molecular orbitals. The

number of these configurations varies considerably with the model employed. With the wavefunction given by eqn (1), a static exchange calculation has a single Hartree-Fock target state in the first sum. The second sum runs over the minimal number of configurations usually 3 or fewer, required to relax orthogonality constraints between the target molecular orbitals and the functions used to represent the configuration. Our fully close-coupled calculation uses the lowest number of target states, represented by a configuration interaction (CI) expansion in the first expansion and over a hundred configurations in the second. These configurations allow for both orthogonality relaxation and short-range polarization effects.

The complete molecular orbital representation in terms of the target and the continuum orbitals is done by using the Gaussian Type Orbitals (GTOs) and the continuum orbitals of Faure et al [26] and include up to g ( $l=4$ ) orbitals. For non-polar targets, the calculations performed up to g orbitals do not affect the accuracy of calculation [27] and this has an added advantage that it will allow us to see the resonance structures which are prominent at low energies. However for molecules with a permanent dipole moment, the dipole potential leads to strong coupling between channels which differ in 'l' values and also, due to the long range nature of the dipole potential which requires a large number of partial waves for convergence [27]. In practice, instead of including large number of partial waves in the expansion, the procedure is developed based on a frame transformation and the adiabatic nuclear rotation (ANR) approximation to account for rotational motion and the finite dipole Born approximation to account for the contribution of higher partial waves. We have performed the calculations with and without a dipole Born correction. The R-matrix provides the link between the inner region and outer region, the inner region is propagated to the outer region potential until its solutions match with the asymptotic functions given by the Gailitis expansion [20]. Thus by generating the wave functions, using equation 1, their eigen values are determined. These coupled single centre equations describing the scattering in the outer region are integrated to identify the K-matrix elements. Consequently the resonance positions, widths and various cross sections can be evaluated using the T-matrix obtained from S-matrix which is in turn obtained by the K-matrix elements.

Higher energy formalism (15 eV – 2 keV)

High energy electron scattering is modeled using the well established SCOP formalism [28, 29] which employs partial wave analysis to solve the Schrödinger equation with various model potentials as its input. The interaction of incoming electron with the target molecule can be represented by a complex potential comprising of real and imaginary parts as,

$$V_{opt}(r, E_i) = V_R(r) + iV_I(r, E_i) \quad (2)$$

such that

$$V_R(r, E_i) = V_{st}(r) + V_{ex}(r, E_i) + V_p(r, E_i) \quad (3)$$

where,  $E_i$  is the incident energy. Equation (3) corresponds to various real potentials to account for the electron target interaction namely, static, exchange and the polarization potentials respectively. These potentials are obtained using the molecular charge density of the target, the ionization potential and the polarizability as inputs. The molecular charge density may be derived from the atomic charge density by expanding it to the center of mass of the system. Our calculation for these TCSs is based on complex scattering potentials, generated from spherically averaged charge densities of the target. The charge density of lighter hydrogen atoms is expanded at the center of heavier atom (Chlorine) by employing the Bessel function

expansion as in Gradshetyn and Ryzhik [30]. This is a good approximation since hydrogen atoms do not significantly act as scattering centers and the cross sections are dominated by the central atom size. Thus, the single-center molecular charge density is obtained by a linear combination of constituent atomic charge densities, renormalized to account for covalent molecular bonding. The atomic charge densities and static potentials ( $V_{st}$ ) are formulated from the parameterized Hartree-Fock wave functions given by Cox and Bonham [31]. The parameter free Hara's 'free electron gas exchange model' [32] is used for the exchange potential ( $V_{ex}$ ). The polarization potential ( $V_p$ ) constructed from the parameter free model of correlation-polarization potential given by Zhang et al. [33]. Here, various multipole non-adiabatic corrections are incorporated in the intermediate region which will approach the correct asymptotic form at large 'r' smoothly. The target parameters like ionization potential (IP) and dipole polarizability ( $\alpha_0$ ) of the target used here are the best available from the literature [34].

Ionization potential (IP) of HCl is 12.74 eV and Dipole polarizability of HCl is  $2.63 \times 10^{-24} \text{ cm}^3$ .

The imaginary part in  $V_{opt}$  called the absorption potential  $V_{abs}$  will account for the total loss of flux scattered into the allowed electronic excitation or ionization channels. The equation (2) is vibrationally and rotationally elastic. We have used here fixed nuclei approximation where the nuclear rotational and vibrational motions are not considered. This is due to the fact that these non spherical terms do not contribute much to the total potential at the present high energy range.

The well-known quasi-free model form of Staszewska et al. [35] is employed for the absorption part given by,

$$V_{abs}(r, E_i) = -\rho(r) \sqrt{\frac{T_{loc}}{2}} \left( \frac{8\pi}{10k_F^3 E_i} \right) \theta(p^2 - k_F^2 - 2\Delta)(A_1 + A_2 + A_3) \quad (4)$$

Where the local kinetic energy of the incident electron is

$$T_{loc} = E_i - (V_{st} + V_{ex} + V_p) \quad (5)$$

Where  $p^2 = 2E_i$ ,  $k_F = [3\pi^2 \rho(r)]^{1/3}$  is the Fermi wave vector and  $A_1$ ,  $A_2$  and  $A_3$  are dynamic functions that depends differently on  $I$ ,  $\theta(x)$ ,  $\Delta$  and  $E_i$ . Here,  $I$  is the ionization threshold of the target, is the Heaviside unit step-function and  $\Delta$  is an energy parameter below which  $V_{abs} = 0$ . Hence,  $\theta(x)$  is the principal factor which decides the values of total inelastic cross section, since below this value, ionization or excitation is not permissible. This is one of the main characteristics of Staszewska model [35]. This has been modified by us by considering  $\Delta$  as a slowly varying function of  $E_i$  around  $I$ . Such an approximation is meaningful since fixed at  $I$  would not allow excitation at energies  $E_i \leq I$ . However, if  $\Delta$  is much less than the ionization threshold, then  $V_{abs}$  becomes unexpectedly high near the peak position. The amendment introduced is to give a reasonable minimum value  $0.8I$  to  $\Delta$  [36] and also to express the parameter as a function of  $E_i$  around  $I$ , i.e.,

$$\Delta(E_i) = 0.8I + \beta(E_i - I) \quad (6)$$

Here the value of the parameter  $\beta$  is obtained by requiring that  $\Delta = I$  (eV) at  $E_i = E_p$ , the value of incident energy at which present  $Q_{inel}$  reaches its peak.  $E_p$  can be found by calculating  $Q_{inel}$  by keeping  $\Delta = I$ . Beyond  $E_p$   $\Delta$  is kept constant and is equal to  $I$ . The expression given in eqn (6) is meaningful since if  $\Delta$  is fixed at the ionization potential it would not allow any inelastic channel to open below  $I$ . Also, if it is very much less than  $I$ , then  $V_{abs}$  becomes significantly high close to the peak position of  $Q_{inel}$ .

The complex potential thus formulated is used to solve the Schrödinger equation numerically through partial wave

analysis. This calculation will produce complex phase shifts for each partial wave which carries the signature of interaction of the incoming projectile with the target. At low impact energies only a few partial waves are significant, but as the incident energy increases more partial waves are needed for convergence. The phase shifts ( $\delta_l$ ) thus obtained are employed to find the relevant cross sections, total elastic ( $Q_{el}$ ) and the total inelastic cross sections ( $Q_{inel}$ ) using the scattering matrix  $S_l(k) = \exp(2i\delta_l)$  [37]. Then the total scattering cross section (TCS),  $Q_T$  [38] is found by adding these two cross sections together.

## RESULTS AND DISCUSSION

The present work reports total cross section for e-HCl scattering. We have employed the ab initio R matrix code below the ionization threshold of the target. In this energy regime the total cross section is sum of vibrationally and rotationally total elastic and total electronic excitation cross sections. Above the ionization threshold of the target we have computed the total cross section as the sum of total elastic and total inelastic cross section using the SCOP formalism [39, 40, 41]. The data sets produced by two formalisms are consistent at the transition energy ( $\sim 15$  eV). All the numerical results of total cross section (in  $\text{\AA}^2$ ) for both the targets from 0.1 eV to 2000 eV are presented in Table III and are also represented graphically along with the available comparisons in Figure 1.

**Table III:** Total Cross Section  $Q_T$  ( $\text{\AA}^2$ )

$E_i$ (eV)	HCl	$E_i$ (eV)	HCl
0.1	588.73	14	27.54
0.2	325.98	15	26.96
0.4	194.85	20	23.01
0.6	134.58	30	16.64
0.8	104.97	40	15.27
1.0	87.41	80	11.43
1.5	64.69	100	10.32
2.0	48.91	200	07.37
3.0	42.10	300	04.48
4.0	39.30	400	03.71
5.0	37.27	500	03.19
6.0	33.96	600	02.81
7.0	33.70	700	02.55
8.0	34.60	800	02.30
9.0	34.75	900	02.11
10	34.70	1000	01.96
11	33.72	1500	01.65
12	28.74	2000	01.16
13	27.65		

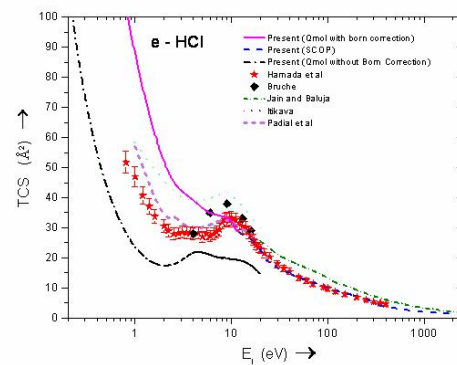


**Fig.1** Total cross sections,  $Q_T$ , for e-HCl scattering

Solid line: Present results (Quantemol with Born correction); Dashed line: Present (SCOP); Dashed Dot line: Present (Quantemol without born correction); Short Dash Dotted line: Jain and Baluja [18]; Short Dash line: Padial et al [15]; Dotted Line: Itikawa and Takayanagi [14]; Stars: Hamada and Sueoka [13]; Squares: Bruche [11].

Figure 1 shows comparison of e – HCl scattering with available comparisons. Looking to its importance in varied fields of applied interest, good amount of work is done at low energies. There are only two measurement data reported for total cross sections. Measurement results of Bruche [11] are very old and there is recent measurement by Hamada and Sueoka [13]. They have measured total cross sections using linear transmission type time of flight method for incident energies 0.8 – 400 eV. Their data were corrected for the effects of forward scattering using the differential cross section (DCS). The magnitude of the correction was very large in the low energy region. It could be easily seen from the graph that present data are in excellent agreement with data of Hamada and Sueoka [13] beyond 10 eV, below which the present data is higher due to Born approximation. A small hump in the total cross section is also observed in the present data without Born correction which is in accordance with the same observed by Hamada and Sueoka [13]. This structure disappears when Born correction is done. The experimental data of Bruche [11] are also in good agreement with present data except the one at 3 eV which is lower. On theoretical side there are relatively more comparisons. The low energy calculations are carried out by Itikawa and Takayanagi [14] and Padial et al [15]. Itikawa and Takayanagi [14] performed close coupling calculations in the energy from 0 to 10 eV. Peak appearing at 10 eV which could be easily observed in all experimental as well as theoretical data including present data is a consequence of shape resonance at this position [14]. Padial and Norcross have also performed ab initio calculation for very low energy (1 to 20 eV). Their results are lower than present results below 10 eV again due to Born approximation. Jain and Baluja [18] have calculated total cross sections from 10 eV to 5000 eV and their values are in good agreement with present results above 100 eV below which they are higher by small amount and this is attributed to the fact that they have considered the contribution of rotational excitation also which is significant for energies below 100 eV.

## CONCLUSION

The main impetus of present work is to compute total cross sections over a wide range of impact energies starting from very low (0.1 eV) to high energy (2 keV) for HCl on electron impact. Since a single formalism cannot be employed over such a wide range, we have used UK molecular R-matrix code using Quantemol-N at low impact energies to yield ab initio results while at high energies SCOP formalism is used. We have illustrated earlier this methodology for three simple polyatomic molecular targets NH<sub>3</sub>, H<sub>2</sub>S and PH<sub>3</sub> [39] for which there exists a good database against which we can benchmark our results. The method has been extended to simple biomolecules [41] and in the present work for HCl. The results are promising since the two methods are consistent at the transition energy (15 eV) and show good agreement with available data throughout the energy range. Therefore now we have confidence that the methodology we propose may be used to calculate such cross sections in other molecular systems where experiments are difficult (e.g. exotic system and radicals). Such data set is needed in a variety of applications from aeronomy to plasma modeling which is the thrust area of research in the present era. Accordingly such a methodology maybe built into the design of on-line databases to provide a 'data user' with the opportunity to request their own set of cross sections for use in their own research. Such a prospect will be explored by the emerging Virtual Atomic and Molecular

Data Centre (VAMDC) [http:// batz.lpm.jussieu.fr/ www\\_VAMDC/](http://batz.lpm.jussieu.fr/www_VAMDC/).

## ACKNOWLEDGMENT

MVK thanks Department of Science and Technology, New Delhi for financial support through Project Grant No: SR/S2/LOP-26/2008 for Major Research project under which part of this work is done.

## REFERENCES

- [1] Morgan, L. A., Tennyson, J., Gillan, C.J.,(1998) The UK molecular R-matrix codes. *Comput. Phys. Commun.*, **114**: 120.
- [2] Tennyson, J., Gorfinkiel, J. D., Ruzum, I., Trevisan, C. S., Vinci, N., (2003) Electron molecule collisions calculations using the R- matrix method. *Radiation. Phys. Chemistry*, **68**: 65.
- [3] Jain, A., (1986) Total (elastic + absorption) cross sections for e-CH<sub>4</sub> collisions in a spherical model at 0.10–500 eV. *Phys. Rev. A*. **34**: 3707.
- [4] Jain, A., (1988) Theoretical study of the total (elastic + inelastic) cross sections for electron -H<sub>2</sub>O (NH<sub>3</sub>) scattering at 10-3000 eV. *J Phys B*, **21**: 905.
- [5] Zhang, X., Sun, J., and Liu, Y. (1992) A new approach to the correlation polarization potential- low-energy electron elastic scattering by He atoms. *J. Phys. B: At. Mol. Opt. Phys.*, **25**: 1893.
- [6] Garcia G., Pablos, J. L. de., Blanco, F. and Williart, A. (2002) Total and elastic electron scattering cross sections from Xe at intermediate and high energies. *J. Phys. B: At. Mol. Opt. Phys.*, **35**: 4657.
- [7] Vinodkumar, M., Joshipura K. N., Limbachiya, C. and Mason, N. J. (2006) Theoretical calculations of the total and ionization cross sections for electron impact on some simple biomolecules. *Phys. Rev. A*, **74**: 022721.
- [8] Vinodkumar, M., Limbachiya, C., Korot K. and Joshipura, K. N. (2008) Theoretical electron impact elastic ionization and total cross sections for silicon hydrides, SiH<sub>x</sub> (X=1,2,3,4) and Disilane, Si<sub>2</sub>H<sub>6</sub> from threshold to 5 keV. *Euro. Phys. J. D*, **48**: 333.
- [9] Vinodkumar, M., Joshipura, K. N., Limbachiya, C. and Antony, B. K. (2006) Electron impact total and ionization cross-sections for some hydrocarbon molecules and radicals. *Euro. Phys. J. D*, **37**: 67.
- [10] Vinodkumar, M., Limbachiya, C., Antony, B. and Joshipura, K. N. (2007) Calculations of elastic, ionization and total cross sections for inert gases upon electron impact: threshold to 2 keV. *J. Phys. B: At. Mol. Opt. Phys.*, **40**: 3259.
- [11] Bruche, E. (1926) Uber die querschnitts kurve des chlorwass erstoffer fregenuber langsammae chlor wasserstoffes Gegenuber Langsamer Electronen, and inren vergieich mitder, Argon kurve, *Ann. Phys., lpz*, **82**: 25-38.
- [12] Radle, M., Konoth, G., Jung K., and Ehrhardt, H. (1989) Rotational and rovibrational excitation of HCl and HF by low-energy electron impact. *J Phys B: At. Mol Opt. Phys.* **22**: 1455.
- [13] Hamada, A. and Sueoka, O. (1994) Total cross section measurements for positrons and electrons colliding with molecules. II. HCl. *J. Phys.B: At. Mol.Opt. Phys.* **27**: 5055.

- [14] Itikawa Y. and Takayanagi, K. (1969) Rotational transition in polar molecule by electron collision: Application to CN and HCl. *J. Phys. Soc. Japan*, **26**: 1254.
- [15] Padial, T. N., and Norcross, W.D. (1984) Ro-vibrational excitation of HCl by electron impact. *Phys. Rev. A*, **29**: 1590.
- [16] Padial, T. N., and W.D. Norcross and L. A. Collins, *Phys. Rev. A*, **27**: 141
- [17] Pifings, K., Thiimmel, T.H. and Peverimhor, D. S. (1992) Near-threshold rotational excitation in electron scattering by the HCl molecule. *J. Phys. B: At. Mol. Opt. Phys.*, **25**: 2107.
- [18] Jain, A. and Baluja, K.L (1992) Total elastic and inelastic cross section for diatomic and polyatomic molecules at 10-5000 eV: H<sub>2</sub>, Li<sub>2</sub>, HF, CH<sub>4</sub>, N<sub>2</sub>, CO, C<sub>2</sub>H<sub>2</sub>, HCN, HCl, O<sub>2</sub>, H<sub>2</sub>S, PH<sub>3</sub>, SiH<sub>4</sub> and CO<sub>2</sub>. *Phys. Rev. A*, **45**: 202.
- [19] Pilling, S., Santos, A.C.F., Wolff, W., Sant'Anna, M. M., Barros, A. L. F., Souza, G. G. B de, castro faria, N. V.de, Boechat-Roberly, H. M. (2006), *Mon. Not. R. Astron. Soc.*, **372**: 1379.
- [20] P. Mozejko, (2007) Calculations of electron input ionization cross section for simple biomolecules ; Formic and acetic acid. *Eur. Phys. J. Special topics* **144**: 233.
- [21] Märk, T. D., Egger, F. J. (1977), *Chem. Phys.* 67 issue **6**, 2629.
- [22] Khare, S. P., Meath, W. J. (1987) Cross sections for the direct and dissociative ionisation of NH<sub>3</sub>, H<sub>2</sub>O and H<sub>2</sub>S by electron impact. *J. Phys. B: At. Mol. Phys.* **20**: 2101.
- [23] National Institute of Standards and Technology Website: <http://srdata.nist.gov/cccbdb>
- [24] Nee, J. B., Masaco Suto; Lee, L. C. (1986) Quantitative spectroscopy study of Hbr in the 105 - 235 nm region, *J. Chem. Phys.* **85**, 4919.
- [25] Shaw, D. A., Cvejanovic, D., King, G.C. Read, F. H. (1984) Inner-shell and outer-shell excitation of HCl, HBr and Br<sub>2</sub> by electron impact with high resolution. *J. Phys. B*: **17**: 1173.
- [26] Faure, A.; Gorfinkiel, J. D.; Morgan, L. A.; and Tennyson, J. (2002) GTOBAS: fitting continuum functions with Gaussian-type orbitals *Comput. Phys. Commun.* **144**: 224.
- [27] Tennyson, J. (2010) Electron- molecule collision methods using R-Matrix method. *Physics Reports*; **491**: 29.
- [28] Vinodkumar, M., Dave, R., Bhutadia, H., Antony, B. K. (2010) Electron impact total ionization cross sections for halogens and their hydrides. *Int. J. Mass. Spectrom* **292**: 7-13.
- [29] Vinodkumar, M., Joshipura, K. N., Limbachiya, C. G., Antony, B. K. (2009) Theoretical study of electron scattering processes with H<sub>2</sub>O (ice). Atomic Structure and Collision Processes' Narosa Publishing House, 177.
- [30] Gradashteyn, I. and Ryzhik, I. M. (1980) Tables of Integrals, Series and Products Associated Press New York.
- [31] Cox, JR., H. L., and Bonham, R. A. (1967) Elastic electron scattering amplitudes for neutral atoms calculated using the partial wave method at 10, 40, 70, and 100 keV for Z=1 to Z=54. *J. Chem. Phys.*, **47**: 8.
- [32] Hara, S. (1967). The Scattering of slow electrons by hydrogen molecules; *J. Phys. Soc. Jpn.* **22**: 710.
- [33] Zhang, X., Sun, J., Liu, Y. (1992) A new approach to the correlation polarization potential-low-energy electron elastic scattering by He atoms. *J. Phys. B*, **25**: 1893.
- [34] Garcia, G., Blanco, F. (2000) Energy dependence of the total cross section for electron scattering by chloromethanes in the energy range 0.5-10 keV. *Phys. Rev. A*, **62**: 044702.
- [35] Garcia, G., Manero, F. (1997) Correlation of the total cross section for the electron scattering by molecules with 10-22 electrons, and some molecular parameters at intermediate energies, *Chem. Phys. Lett.*, **280**: 419-422.
- [36] Zecca, A., Karwasz, G. P., Brusa, R. S. (1992) Absolute total-cross-section measurements for intermediate-energy electron scattering on CF<sub>4</sub>, CClF<sub>3</sub>, CCl<sub>2</sub>F<sub>2</sub>, CCl<sub>3</sub>F, and CCl<sub>4</sub>. *Phys. Rev. A*, **46**: 3877.
- [37] Vinodkumar, M., Korot, K. Vinodkumar, P. C. (2011) Computation of the Electron impact total ionization cross sections of the C<sub>n</sub>H(2n+1)OH molecules from threshold to 2KeV energy range. *International Journal of Mass and Spectroscopy* **305**: 26-29.
- [38] Szymystkowski, C., Krzysztofowicz, A. M. (1995) Electron scattering from isoelectronic, Ne = 18, CH<sub>3</sub>X molecules (X = F, OH, NH<sub>2</sub> and CH<sub>3</sub>). *J. Phys. B: At. Mol. Opt. Phys.* **28**: 4291.
- [39] Vinodkumar, M., Limbachiya, C., Joshipura, K. N., Mason, N. J. (2011) Electron impact calculations of total elastic cross sections over a wide energy range - 0.01 eV to 2 keV for CH<sub>4</sub>, SiH<sub>4</sub> and H<sub>2</sub>O, *Euro. Phys. J. D*: **61**: 579-585.
- [40] Limbachiya, C., Vinodkumar, M., Mason, N. J. (2011) Calculation of the electron impact rotationally elastic cross section for NH<sub>3</sub>, H<sub>2</sub>S and PH<sub>3</sub> over the energy range from 0.01 eV to 2 keV, *Phys. Rev. A*, **83**: 042708.
- [41] Vinodkumar, M., Bhutadia, H., Antony, B. Mason, N. J. Electron impact rotationally elastic total cross sections for H<sub>2</sub>CO and HCOOH over a wide range of incident energy (0.01-2000eV). *Phys. Rev. A*. (Accepted, 2011).



## A CASE STUDY OF HYBRID MICROCIRCUIT ASSEMBLY PROCESS USING TAGUCHI DESIGN METHOD AND RESPONSE SURFACE METHOD

**D.P. Raykundaliya\* and A. Shanubhogue**

*P. G. Department of Statistics, Sardar Patel University, Vallabh Vidyanagar – 388 120, Gujarat, India*

### ABSTRACT

**In this paper we investigate the choice of best combination of factors for  $3^7 \times 2^1$  mixed factorial design in 18 runs through Taguchi Design Method and Response Surface Method (RSM). Further we show that Response Surface Method predicts better optimal response as compared to optimal response obtained through Taguchi Design Method. The comparison of methods is done with the help of a case study on Hybrid Microcircuit Assembly Process conducted by Taguchi et al [5]. We do analysis using MINITAB, for the methods.**

**Key words :** *shear strength; Taguchi design method; signal-to-noise ratio; response surface method; choice of the best factors combination; hybrid microcircuit; ANOVA*

### INTRODUCTION

There are mainly two types of circuits used in electronic devices, namely, digital circuit and analogue circuit. The Hybrid Microcircuit is hybrid structure of one of the types of circuit. The steps required in the production of hybrid microcircuit are (1) screen (2) profile (3) atmosphere (4) gas flow rate (5) belt speed (6) drying temperature. For detail refer Condra [2]. The experiment was conducted by Taguchi et al [5] for production of hybrid microcircuit process in which they measured the shear strength of circuit. The shear strength, in engineering is a term used to describe the strength of a material or component against the type of yield or structural failure where the material or component fails in shear. A shear load is a force that tends to produce a sliding failure on a material along a plane that is parallel to the direction of the force.

Our objective in this paper is to investigate choice of the best factors combination to increase the shear strength of hybrid microcircuit. In Section 2, we discuss the principle of design of experiment and the data collected through experiment, which are given in Condra [2]. In Section 3, we discuss the results of analysis of shear strength data of hybrid microcircuit through Taguchi Design Method and Response Surface Method. We also discuss conclusions of comparative study of both designs and provide advantages of Response Surface Method over Taguchi Design Method.

### THE DESIGN OF EXPERIMENT FOR THE SHEAR STRENGTH OF HYBRID MICROCIRCUIT

To use statistical approach in designing and analyzing an experiment, it is necessary to follow the basic guideline for conducting the experiment. The basic steps of guideline of design of experiments are:

*(i) Recognition of problem and statement of the problem:*

Here our approach is to investigate choice of best combination of factors as a result optimum value of shear strength of hybrid microcircuit.

*(ii) Choice of factors, levels and ranges:*

Brainstorming with experienced engineers and feasible operating ranges of machines and materials help to decide the experimental factors.

*(iii) Choice of experimental design:*

The study conducted for eight factors in 18 runs. The seven factors at three levels and one factor at two levels. The descriptions of these factors are given in Table 1 following Condra [2]. In statistical language our objective is to study main effects and interaction effects in this mixed factorial experiment. To conduct such an experiment one can use both  $L_{18}$ , orthogonal array given by Taguchi or one can generate it using Fractional Factorial Design (Montgomery [4]; Taguchi et al [5]).

**Table 1:** Description of Factors and Levels for Hybrid Component Attachment Experiment

Description	Factor (variable)	Level 1	Level 2	Level 3
Screen	A ( $x_1$ )	80 mesh, 0.0037 in. wire diameter, 0.003 in. emulsions	80 mesh, 0.0020 in. wire diameter, 0.002 in. emulsions	-
Profile (°C)	B ( $x_2$ )	150-200-250-300-350-350-290-240	150-200-250-300-370-370-290-240	150-200-250-300-390-390-290-240
Atmosphere	C ( $x_3$ )	100% nitrogen	50% nitrogen – 50% hydrogen	100% hydrogen
Gas Flow Rate	D ( $x_4$ )	40 cfh	60 cfh	80 cfh
Empty	E ( $x_5$ )	Dummy Variable		
Belt Speed	F ( $x_6$ )	4.5 in./min	5.5 in./min	6.0 in./min
Drying temperature	G ( $x_7$ )	Room Temperature	50°C	90°C
Empty	H ( $x_8$ )	Dummy Variable		

To analyze the data through Taguchi Design Method we require minimum two replications. Here we have three replications to measure shear strength of each factor combination. For detail regarding Taguchi Design Method and Fractional Factorial experiment readers may refer Taguchi et al [5] and Montgomery [4].

*(iv) Performing the experiment and collection of data:*

As the experiments are conducted in laboratory or like laboratory environment, the experimenter should first create the same environment which is actual environment prevailing while producing in a factory. The collected data on shear strength through  $L_{18}$  experiment is given in Table 2.

*(v) Statistical Analysis of Data*

*(vi) Conclusions and recommendation*

Step (v) and (vi) are discussed in details in the section of statistical analysis for Taguchi Design Method and Response Surface Method.

\*Corresponding author: dp\_raykundaliya@spuvvn.edu

**Table 2:** Experimental Design and observed Shear Strength

Run No.	A	B	C	D	E	F	G	H	Strength		
									Replication 1	Replication 1	Replication 1
1	1	1	1	1	1	1	1	1	1.65	0.01	0.45
2	1	1	2	2	2	2	2	2	0.25	0.65	0.75
3	1	1	3	3	3	3	3	3	0.01	0.25	0.25
4	1	2	1	1	2	2	3	3	0.20	0.25	0.30
5	1	2	2	2	3	3	1	1	0.60	0.35	0.40
6	1	2	3	3	1	1	2	2	2.55	2.90	2.90
7	1	3	1	2	1	3	2	3	1.40	0.65	0.40
8	1	3	2	3	2	1	3	1	2.95	2.85	3.45
9	1	3	3	1	3	2	1	2	1.95	1.95	1.30
10	2	1	1	3	3	2	2	1	0.40	0.50	0.01
11	2	1	2	1	1	3	3	2	0.01	0.01	0.25
12	2	1	3	2	2	1	1	3	0.85	1.05	1.60
13	2	2	1	2	3	1	3	2	2.50	3.15	2.75
14	2	2	2	3	1	2	1	3	2.70	2.80	1.25
15	2	2	3	1	2	3	2	1	0.01	0.20	0.01
16	2	3	1	3	2	3	1	2	0.55	0.55	0.50
17	2	3	2	1	3	1	2	3	1.35	0.70	0.50
18	2	3	3	2	1	2	3	1	0.85	1.20	0.60

**STATISTICAL ANALYSIS FOR TAGUCHI DESIGN METHOD AND RESPONSE SURFACE METHOD**

(a) Taguchi Design Method:

Here we note that the shear strength of hybrid microcircuit is a “larger-the better” type of characteristic. The signal-to-noise ratios are calculated through the equation for “larger-the-better” type

$$\eta_i = -10 * \log \left( \frac{1}{n} \sum_{j=1}^n \frac{1}{y_{ij}^2} \right) \tag{1}$$

where  $y_{ij}$  is the  $j^{th}$  observation from the  $i^{th}$  run and  $n$  is number of replications of the  $i^{th}$  run. In our case we have  $n=3$  and values for  $\eta_i$  can be calculated for shear strength of hybrid microcircuit. The resultant output obtained by analyzing data in Table 2 by considering only main effects A, B, C, D, F and G, using MINITAB software, is given in Table 3. Here again, it is to be noted that Taguchi Design is analyzed for main effects for all factors except E and H suggested by engineers. The reason is E and H are two dummy factors added to perform Taguchi Design Method using  $L_{18}$ .

**Table 3:** Response Value Table for Signal-to-Noise Ratio

Level	Factor					
	A	B	C	D	F	G
1	-8.9704	-25.2888	-14.0590	-20.5409	-1.7999	-6.3864
2	-12.0218	-5.8914	-7.1023	-2.2437	-8.0832	-13.5258
3	--	-0.3080	-10.3269	-8.7036	-21.6050	-11.5760

In Taguchi Design Method the level of factor is considered for optimum response is based on the maximum value of signal-to-ratio among the levels of each factor (Dharmadhikari et al [3]). The resultant recommended level of factors for the production of hybrid microcircuit having optimum shear strength is given in Table 4.

**Table 4:** Recommended Levels of Factors for the Production Hybrid Microcircuit

Level	Factor					
	A	B	C	D	F	G
1	1	3	2	2	1	1

The predicted shear strength of hybrid microcircuit for recommended choice of factor combinations can be obtained by the optimum noise-to-signal ratio as a function of  $y$ . The optimum value of noise-to-signal ratio for the factor combination recommended is 25.67 and the corresponding optimum shear strength of hybrid microcircuit is 2.44.

(b) Response Surface Method:

Response Surface Methodology (RSM), is a collection of mathematical and statistical techniques those are useful for modelling and analysing response of interest as a function of several variables (factors) and objective is to optimize this response (Montgomery [4]). In RSM problems, the form of the relation is unknown. Hence, the first step is to find approximate functional relationship between  $y$  and set of independent variables  $x$ . The statistical form of RSM is

$$Y = f(x) + \epsilon \tag{2}$$

where  $\epsilon$  represents the noise or error observed in the response  $y$ . Our objective is to investigate the best choice of factor combinations which give optimum value of response on the surface of response. The first step of RSM is to investigate the distribution of average shear strength of hybrid microcircuit ( $y$ ). The distribution of average shear strength of hybrid microcircuit is found to be Lognormal from its Normal Probability Plot (Figure 1). Further the p-value of Anderson-Darling test of fitting of normal distribution for  $y$ , is 0.637 ( $> 0.05$ ) which indicates, the Lognormal distribution fits well to shear strength of hybrid microcircuit.

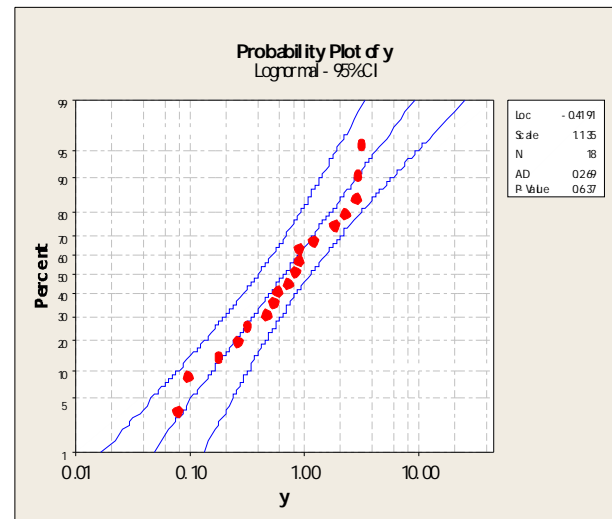


**Figure 1:** Normal Probability Plot of Shear Strength of Hybrid Microcircuit

The maximum likelihood estimators of parameters of the Lognormal distribution and its properties have been studied (Aitchison and Brown [1]). A positive continuous random variable  $X$  is said to follow the Lognormal distribution if the variable  $\log_e X$  has Normal distribution with mean  $\mu$  and variance  $\sigma^2$ . Before fitting RSM to the data in Table 2 for identifying which effect to be included in the model, we draw main effect plots for all factors given in Figure 2.

The analysis of the log transformed average shear strength of hybrid microcircuit is carried out through MINITAB by considering main effects A, B, C, D, F and G. The reason is that the experiment is carried out for the first time and the analysis is done for un-coded observations in MINITAB. The resultant output is given in Table 5 (Estimates of effects) and Table 6 (Analysis of Variance Table).

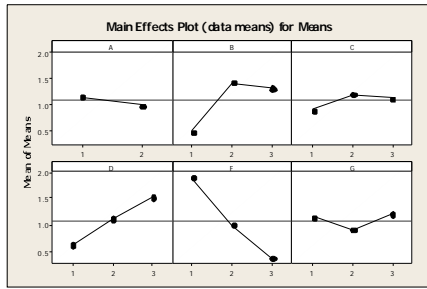


**Figure 2:** Main Effect Plots for log of average Shear Strength of Hybrid Microcircuit

**Table 5:** Estimated Regression Coefficients for log (average shear strength of hybrid microcircuit)

Term	Coefficient	SE coefficient	T	P-value
Constant	0.384205	0.8475	0.453	0.659
A	-0.30275	0.2680	-1.130	0.283
B	0.560566	0.1641	3.416	0.006**
C	-0.00402	0.1641	-0.024	0.981
D	0.478207	0.1641	2.914	0.014**
F	-0.93677	0.1641	-5.708	0.000**
G	-0.27256	0.1641	-1.661	0.125

S=0.5685 R-sq = 83.8% R-Sq (Adj) = 74.9% \* p-value (<0.05) \*\* p-value (<0.01)

**Table 6:** Analysis of Variance of ln (Average Shear Strength of Hybrid Microcircuit)

Source	DF	Adj. SS	Adj. MS	F	P-value
Regression	6	18.3496	3.05827	9.46	0.001**
Linear	5	18.3496	3.05827	9.46	0.001**
Residual Error	11	3.5551	0.32319		
Total	17	21.9047			

\*\* p-value (<0.01)

The R-Square value given in Table 5 indicates that 83.8% of total variation in ln(y) is explained by the fitted model. Further from ANOVA given in Table 6 we observe that both linearity assumptions and fitted regression model for main effects are highly significant. It is observed that only main effects B, D and F are significant at 1% level of significance. Thus the fitted Response Surface Model for ln(y) is :

$$\ln(y) = 0.384205 - 0.30275x_1 + 0.560566x_2 - 0.00402x_3 + 0.478207x_4 - 0.93677x_6 - 0.27256x_7 \quad (3)$$

From the study of main effect plots of average shear strength of hybrid microcircuits for selected factors (Figure 3), the recommended best combination of level of factors is given in Table 7.

**Table 7:** Recommended Levels of Factors for the Production of Hybrid Microcircuit through RSM

Level	Factor					
	A	B	C	D	F	G
1	1	2	1	3	1	1

The optimum value of ln(y) for above recommended levels of factor for the production of hybrid microcircuit using equation (3) is 1.424 and corresponding average shear strength of hybrid microcircuit is 4.14. It is interesting to note that RSM gives 69.6% more optimal value as compared to Taguchi Design Method.

**Advantages of using Response Surface Methodology:**

1. It is a Statistical/Mathematical modelling technique.
2. It can help to find optimum value for response beyond or within the range of level of factors suggested by the engineers.
3. It will help to identify the future direction of optimum response.
4. It can also identify the interaction or curvature effects beyond the imagination of engineers.
5. It can also investigate whether the effects are statistically significant. As a result on can construct 95% confidence interval for main effects which can help to identify future range of level of factors.

**Disadvantages of Taguchi Design Method:**

1. It is purely a philosophy, no Mathematics involved.
2. It gives only the optimum value at any of the levels specified by experimenter.
3. It will not give the future direction of optimum response in experiments. Further, to know the future direction of optimum value we require conducting a new experiment.

**REFERENCES:**

- [1] Atchinson, J. and Brown, J.A.C. (1957). The Lognormal Distribution. Cambridge University Press, Cambridge.
- [2] Condra, L.W. (2001). Reliability Improvement with Design of Experiments, Edition II, Marcel Deker, 47-61
- [3] Dharmadhikar, D.A., Kharshikar, V.A., Ratnaparkhi, M.V. and Prasad, K. (2000). "Analyzing the Censored Life Data arising in Fractional Factorial Designs: Spin-on-filter Case Study". Quality Engineering, 13(1), 65-72.
- [4] Montgomery, D.C. (2004). Design and Analysis of Experiments. Edition V, John Wiley and Sons (Asia).
- [5] Taguchi, G. and Konish, S. (1987). Orthogonal Arrays and Linear Graphs. American Supplier Institute, Dearborn, MI.

**ACKNOWLEDGMENT:**

This research is funded by University Grant Commission (UGC) for Minor Research Project (F.37-549/2009(SR)). The First author wishes to thank Prof. D.K.Ghosh for helpful discussion during his visit in Department and Dr.Jyoti M.Divecha for helpful discussion.



## ACCEPTANCE DECISION RULE FOR TYPE-I GENERALIZED HALF LOGISTIC DISTRIBUTION

\*K. Rosaiah, \*R.R.L. Kantam and \*\*V. Rama krishna

*Department of Statistics, Acharya Nagarjuna University, Guntur – 522 510, India*

*\*Koneru Lakshmaiah College of Engineering, Vaddeswaram, Guntur (Dt.), India*

### ABSTRACT

The well known half logistic distribution is considered and its generalization through failure probability of a parallel system of independently identically distributed components is suggested. With the probability model as the suggested generalized version, a new life testing model is assumed for the life of a product. Based on the observed failure times before a prefixed time, the decision rule for acceptance or otherwise of a submitted lot of products is constructed involving a minimum sample size required for the decision rule. The operating characteristic of the decision rule and the tolerance range of the population average are also worked out. Comparison with similar procedures that exist in literature is presented.

**Key words :** Type-I generalized half logistic distribution, acceptance decision rule

### INTRODUCTION

If  $\theta$  is a positive real number,  $F(x)$  is the cumulative distribution function (cdf) of continuous random variable, then  $[F(x)]^\theta$  and the corresponding probability distribution may be named as exponentiated or generalized version of  $F(x)$ , according to Mudholkar et al [1]; Gupta and Kundu [2]. Whether it is exponentiated version of Mudholkar et al [1], generalized version of Gupta and Kundu [2], the model in either of the cases is obtained by considering the positive power of the cdf of a given continuous distribution. The life of a parallel system of components with independent and identical lifetime distribution given by exponential/Weibull for each component will have a cdf given by integral power of the common cdf governing the life of individual components. Such a system's lifetime model turns to be exponentiated/generalized version of Exponential / Weibull models. We adopt this generalization to half logistic distribution.

Half logistic model obtained as the distribution of absolute standard logistic variate is another probability model of recent origin [3]. The probability density function (pdf), cumulative distribution function (cdf) and hazard function (hf) are given by

$$f(x) = \frac{2e^{-x}}{(1+e^{-x})^2}; \quad x \geq 0 \quad (1)$$

$$F(x) = \left[ \frac{1-e^{-x}}{1+e^{-x}} \right]; \quad x \geq 0 \quad (2)$$

$$h(x) = \frac{1}{1+e^{-x}}; \quad x \geq 0 \quad (3)$$

It can be seen that the model is an increasing failure rate (IFR) model and free from any shape parameter. It would be more useful in reliability studies and survival analysis. This model is parallel to half normal distribution as an underlying probability model in the studies of reliability and quality control.

### THE PROPOSED MODEL

As narrated above, the distribution of the random variable representing life of a parallel system of  $\theta$  components ( $\theta$  is natural number) whose individual lifetimes are identically independently distributed with common distribution as that of standard half logistic distribution given by the equations (1), (2)

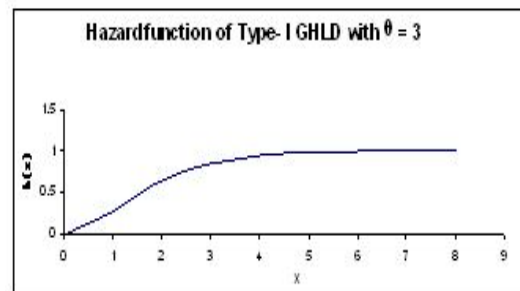
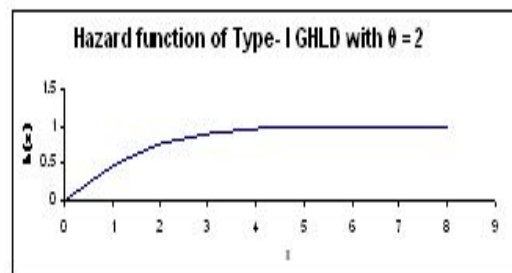
and (3) shall be considered by us in this paper as standard Type-I generalized half logistic distribution (Type-I GHLD). Its pdf, cdf and hazard function are given by

$$f(x) = \frac{2\theta e^{-x}(1-e^{-x})^{\theta-1}}{(1+e^{-x})^{\theta+1}} \quad (4)$$

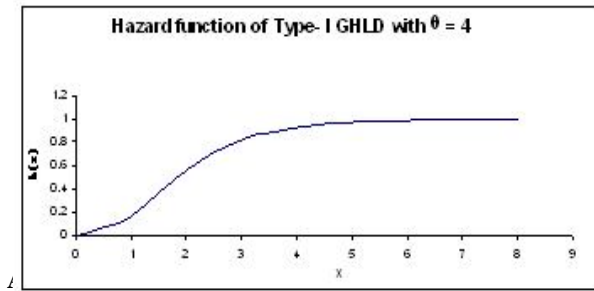
$$F(x) = \left[ \frac{1-e^{-x}}{1+e^{-x}} \right]^\theta \quad (5)$$

$$h(x) = \frac{2\theta e^{-x}(1-e^{-x})^{\theta-1}}{(1+e^{-x})[(1+e^{-x})^\theta - (1-e^{-x})^\theta]} \quad (6)$$

The graphs of hazard function are shown in the following Figures, which show CFR nature on and after some stage of  $x$  for various values of  $\theta$ . We consider the Type-I generalized version of half logistic distribution and study the construction of reliability test plans using this distribution as the model for a lifetime variable.



\*Corresponding author: rosaiah1959@gmail.com



A typical application of acceptance sampling is as follows. A company receives shipment of product from a vendor. This product is often a component or raw material used in the company's manufacturing process. A sample is taken from the lot and some quality characteristic of the unit in the sample is inspected. On the basis of the information in this sample, a decision is made regarding lot disposition. Usually, this decision is either to accept or to reject the lot.

If the distribution of the quality characteristic is non-normal, and a plan based on the normal assumption is employed, serious departures from the advertised risks of accepting or rejecting lots of given quality may be experienced.

Based on the notion of testing a null hypothesis about a population average with a specified minimum, we can think of sampling inspection plans where the sample observations are lifetimes of products put to test. In such a sampling plan the population average stands for average life of the product say  $\sigma$ ,  $\sigma_0$ , is a specified value of  $\sigma$  and if a null hypothesis is formulated as  $\sigma \geq \sigma_0$ , this means that the true unknown population average life of the product exceeds a specified value, which decides a submitted lot of products to be good. The test criterion shall naturally be on the basis of the observed failures in a sample product of size  $n$  before a specified time  $t$ . If the observed number of failures is large say  $\geq$  a number 'c', the hypothesis cannot be accepted and hence lot cannot be accepted. That is, a parallel between a test of hypothesis and a sampling plan can be considered provided the decision rules in either case are with minimum associated risks. Such a sampling plan is named as "Reliability Test Plan" or "Acceptance sampling plan on life tests".

In this paper, we assume that the life of product follows a non-normal distribution called Type-I generalized half logistic distribution (GHLD). If a lot of products with this as the model is submitted for inspection, we develop the necessary sampling plan of characteristics' to decide about the acceptance or otherwise of the submitted lot. Similar sampling plans in other models are developed by many researchers - [4 - 13] and the references therein. Constructing the reliability test plan and its theory, operating characteristics and the sensitivity of sampling plan for the model is described in the following sections.

**RELIABILITY TEST PLAN**

We consider the cumulative distribution function and probability density function of Type-I generalized half logistic distribution with scale parameter  $\sigma$  are given by

$$G(t) = [F(t)]^\theta = \left[ \frac{1 - e^{-t/\sigma}}{1 + e^{-t/\sigma}} \right]^\theta, \quad t > 0, \sigma > 0 \quad (7)$$

$$g(t) = \frac{2\theta (1 - e^{-t/\sigma})^{\theta-1} e^{-t/\sigma}}{\sigma(1 + e^{-t/\sigma})^{\theta+1}}, \quad t > 0, \sigma > 0 \quad (8)$$

We assume that the life of a product follows a Type-I generalized half logistic distribution defined by [5]. A common practice in life testing is to terminate the life test by a pre-determined time 't' and note the number of failures (assuming that a failure is well defined). One of the objectives of these

experiments is to set a lower confidence limit on the average life. It is then desired to establish a specified average life with a given probability of at least 'p'. the decision to accept the specified average life occurs if and only if the number of observed failures at the end of the fixed time-t does not exceed a given number c-called the acceptance number. The test may get terminated before the time-t is reached when the number of failures exceeds in which case the decision is to reject the lot. For such a truncated life test and the associated decision rule, we are interested in obtaining the smallest sample sizes necessary to achieve the objective.

A sampling plan consists of, the number of units  $n$  on test, the acceptance number  $c$ , the maximum test duration  $t$ , and the ratio  $t/\sigma_0$ , where  $\sigma_0$  is the specified average life.

The consumer's risk, i.e., the probability of accepting a bad lot (the one for which the true average life is below the specified life- $\sigma_0$ ) not to exceed  $1-p^*$ , so that  $p^*$  is a minimum confidence level with which a lot of true average life below is rejected by the sampling plan. For a fixed  $p^*$ , our sampling plan is characterized by  $(n, c, t/\sigma_0)$  Here we consider sufficiently large lots so that the binomial distribution can be applied. The problem is to determine the smallest positive integer  $n$  for given values of  $p^*$  ( $0 < p^* < 1$ ),  $\sigma$ , and  $c$  such that

$$\sum_{i=0}^c \binom{n}{i} p^i (1-p)^{n-i} \leq 1 - p^* \quad (9)$$

holds, where  $p = G(t; \sigma_0)$  given by[5] which indicates the failure probability before time  $t$ , and depends only on the ratio  $t/\sigma_0$ . It is sufficient to specify this ratio for designing the experiment.

The minimum values of  $n$  satisfying the inequality (9) are obtained for  $\theta = 2, 3, 4; p^* = 0.75, 0.90, 0.95, 0.99$  and  $t/\sigma_0 = 1, 1.5, 2, 2.5, 3, 3.5, 4, 4.5$  and are presented in Table-1 only for  $\theta = 2$ .

If  $p = G(t; \sigma_0)$  is small and  $n$  is large (as is true in some cases of our present work), the binomial probability may be approximated by Poisson probability with parameter  $\lambda = np$  so that the left side of (9) can be written as

$$\sum_{i=0}^c \frac{\lambda^i}{i!} e^{-\lambda} \leq 1 - p^* \quad (10)$$

where  $\lambda = n G(t; \sigma_0)$ . The minimum values of  $n$  satisfying (10) are obtained for the same combination of  $\theta, p^*, t/\sigma_0$  as those used for (9). The results are given in Table-2 only for  $\theta = 2$ .

The operating characteristic function of sampling plan  $(n, c, t/\sigma_0)$  gives the probability  $L(p)$  of accepting the lot as

$$L(p) = \sum_{i=0}^c \binom{n}{i} p^i (1-p)^{n-i} \quad (11)$$

where  $p = G(t; \sigma_0)$ . It is considered as a function of  $\sigma$ , the lot quality parameter. It can be seen that the operating characteristic is an increasing function of  $\sigma$  for given  $p^*, t/\sigma_0$ . Values of the operating characteristic as a function of  $\sigma/\sigma_0$  for a few sampling plans are given in Table -3.

The producer's risk is the probability of rejecting a lot when  $\sigma > \sigma_0$ . We can compute the producer's risk by first finding  $p = G(t; \sigma)$  and then using the binomial distribution function. For a given value of the producer's risk 0.05, one may be interested in knowing what value of  $\sigma/\sigma_0$  will ensure a producer's risk less than or equal to 0.05 if a sampling plan under discussion is adopted. It should be noted that the probability  $p$  may be obtained as function of  $\sigma/\sigma_0$  as  $p = G[(\sigma/\sigma_0) (\sigma_0/\sigma)]$ . The value  $\sigma/\sigma_0$  is the

smallest positive number for which the following inequality holds

$$\sum_{i=0}^c \binom{n}{i} p^k (1-p)^{n-i} \geq 0.95 \tag{12}$$

For a given sampling plan (n, c, t/σ<sub>0</sub>) and specified confidence level p\* the minimum values of σ/σ<sub>0</sub> satisfying the inequality (12) are given in Table-4.

Our results of Table-1 on comparison with similar results of Gupta and Groll [4] for the gamma distribution reveal that, the sample size of Type-I generalized half logistic distribution (Type-I GHLD) plans are uniformly smaller than those of Gupta and Groll [4] for the gamma distribution, thus giving a saving in cost of experimentation with the same risk probability. Hence, we may say that if type-I GHLD and gamma distribution are good fits for a given data, our decision rule with the present model can be applied with less cost and same risk.

**CONCLUSION**

In this paper an acceptance decision rule is developed based on the truncated life test when the life distribution of test items follows Type-I generalized half logistic distribution. For the use of plans by the practitioners, we provided some Tables.

**Table – 1** Minimum sample size necessary to assert the average life to exceed specified average life σ<sub>0</sub>, with probability p\* and the corresponding acceptance number c, using binomial probabilities under Type-I generalized half logistic distribution for θ=2

p*	c	t/σ <sub>0</sub> =1.0	1.5	2.0	2.5	3.0	3.5	4.0	4.5
.75	1	12	6	4	3	3	2	2	2
.75	2	18	9	6	5	4	4	3	3
.75	3	23	12	8	6	5	5	4	4
.75	4	29	15	10	8	7	6	6	5
.75	5	34	18	12	9	8	7	7	6
.75	6	39	20	14	11	9	8	8	8
.75	7	44	23	16	12	11	10	9	9
.75	8	50	26	18	14	12	11	10	10
.75	9	55	28	19	15	13	12	11	11
.75	10	60	31	21	17	14	13	12	12
.90	1	17	9	6	4	3	3	2	2
.90	2	24	12	8	6	5	4	4	4
.90	3	30	15	10	8	6	5	5	5
.90	4	36	18	12	9	8	7	6	6
.90	5	42	21	14	11	9	8	7	7
.90	6	47	24	16	12	10	9	8	8
.90	7	53	27	18	14	12	10	10	9
.90	8	59	30	20	15	13	12	11	10
.90	9	64	33	22	17	14	13	12	11
.90	10	70	36	24	19	16	14	13	12
.95	1	21	10	7	5	4	3	3	3
.95	2	28	14	9	7	5	4	4	4
.95	3	34	17	11	8	7	6	5	5
.95	4	41	20	13	10	8	7	7	6
.95	5	47	24	15	12	10	9	8	7
.95	6	53	27	18	13	11	10	9	8
.95	7	59	30	20	15	12	11	10	10
.95	8	65	33	22	17	14	12	11	11
.95	9	71	36	24	18	15	14	12	12
.95	10	76	39	26	20	17	15	14	13
.99	1	29	14	9	6	5	4	4	3
.99	2	37	18	11	8	7	6	5	5
.99	3	44	22	14	10	8	7	6	6
.99	4	51	25	16	12	10	8	7	7
.99	5	58	29	18	14	11	10	9	8
.99	6	64	32	21	15	13	11	10	9
.99	7	71	35	23	17	14	12	11	10
.99	8	77	38	25	19	16	14	12	12
.99	9	83	42	27	21	17	15	14	13
.99	10	90	45	29	22	18	16	15	14

**Table - 2** Minimum sample size necessary to assert the average life, to exceed specified average life σ<sub>0</sub>, with probability p\* and the corresponding acceptance number c, using Poisson approximation under Type-I generalized half logistic distribution for θ=2

p*	c	t/σ <sub>0</sub> =1.0	1.5	2.0	2.5	3.0	3.5	4.0	4.5
.75	1	13	7	5	4	4	4	3	3
.75	2	19	10	7	6	5	5	5	5
.75	3	24	13	9	8	7	6	6	6
.75	4	30	16	11	9	8	8	7	7
.75	5	35	19	13	11	10	9	8	8
.75	6	41	22	15	12	11	10	10	9
.75	7	46	25	17	14	12	11	11	11
.75	8	51	27	19	16	14	13	12	12
.75	9	56	30	21	17	15	14	13	13
.75	10	61	33	23	19	16	15	15	14
.90	1	19	10	7	6	5	5	5	5
.90	2	25	14	10	8	7	7	6	6
.90	3	32	17	12	10	9	8	8	7
.90	4	38	20	14	12	10	10	9	9
.90	5	44	23	16	13	12	11	10	10
.90	6	50	27	19	15	13	12	12	12
.90	7	56	30	21	17	15	14	13	13
.90	8	61	33	23	19	16	15	14	14
.90	9	67	36	25	20	18	17	16	15
.90	10	73	39	27	22	19	18	17	17
.95	1	23	12	9	7	6	6	6	5
.95	2	30	16	11	9	8	8	7	7
.95	3	37	20	14	11	10	9	9	9
.95	4	43	23	16	13	12	11	10	10
.95	5	50	27	19	15	13	12	12	11
.95	6	56	30	21	17	15	14	13	13
.95	7	62	33	23	19	17	15	15	14
.95	8	68	36	25	21	18	17	16	16
.95	9	74	39	28	22	20	18	17	17
.95	10	80	43	30	24	21	20	19	18
.99	1	32	17	12	10	9	8	8	7
.99	2	40	21	15	12	11	10	10	9
.99	3	48	25	18	14	13	12	11	11
.99	4	55	29	21	17	15	14	13	13
.99	5	62	33	23	19	16	15	15	14
.99	6	69	37	26	21	18	17	16	16
.99	7	75	40	28	23	20	19	18	17
.99	8	82	44	31	25	22	20	19	19
.99	9	88	47	33	27	23	22	21	20
.99	10	95	50	35	28	25	23	22	22

**Table - 3** Operating characteristic values of the sampling plan (n, c, t/σ<sub>0</sub>) for a given p\* under Type-I generalized half logistic distribution for θ=2

p*	n	c	t/σ <sub>0</sub>	σ/σ <sub>0</sub> = 2	4	6	8	10	12
.75	23	3	1.000	.9541	.9996	1.0000	1.0000	1.0000	1.0000
.75	12	3	1.500	.9425	.9994	1.0000	1.0000	1.0000	1.0000
.75	8	3	2.000	.9304	.9993	1.0000	1.0000	1.0000	1.0000
.75	6	3	2.500	.9233	.9991	1.0000	1.0000	1.0000	1.0000
.75	5	3	3.000	.9103	.9988	.9999	1.0000	1.0000	1.0000
.75	5	3	3.500	.8181	.9964	.9998	1.0000	1.0000	1.0000
.75	5	3	4.000	.6967	.9914	.9995	.9999	1.0000	1.0000
.75	4	3	4.500	.8160	.9954	.9997	1.0000	1.0000	1.0000
.90	30	3	1.000	.8975	.9989	.9999	1.0000	1.0000	1.0000
.90	15	3	1.500	.8837	.9986	.9999	1.0000	1.0000	1.0000
.90	10	3	2.000	.8541	.9980	.9999	1.0000	1.0000	1.0000
.90	8	3	2.500	.7919	.9964	.9998	1.0000	1.0000	1.0000
.90	6	3	3.000	.8160	.9967	.9998	1.0000	1.0000	1.0000
.90	6	3	3.500	.6647	.9908	.9994	.9999	1.0000	1.0000
.90	5	3	4.000	.6967	.9914	.9995	.9999	1.0000	1.0000
.90	5	3	4.500	.5620	.9819	.9988	.9999	1.0000	1.0000
.95	34	3	1.000	.8555	.9982	.9999	1.0000	1.0000	1.0000
.95	17	3	1.500	.8344	.9977	.9999	1.0000	1.0000	1.0000
.95	11	3	2.000	.8076	.9970	.9998	1.0000	1.0000	1.0000
.95	8	3	2.500	.7919	.9964	.9998	1.0000	1.0000	1.0000
.95	7	3	3.000	.7036	.9931	.9996	1.0000	1.0000	1.0000
.95	6	3	3.500	.6647	.9908	.9994	.9999	1.0000	1.0000
.95	5	3	4.000	.6967	.9914	.9995	.9999	1.0000	1.0000
.95	5	3	4.500	.5620	.9819	.9988	.9999	1.0000	1.0000
.99	44	3	1.000	.7300	.9953	.9998	1.0000	1.0000	1.0000
.99	22	3	1.500	.6895	.9938	.9997	1.0000	1.0000	1.0000
.99	14	3	2.000	.6509	.9920	.9996	.9999	1.0000	1.0000
.99	10	3	2.500	.6293	.9906	.9995	.9999	1.0000	1.0000
.99	8	3	3.000	.5861	.9876	.9993	.9999	1.0000	1.0000
.99	6	3	4.500	.3429	.9569	.9967	.9996	.9999	1.0000
.99	6	3	4.000	.4970	.9785	.9986	.9998	1.0000	1.0000

**Table – 4** Minimum ratio of true mean life to specified mean life for the acceptability of a lot under Type-I generalized half logistic distribution with producer's risk of 0.05 for  $\theta = 2$ .

$\theta$	$p^*$	$c$	$t/\sigma = 1$	1.5	2	2.5	3.0	3.5	4.0	4.5
2.00	.75	1	1.96	2.33	2.59	3.25	2.92	3.41	3.90	4.40
2.00	.75	2	1.55	1.82	2.15	2.29	2.75	2.49	2.84	3.20
2.00	.75	3	1.37	1.59	1.73	1.87	2.24	2.61	2.37	2.68
2.00	.75	4	1.26	1.47	1.67	1.87	1.95	2.28	2.10	2.36
2.00	.75	5	1.20	1.38	1.49	1.68	1.76	2.06	1.92	2.16
2.00	.75	6	1.11	1.32	1.47	1.54	1.63	1.90	2.17	2.44
2.00	.75	7	1.08	1.28	1.37	1.58	1.72	1.78	2.03	2.29
2.00	.75	8	1.06	1.24	1.37	1.48	1.62	1.68	1.92	2.17
2.00	.75	9	1.02	1.17	1.29	1.41	1.54	1.61	1.83	2.06
2.00	.75	10	1.00	1.15	1.30	1.34	1.48	1.54	1.76	1.98
2.00	.90	1	2.44	2.93	3.09	3.25	3.39	4.55	5.40	4.90
2.00	.90	2	1.82	2.17	2.42	2.68	2.75	3.20	3.65	3.45
2.00	.90	3	1.56	1.84	2.12	2.17	2.60	2.61	2.99	2.68
2.00	.90	4	1.41	1.65	1.82	2.08	2.25	2.28	2.61	2.32
2.00	.90	5	1.31	1.53	1.73	1.86	2.01	2.06	2.35	2.16
2.00	.90	6	1.24	1.45	1.58	1.70	1.85	2.16	2.17	2.01
2.00	.90	7	1.19	1.39	1.55	1.71	1.72	2.01	2.03	1.90
2.00	.90	8	1.16	1.34	1.45	1.61	1.78	1.89	1.92	1.81
2.00	.90	9	1.12	1.30	1.43	1.52	1.69	1.80	1.83	1.74
2.00	.90	10	1.10	1.27	1.42	1.54	1.61	1.79	1.76	1.67
2.00	.95	1	2.58	3.19	3.53	3.87	3.89	4.55	5.20	4.40
2.00	.95	2	1.98	2.32	2.67	2.68	3.23	3.20	3.65	3.20
2.00	.95	3	1.67	1.95	2.12	2.43	2.60	2.61	2.99	2.68
2.00	.95	4	1.50	1.74	1.96	2.08	2.25	2.62	2.61	2.36
2.00	.95	5	1.42	1.60	1.84	2.02	2.23	2.35	2.96	2.16
2.00	.95	6	1.33	1.57	1.67	1.84	2.04	2.16	2.17	2.01
2.00	.95	7	1.27	1.49	1.63	1.71	1.89	2.01	2.30	2.29
2.00	.95	8	1.22	1.43	1.59	1.71	1.78	1.89	2.17	2.18
2.00	.95	9	1.18	1.38	1.50	1.61	1.82	1.80	2.06	2.08
2.00	.95	10	1.15	1.34	1.48	1.62	1.73	1.88	1.97	1.98
2.00	.99	1	3.08	3.85	3.90	4.42	4.64	5.42	5.70	4.40
2.00	.99	2	2.27	2.61	2.89	3.33	3.64	3.76	4.29	4.12
2.00	.99	3	1.93	2.25	2.45	2.66	2.92	3.03	3.47	3.36
2.00	.99	4	1.70	1.97	2.20	2.44	2.50	2.62	2.99	2.92
2.00	.99	5	1.58	1.79	2.04	2.17	2.43	2.60	2.68	2.64
2.00	.99	6	1.47	1.72	1.85	2.09	2.21	2.38	2.66	2.44
2.00	.99	7	1.39	1.62	1.78	1.93	2.05	2.21	2.30	2.29
2.00	.99	8	1.33	1.55	1.72	1.90	2.05	2.08	2.37	2.17
2.00	.99	9	1.30	1.49	1.68	1.79	1.93	2.12	2.25	2.32
2.00	.99	10	1.25	1.44	1.59	1.70	1.84	2.02	2.15	2.22
3.00	.75	1	1.45	1.78	2.01	2.21	2.64	2.49	2.84	3.25
3.00	.75	2	1.23	1.43	1.67	1.91	2.03	2.37	2.22	2.54
3.00	.75	3	1.11	1.32	1.52	1.62	1.73	2.02	1.92	2.23
3.00	.75	4	1.06	1.22	1.35	1.57	1.74	1.81	1.74	1.96
3.00	.75	5	1.00	1.18	1.30	1.44	1.59	1.67	1.90	1.81
3.00	.75	6	.98	1.12	1.26	1.34	1.48	1.56	1.78	1.71
3.00	.75	7	.95	1.11	1.24	1.34	1.40	1.48	1.69	1.62
3.00	.75	8	.93	1.07	1.21	1.28	1.44	1.56	2.04	1.56
3.00	.75	9	.91	1.06	1.16	1.28	1.38	1.49	1.55	1.74
3.00	.75	10	.90	1.04	1.15	1.23	1.33	1.44	1.50	1.43
3.00	.90	1	1.64	1.99	2.21	2.51	2.64	3.09	3.53	3.20
3.00	.90	2	1.38	1.64	1.80	2.10	2.30	2.37	2.71	2.50
3.00	.90	3	1.24	1.47	1.61	1.77	1.95	2.02	2.31	2.16
3.00	.90	4	1.15	1.34	1.50	1.68	1.74	2.03	2.07	1.95
3.00	.90	5	1.09	1.28	1.42	1.54	1.73	1.86	1.90	1.81
3.00	.90	6	1.05	1.23	1.37	1.51	1.61	1.73	1.78	1.71

**REFERENCES**

[1] Mudholkar S Govind., Srivastava Deo Kumar. (1995). The exponentiated Weibull family, A reanalysis of the bus-motor failure data, *Technometrics*, **37**(4), 436-445.  
 [2] Gupta, R.D. and Kundu, D. (2001). Generalized exponential distribution. Different methods of estimation, *J. of Statistical Computation and Simulation*, **69**, 315-338.

[3] Balakrishnan, N. (1985). Order statistics from the half logistic distribution, *J. Statist. Comput. Simul.*, **20**, 287-309.  
 [4] Gupta, S.S. and Groll, P.A. (1961). Gamma distribution in acceptance sampling based on life tests, *Journal of American Statistical Association (JASA)*, **56**, 942-970.  
 [5] Kantam, R.R.L. and Rosaiah, K. (1998). Half logistic distribution in acceptance sampling based on life tests, *Journal of the Indian Association for Productivity, Quality & Reliability (IAPQR Transactions)*, **23**(2), 117-125.  
 [6] Kantam, R.R.L., Rosaiah, K. and Srinivasarao, G. (2001). Acceptance sampling based on life tests : Log-logistic model, *Journal of Applied Statistics (U.K.)*, **28**(1), 121-128.  
 [7] Rosaiah, K. and Kantam, R.R.L. (2005). Acceptance Sampling based on the Inverse Rayleigh distribution, *Economic Quality Control*, **20**(2), 277-286.  
 [8] Kantam, R.R.L., Srinivasarao, G. and Sriram, B. (2006). An economic reliability test plan : Log-logistic distribution, *Journal of Applied Statistics (U.K.)*, **33**(3), 291-296.  
 [9] Rosaiah, K., Kantam, R.R.L. and Santosh Kumar, Ch. (2006). Reliability test plans for exponentiated log-logistic distribution, *Economic Quality Control*, **21**(2), 165-175.  
 [10] Rosaiah, K., Kantam, R. R. L. and Santosh Kumar, Ch. (2007). Exponentiated log- logistic distribution-An economic reliability test plan, *Pakistan J. of Statistics*, **23**(2), 147-156.  
 [11] Rosaiah, K., Kantam, R. R. L. and Pratap Reddy, J. (2008). An economic reliability test plan with Inverse Rayleigh variate, *Pakistan J. of Statistics*, **24**(1), 57-65.  
 [12] Balakrishnan, N., Leiva, V. and Lopez, J. (2007). Acceptance sampling from truncated life tests based on the generalized Birnbaum-Saunders distribution, *Commun. Statist. Simul.-Comput.*, **36**, 643-656.  
 [13] Rosaiah, K., Kantam, R. R. L. and Srinivasa Rao, B. (2009). Reliability test plan for half logistic distribution, *Calcutta Statistical Association Bulletin*, **61**(241-244), 183-196.



## ON VARIANCE ESTIMATION FOR THE GREG ESTIMATOR

P.A. Patel<sup>1</sup> and R.D. Chaudhari<sup>2</sup>

<sup>1</sup>Department of Statistics, Sardar Patel University, Vallabh Vidhyanagar-388120, Gujarat, India

<sup>2</sup>Department of Statistics, M. G. Science College, Ahmedabad, Gujarat, India

### ABSTRACT

This article extends the  $\pi$ -weighted ratio-type variance estimator of the Horvitz–Thompson estimator, suggested by Patel and Chaudhari (2006), for the generalized regression (GREG) estimation. The suggested variance estimator based on the empirical mean squared error yields some gain over the available variance estimators in simulations when the underlying assumptions are satisfied.

**Key words:** Finite population, Generalized regression estimator, Variance estimation.

### INTRODUCTION

Recently more attention has been given to the generalized regression estimator of the finite population total. Some of the reasons are given in Särndal (1996). Important references on GREG estimation and on its variance estimation are Särndal (1980, 1996), Robinson and Särndal (1983), Wright (1983), Särndal et al. (1989, 1992), Deville and Särndal (1992), Kott (1990), Chaudhuri and Maiti (1994), Singh et al. (1999) and Duchesne (2000) and references cited there.

Following the notations of Patel and Chaudhari (2006), we postulate the model

$$\left. \begin{aligned} y_i &= \beta x_i + \varepsilon_i, \quad i \in U = \{1, \dots, N\} \\ E_{\xi}(\varepsilon_i / x_i) &= 0 \\ V_{\xi}(\varepsilon_i / x_i) &= \sigma^2 = \sigma^2 x_i^{\gamma}, \quad 0 \leq \gamma \leq 2 \\ C_{\xi}(\varepsilon_i, \varepsilon_j / x_i, x_j) &= 0 \quad (i \neq j) \end{aligned} \right\} \quad (1)$$

Where  $\beta, \sigma^2 > 0$  are the parameters. Here  $E_{\xi}(\cdot), V_{\xi}(\cdot)$  and  $C_{\xi}(\cdot)$  denote  $\xi$ - expectation,  $\xi$ - variance and  $\xi$ - covariance. Under Model (1) the GREG-estimator of  $Y = \sum_{i \in U} y_i$  is given by

$$\hat{Y}_{GREG} = \sum_s \frac{g_s y_s}{\pi_s} \quad (2)$$

where  $g_s = 1 + (X - \hat{X}_{HT}) \frac{x_s q \pi_s}{\sum_s x_s^2 q_s}$  is the g-adjustment factors,  $\hat{X}_{HT} = \sum_s \frac{x_s}{\pi_s}$  is the Horvitz. Thompson estimator of  $x = \sum_U x_i$  and  $q_i$  is chosen by the user.

The estimator  $\hat{Y}_{GREG}$  is optimal in the following way: Starting from the basic estimator  $\hat{Y}_{HT} = \sum_s a_s y_s$  with  $a_s = 1/\pi_s$ , create a new estimator  $\hat{Y} = \sum_s w_s y_s$  with weight  $w_i$  lying as close as possible to the basic weights  $a_s$ , subject to the calibration constraint  $\sum_s w_s x_s = X$ . when the distance to minimize is given as  $\sum c_i (w_i - a_i)^2 / a_i$ , where  $c_i$ 's are constants, the optimal weights  $w_i$  are precisely  $w_i = a_i g_i$ .

The Taylor expansion variance for the GREG – estimator (See, Särndal et al. 1992) is

$$V_T = \sum_{i < j \in U} \Delta_{ij} \left( \frac{E_i}{\pi_i} - \frac{E_j}{\pi_j} \right)^2$$

where

$$\Delta_{ij} = \pi_i \pi_j - \pi_{ij}, \quad E_i = y_i - B Q_i x_i \quad \text{and} \quad B = \frac{\sum_U y_i x_i Q_i}{\sum_U x_i^2 Q_i}.$$

\*Corresponding author: patelpraful\_a@indiatimes.com

Two versions of Yates-Grundy type variance estimators of  $V_T$  are

$$v_s = \sum_{i < j \in s} \frac{\Delta_{ij}}{\pi_{ij}} \left( \frac{e_i}{\pi_i} - \frac{e_j}{\pi_j} \right)^2 \quad \text{and} \quad v_g = \sum_{i < j \in s} \frac{\Delta_{ij}}{\pi_{ij}} \left( \frac{e_i g_i}{\pi_i} - \frac{e_j g_j}{\pi_j} \right)^2 \quad (3)$$

where  $e_i = y_i - \hat{\beta} x_i$  and  $\hat{\beta} = \frac{\sum_s x_i y_i q_i}{\sum_s x_i^2 q_i}$

Kott (1990) proposed an estimator of  $V_T$  (see Appendix A) that is design-consistent and model-unbiased. Chaudhuri and Maiti (1994), following Kott's estimator, suggested various model-assisted estimator of  $V_T$ .

We suggest in the next section an estimator of  $V_T$ . To study the repeated sampling properties relative to standard one a limited simulation study is conducted in Section 3. The conclusions and recommendations are given in section 4.

### THE RATIO-TYPE VARIANCE ESTIMATOR

Patel and Chaudhari (2006) suggested a  $\pi$ - weighted ratio- type estimator ( $v_{\pi}$ ) for the variance of Horvitz- Thompson estimator of population total. They showed that this estimator is asymptotically design-unbiased (ADU) and asymptotically design consistent (ADC). Empirically this estimator has performed very well when the relationship between  $y$  and  $x$  is linear passing through the origin and the  $V_{\xi}(y_i) \propto x_i^{\gamma}$ ,  $\gamma \in [1, 2]$ , under fixed size or non-fixed size sampling design. Motivated by this we suggest the following estimator for  $V_T$ :

$$v_{\pi} = \frac{\sum_s \phi_{ii} g_i^2 e_i^2 / \pi_i}{\sum_s \phi_{ii} g_i^2 x_i^2 / \pi_i} \sum_U \phi_{ii} x_i^2 + \frac{\sum_s \sum_{i < j} \phi_{ij} g_i e_i g_j e_j / \pi_{ij}}{\sum_s \sum_{i < j} \phi_{ij} g_i x_i g_j x_j / \pi_{ij}} \sum_U \phi_{ij} x_i x_j$$

where  $\phi_{ij} = \frac{1}{\pi_i} - 1$ , if  $i=j$  and  $= \frac{\pi_{ij}}{\pi_i \pi_j} - 1$  if  $i \neq j$ .

**Remark :** The construction of  $v_{\pi}$  would suggest that  $v_{\pi}$  performs well if the ratios  $y/x_i$  is more or less constant and the variance of  $y_i$  is proportional to  $x_i$ .

### SIMULATION

A finite population of size  $N=400$  was created. The characteristics  $x$  and  $y$  for the  $i^{th}$  unit were generated using the model

$$y_i = \beta x_i + x_i^{\gamma/2} \varepsilon_i, \quad i = 1, \dots, N$$

for specified values of  $\beta, \gamma, g, h$  and  $\sigma_{\varepsilon}^2, \varepsilon_i \sim N(0, \sigma_{\varepsilon}^2)$  were independent of  $x_i \sim \text{Gamma}(g, h)$ . Thus the mean, variance and coefficient of variation of  $x_i$  are given by  $\mu_x = gh, \sigma_x^2 = gh^2$  and  $C_x = \sigma_x / \mu_x = g^{-1/2}$ .

Further the mean of  $y_i$  is  $\mu_y = \beta \mu_x$ , variance of  $x_i$  is  $\sigma_y^2 = \beta^2 \sigma_x^2 + \sigma_{\varepsilon}^2 E(x_i^{\gamma})$

and the correlation coefficient  $Corr(x_i, y_i) = \rho = \beta \sigma_x / \sigma_y$ , vary depending on the choice of  $\gamma$ . Here  $\gamma = 0, 1$  and  $2$  were considered so that  $E(x_i^{\gamma/2}) = 1, \mu_x$  and  $\mu_x^2 + \sigma_x^2$ ; for each of these cases  $\sigma_y^2$  and  $\sigma_x^2$  were then chosen to match various values of  $\rho$  and  $C_x$ . The three  $(\beta, \mu_x, \gamma)$  combinations were: (a)  $\beta=1, \mu_x = 100, \gamma=0$ ; (b)  $\beta=1, \mu_x = 100, \gamma = 1$ ; and (c)  $\beta=1, \mu_x = 100, \gamma=2$ .

A finite population was created for each of (a) - (c) and each combination of  $(\rho, C_x)$  and a sample of size  $n = 30$  was drawn using Sunter's (1986) sampling design. The variance estimators were computed from each sample. This process was repeated  $M = 10,000$  times. For each of these samples, we computed the estimators  $v_g, v_k$  and  $v_\pi$  corresponding to different values of  $q_i, i = 1, 2, 3$  given by

Choice of $q_i$	Form of Estimator
$q_1 = 1/x_i$	$\hat{Y}_{GREG} = \hat{Y}_{HT} + \frac{\bar{y}}{x} (X - \hat{X}_{HT})$
$q_2 = 1/\pi_i x_i$	$\hat{Y}_{GR} = \frac{\hat{Y}_{HT}}{\hat{X}_{HT}} X$
$q_3 = (1 - \pi_i) / \pi_i x_i$	$\hat{Y}_b = \hat{Y}_{HT} + \frac{\sum_i \left( \frac{1 - \pi_i}{\pi_i} \right) y_i}{\sum_i \left( \frac{1 - \pi_i}{\pi_i} \right) x_i} (X - \hat{X}_{HT})$

The performance of the different variance estimators was measured and compared in terms of relative bias in percentage (RB), relative efficiency (RE) and empirical coverage rate (ECR). The simulated values of RB and RE for a particular variance estimator were computed as

$$RB(v) = 100 \times \frac{\bar{v} - V}{V} \quad \text{where} \quad \bar{v} = \frac{1}{M} \sum_{j=1}^M v_{(j)}$$

and relative efficiency of  $v$  is given by

$$RE(v) = \frac{MSE(v_{YG})}{MSE(v)} = \frac{RSE(v_{YG})^2}{RSE(v)}$$

where  $MSE(v) = \frac{1}{M-1} \sum_{j=1}^M (v_{(j)} - \bar{v})^2$  and  $RSE(v) = 100 \times \sqrt{\frac{MSE(v)}{V}}$

The REs of the estimators is presented in Table 1 whereas the RBs in the table 2 given in Appendix A.

**Table 1** RE under Sunter's Sampling Scheme

$q_i$	Est.	$\gamma$	0			1			2		
			$\rho \setminus C_x$	1.5	0.75	0.33	1.5	0.75	0.33	1.5	0.75
$q_1$	$v_g$	0.9	1.000	1.000	1.000	1.000	1.000	1.000	1.000	1.000	1.000
		0.8	1.000	1.000	1.000	1.000	1.000	1.000	1.000	1.000	1.000
		0.7	1.000	1.000	1.000	1.000	1.000	1.000	1.000	1.000	1.000
	$v_k$	0.9	1.057	1.047	1.047	1.049	1.033	1.093	1.024	1.039	1.034
		0.8	1.041	1.030	1.022	1.050	1.028	1.053	1.020	1.069	1.026
		0.7	1.041	1.033	1.029	1.056	1.052	1.064	1.023	1.082	1.034
	$v_\pi$	0.9	1.112	1.968	1.065	<b>1.131</b>	<b>4.519</b>	<b>1.221</b>	1.077	1.033	1.075
		0.8	1.124	1.741	1.150	<b>1.106</b>	<b>3.163</b>	<b>1.149</b>	1.073	2.954	1.028
		0.7	1.137	1.836	1.102	<b>1.198</b>	<b>4.652</b>	<b>1.189</b>	1.001	3.827	1.035
$q_2$	$v_g$	0.9	1.000	1.000	1.000	1.000	1.000	1.000	1.000	1.000	1.000
		0.8	1.000	1.000	1.000	1.000	1.000	1.000	1.000	1.000	1.000
		0.7	1.000	1.000	1.000	1.000	1.000	1.000	1.000	1.000	1.000
	$v_k$	0.9	1.048	0.933	1.048	1.039	0.740	1.073	1.019	0.927	1.028
		0.8	1.026	0.923	0.978	1.044	0.763	1.037	1.016	0.813	1.025
		0.7	1.024	0.911	1.010	1.041	0.740	1.039	1.019	0.800	1.031
	$v_\pi$	0.9	1.101	1.287	1.056	<b>1.120</b>	<b>3.957</b>	<b>1.207</b>	1.066	0.528	1.062
		0.8	1.112	1.251	1.143	<b>1.098</b>	<b>2.357</b>	<b>1.145</b>	1.063	1.200	1.025
		0.7	1.120	1.402	1.091	<b>1.177</b>	<b>2.650</b>	<b>1.169</b>	0.996	1.591	1.030
$q_3$	$v_g$	0.9	1.000	1.000	1.000	1.000	1.000	1.000	1.000	1.000	1.000
		0.8	1.000	1.000	1.000	1.000	1.000	1.000	1.000	1.000	1.000
		0.7	1.000	1.000	1.000	1.000	1.000	1.000	1.000	1.000	1.000
	$v_k$	0.9	1.048	0.932	1.049	1.038	0.704	1.071	1.018	0.926	1.028
		0.8	1.025	0.921	0.971	1.043	0.730	1.034	1.016	0.796	1.025
		0.7	1.022	0.904	1.008	1.040	0.704	1.036	1.019	0.777	1.031
	$v_\pi$	0.9	1.099	1.218	1.054	<b>1.119</b>	<b>3.862</b>	<b>1.205</b>	1.065	0.487	1.060
		0.8	1.111	1.197	1.142	<b>1.097</b>	<b>2.255</b>	<b>1.145</b>	1.062	1.045	1.024
		0.7	1.117	1.345	1.090	<b>1.174</b>	<b>2.316</b>	<b>1.167</b>	0.996	1.361	1.030

Table 1 reveals the following comments

- The absolute values of RBs of  $v_g$  for  $C_x = 0.33, 1.5$  and  $\gamma = 2$  are all within reasonable range of 1%, whereas for  $C_x = 0.33, \gamma = 2$  it has large absolute values of RBs ranging from 1-19%. However, for  $\gamma = 2$   $v_g$  has performed well.
- For  $\gamma = 1, C_x = 0.75$  the absolute RBs of  $v_\pi$  are small compare to  $v_g$  and has performed extremely well. This improvement of  $v_\pi$  over  $v_g$  is from 125-350%.
- For  $\gamma = 1, C_x = 0.33, 1.5$  the absolute RBs of  $v_\pi$  and  $v_g$  are in the reasonable range with the largest occurring as 3% and 4.67% respectively. But  $v_\pi$  has 10-20% more efficiency compared to  $v_g$ .
- For  $\gamma = 1, C_x = 1.5$  the estimator  $v_\pi$  should be avoided. However, in case for the other values of  $C_x, v_\pi$  is fractionally more efficient and has reasonable absolute RBs than  $v_g$ .
- Overall the variance estimator  $v_k$  of  $\hat{Y}_{GREG} = \hat{Y}_{HT} + \frac{\bar{y}}{x} (X - \hat{X}_{HT})$  is slightly more efficient than  $v_g$ , but less efficient than  $v_\pi$  when  $\gamma = 0, 1, 2$  and  $C_x = 0.33, 0.75, 1.5$ . In rest of all cases it should be avoidable.

**Remark 3.** In our simulation study it was borned out that the estimators suggested by Chaudhari and Maiti (1994) performed poorly. Therefore, the results corresponding to these estimators were not presented in respective tables.

**Appendix A**

The following estimator is included for the comparison.

Kott's Estimator: A variance estimator somewhat similar in spirit to that in equation (3) was proposed by Kott (1990). His point of departure is to create a variance estimator that is unbiased with respect to the model but is still design consistent. The objective is achieved by attaching a ratio adjustment to the estimator (3). Kott's variance estimator is given as

$$v_k = \frac{v_g v_1}{v_2}$$

where  $v_1 = v(\hat{Y}_{GREG} - Y)$

$$= \sigma^2 \left[ \frac{\sum_i f_i x_i^2 Q_i^2}{\left( \sum_i x_i^2 Q_i \right)^2} (X - \hat{X}_{HT})^2 + \sum_i \frac{f_i}{\pi_i^2} + \sum U_i f_i + \frac{2}{\sum_i x_i^2 Q_i} (X - \hat{X}_{HT}) \sum_i \frac{1 - \pi_i}{\pi_i} f_i x_i Q_i - 2 \sum_i \frac{f_i}{\pi_i} \right]$$

and

$$v_2 = \sigma^2 \left[ \sum_{i < j} \frac{\Delta_{ij}}{\pi_{ij}} \left( \frac{f_i g_i^2}{\pi_i^2} + \frac{f_j g_j^2}{\pi_j^2} + \frac{\sum_i f_i x_i Q_i^2}{\left( \sum_i x_i^2 Q_i \right)^2} \left( \frac{x_i g_i}{\pi_i} - \frac{x_j g_j}{\pi_j} \right) \right) \right. \\ \left. - \frac{2}{\left( \sum_i x_i^2 Q_i \right)} \left( \frac{x_i g_i}{\pi_i} - \frac{x_j g_j}{\pi_j} \right) \left( \frac{x_i Q_i f_i g_i}{\pi_i} - \frac{x_j Q_j f_j g_j}{\pi_j} \right) \right]$$

**Appendix B**

**Table 2.** RB (%) under Sunter's Sampling Scheme

$q_i$	Est.	$\gamma$	0			1			2		
			$\rho \setminus C_x$	1.5	0.75	0.33	1.5	0.75	0.33	1.5	0.75
$q_1$	$v_g$	0.9	0.44	7.34	-9.67	0.58	95.28	1.59	0.49	2.07	0.95
		0.8	3.12	2.45	7.91	1.18	80.35	4.67	0.10	12.99	0.15
		0.7	1.72	9.67	0.13	1.63	45.41	2.32	0.46	18.28	0.72
	$v_k$	0.9	0.33	7.78	-9.77	0.40	94.79	1.46	-0.60	0.78	-0.61
		0.8	3.09	3.03	8.02	1.04	80.39	4.46	-0.84	11.20	-1.19
		0.7	1.68	10.05	0.19	1.52	45.32	2.20	-0.65	16.27	-0.96
	$v_\pi$	0.9	-1.40	-2.727	-10.93	-0.96	27.44	-0.36	-0.71	-15.75	-0.27
		0.8	0.95	-2.375	4.85	-0.29	21.90	3.02	-1.48	-8.33	-1.17
		0.7	-0.91	-18.37	-2.13	0.11	3.69	0.22	-1.34	-5.54	0.22
$q_2$	$v_g$	0.9	-0.82	-18.34	-10.15	-0.18	44.20	0.86	0.17	-2.39	0.67
		0.8	1.46	-17.24	4.86	0.61	39.94	3.82	-0.20	2.26	0.09
		0.7	-0.33	-1.666	-1.67	0.64	16.39	1.13	0.26	5.78	0.57
	$v_k$	0.9	-0.59	-10.73	-10.02	-0.15	59.65	1.08	-0.80	-0.26	-0.81
		0.8	1.91	-10.59	6.05	0.65	55.13	3.91	-1.05	5.16	-1.21
		0.7	0.20	-4.80	-0.95	0.82	27.25	1.54	-0.73	9.02	-1.06
	$v_\pi$	0.9	-2.57	-3.961	-11.35	-1.62	2.13	-1.14	-1.12	-19.02	-0.43
		0.8	-0.59	-3.328	2.03	-0.89	2.41	2.01	-1.86	-13.27	-1.47
		0.7	-2.76	-3.048	-3.79	-0.84	-9.28	-0.89	-1.96	-11.21	0.07
$q_3$	$v_g$	0.9	-1.02	-2.177	-10.22	-0.30	37.33	0.72	0.12	-2.78	0.60
		0.8	1.19	-2.016	4.34	0.53	33.98	3.68	-0.25	1.00	0.08
		0.7	-0.66	-14.68	1.97	0.50	11.76	0.95	0.24	4.10	0.55
	$v_k$	0.9	-0.74	-13.57	-10.07	-0.23	54.19	1.01	-0.83	-0.21	-0.86
		0.8	1.72	-12.93	5.70	0.59	50.73	3.81	-1.08	4.36	-1.21
		0.7	-0.06	-7.17	-1.15	0.72	23.91	1.44	-0.73	7.87	-1.07
	$v_\pi$	0.9	-2.77	-41.36	-11.43	-1.72	-1.55	-1.30	-1.19	-19.53	-0.47
		0.8	-0.85	-34.79	1.53	-0.98	-0.86	1.82	-1.92	-13.91	-1.54
		0.7	-3.08	-32.27	-4.08	-0.97	-11.60	-1.07	-2.07	-12.07	0.04

**References**

- [1] Patel, P. A. and Chaudhari, R. D. (2006). Design-Based Horvitz-Thompson Variance Estimation:  $\pi$ -Weighted Ratio Type estimator. *Statistics in Transition*, 7(6), 1277-1293.
- [2] Särndal, C.E. (1996). Efficient estimators with simple variance in unequal probability sampling. *Journal of the American Statistical Association*, 91, 1289-1300.
- [3] Särndal, C.E. (1980). On  $\pi$ -inverse weighting versus best linear unbiased weighting in probability sampling. *Biometrika*, 67, 639-650.
- [4] Robinson, P. M. and Särndal, C.E. (1983). Asymptotic properties of the generalized regression estimator in probability sampling. *Sankhya, Series B*, 45, 240-248.
- [5] Wright, R. L. (1983). Finite population sampling with multivariate auxiliary information, *Journal of the American Statistical Association*, 78, 879-884.
- [6] Särndal, C.E., Swensson, B. and Wretman, J.H. (1989). The weighted residual technique for estimating the variance of the general regression estimator of the finite population total. *Biometrika*, 76, 527-537.
- [7] Särndal, C.E., Swensson, B. and Wretman, J.H. (1992). *Model Assisted Survey Sampling*. Springer Verlag, New York.
- [8] Deville, J.C., Särndal, C.E. (1992). Calibration using auxiliary information. *Journal of the American Statistical Association*, 78, 117-123.
- [9] Chaudhari, A. and Maiti, T. (1994). Variance estimation in model assisted survey sampling. *Communication in Statistical Theory and Methods*, 23(4), 1203-1214.
- [10] Singh, S., Horn, S., Chowdhury, S. and Yu. S. (1999). Calibration of the estimators of variance. *Australian and New Zealand Journal of Statistics*, 41, 199-212.
- [11] Duchesne, P. (2000). A note on jackknife variance estimation for the general regression estimator. *Journal of Official Statistics*, 16(2), 133-138.
- [12] Kott, P. S. (1990). Estimating the conditional variance of a design consistent regression estimator. *Journal of Statistical Planning and Inference*, 24, 287-296.
- [13] Sunter, A. B. (1986). Solution to the problem unequal probability sampling without replacement. *International Statistical Review*, 54, 33-50.

## GUIDELINES FOR CONTRIBUTORS

The Editorial Board of 'PRAJNA' – Journal of Pure and Applied Sciences invites Original Research Papers in the fields of Basic and Applied Sciences (Biosciences, Chemistry, Computer Science, Electronics Science, Home Science, Materials Science, Mathematics, Physics and Statistics) for the Next Volume of PRAJNA, *published by Sardar Patel University, Vallabh Vidyanagar, Gujarat – 388120, INDIA.*

The soft copies of regular (full-length) research papers (not exceeding 15 typed pages), prepared as per the file format shown below may be submitted for publication through e-mail to Prof. T. V. Ramana Rao, Managing Editor (spu.prajna@gmail.com) OR to a Member of the Editorial Board who represents the author's broad research area with a cc to the Managing Editor.

Each manuscript must be accompanied by a statement that it has not been published elsewhere and that it has not been submitted simultaneously for publication elsewhere.

**Review process:** Submitted papers are peer-reviewed by two to three independent reviewers after approval by the Editorial Board. Authors are encouraged to suggest three names of expert reviewers with their e-mail IDs, but selection remains the prerogative of the Editorial Board.

### Articles of the following categories are also considered for publication in PRAJNA:

**Short Communications** are limited to a maximum of two figures and one table. They should present a complete study that is more limited in scope than is found in full-length papers. The items of manuscript preparation listed above apply to Short Communications with the following differences: (1) Abstracts are limited to 100 words; (2) instead of a separate Materials and Methods section, experimental procedures may be incorporated into Figure Legends and Table footnotes; (3) Results and Discussion should be combined into a single section.

**Review Articles** intended to provide concise in-depth reviews of both established and new areas and summarize recent insights in specific research areas within the scope of PRAJNA are solicited by the Editorial Board from leading researchers. The manuscript of this category should be limited to 5,000 words with an abstract of no more than 250 words, a maximum of 5 tables and figures (total), and up to 50 references. Word count includes only the main body of text (i.e., not tables, figures, abstracts or references).

**Commentaries** call attention to papers of particular note and are written at the invitation of the Editorial Board.

**Perspectives** present a viewpoint on an important area of research and are written only at the invitation of the Editorial Board. Perspectives focus on a specific field or subfield within a larger discipline and discuss current advances and future directions. Perspectives are of broad interest for non-specialists and may add personal insight to a field.

**Letters** are brief comments that contribute to the discussion of a research article published in the last issue of PRAJNA. Letters may not include requests to cite the letter writer's work, accusations of misconduct, or personal comments to an author. Letters are limited to 500 words and no more than five references. Letters must be submitted within 3 months of the publication date of the subject article.

**Also announcement of forthcoming Seminars / Conferences / Symposia / Workshops etc. will be considered for publication in PRAJNA.**

### File format for soft copies:

Texts (should be of Times New Roman with 9 point for Abstract and 11 point for other matter) and Tables, if any, must be saved in \*.doc (Word) or \*.rtf (rich text format), graphs in Excel and for illustrations (diagrams, maps, drawings, etc.), the TIF format (300 dpi minimal resolution) is the most appropriate (\*.TIF or \*.JPEG extension).

### Instructions for preparation of manuscripts:

1. The paper should be written in English and neatly typed with double spacing.
2. The title of the paper and the name(s) of the author(s) be in capital letters. The name of the institution be given in small letters below the name (s) of the author(s).
3. The Abstract of the paper, in not more than 150 words, should be provided on a separate page along with 4-6 keywords.
4. The sub-titles, e.g. INTRODUCTION, should be written in capital letters.
5. Displayed formulae, mathematical equations and expressions should be numbered serially. Table should be with a title in addition to a serial number for it.
6. Photographs / Figures should be original with good contrast so as to be in a form suitable for direct reproduction / scanning.

7. Footnotes are not normally allowed, except to identify the author for correspondence.
8. All figures must be numbered serially as they appear in the text, and their legends / captions should necessarily be provided.
9. References should be numbered in brackets [ ] in the order of appearance in the text. All the references in the bibliographic list must correspond to in-text references and vice versa. Abbreviated periodical titles should follow standard subject Abstracts. Names which are not listed by any standard subject indexing organizations should be spelled out in full.
10. All references should be clear and follow the examples below:

**Periodical articles**

- [2] Sadqui, M., Fushman, D. and Munoz, V. (2006) Atom – by – atom analysis of global downhill protein folding. *Nature*, **442**: 317–321.

**Books**

- [16] Stebbins, G. L. (1974) *Flowering plants: Evolution above the species level*, Arnold Press, London, pp. 1–399.

**Chapters from a book**

- [19] Schafer, H. and Muyzer, G. (2001) Denaturing gradient gel electrophoresis in marine microbial ecology. In *Methods in Microbiology* (Ed. Paul, J. H.), Academic Press, London, Vol. 30, pp. 425–468.

**Thesis or other diplomas**

- [21] Nayaka, S. (2004) *The visionary studies on the lichen genus Lecanora sensu lato in India*. Ph. D. Thesis, Dr. R. M. L. Avadh University, Faizabad, India.

**Conference proceedings**

- [4] Mohapatra, G. C. (1981) Environment and culture of early man in the valley of rivers Chenab and Ravi, Western sub-Himalayas. In *Proceedings X Congress of IUPPS*, Mexico, pp. 90–123.

**Online documentation**

- [9] Koning, R. E. (1994). Home Page for Ross Koning. Retrieved 26-6-2009 from Plant *Physiology Information* Website: <http://plantphys.info/index.html>.

**Note:**

**Manuscripts prepared faithfully in accordance with the instructions will accelerate their processing towards publication; otherwise it would be delayed in view of their expected re-submission.**

**For and on behalf of Editorial Board, PRAJNA**

**Prof. T. V. Ramana Rao**  
**Managing Editor, PRAJNA**  
**B R Doshi School of Biosciences,**  
**Satellite Campus, Vadtal Road,**  
**Sardar Patel University,**  
**VALLABH VIDYANAGAR**  
**Gujarat – 388120**  
**Phone: (Lab): 02692-234412 Extn. 111**  
**Mobile: 98254 38147**  
**Fax: 02692-237258 / 236475**  
**e-mail: [spu.prajna@gmail.com](mailto:spu.prajna@gmail.com)**  
**Website: [www.spuvvn.edu](http://www.spuvvn.edu)**

**Note:** This information may be kindly circulated among your colleagues.